THE DEPOSITION OF SILICA ON TITANIUM DIOXIDE SURFACES

Thesis Submitted for the Degree of
Doctor of Philosophy of Brunel University

BY

DONALD NEIL FURLONG

Brunel University
Kingston Lane
Uxbridge
Middlesex
England

September 1975

CONTENTS

ABSTRACT

The deposition of amorphous silica from aqueous solution on to rutile particles has been studied with the aim of elucidating the nature of the silica-titania interactions occurring and of following the progressive build up of the silica coating.

The coating process, which involves the addition of an aqueous sodium silicate solution to an aqueous dispersion of titanium dioxide, has been investigated by performing a series of controlled preparations and using the technique of microelectrophoresis. Prepared silica-coated rutile samples ranging from partial to full silica coatings have been characterized using transmission electron microscopy, microelectrophoresis and nitrogen, argon and water sorption. Nitrogen and argon adsorption isotherms have been analysed using the equation of Brunauer, Emmett and Teller (BET). Differential energies of adsorption of nitrogen and argon have been determined calorimetrically. Water sorption isotherms have been analysed using the BET equation and the Frenkel - Halsey - Hill (FHH) equation.

It has been shown that uniform silica coatings can be produced if adsorption of monomeric silica is followed by polymerization of silica at the solid/liquid interface. Surface cations on rutile may be hydroxylated or co-ordinately bound to water molecules and it appears that monomeric silica adsorbs preferentially by replacing ligand water molecules.

Rutile particles with silica coatings thicker than approximately 2.5nm exhibit characteristics typical of silica and not of the base

rutile.

Silica coatings deposited at pH 10 contain narrow channels which are accessible to water molecules but not to nitrogen or argon. Neutralization to pH 7 reduces the volume in the coating accessible to water molecules.

ACKNOWLEDGEMENTS

The author wishes to thank the many people who have helped to make this thesis possible. To my supervisors, Professor K.S.W. Sing and Professor G.D. Parfitt, I say thank you for your help and advice over the past three years and for your discussion and criticisms of the work described in this thesis. I thank Tioxide International Ltd. for their financial support.

To Dr. T.W. Healy I express appreciation for introducing me to the realms of surface chemistry and for discussions of the electrokinetic data presented in this thesis.

The author has benefited from the experience of Dr. S.J. Gregg and Dr. R.E.Day, and is grateful for discussions and advice.

Many of the staff of Tioxide International Ltd. have assisted with electron micrographs and X.R.F. analyses and in particular I thank Dr. D. Urwin for his time and efforts.

The author had the privilege of spending a part of 1974 working under the guidance of Drs. J. and F. Rouquerol at the "Centre de Recherches de Microcalorimétrie et Thermochimie" - Marseille. I am very grateful to the Rouquerols and their colleagues for advice and friendship, and to the "Centre National de la Recherche Scientique" and "Tioxide International Ltd." for financial support for this project.

The author has been fortunate in being able to call upon the services of the technical staff at Brunel University. In particular

I am grateful to Mr. W. Wilkings and to Brunel's expert glass-blower Mr. A. Williams. My thanks also go to Miss J. Ridge and Mrs. D. Wray in the Chemistry School Office.

To fellow students, past and present, I extend my thanks for friendliness and good times.

My thanks are extended to Mrs. Z. Curry for the typing of this thesis. Her friendliness and co-operation, in addition to her typing skills, were greatly appreciated.

Finally, I thank my family for their support which has continued for many years. I dedicate this thesis to my wife Bena and extend to her my love and appreciation.

LIST OF FIGURES

CHAPTER 1: INTRODUCTION

World annual production of titanium dioxide has increased ten fold since 1930 and is currently approximately two million tons[1,2]. The high refractive index[2], uniform reflectance[2], physical and chemical stability[3] and intrinsic semiconductor properties[4,5] of titanium dioxide have led to its application in such diverse fields as pigments, ceramics and microelectronics[10] and photocatalysis[6-9].

The most widespread application of titanium dioxide (about 75% of total usage in 1969[2,10,11]) is as a pigment in paint, textile and paper manufacture. Naturally occurring titanium dioxide is too impure and of the wrong particle size for use as a pigment. Pigmentary titanium dioxide is produced commercially either by aqueous hydrolysis of titanyl sulphate obtained by digestion from Ilmenite ore (45 to 70% TiO_2)[16] or by high temperature oxidation of titanium tetrachloride obtained from Rutile ore (95% TiO_2)[16,17]. Both processes[18,19] can be used to produce either the anatase or rutile polymorphic forms of titanium dioxide[12-15]. Although "chloride process" rutile pigments have been preferred for many applications, the use of the sulphate and chloride processes currently depends on a fine balance of ore supply and cost against production efficiency and pollution control.

A major problem in the use of titanium dioxide pigments in organic based paints has been the occurrence of "chalking" - a term used to denote oxidative degradation of organic media in the presence of ultra-violet radiation and titanium dioxide. Oxidation leads to the destruction of wetted pigment particle/organic medium interfaces.

This destruction is attributed to a film of carbon dioxide between particle and medium[20] and results in dry pigment powder ("chalk") appearing on the paint film surface. Chalking drastically reduces pigment efficiency[21]. The link between chalking and the photochemical activity of the titanium dioxide has long been recognised[22,23] and the mechanism of the oxidation process has been studied in detail[20,24-28]. In pigments, the photocatalytic activity of titanium dioxide is reduced by coating its surface with a relatively uniform layer of inorganic oxides. Silica, alumina and titanium dioxide mixed coatings are most often used. Coating methods vary with pigment application[29,30] but the most common involves precipitation of the oxides in amorphous form from solution.

Although these surface coatings do not significantly affect the optical properties of the pigment particle, they do control chemical behaviour at pigment/medium interfaces. A vast range of coated pigments has been developed[31,32] as well as numerous empirical methods designed to assess pigment performance with respect to hiding power, colour stability and durability[33-37].

As pigment technology has become more complex precise analytical techniques such as electron microscopy[2,39-44], gas adsorption[43,45-47], microelectrophoresis[48-53], heats of immersion[43,54-56], infra-red spectroscopy[51,57] and adsorption of organics[45,57] have been used to investigate the physical and chemical nature[38] of coated titanium dioxide surfaces. However little has been reported of attempts to study the interactions which lead to a uniform coating of an inorganic oxide on the surface of titanium dioxide. Similarly the physical and

chemical nature of partially coated titanium dioxide surfaces has not been systematically investigated.

The work described in this thesis was directed towards further understanding of the deposition of amorphous silica onto the surfaces of titanium dioxide particles. The single coating component, silica, was chosen for the following reasons:

(1) silica is a major component in commercial pigment coatings

(2) standard procedures for coating pigmentary titanium dioxide with silica have been developed[59,60]

(3) mixed silica-titania surfaces have been studied previously, particularly with regard to their properties as catalysts[61-63]

(4) reports of studies on mixed oxide coatings[53,58] indicate that the interpretation of their properties requires fuller understanding of single component coating systems.

The coating procedures employed in the present work involved the use of aqueous solutions of silica. The nature of silica in aqueous solution, and its polymerization behaviour in supersaturated solution, have been extensively studied over the last thirty years and a brief review of the aqueous chemistry of silica is given in Chapter 2-3.

Microelectrophoresis has been used in the present study to investigate the nature of aqueous silica - titania interactions and to characterize prepared silica-coated rutile surfaces. The interpretation. of electrokinetic data such as that obtained by microelectrophoresis requires a model for the electrical double layer at the solid/liquid interface. The development of electrical double layer theory, with

particular reference to those models developed in recent years for oxides, is outlined in Chapter 2-1.

The surfaces of silica-coated rutile samples have been characterized by gas adsorption using three adsorbates. Water vapour adsorption isotherms at 25°C have been determined using a gravimetric technique. The adsorption isotherms of nitrogen and argon at 77K have been determined volumetrically. Differential energies of adsorption of nitrogen and argon were measured using a Tian-Calvet microcalorimeter. An introduction to the way in which gas adsorption is used to characterize oxide surfaces is given in Chapter 2-2.

The results obtained by each experimental technique are discussed separately in Chapters 6,7 and 8 and general conclusions given in Chapter 9.

All the work reported in this thesis, except for electron micrographs and X-ray fluorescence analyses, was performed by the author during the period: June 1st 1972 to May 31st 1975.

CHAPTER 2: BACKGROUND

2 - 1 INTERPRETATION OF ELECTROKINETIC STUDIES OF THE OXIDE/AQUEOUS SOLUTION INTERFACE

2-1-1 Introduction

Electrokinetic phenomena have been defined as those "involving electricity and connected with a tangential movement of two phases along one another"[64].

For inorganic colloids such phenomena involve two basic processes:

(A) The establishment of a potential difference between a particle and its surrounding medium.

(B) The measurement of a potential difference (or related parameter) at the "plane of shear" between solid particle and supporting medium.

Quantitative measurements of particle surface parameters can be obtained using electrokinetic data by postulating mathematical models for (a) the location of particle charge, (b) the distribution of charge and potential across the region of charge separation (known as the electrical double layer), and (c) the location of the experimental shear plane within that region. Detailed models are not required, however, when electrokinetic experiments are performed in order to follow changes in the nature of particle surfaces. Nevertheless as these techniques involve measurement at the plane of shear and not at the surface, understanding of the mode of formation and structure

of the double layer is necessary.

The general concepts of double layer theory have been derived and tested using the mercury/aqueous electrolyte interface. As a model system this interface combines the advantages of insignificant surface impurity effects with good reproducibility and precision of measurement of surface properties. Insoluble oxides on the other hand form reversible interfaces in which impurity adsorption, finite solubility, irreproducibility of surface preparation and chemical reactivity restrict the reproducibility and precision of measurement of double layer properties[65]. These limitations are partially offset by the applicability of additional techniques such as microelectrophoresis to oxide double layer studies.

Many of the fundamental principles developed for the mercury/aqueous electrolyte interface can be applied to oxide/aqueous electrolyte interfaces. However, when attempts are made to quantitatively extend the mercury theory many inconsistencies occur. For this reason much work has been performed in recent years to develop new models which enable quantitative description of the oxide/aqueous electrolyte interface.

2-1-2 Theory of the Electrical Double Layer

The vast amount of work in the literature on aspects of this subject have been reviewed many times[66-69].

(i) Potentials in the Double Layer: The total work done in transporting unit electric charge from one phase to another is an

unambiguous quantity termed the ELECTROCHEMICAL POTENTIAL DIFFERENCE - $\Delta\eta$[70]. Although most interactions are fundamentally electrostatic in origin, $\Delta\eta$ is normally considered to be the sum of the chemical potential difference $\Delta\mu$ and the electrical or GALVANI potential difference $\Delta\varphi$[67]. Although the total Galvani potential difference between two phases is not measureable by experiment, it is this potential difference that determines many of the properties of colloids. In the case of a charged solid particle suspended in solution the INNER potential is conveniently subdivided:

$\varphi = \psi + \chi$ where $\psi \equiv$ OUTER potential $\equiv$ potential due to the nett charge separation between solid and solution

$\chi \equiv$ KI potential $\equiv$ potential due to orientated dipoles at the interface.

The position of zero reference for these potentials is usually taken at the interior of the solution. Many treatments of the analysis of double layer potentials use the Poisson equation which is concerned with free charges and hence gives the distribution of the ψ potential. In such models, dipoles, and hence the χ potential, were only introduced in terms of the permittivity of the double layer. Later models are modified to take account of special orientations of dipoles at the interface.

(ii) The Diffuse Layer Model: The early "parallel plate capacitor" models of the double layer proposed by Helmholtz and others[70,71] proved of little use. They were modified by Gouy[72-74] and Chapman[75], who proposed that the ions in solution formed a diffuse layer of

charge in which the ordering effect of the surface field tended to be randomized by thermal motions in the liquid (Figure 2-1). Expressions for the distribution of diffuse layer charge and potential were derived using a combined Poisson-Boltzman equation for a flat surface[68], and considering only electrostatic contributions to adsorption of ions. The model predicts an approximately exponential decay of $\psi(x)$ with distance from the surface (x)[89] and a quantity $1/\kappa$ is often designated as double layer thickness[85,92], in that it represents that distance from the surface where $\psi = 1/e[\psi(0)]$. The model is consistent with experimental observation in that it predicts a dependence of diffuse layer potential on electrolyte concentration and a minimum in double layer capacitance when the surface carries no charge[67,77]. However, it does not predict realistic ion adsorption densities at the interface[67,77,85] nor does it help to explain the concept of a shear plane.

The Gouy-Chapman model has been reviewed many times[67,68,76-79], and the assumptions of the model which lead to it being invalid for the entire electrified interface may be summarized:

(1) Ions behave as point charges.

(2) Solvent properties are continuous around ions and near the interface. This has been shown not to be the case with the dielectric constant[81,86].

(3) Non-coulombic interactions such as specific adsorption[83], changes in solvation[82], self atmosphere[79,80] and cavity potentials[79,84] are not significant.

It has been shown that the effects of these assumptions largely cancel out for electrolyte concentrations less than 10^{-2}m [68,79]. However because of assumption (1) $\psi(0)$ should be defined as the potential at the plane of closest approach of ions, not as the surface potential as in the Gouy-Chapman model[76].

(iii) The Compact Double Layer: Stern[87] proposed a model (Figure 2-2) which was essentially a combination of the Helmholtz and Diffuse Layer models and in which:

(A) The distance of closest approach of ions depends on their radii and degree of hydration. The locus of centres of ions at their closest approach forms the Stern plane.

(B) A non-coulombic or specific adsorption energy term ($\Phi\pm$) is included in the total work of adsorption.

Stern derived an isotherm for ion adsorption in the Stern plane based on the configurational Boltzmann equation approach of Langmuir[88]. Stern's model has been often reviewed[66-67,76,89], and whilst it suffers the disadvantages of a Langmuir treatment[90] it does predict

(A) realistic adsorption densities of ions at the interface

(B) specific adsorption of ions ($\Phi \neq 0$) leading to a surplus of counterions at the interface (See Figure 2-3). If the electrokinetic shear plane is located at or outwards of the Stern plane then this specific adsorption would explain the often observed reversal of sign of surface charge[91,93].

The Stern model was modified by Grahame[76] to allow for the smaller primary hydration numbers of anions and the likelihood of their being partially dehydrated on adsorption. The locus of the "electrical" centres[94] of these anions was termed the INNER HELMHOLTZ plane and that of the cations the OUTER HELMHOLTZ plane (Figure 2-4). The charge distribution in the region of the interface has been derived for both metallic[95] and non-metallic[96] surfaces. Grahame's model has given better agreement with experimental analyses.

(iv) Further Developments: There have been many modifications to Grahame's model. Bockris and co-workers[97,98] introduced orientated water dipoles between the surface and the I.H.P. which gave improved agreement with experimental capacitance data. These workers also separated the energy of adsorption into various ion-solvent interactions[99] and concluded that the specific adsorption energy $\Phi\pm$ is more closely correlated to primary solvation of ions rather than their tendency to form covalent bonds as initially suggested by Grahame[76].

Some experimental observations such as the variation of $\Phi\pm$ with surface charge and a maximum in ψ_{IHP} with surface potential are not consistent with the Stern-Grahame model. They can however be explained by using the MICROPOTENTIAL ψ_A, that is the mean electrostatic potential at the centre of an adsorbed ion due to its coulombic interactions with all surrounding ions, rather than the Stern-Grahame MACROPOTENTIAL ψ[100]. The latter is the mean electrostatic potential in the adsorption plane; surface and adsorbed

charges are assumed uniformly distributed. The difference between ψ and ψ_A, caused by the rearrangement of ions when an ion is adsorbed into (say) the I.H.P., is concerned with the calculation of the self-atmosphere potential[100-102]. This calculation forms the basis of the so called DISCRETENESS OF CHARGE effect. The concept of a micropotential allows yet another explanation of the relative adsorption tendencies of anions[101], distinct from those of Grahame and Bockris mentioned above.

For metals there can be no potential gradient within the solid, and the region of space charge separation is restricted to the solution side of the interface. However, with ionic solids and inorganic oxides, solid state defects and surface texture may mean that a significant fraction of the total double layer potential occurs within the solid. Attempts have been made, both general[103] and in terms of specific crystal defects[104-109], to derive double layer potential distributions for both the solution and solid sides of the interface. These attempts have not been incorporated into a general theory which may be applied to oxides and the effect of a solid phase space charge separation remains unresolved[109].

2-1-3 The Electrical Double Layer at the Oxide/Aqueous Solution Interface

At the mercury/solution interface any potential can be applied within quite wide limits and the resulting charge on the metal measured. On the other hand, at the oxide/solution interface, whilst the potential difference between the bulk of the solution

and the solid can be changed by changing the solution concentrations of some ions, the size of this potential difference, or changes in it, cannot be unequivocally determined. Instead, as outlined in the next section, a model dependent analysis must be used to relate concentration changes to potentials and potential changes.

Many of the concepts developed for the mercury interface can be modified for oxides but parallels are generally limited to the diffuse layer region. The Gouy-Chapman theory is considered to give an adequate description of diffuse layer behaviour under the conditions of micro-electrophoresis experiments[146]. It is apparent, however, that for many oxides the charge on the solid side of the interface is developed over a region of finite depth, which may be more or less disordered and may be penetrated by solvent molecules and electrolyte ions. New models have therefore been developed to describe the "inner" region of the double layer at oxide/aqueous electrolyte interfaces.

(i) Potential Determining Ions: The charge transfer processes that are responsible for the establishment of electrochemical equilibrium between a solid oxide and an aqueous solution are of two types[110]:

PRIMARY - the hydrolysis and complexing of surface atoms and the dissociation of surface groups.

SECONDARY - the dissolution of oxide leading to hydrolysis, complexing and readsorption of dissolved species.

If the processes are summarized as follows:[77]

$$MO_x \text{ (solid)} \rightleftharpoons M^{Z+}(aq) + x\, O^{=}(aq)$$

$$MO_x \text{ (solid)} + x\, H_2O \rightleftharpoons M^{Z+}(aq) + 2x\, OH^-(aq)$$

$$\rightleftharpoons [M(OH)_n]^{(Z-n)+}(aq) + (2x-n)OH^-(aq)$$

$$\rightleftharpoons [M(OH)_{2x}]\ (aq)$$

$$\rightleftharpoons [MO_{2x}\, H_{2x-n}]^{-n}(aq) + nH^+(aq)$$

and the formation of polynuclear complexes is ignored, it can be shown that[77]

$$d\psi(0) = (RT/F)\, d \ln [a_{H^+}\ (\text{solution})/a_{H^+}\ (\text{solid})] \qquad (2\text{-}1)$$

χ potentials are assumed constant[77,112] in the derivation of equation (2-1). This equation shows, therefore, that changes in the magnitude of the total double layer potential on oxides are a function of the activity of protons. Protons (and hydroxyl ions) are called POTENTIAL DETERMINING IONS of the SECONDARY type - secondary as they are not, strictly speaking, lattice constituents[117]. If it is assumed that a_{H^+} (solid) is independent of the composition of the solution the familiar Nernst equation is obtained from equation (2-1):

$$\psi(0) = 2.303\, (RT/F)\, (pH_{pzc} - pH) \qquad (2\text{-}2)$$

where $pH_{pzc} = -\log_{10} a^0_{H^+}$ (solution)

The Nernst equation has often been used in conjunction with a Grahame type of double layer model for the calculation of double layer parameters on oxides[19,60,66]. This model is, however, very often at variance with experimental data[111,118] on three counts:

(1) Δ(Electrokinetic Potential)/ΔpH $\neq$ 0.059 when the electrokinetic potential (ζ) = $\psi(0)$ (i.e. no specific adsorption) = 0,

(2) surface charge densities are much higher for oxides than for corresponding mercury or silver halide systems,

(3) the high surface charge densities do not give rise to correspondingly large electrokinetic potentials.

The assumption concerning the independent nature of a_{H^+} (solid) has been criticised as unrealistic[65,121], and recently a modified form of the Nernst equation has been derived for very insoluble oxides[114,115], like titanium dioxide. For such oxides it is proposed that the surface gains charge according to the equilibria:

$$A^- \underset{OH^-}{\rightleftharpoons} AH \overset{H^+}{\rightleftharpoons} AH_2^+ \qquad (2\text{-}3)$$

where AH might be a simple hydroxylated cation site[116] or a neutral aquo-complex site [$\equiv M(H_2O)(OH)_2$][110]. For such a surface it is shown[114,115] that the Nernst equation (equation 2-2) only applies if all sites are uncharged at the point of zero total surface charge. Even though it cannot always be used quantitatively to calculate $\psi(0)$, the Nernst equation does provide a basis for the potential determining role of solution pH in electrokinetic studies on oxides.

(ii) Models of the Double Layer: The Grahame model[76] has often been used in conjunction with a Nernst type equation to give qualitative understanding of the double layer on oxides. It has been suggested[139] that the number of adjustable parameters in a Grahame treatment means that its limitations are often not recognised when applied to oxides. Many workers have attempted to modify the Grahame model to give quantitative agreement with experimental data on oxides. Herczyńska[132,138] proposed a "uniform surface" model for aluminium oxide films on aluminium; Atkinson and co-workers used a similar approach for iron oxide[133]. Although Atkinson's model has been criticised[131] it was the first to propose that counterions may penetrate into the surface charge layer. Blok and de Bruyn[135-136] proposed a model for zinc oxide based on the specific adsorption of counterions. Ahmed[134] generalised this treatment for iron oxide, tin oxide, alumina and silica and stressed that double layer structure on positively charged oxide surfaces is more complex than that on negative surfaces and depends on the nature of co-ordination between surface metal atoms and water molecules, anions and the potential determining ions. Bowden[137] later proposed a generalised version of Blok and de Bruyn's model and used it to obtain good agreement with experimental data on the adsorption of zinc and silicate ions on goethite. All of the above models represented modifications of a Grahame "flat surface charge layer approach" and each model was usually of very limited application. More significant advances in recent years have been made using models which use concepts derived specifically for oxides.

A model designed to explain experimental data on the rutile/aqueous electrolyte interface was put forward by Bérubé and de Bruyn[77,121]. The workers proposed that the solution adjacent to the solid phase was of "ordered" structure and that this ordered region was anchored to the surface via hydroxyl groups. Ordering was promoted by the chemisorption of water and by polarization effects due to the strong crystal field of rutile. Hydrogen bonding sustained the ordering through the liquid phase. This model is consistent with the known "cluster" or "cage" structuring models in water[122] and with data showing that removal of chemisorbed water from titanium dioxide alters its double layer properties[123,152]. Ahmed also used a model in which protons and hydroxyls function as potential determining and structure promoting ions[113]. He related the distribution of double layer potential to the rearrangement of the hydrogen bonded structure extending beyond the Helmholtz region, and claimed that agreement with electrokinetic potentials for quartz and germanium oxide could only be achieved if both χ and ψ were assumed to vary with solution pH. Some important consequences of the Bérubé-de Bruyn model are:

(A) The focal point of the double layer lies in the region of greatest disorganisation in the liquid, and the charging process need not be located at the hydroxylated surface. Instead the unit in the charging process is of the form $[\equiv M\text{-}OH\text{-}H_2O]$.

(B) Counterions penetrate into the charge forming layer depending on their degree of hydration. Counterion penetration accounts for the high double layer capacitance but small electrokinetic potentials observed with oxides.

Another attempt to develop a double layer model specifically for oxides was made by Lyklema[65,119]. The planar surface charge concept of Grahame was discarded in favour of a surface which was porous to both potential determining ions and electrolyte counterions. Lyklema derived a Poisson-Langmuir based expression for the distribution of ions in this porous region. The model predicts that with sufficient counterion penetration very little charge separation would occur in the solution diffuse layer. The experimental observations (1) (2) (3) (page 14) are consistent with this model. Lyklema also claims that the low surface charge for some silicas over a wide range of pH[120], and the trends in adsorption specificity of counterions on silica[130], can be accounted for using this "porosity" model for silica.

In recent years most attempts at oxide double layer analysis have evolved around the so called "gel layer"[126-129] model, in which the surface of the oxide consists of a layer of hydrated oxide into which both potential determining ions and electrolyte counterions can penetrate. The development of this model seems not to have arisen from the suggestions of Atkinson[133] but more from the experimental evidence of gel layers on some silicas[124-125] and the desire to generalise treatments such as that of Lyklema[65,119] for porous silicas and of Bérubé and de Bruyn[77,121] for titanium dioxide. Levine has[126] used a simple $A^- \rightleftharpoons AH \rightleftharpoons AH_2^+$ charging process in the gel with a Poisson-Boltzmann approach to derive the distribution of potential determining ions and electrolyte ions in the gel layer. Perram[127-128] used a more complex charging process:

$$[\equiv M\text{-}(OH)_{n-1}\ O]^- \rightleftharpoons [\equiv M\text{-}(OH)_n] \rightleftharpoons [\equiv M\text{-}(OH)_{n-1}H_2O]^+$$

and derived a modified Poisson-Boltzmann distribution in which any Stern layer at the gel/electrolyte boundary is ignored. Similarly Helmy[129] has given a brief mathematical analysis of the three region "double layer" in which regions are distinguished only by different values of dielectric constant. All three treatments[126-129] show that the gel layer model is consistent with the experimentally high surface charges and low electrokinetic potentials observed with silica, titania, alumina and hematite if the shear plane is located at the gel electrolyte boundary. However, it was recognised by Perram[127] that the gel layer model applies only to oxides with high surface charges as measured by titration. Bérubé and de Bruyn's results[121] for titanium dioxide indicate that this oxide shows behaviour consistent with a gel layer type interface when suspended in aqueous electrolyte.

It can be seen from this review of models of oxide double layers that different oxides follow different patterns of behaviour that are consistent with different models. Whilst the gel layer model is probably the most successful in that it seems to cover more oxides than any previous model, no single model has been developed to fully explain the behaviour of all inorganic oxides.

2-1-4 Some Practical Aspects

(i) Surface Charge: The pH dependence of various mononuclear hydrolysis products of Ti(IV) in equilibrium with rutile at 25°C have been calculated from solubility[140,154] and thermodynamic data[141-2,153] and are shown in Figure 2-5. It can be seen from this diagram that rutile has a maximum solubility of 10^{-6} moles/litre over the pH range

3 to 12. Because of this low solubility, surface dissolution and subsequent adsorption of hydrolysis products is not normally considered to be a significant charging mechanism. Surface charge is produced principally by the adsorption/desorption of protons and hydroxyls at surface hydroxyl groups on the titanium dioxide surface. Solution pH is a parameter which controls the magnitude of the total double layer potential on titanium dioxide.

(ii) Supporting Electrolyte: Gouy-Chapman diffuse layer theory showed that at constant total double layer potential, the potential at any point in the diffuse layer changes with solution ionic strength. Stern's and subsequent models have shown that specific adsorption of ions in the inner region of the double layer can lead to apparent reversal of the sign of surface charge. Hence in electrokinetic experiments where pH is the varying parameter, a supporting electrolyte must be used to maintain constant ionic strength. The electrolyte ions must only adsorb in the inner region of the double layer in response to simple electrostatic free energy changes. The most common indifferent electrolytes used in electrokinetic studies of titanium dioxide have been KNO_3[143-144], NaCl[145] and KCl[146].

(iii) Iso-Electric Point and Point of Zero Charge: The velocity of a particle suspended in electrolyte when that system is subject to an applied electric field, can be used to estimate changes in the electrical double layer potential at the plane of shear between particle and solution. The velocity per unit field strength is termed the ELECTROPHORETIC MOBILITY, and a useful quantity to emerge from measurements of mobility as a function of solution pH is that pH at

which the electrophoretic mobility is zero. This pH will be called the ISOELECTRIC POINT (i.e.p.) for data presented in this thesis. This definition is consistent with I.U.P.A.C. recommendations[155] but should not be confused with definitions of i.e.p. used by others[146-147]. The i.e.p. enables different solid surfaces to be compared when it is believed that their double layer structures are similar - for example a series of titanium dioxide samples having different pre-treatments.

The point of zero charge (pzc) is a term often used in the literature with respect to oxides but not always rigorously defined. Parks[147] has used this term to denote "that pH in any system, however complex, at which there is no nett charge on the solid particles of interest". Other definitions of pzc include "the pH at which an oxide surface acquires a zero effective charge as a result of H^+ and OH^- adsorption[131], and "the pH at which the surface excesses of H^+ and OH^- are equal"[148]. All quoted values of pzc or iep must be placed in context by understanding of their definitions and the experimental method by which they were measured. The term pzc will not be used in reference to any microelectrophoresis data obtained by the author and presented in this thesis.

(iv) Location of the Shear Plane: The isoelectric point enables a model independent characterization of a solid. However, interpretation of changes in the inner region of the double layer, whether such changes are estimated by double layer potential or electrophoretic mobility measurement, requires a model dependent location of the experimental shear plane. The Grahame model of the double layer predicts a plane of viscosity discontinuity at the Outer Helmholtz Plane. It can be shown that experimental data are not consistent with placing

the shear plane further out into the solution than the OHP[69,118,150], although this may well mean the model itself is inconsistent. Nevertheless many workers using Grahame's model have placed the shear plane at the OHP[83,139,149]. The concept of a discrete slipping plane has been criticised by Lyklema and Overbeek[151] who suggest a gradual transition from bulk to zero fluidity rather than a plane discontinuity. They and others[68,151] have shown that high surface potential lead to the slipping region moving outwards from the surface such that potential changes in the inner region of the double layer are not "seen" at the shear region. This does not, however, appear to occur with the systems used in this work.

Of all the recent models of oxide double layers, the "gel layer" model incorporates the most feasible location of the shear plane. Perram[127-128] has shown that all double layer calculations are consistent with a slipping plane at the gel/electrolyte boundary and Levine[126] concludes that a shear plane further out into solution leads to incorrect estimation of double layer parameters.

In conclusion it can be said that although double layer models may not be completely consistent with all experimental data, all evidence is that the experimental shear plane can be put at the boundary between the solution diffuse layer and the inner region of the double layer. Data obtained at the shear plane represent the sum of all effects between it and the surface. It should also be recognised that shear plane measurements represent average quantities over a region of slipping between the particle with its attached layers and the mobile solution.

CHAPTER 2 - 2 CHARACTERIZATION OF OXIDE SURFACES BY GAS ADSORPTION

2-2-1 The Nature of Metal Oxide Surfaces

Although oxide particles can be prepared in many different ways one approach to describing the structure of an oxide surface is to consider it as resulting from the cleavage of a bulk oxide crystal[162-165]. The surface formed by cleavage would consist of oxygen and metal atoms, unsaturated with respect to co-ordination and carrying formal charges. This surface would be highly unstable and in the absence of foreign reactive species would form highly strained M-O-M surface bonds[157,164]. However in the presence of water vapour dissociative chemisorption of water molecules would occur on the strained surface giving a layer of surface hydroxyl groups. This chemisorption process presupposes that hydroxyl groups can be accommodated on adjacent metal atoms. It has been suggested, on the basis of bulk crystal cleavage occurring along known crystal planes, that for some crystal planes this degree of hydroxyl accommodation is not sterically possible[162-163]. In such instances it is likely that co-ordination of the metal cation is completed by the adsorption of a water molecule as a σ bonded ligand[162-163].

In addition to the two possible forms of chemisorbed "water" on oxides, hydroxyl groups and ligand water molecules, physical adsorption of molecular water will occur to give layers of relatively loosely held water molecules. Hence the interaction of gases with oxide surfaces may involve interactions with metal cations, oxide anions, hydroxyl groups and water molecules.

2-2-2 Interactions at Gas/Solid Interfaces

(i) Introduction: When a gas molecule approaches an outgassed solid surface (the adsorbent) it will experience forces which lead to increased concentration of gas near this surface (adsorption) relative to the bulk gas phase (the adsorptive[155]). Because exact calculation of the interactions of quantum states of gas molecules with those of the solid surface is not possible[161], it is usual to simplify the treatment of adsorption by assuming that adsorption can be one of two types[156]:

Physisorption: in which the equilibrium distribution of the electrons of the solid and the gas molecule may be modified, but in which electrons are not shared or transferred between the solid and gas molecules.

Chemisorption: in which electrons are shared or transferred during adsorption.

These two types of interaction will be discussed as though they are independent, although during adsorption on oxides both are likely to occur simultaneously[157]. Lateral adsorbate-adsorbate interactions, and their effects on adsorbate-adsorbent interactions will not be discussed.

(ii) Physisorption: The interactions involved in physisorption are of the van der Waals type, and the total physical adsorption energy for each adsorbed molecule ($\phi_{PHYSICAL}$) can be expressed as[158]

$$\phi_{PHYSICAL} = \phi_D + \phi_R + \phi_P + \phi_{F\mu} + \phi_{FQ} + \phi_X$$

The dispersion energy (ϕ_D) and short range repulsion energy (ϕ_R) are non-specific in that they are non-zero for any adsorbate/adsorbent system[161]. Many complex expressions have been derived for ϕ_D and ϕ_R[156-157], and the energy ($\phi_D + \phi_R$) has been shown to have a minimum value at about one molecular diameter out from the solid surface[157,159]. The energies ϕ_P and $\phi_{F\mu}$ arise from the interaction between the surface electric field and the electric moment it induces in a polarizable molecule (ϕ_P) and the permanent dipole moment of the adsorbate molecule ($\phi_{F\mu}$). The energy $\phi_{\dot{F}Q}$ arises from the interaction between the surface electric field gradient ($\dot{F}$) and any permanent quadrupole moment of the adsorbed molecule. The term ϕ_X represents the sum of any interactions arising from a multipole moment of the surface, and will not be further discussed in the present work. The energies ϕ_D, $\phi_{F\mu}$, $\phi_{\dot{F}Q}$ and ϕ_X are termed specific in that their magnitude depends on the nature of the particular adsorbent-adsorbate system[161].

(iii) Chemisorption: The distinction is often made between weak chemisorption, which involves covalent bond formation on adsorption, and strong chemisorption which involves ionic bond formation[156]. As either electron sharing or transfer is involved, the chemisorbed layer cannot exceed a single molecule in thickness[160]. Bond formation although a spontaneous process from a thermodynamic viewpoint (negative change in total free energy) may involve an energy barrier arising for example from an initial bond breaking. Approach to equilibrium may therefore be slow.

2-2-3 Methods of Characterization

Extensive reviews of the numerous experimental techniques that

can be used to characterize gas-solid interactions are given elsewhere[157,170,172] and discussion here will be restricted to adsorption isotherms and heats of adsorption.

(i) Adsorption Isotherms: At constant temperature (T) the amount of gas (x) adsorbed at a gas-solid interface depends on the concentration of gas (i.e. pressure, P) and the strength of gas-solid interactions. An experimental adsorption isotherm may be represented by

$$x = f(P/Ps)_{T,\ gas,\ solid}$$

where Ps is the saturation pressure of the adsorptive at temperature T. The most commonly observed isotherm shapes have been classified by Brunauer et al.[171] and the isotherms reported in this thesis are Type II according to this BDDT classification (See Figure 2-6). Type II isotherms are associated with monolayer-multilayer adsorption[160,173] and many mathematical equations have been derived to analyse the adsorption isotherms. The BET and FHH models have been used to analyse adsorption data presented in Chapters 7 and 8 of this thesis and these two models are described in following sections of this Chapter.

Many adsorbents give greater uptakes of gas during a desorption run than occurred at the same relative pressure during the adsorption [increasing (P/Ps)] run. The reasons for this hysteresis may be:
(A) Irreversible chemisorption of adsorbate during the adsorption run. This chemisorption may not occur until high (P/Ps) values are reached and the hysteresis loop remains open over the whole (P/Ps) range.

(B) Activated entry of adsorbate into pores or cracks in the surface[176]. The term "activated" implies that a threshold (P/Ps) is required before entry occurs. In this case the hysteresis loop may also stay open to low (P/Ps) values.

(C) Capillary condensation of liquid adsorbate in surface pores or interparticle voids. A liquid meniscus is formed and the radius of curvature of this meniscus controls the relative pressure at which liquid will evaporate from the capillary. Hence as (P/Ps) is reduced, adsorbate is removed from progressively smaller pores. The lower (P/Ps) limit for the existence of the liquid meniscus is considered to be controlled by the tensile strength of the adsorbate[167].

The BET Equation

Brunauer, Emmett and Teller[190] extended the dynamic condensation-evaporation adsorption mechanism previously applied by Langmuir[191-192] to describe localised monolayer adsorption, to the monolayer and multilayer adsorption of gases on solid surfaces. The BET isotherm equation

$$\frac{P}{V(Ps-P)} = \frac{1}{VmC} + \frac{C-1}{VmC}\,\frac{P}{Ps}$$

where V is the amount of gas adsorbed at equilibrium pressure P, Vm is the amount of gas required to give monolayer coverage, Ps is the saturated vapour pressure of the adsorptive and C is a constant ≥ 2;

corresponds to a sigmoid shape (Type II) adsorption isotherm. The BET equation predicts that a plot of P/ V(Ps-P) against (P/Ps) should be linear, enabling ready calculation of the monolayer capacity (Vm) and

the constant C. In practice most adsorbate-adsorbent systems only give linear BET plots in the range $0.05 < (P/Ps) < 0.35$ (0.5 V/Vm→ 1.5 V/Vm) and this linear portion must be extrapolated to enable calculation of Vm and C.

The derivation of the BET equation has often been reviewed[159,193] and the main approximations in the derivation are:

(1) the adsorbent surface is energetically homogeneous

(2) lateral adsorbate-adsorbate interactions are absent

(3) molecules in the second and subsequent adsorbed layers are energetically equivalent

(4) the number of adsorbed layers is infinite at saturation pressure.

These approximations have been shown to be invalid for various systems[194-197] and numerous modifications to the BET equation have been proposed. The modified models often involve extra parameters[215] and result in equations much more complex[198] than the BET equation. The practical utility of the BET equation has led to its wide-spread use in preference to more complex models.

In light of the assumptions (1) to (4) it is not surprising that the BET equation does not completely describe all experimental isotherms. In regions of low surface coverage where adsorption occurs in response to the strongest adsorbate-adsorbent interactions, both surface energy heterogeneity and enhanced dispersion forces[174,175] in micropores[155] may contribute to non-BET adsorption behaviour. At higher coverages lateral adsorbate-adsorbate interactions will occur. A linear section in the BET plot may indicate that assumptions (1)

to (4) are valid, but is more likely to result from the mutual compensation of various sources of error[193,237] in this region of adsorption. Lengthy and vigorous consistency tests for the BET equation have recently been proposed[201] but have not been applied to adsorption data presented in this thesis.

The BET Surface Area

The BET specific surface area (S_{BET} in m^2/gm) can be calculated from the monolayer capacity (Vm in cm^3/gm, STP) using the equation

$$S_{BET} = \frac{Vm \cdot N \cdot Am \cdot 10^{-19}}{22414}$$

where N is Avogadro's Number and Am is the area (in nm^2) occupied by each adsorbed species in the completed adsorbed monolayer. Am cannot be independently measured and its value is usually estimated by assuming (i) close hexagonal packing of species in the monolayer and (ii) a packing density in the monolayer equal to the bulk liquid density of the adsorbate[160]. With these assumptions the Am values for nitrogen, argon and water are 0.162 nm^2, 0.138 nm^2 and 0.106 nm^2 respectively. The assumptions (i) and (ii) require that the value of Am is independent of the nature of the adsorbent. For systems where localised adsorption can occur assumptions (i) and (ii) may not be valid. For water sorption on oxides, chemisorption and strong physisorption may lead to localised adsorption of water and the value of 0.106 nm^2 per adsorbed water molecule may be incorrect. Nitrogen, because of its quadrupole moment, may also undergo localised adsorption and Am (N_2)

values of from 0.129 to 0.177 nm^2 have been reported[203-204] for nitrogen adsorbed on silica and titania.

Argon adsorption presents two additional problems when used to estimate BET surface areas.(i) Argon isotherms often do not possess a well defined point B (See Figure 2-6) and the use of the BET equation to evaluate the monolayer capacity may be in doubt[159-160]. (ii) It is often uncertain whether argon adsorbed at 77K exists in a liquid or solid like state. This uncertainty is manifest in the calculation of the saturated vapour pressure of argon for isotherm representation, and in the calculation of the cross-sectional area per adsorbed atom. For the argon adsorption isotherms presented in Chapter 7 it has been assumed that argon exists as a supercooled liquid at 77K. This is consistent with the approach of other workers[208-209].

The BET C Constant

For adsorption which follows the BET equation the magnitude of the BET C constant determines the amount of gas adsorbed at any relative pressure. An increased C constant gives rise to a sharper "knee" in the adsorption isotherm (See Figure 2-6). The C constant can be expressed as follows:

$$C = A \exp[(\epsilon_1 - \epsilon_L)/RT] \qquad (2\text{-}5)$$

where ϵ_1 and ϵ_L are the potential energies of adsorption[216] in the first and all subsequent adsorbed layers respectively. From a statistical mechanics viewpoint[216] C can be related to the ratio of molecular partition functions for adsorbed and non-adsorbed molecules. Each

molecular partition function is the product of a configurational entropy term and an exponential energy term, and hence by analogy the term ($\epsilon_1-\epsilon_L$) in equation (2-5) is often called the NETT MOLAR HEAT OF ADSORPTION and the pre-exponential term (A) the NETT ENTROPY OF ADSORPTION. The calculation of the molar enthalpy of adsorption from an experimental BET C constant, using equation (2-5), involves three sources of uncertainty:

(a) It must be assumed that the term $\Delta\epsilon$ ($= \epsilon_1 - \epsilon_L$) can be set equal to the difference in total internal energies, which may be termed the surface excess energy[155]. According to Schay[178] the surface excess energy is equal to the excess enthalpy of adsorption.

(b) Estimation of the pre-exponential factor A requires values for the entropy changes during adsorption[217]. These entropy changes are often unknown and in these cases A is often set equal to unity. Kemball and Schreiner[217] have given values of A for different systems which vary by up to 7 orders of magnitude. However, entropy data reported for nitrogen, argon and water sorption on rutile[179,218] indicate that for these adsorption systems the assumption that A = 1 might lead to errors of the order of 10% in calculated enthalpies of adsorption.

(c) The derivation of the BET equation requires the assumption that the energy of adsorption is constant up to monolayer completion (ϵ_1); and for multilayer adsorption is equal to the energy of liquefaction of the adsorbate (ϵ_L). Experimentally, enthalpies of adsorption of gases on heterogeneous surfaces are not constant during monolayer formation[179,219,220]. The BET C constant is only applicable to the

region of linearity of the BET plot (normally $0.5 < V/Vm < 1.5$) and has been claimed to represent an inverse mean quantity[201] for this BET region.

In summary then it can be said that whilst the BET C constant may be used to give an approximate estimate of the average enthalpy of adsorption its value is limited and in some circumstances it may bear no relation to the real differential enthalpy of adsorption[237].

The Frenkel-Halsey-Hill Equation

A theory for the analysis of adsorption isotherms in the multilayer region was developed independently by Frenkel[221], Halsey[222] and Hill[223], and is based on the following model for the adsorption process:

(1) the first part of the adsorption isotherm consists of adsorption, without lateral adsorbate-adsorbate interactions, on the more active parts of the surface. Calculations by Halsey[224] showed that smooth isotherms (e.g. type II) were not consistent with an energetically homogeneous surface.

(2) "co-operative" adsorption (i.e. lateral interactions occur) then takes place on the still heterogeneous surface resulting from the initial adsorption.

(3) "co-operative" multilayer condensation occurs under the influence of the van der Waals field transmitted from the surface.

If the van der Waals forces (ΔF) are expressed in the form $\Delta F = a\theta^{-r}$ (2-6) then the following adsorption isotherm can be

derived:

$$P/Ps = \exp(-a/RT\theta^{r}) \qquad (2\text{-}7)$$

where $\theta = V/Vm$, T = Temperature (K), R = Gas constant, r is a constant and a is a constant related to the energy of adsorption in the first layer. It follows from postulates (1) (2) and (3) and equation (2-6) that this isotherm equation (2-7) applies only in the multilayer region of adsorption where the effects of surface heterogeneity will be of decreasing importance. If the FHH equation is applicable a plot of $\log[\log(Ps/P)]$ against $\log\theta$ (the FHH plot) should be linear with a slope of -r. In further discussion the term "slope of the FHH plot" will be used to indicate the magnitude of r..

For energetically heterogeneous surfaces, such as titanium dioxide[235,236], Pierce has suggested[228] that an FHH plot that is non-linear in the multilayer region indicates restricted adsorption. An upward deviation from linearity at higher relative pressures may be interpreted in terms of capillary condensation[228,229], whilst a generally curved plot (or a linear plot of very low slope) indicates micropore filling[228].

As r represents the exponent of decay of the surface force field, a large value of r indicates short range adsorbate-adsorbent interactions; that is "specific" interactions. Smaller values of r indicate longer range interactions. The exact theoretical values of r for different types of interaction are not known[225-227] and it is necessary to review the results of those workers who have applied the FHH equation, to assess the dependence of r on the nature of the adsorbate and adsorbent.

For the adsorption of nitrogen on anatase, Halsey[222] obtained

a value of r = 2.67 by replotting the adsorption data of Harkins and Jura[234]. Pierce[230], for the adsorption of nitrogen on silica and titania, claimed that all adsorption at (P/Ps) > 0.2 on "free" surface (no capillary condensation) fitted the ideal isotherm equation $(V/Vm)^{2.75} = 1.30/\log(Ps/P)$, i.e. r = 2.75. Zettlemoyer[231] has confirmed this value, but restricts it to high energy (polar) surfaces. Zettlemoyer gave a range of r values less than 2.75, the lower values for low energy surfaces such as Teflon being around 2.12.

For the adsorption of water vapour, Halsey[222], using the data of Harkins and Jura for the adsorption of water vapour on anatase outgassed at room temperature, obtained r = 2.50. The FHH isotherm with this value of r coincides within experimental error with the experimental isotherm from (P/Ps) 0.2 up to saturation, indicating that no capillary condensation of water occurred. Jurinak[233] has obtained an r value of 2.45 and McCafferty and Zettlemoyer 2.33[232] for the adsorption of water vapour on Fe_2O_3 outgassed at 25°C; Zettlemoyer[231] has shown that for water vapour adsorption, r varies from 1.4 for a dehydrated silica to 2.5 for an hydrated silica. It appears then, from the limited amount of data available that hydrophilic oxide surfaces give r values near 2.5 and hydrophobic oxide surfaces give r values less than 2.0 for the sorption of water vapour.

(ii) Heats of Adsorption: Many experimental techniques can be used to estimate "heats of adsorption"[170,180], and for each method the precise conditions must be specified so that the heat obtained can be related to quantities given by other techniques[182].

The formal treatment of adsorption in thermodynamic terms can procede by defining adsorption according to[155,178]:

(a) the concept of surface excess quantities, or

(b) the concept of an interfacial layer as a distinct phase[188].

Everett[155,182-185] has shown how the usual thermodynamic functions[186], in particular internal energy, entropy and enthalpy, can be defined for adsorption in terms of both concepts (a) and (b). Relationships between these functions for adsorption at the gas/solid interface, can be developed according to the principles of solution thermodynamics[181] with the introduction of surface area as an independent variable[182]. The formal development of adsorption thermodynamics has shown that experimentally determined "differential heats of adsorption" (differential with respect to amount adsorbed) are of numerous forms[180], the two most important being[155,185]:

— DIFFERENTIAL ENERGY OF ADSORPTION — q_D

and — DIFFERENTIAL ENTHALPY OF ADSORPTION — q_{st}

The latter (q_{st}) is also known as the ISOSTERIC heat of adsorption. The quantities q_D and q_{st} can be related by the equation:[182,185]

$$q_D - q_{st} = RT$$

Both q_D and q_{st} can be estimated directly by calorimetry[189]. The calculation of q_D from experimental parameters for the continuous adsorption calorimetry reported in the present work is given in detail in Chapter 4.

The most common indirect method for estimating q_{st} involves the application of a particular form[181] of the Clausius-Clapeyron equation

$[(d\ln P/dT)_X = q_{st}/RT^2)]$ to adsorption data measured over a range of adsorption temperatures. Whether X should be surface coverage (θ) or amount adsorbed (V) has been in doubt[187], but the latter is normally chosen. Use of the Clausius-Clapeyron equation involves four assumptions:

(1) Ideal gas behaviour (a non-ideality correction can however be included[180])

(2) Volume of adsorbate negligible compared to volume of adsorptive

(3) Thermodynamically reversible adsorption[170]

(4) Thermodynamic quantities q_{st} and entropy of adsorption do not change over the pressure and temperature range used[183].

Assumptions (1) and (2) may lead to small errors (< 3%[183]) and (3) should always be verified experimentally[187]. A change of state of the adsorbed layer within the temperature range used will invalidate (4), but the range used is normally small to minimise the possibility of this occurring.

The relative precision of calorimetric and isotherm methods varies with pressure. In most calorimetric methods (See Chapter 4-3) it is necessary to correct calorimetric energies of adsorption for energies of compression of the adsorbing gas entering the adsorption ampoule. These correction factors are greater, and more difficult to calculate accurately, as the pressure increases. Hence calorimetric methods are most precise in regions of low pressure. It is difficult to measure adsorption isotherms with sufficient precision, and

moreover assumption (3) may be inapplicable (e.g. chemisorption), in very low pressure regions to enable the calculated values of q_{st} to rival in precision those determined calorimetrically. At pressures greater than (say) 10^{-1} torr ($13 N/m^2$) and provided assumptions (1) to (4) apply, q_{st} values calculated from adsorption isotherms are sufficiently precise for most purposes[179].

The DIFFERENTIAL ENERGY OF ADSORPTION (q_D) can be defined[185] as "the total change in energy of all the extra molecules which come under the influence of the solid when the pressure is increased, divided by the change in the excess number of molecules". In most cases, particularly at low pressures[185], this change in total energy may be well approximated to the change in energy of the molecules moving from the gas phase to the neighbourhood of the surface, the contributions of molecules already adsorbed being ignored. It will be assumed throughout the discussions that q_D involves principally a consideration of the decrease of the potential energy of adsorbate molecules due to adsorption[182].

CHAPTER 2 - 3 THE AQUEOUS CHEMISTRY OF SILICA

2-3-1 The Solubility of Amorphous Silica

Amorphous silica will form, given time, in any supersaturated aqueous silica solution[239]. The form of the amorphous silica can vary from loose flocculent masses to rigid gel structures depending on the conditions of supersaturation[238-244]. The maximum equilibrium concentration of aqueous silica is the same whether that equilibrium has been obtained from solid amorphous silica by dissolution or from a supersaturated aqueous silica solution[270]. It is often convenient experimentally, to measure that equilibrium concentration by a controlled solubility experiment.

Although some experimental data indicate that the various crystal modifications of silica have different solubilities[238,239], it is believed that the mechanism of dissolution is the same for all silicas[60] and involves the hydrolysis of siloxane (Si-O-Si) bonds with the release of hydrated silicic acid molecules into solution[239,254]:

$$(SiO_2)_x + 2H_2O \xleftarrow{OH^-} Si(OH)_4 \text{ (aqueous)} + (SiO_2)_{x-1}$$

From studies of the depolymerization of silica in sodium hydroxide solution, Greenberg[269] concludes that two important rate controlling factors in the above reaction are: (i) the strength of the siloxane bonds (ii) the ability of NaOH and low molecular weight hydrolysis products to diffuse through the porous structure of the solid. The solubility would be expected to show variation from one sample to another. However, it is believed[239] that the hydrated silicic acid readsorbs onto the solid and this readsorption controls the final

equilibrium solubility. This was also illustrated by Jorgensen[240] who showed that supersaturation is always obtained initially with silica while the stable "readsorbed" surface phase is being formed. Acceptance of the above mechanism means that direct relationships between dissolution and depolymerization, such as the calculation of a free energy of depolymerization from solubility data[241], may not apply quantitatively. Iler's suggestion[244] that solubility may be related to the similarity between the oxygen packing density in the silica and in water also seems unlikely. The dissolution/readsorption model does not preclude varying rates of dissolution between different forms of silica and equilibrium times have been reported as from two days[242] to six months[243]. Lack of equilibrium seems the likely reason for the wide variety of values for the solubility of various forms of silica.

The major factors which control the aqueous solubility of amorphous silica have been summarized by Shell[245] and investigated by many workers. The parameters are: temperature[251,254-256], pH[238,242-243, 249,251], electrolyte[242] and foreign ion concentration[250] and particle size[60]. From the point of view of the precipitation of amorphous silica from a solution of soluble silica the two most important of these parameters are pH and temperature.

a) pH: as a result of many studies it has been established that the solubility of amorphous silica at a given temperature is constant over the pH range 3 to 8 and increases markedly at pH values greater than 8. The data for pH less than 3 are not conclusive, both

increased[251] and decreased[253] solubility having been reported. The rate of dissolution apparently varies over the whole pH range[252]. The solubility/pH data of some workers[238,242-243,249] are summarized in Figure 2-7.

b) Temperature: the solubility of amorphous silica increases with temperature, and the results of some studies are given in Figure 2-8. The rate of dissolution has also been shown to increase with temperature[238,246].

The data given in Figures 2-7 and 2-8 show that at pH above 3, and over a temperature range of 25 to 95°C, the maximum equilibrium concentration of silica in aqueous solution has been reasonably well defined.

2-3-2 The Nature of Silica in Solution

The many experimental techniques that have been used to determine the formulae of silica in aqueous solution have been reviewed by Lagerstrom[255] and Freund[256]. Techniques such as potentiometric titration, ultracentrifugation, conductometric titration and light scattering provide information on well defined solutions but require detailed models for interpretation in terms of the nature of the silica. In contrast, molybdic acid titration and chemical reaction/chromatographic methods are easier to interpret but suffer from some uncertainty as to the state of the solution studied. Whilst the recent laser Raman studies[256] offer improved precision, because of the complexity of silica solutions and the experimental limitations described, the exact forms

of many silica species are still in doubt.

Experiment has shown that at pH less than 9, the solubility/pH curve (Figure 2-7) represents equilibrium between high molecular weight polymeric silica and dissolved monomeric silica - $Si(OH)_4$[255,258-260]. This orthosilicic acid will react with hydroxyl ions to form silicate ions, and although $SiO_3^{=}$[261] and $Si(OH)_6^{=}$[60] have been suggested to describe silicate ions, the weight of evidence[255-256,258,262-263] supports 4 co-ordinated silicon in the forms $SiO(OH)_3^{-}$, $SiO_2(OH)_2^{=}$ and $SiO_3(OH)^{\equiv}$. The latter species only forms in significant amounts at pH greater than 15[256].

At pH greater than 9, the solubility/pH curve (Figure 2-7) represents equilibrium between high molecular weight polymer and soluble oligomeric silica species. These oligomers are stable over a narrow pH - silica concentration range, and although their structures are not known precisely, they do not appear to contain more than eight silicon atoms[256-257,263]. Experimental evidence has been claimed for dimers[256-257,259-260,265], trimers[259,264-5], tetramers[256-257,258-259,265], hexamers[256,283] and octamers[256,283]. Lagerstrom[255] has claimed that the nature of the multimeric species depends on electrolyte concentration. This concept has been criticised by Aveston[266] who, together with Freund[256], claims that a wide range of oligomers can exist and the dominating species depends on silica concentration and pH.

An overall picture of the nature of aqueous silica as a function of pH and concentration was given by Stumm, Hüper and Champlin[267] and is reproduced in Figure 2-9. This diagram has been constructed using published solubility data, the equilibrium constants calculated by Lagerstrom[255] for the hydrolysis of $Si(OH)_4$ and the formation of

$Si_4O_6(OH)_6^{=}$, and the assumption that $Si_4O_6(OH)_6^{=}$ is the only stable oligomer formed. The mononuclear wall, which is used to represent the lower concentration limit for stable oligomers, is calculated from Lagerstroms data given the condition that [Si] monomeric = 100 [Si]multimeric. Superimposed on Stumms diagram in Figure 2-9 are the results of Iler[244] showing that for a 1 molar solution of silica. 97% would be dimeric at pH 13.5 (Point B, Figure 2-9) and polymerization would occur at pH < 10.9 (Point A, Figure 2-9). Also shown on Figure 2-9 are points obtained from the light scattering data of Debye and Nauman[268]. They observed that the turbidity of a 0.13 molar solution of silica at pH 12.5 (Point C, Figure 2-9) was constant for 20 days and increased very slightly over a period of six months. This indicates very slow polymerization of silicic acid. Solutions with lower pH, and silica concentrations 0.1 to 0.5m, (Range D, Figure 2-9) gave large turbidity increases within a few days. These are consistent with point C being close to the monomer-stable multimer boundary and range D being close to the stable multimer-polymer boundary.

The equilibrium diagram given in Figure 2-9, allowing for the approximations in its calculation and the degree of consistency with other experimental data, can be used to indicate the domains of existence of the three types of silica - monomeric, oligomeric and polymeric.

2-3-3 Equilibrium in Solution

It has been shown that if a solution, or any part of it, does not enter into the insolubility or polymerization region of pH and concentration (Figure 2-9), equilibria between the various monomeric

and stable oligomeric silica species are reversible and rapidly established[255,258]. The state of any solution outside the polymerization region is therefore well defined.

2-3-4 Polymerization

From a thermodynamic viewpoint, the conversion of monosilicic acid through intermediate polymers to a form of amorphous silica (colloidal particle, precipitate or gel) is to be expected, as the change represents conversion to the state of lowest surface energy[244]. Iler[60] has defined four processes to describe the aggregation of colloidal silica particles, two of which are relevant to the polymerization processes occurring in a supersaturated aqueous solution of silica:

(A) Gelling: "particles" are linked together throughout the volume to form a network in which there is no increase in silica concentration in any macroscopic region in the medium.

(B) Coagulation: "particles" come together in relatively close packed clumps in which the concentration of silica is increased relative to the original solution. The coagulate settles as a relatively dense precipitate.

The aggregation of silica in supersaturated solutions has been shown to depend on the values of numerous parameters, principally salt concentration[271,274], temperature[275-276], total silica concentration[272,279], adsorbed carbon dioxide[274] and pH[254,264,271-276]. pH is a most important parameter in determining both the state and rate of aggregation of silica in supersaturated solutions.

From the summary of literature data given in Table 2-1, it can be seen that the rate of aggregation is slowest around pH 2 and rapid in neutral or slightly alkaline solution. This pattern of behaviour can be utilised to prepare supersaturated silica solutions with an initial degree of polymerization of less than two[278] and stable to apparently less than trimer formation for more than 24 hours. The key step in such preparations is rapid passage through the neutral pH region.

Understanding of the rate/pH behaviour can be gained by considering the mechanism of interaction leading to aggregation. Although primarily concerned with interactions between colloidal silica particles Depasse and Watillon[279] have described three types of silica-silica interaction which may also apply to the polymerization of silica from aqueous solution.

(A) The hydration/dehydration model in which silanol groups (≡Si-OH) associate by forming hydrogen bonds via water molecules. This mechanism has been proposed by Acker[280] for the formation of silica hydrosols in the pH range 0.5 to 4. From viscosity, elasticity and syneresis studies Acker concludes that even in acid set hydrogels hydrogen bonding predominates; a model with only one siloxane bond (≡Si-O-Si≡) per three trisilicic acid units giving the best fit with experimental data. Acker further claims that only on drying to a rigid gel is a three dimensional network of siloxane bonds formed.

(B) Particle binding via van der Waals forces, as proposed by Debye and Nauman[271] to account for increases in turbidity of their silicate solutions due to the formation of "loosely bound aggregates".

TABLE 2-1

RATES OF AGGREGATION OF SILICATE SOLUTIONS

MOLAR CONCENTRATION	RATE	pH	METHOD	REFERENCE
0.1	Maximum	7.2	Trimethylsilylation	259
0.02	Slow	2.5	Molybdic Acid	260
APPROX 5	Maximum	7.5	Gel Time	255
APPROX 5	Minimum	1.8	Gel Time	255
0.02-0.01	Fast	7-8	Coagulation	267
0.02-0.01	Slow	2-3	Coagulation	267
0.07	Maximum	7.6	Light Scattering	271
APPROX 0.1	Maximum	8.0	Light Scattering	272
0.3	Maximum	5.1-5.9	Gel Time	273
0.25	Maximum	7.0-7.7	Gel Time	274
0.08-1.7	Maximum	8.6	Light Scattering	275
0.1	Minimum	1.8	Freezing Point	276
1.0	Minimum	1.7	Freezing Point Titration	264

(C) Condensation of silanol groups to form siloxane bonds. This model has been widely used and of the three models enables the most plausible explanation of the observed aggregation rate/pH behaviour. The exact nature of the condensing species are not known, the following have been suggested:

(1) $(HO)_3\ SiO^-$ / $Si(OH)_4$ [275]

(2) $(HO)_3\ SiO^-$ / $Si_2O_3(OH)_3^-$ [266]

(3) $(HO)_3\ Si\text{-}O\text{-}Si(OH)_2\text{-}O\text{-}Si(OH)_3$ / $(OH)_3\ Si\text{-}O\text{-}Si(OH)_2\text{-}O\text{-}Si(OH)_3$ [282]

(4) The condensation mechanism involves a temporary increase of co-ordination number of silicon of from 4 to 6[244] viz:

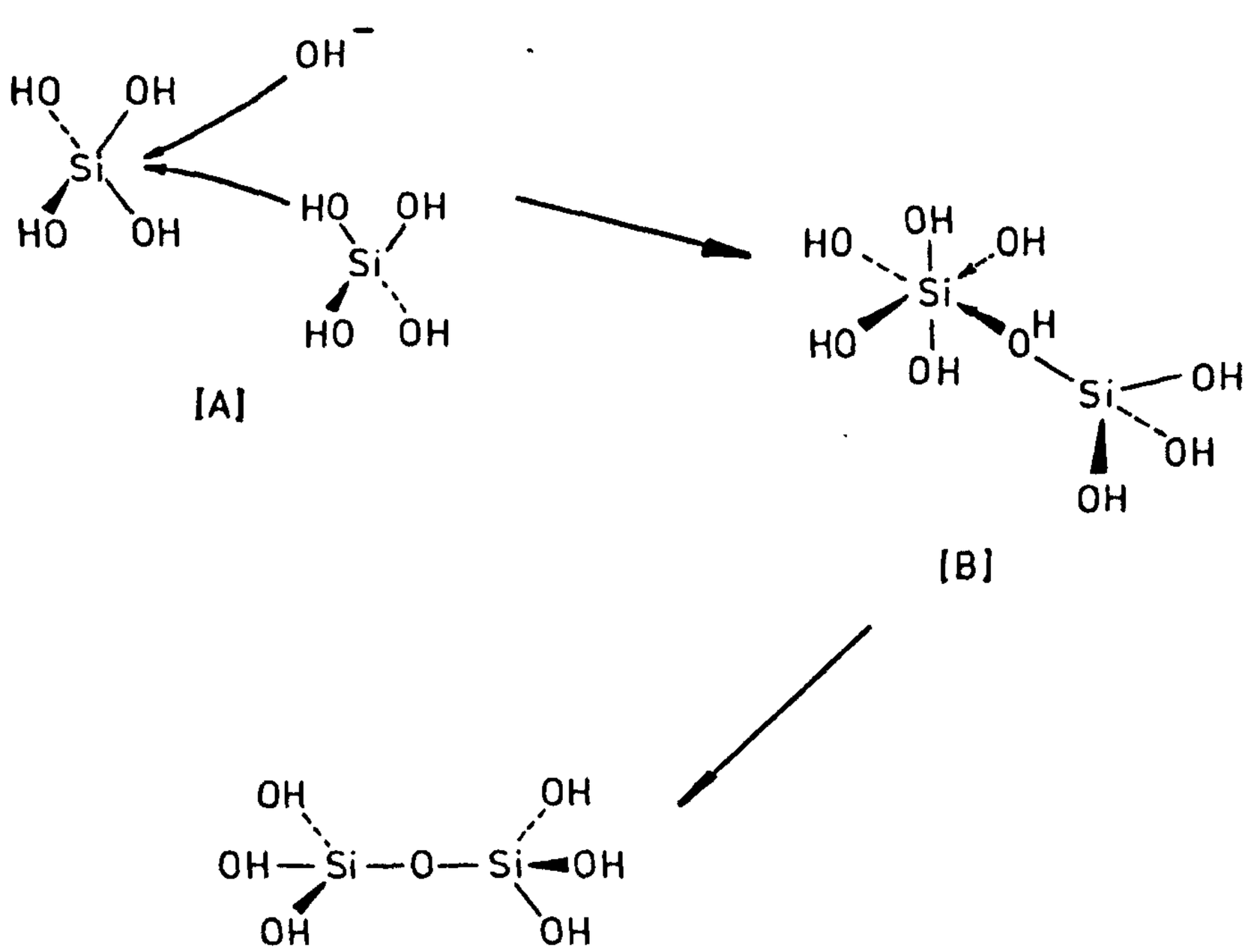

The monomer/monomer pair (1) is in agreement with a maximum rate of

aggregation around pH 7, as this is the region of pH in which both $(HO)_3SiO^-$ and $Si(OH)_4$ co-exist in significant amounts. In support of mechanism (4) Iler[60] claims that the decreasing rate above pH 7 is consistent with the catalytic effect of hydroxyl ions being offset by the repulsion of charged species $(HO)_3SiO^-$.

As well as controlling the rate of aggregation, the pH determines the structure of the resulting polymer. At low pH, the initial condensation reactions have been shown, using techniques such as ultracentrifugation, n.m.r. and light scattering, to be bimolecular and bifunctional[273,281-282]. This would appear to rule out mechanism (4) at low pH. The polymers formed initially are open branched/linear polymers with relatively little cross linking[60,282] and have been represented as follows

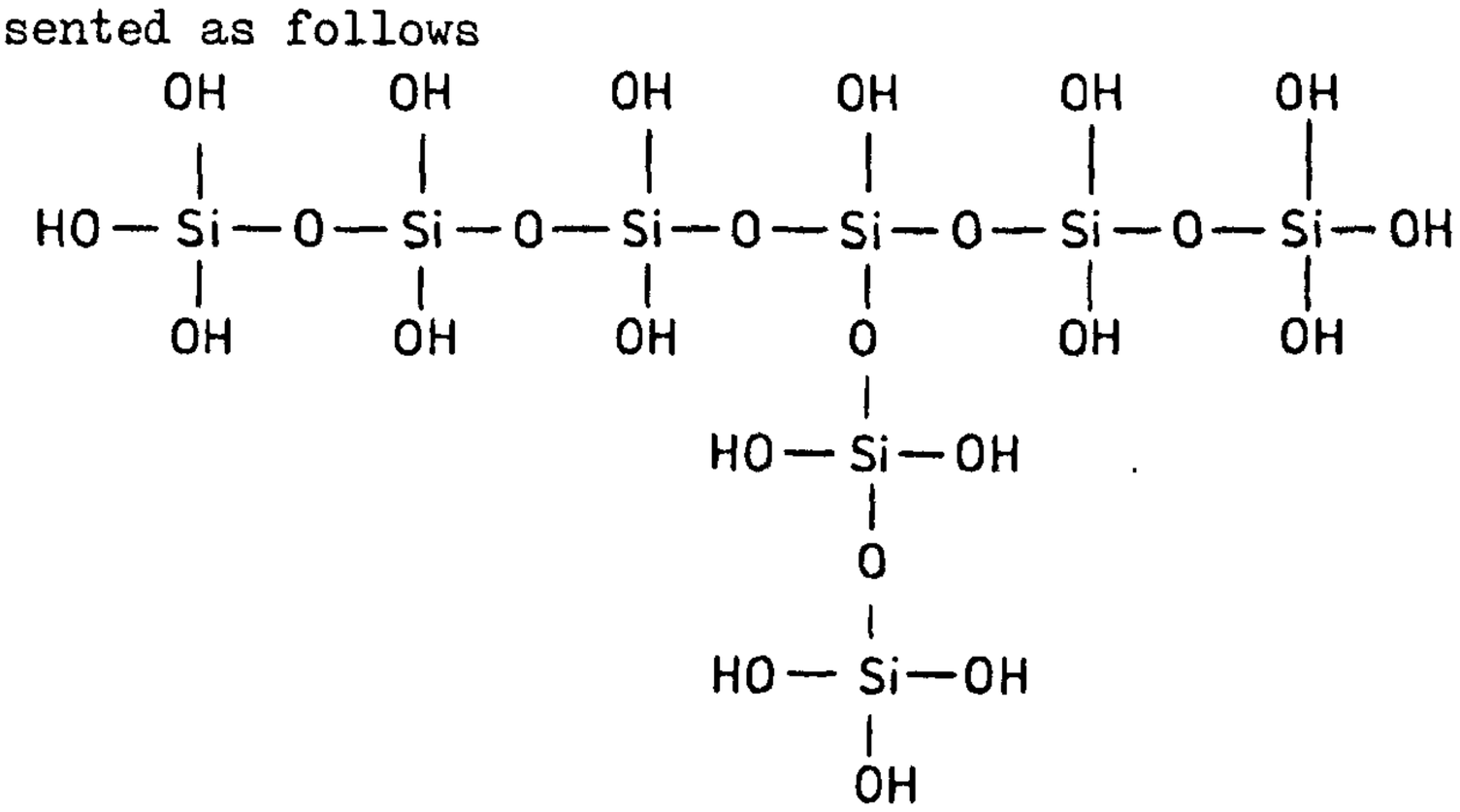

There is however some evidence that this picture is oversimplified in that the "building units" are not monomeric but low molecular weight cyclic acids[283]. In acid solution the open polymers can continue to grow, and as they are not charged may aggregate to form an open three dimensional gel network; as is evidenced by a functionality for the condensation reaction of greater than two[282].

In alkaline solution the hydroxyl ion catalyzes the rearrangement of small polymer units leading to internal condensation and crosslinking to give particles of which the interior consists essentially of silicon and oxygen atoms. The particle charge occurring in alkaline solution opposes the aggregation that occurred in acid solution. The colloidal particle formed represents the maximum dehydration attainable, in that silanol groups occur only around the outside of the particle. The particle has been depicted by Iler[60] as:

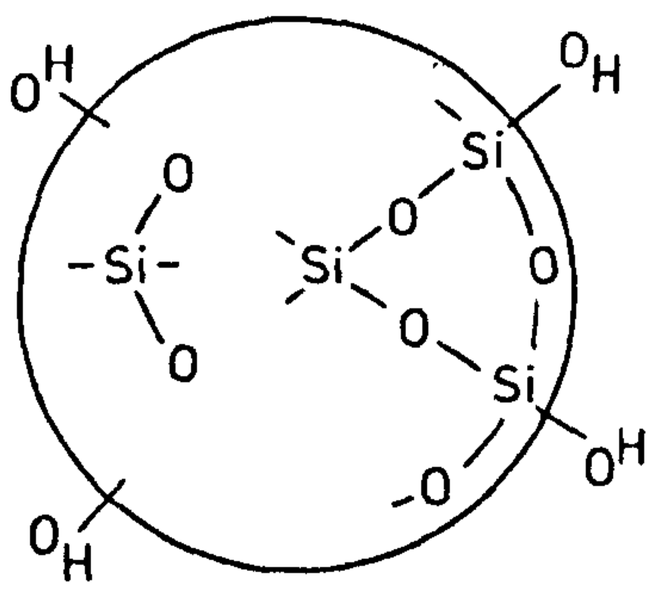

The overall polymerization behaviour as a function of solution pH is given in Figure 2-10. Apart from emphasizing the two types of polymerization product, it can be seen from Figure 2-10 that colloidal particles can be grown to different sizes in alkaline solution and then aggregated to form three dimensional gel networks by lowering the solution pH.

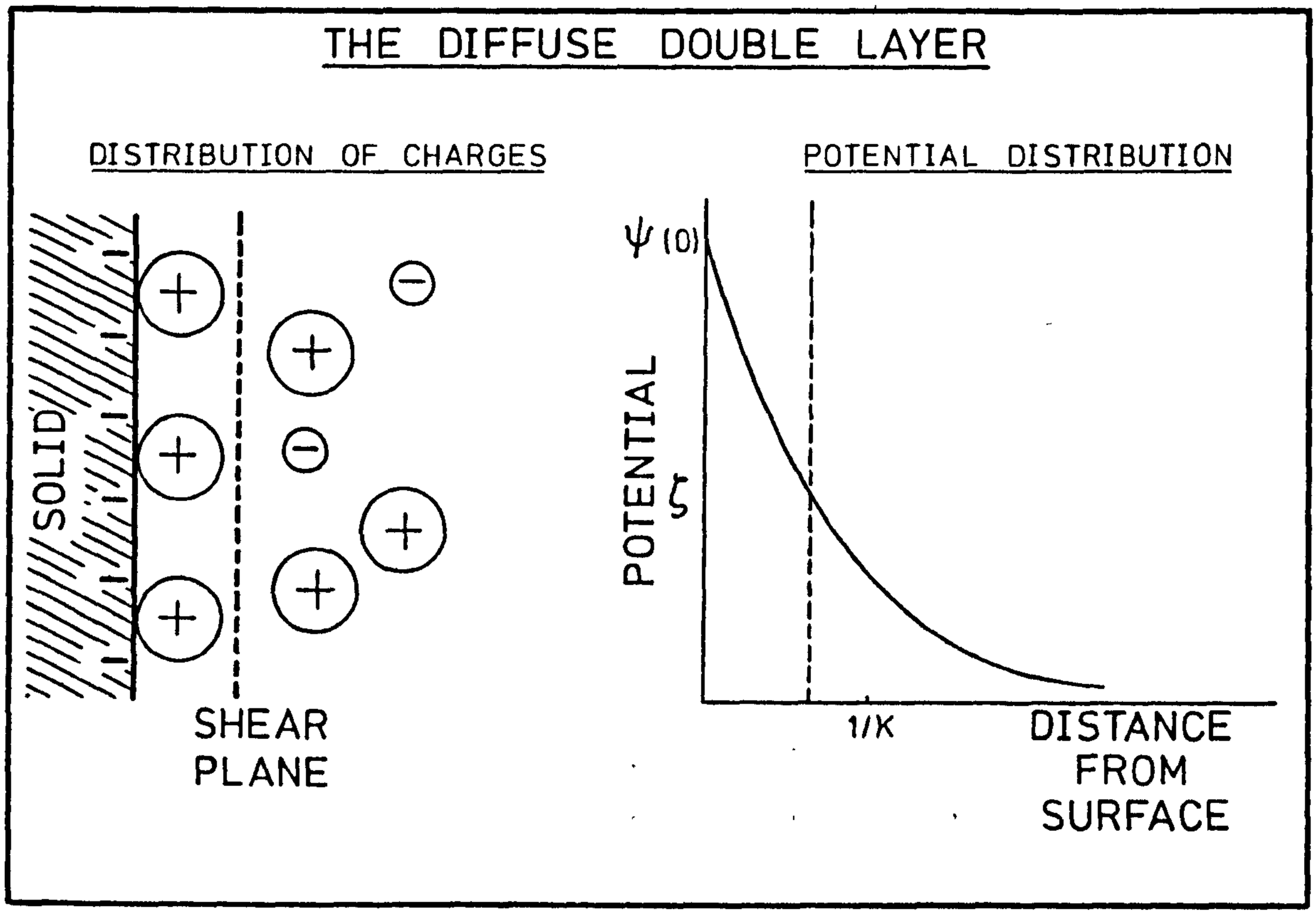

FIGURE 2-1

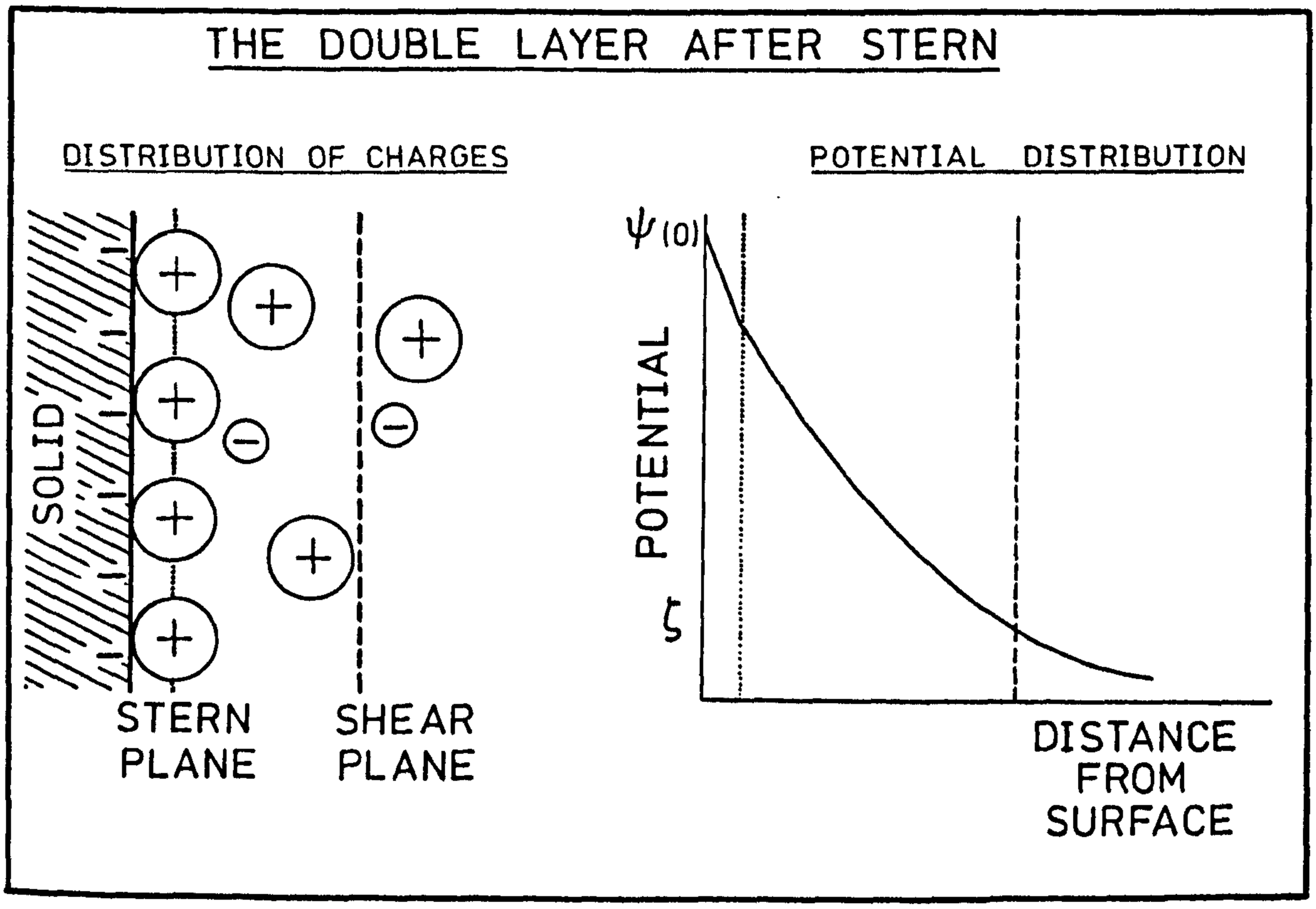

FIGURE 2-2

THE STERN MODEL FOR VARYING SPECIFIC ADSORPTION ENERGIES

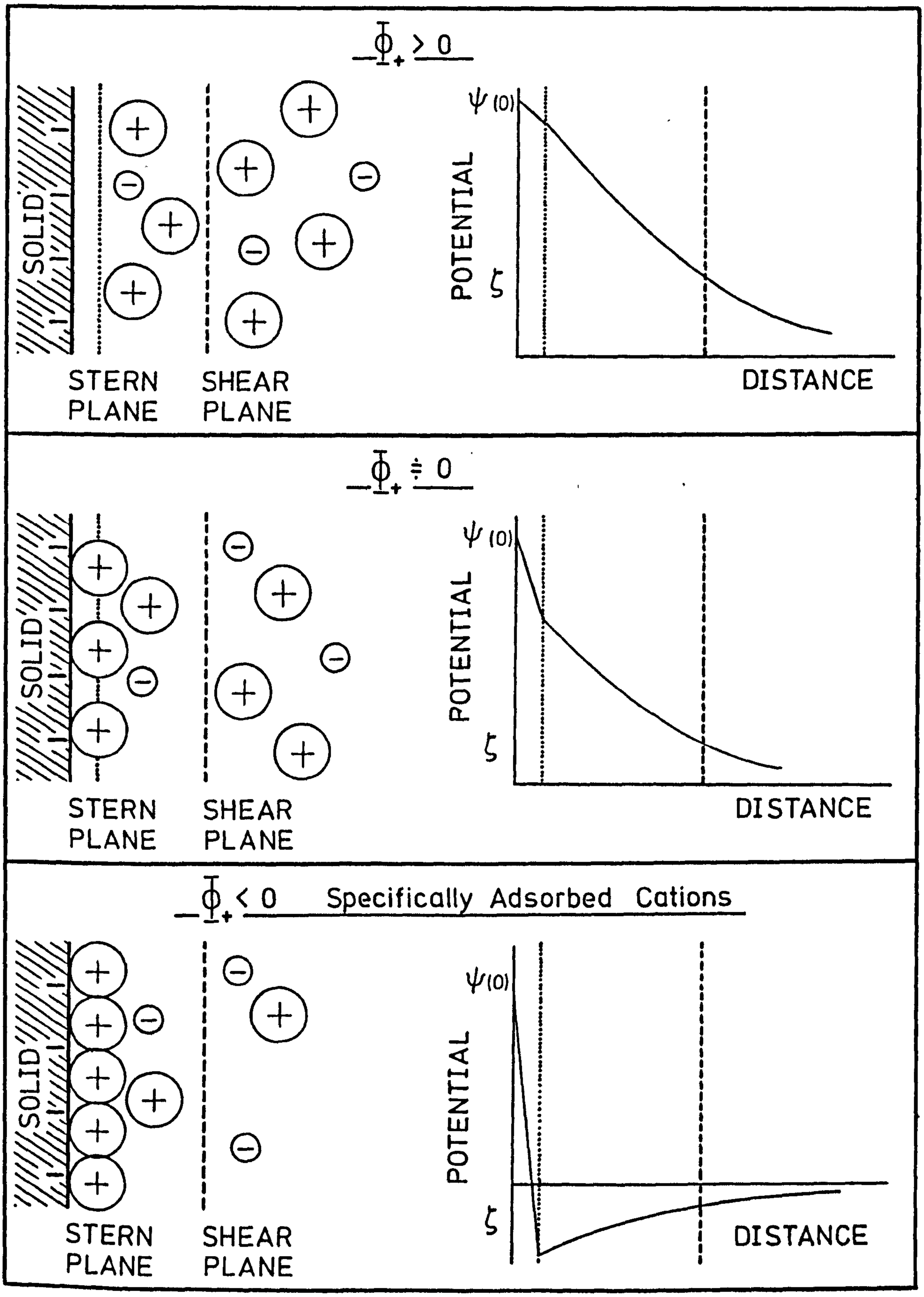

FIGURE 2-3

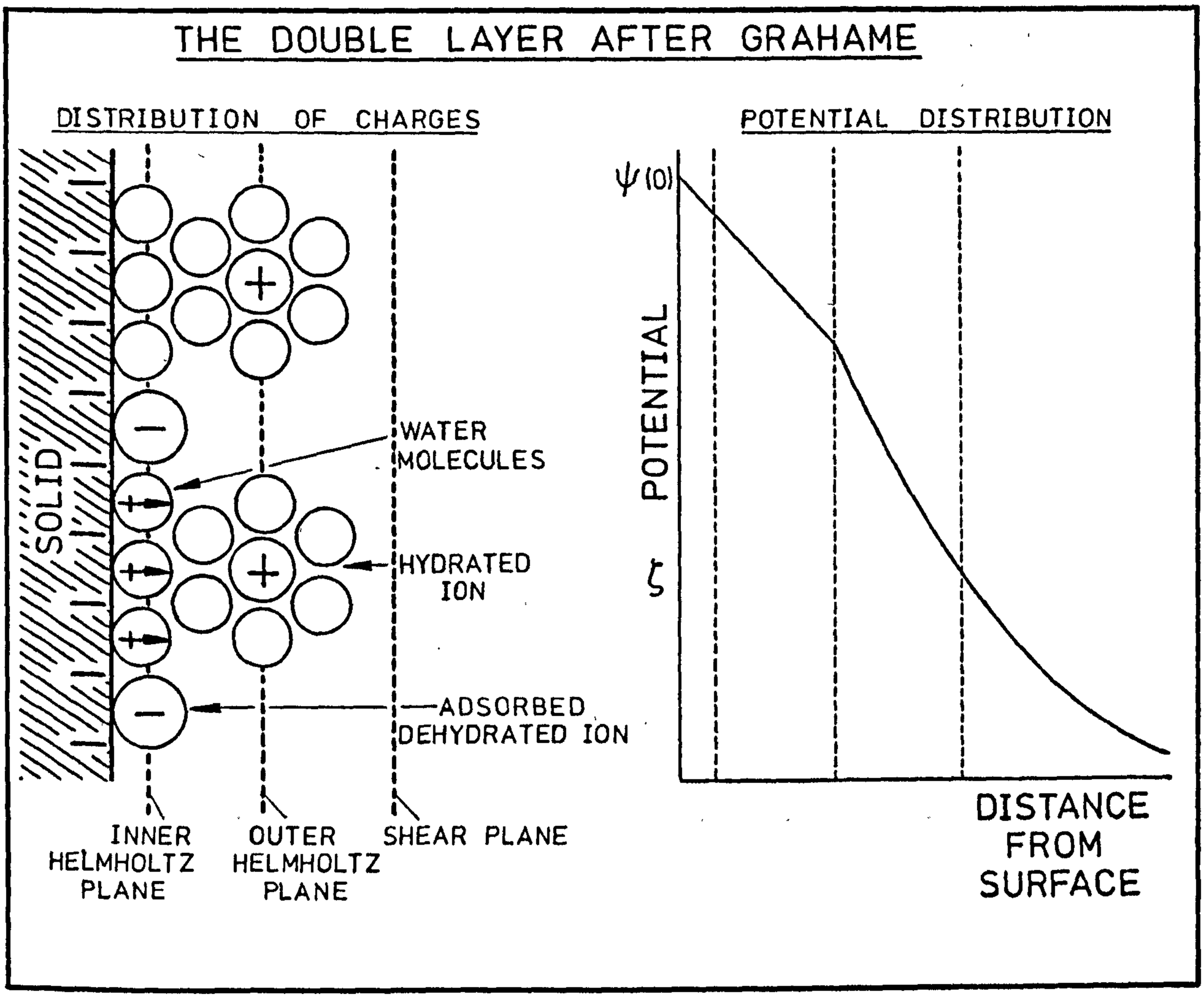
THE DOUBLE LAYER AFTER GRAHAME
DISTRIBUTION OF CHARGES
SOLID
WATER MOLECULES
HYDRATED ION
ADSORBED DEHYDRATED ION
INNER HELMHOLTZ PLANE
OUTER HELMHOLTZ PLANE
SHEAR PLANE
POTENTIAL DISTRIBUTION
ψ(0)
ζ POTENTIAL
DISTANCE FROM SURFACE

FIGURE 2-4

AQUEOUS Ti(IV) SPECIES IN EQUILIBRIUM
WITH RUTILE AT 25°C

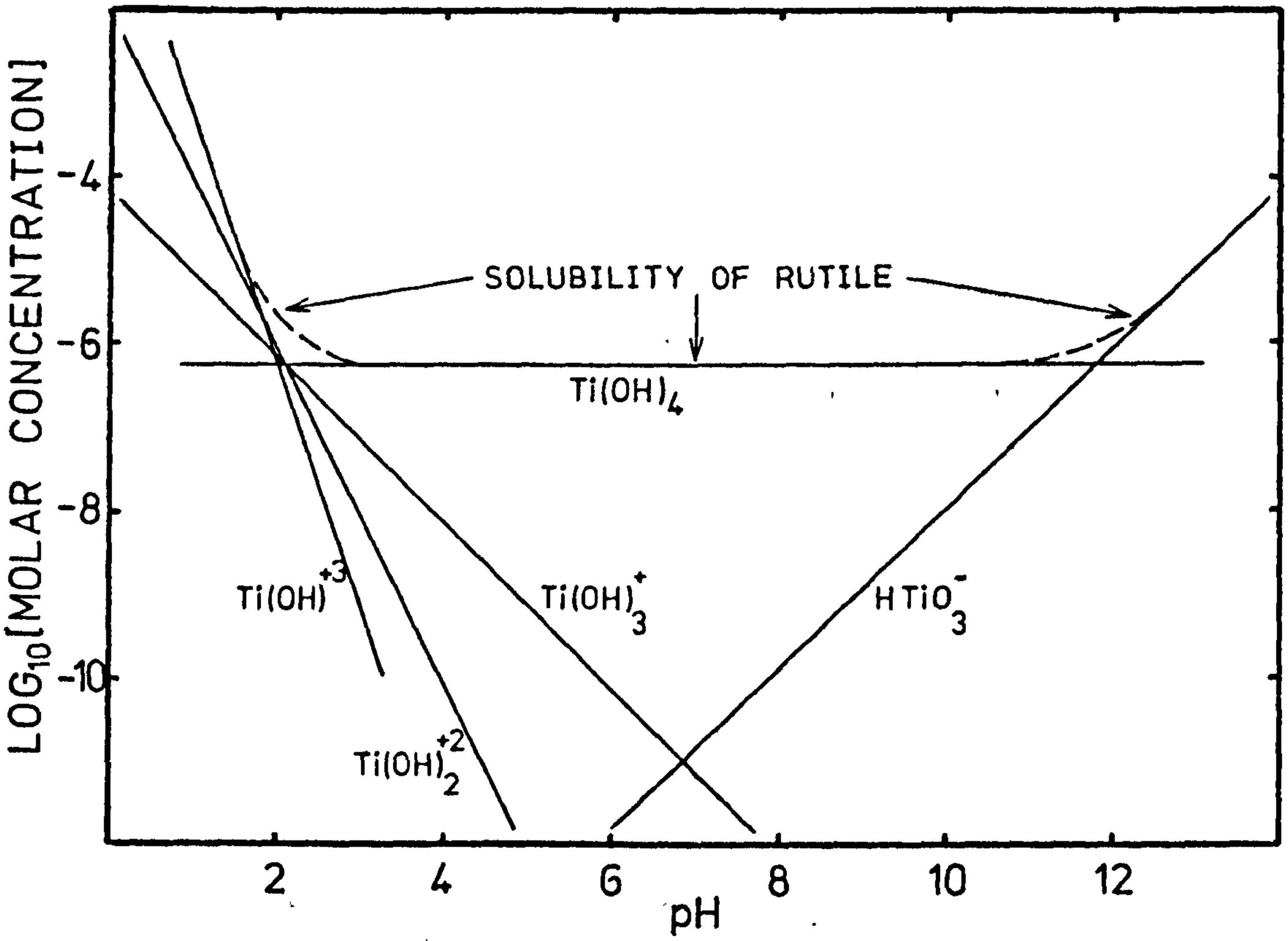

FIGURE 2-5

ISOTHERMS OF THE B.D.D.T. CLASSIFICATION

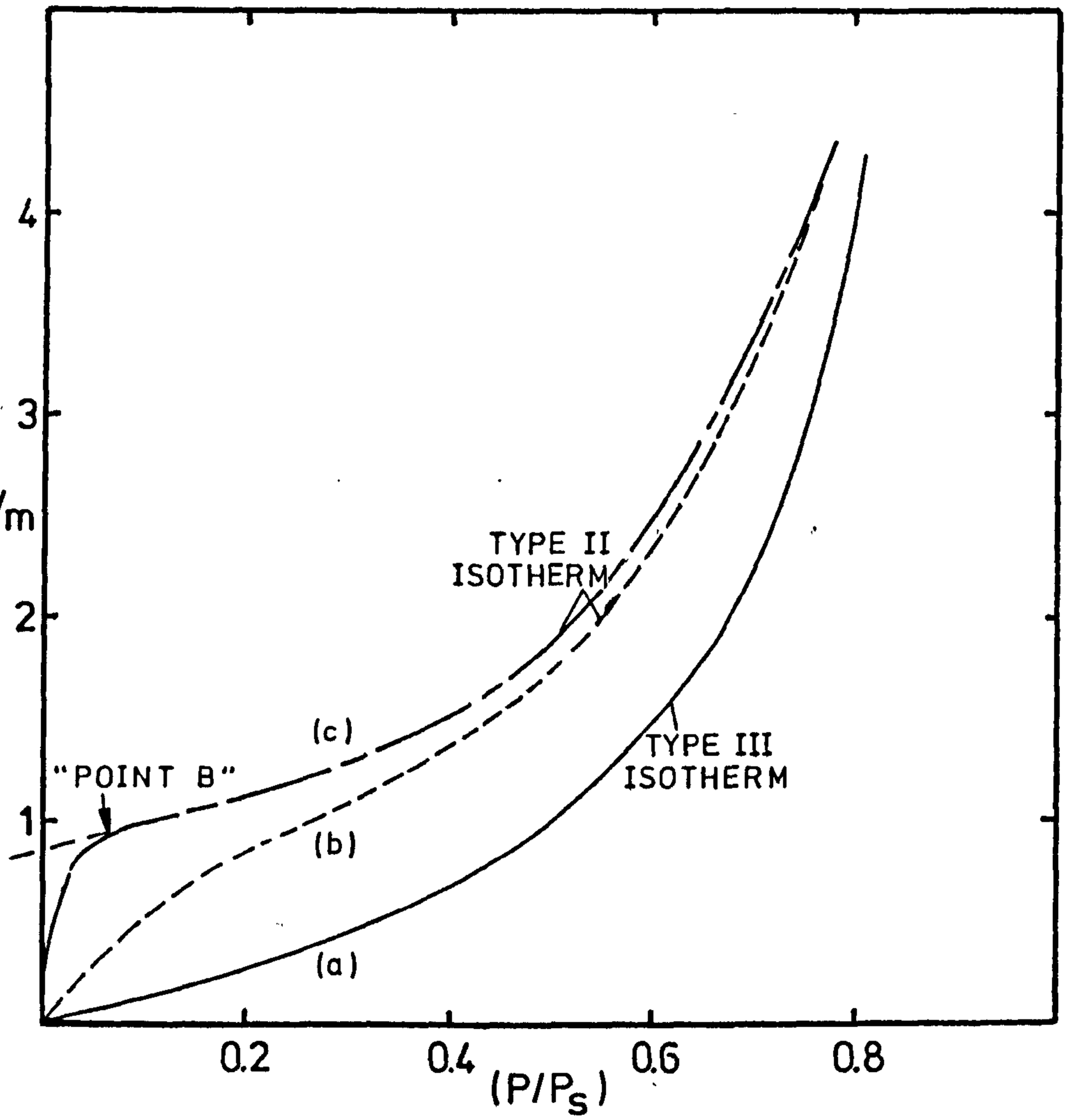

BET ADSORPTION ISOTHERMS

CURVE (a) BET C CONSTANT ≒ 1

" (b) " " ≒ 11

" (c) " " = >100

FIGURE 2-6

SOLUBILITY OF AMORPHOUS SILICA
IN WATER

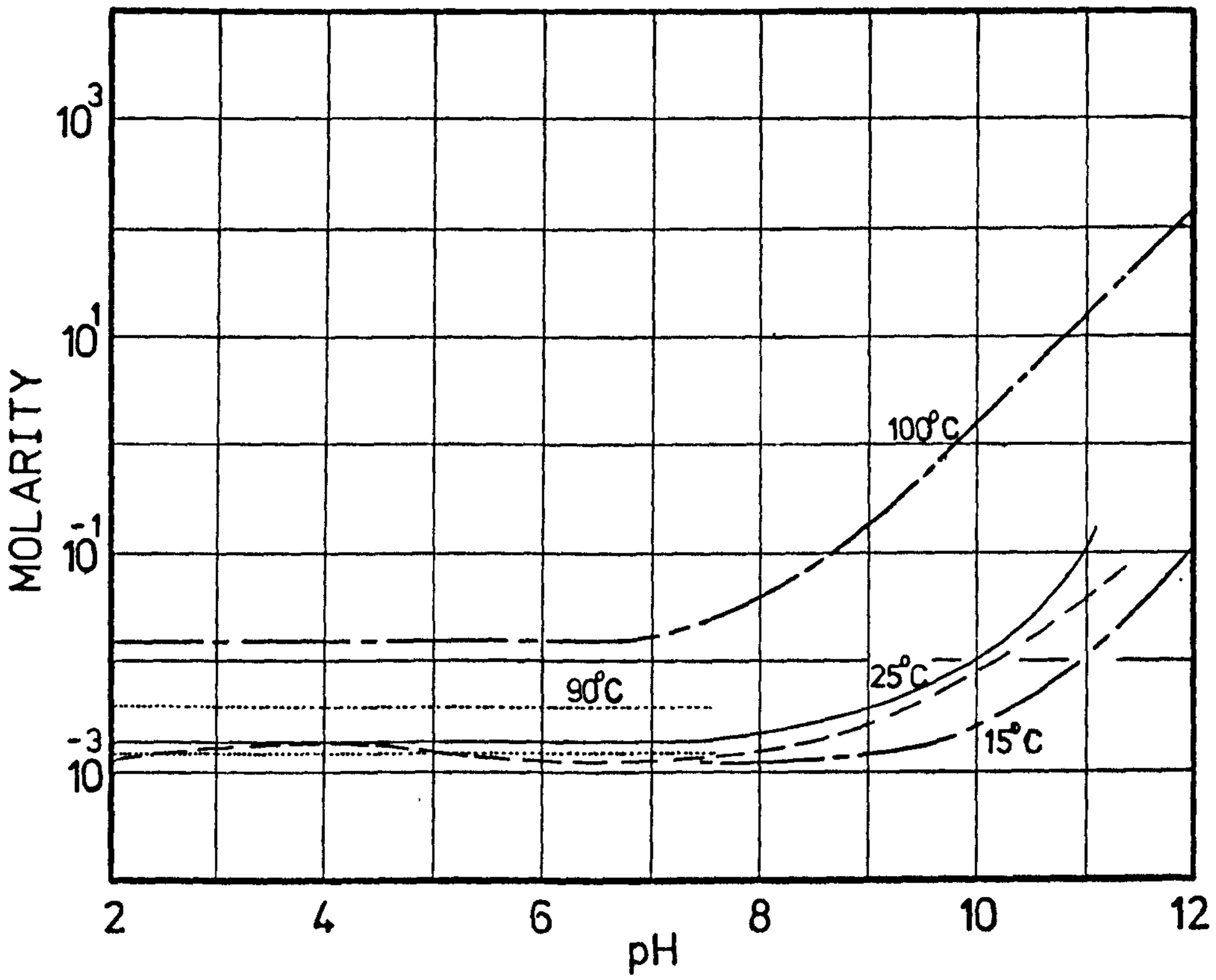

——— DATA OF SMITH [249]
..... " " KRAUSKOPF [238]
——— " " GREENBERG and PRICE [242]
— — — " " ALEXANDER, HESTON and ILER [243]

FIGURE 2-7

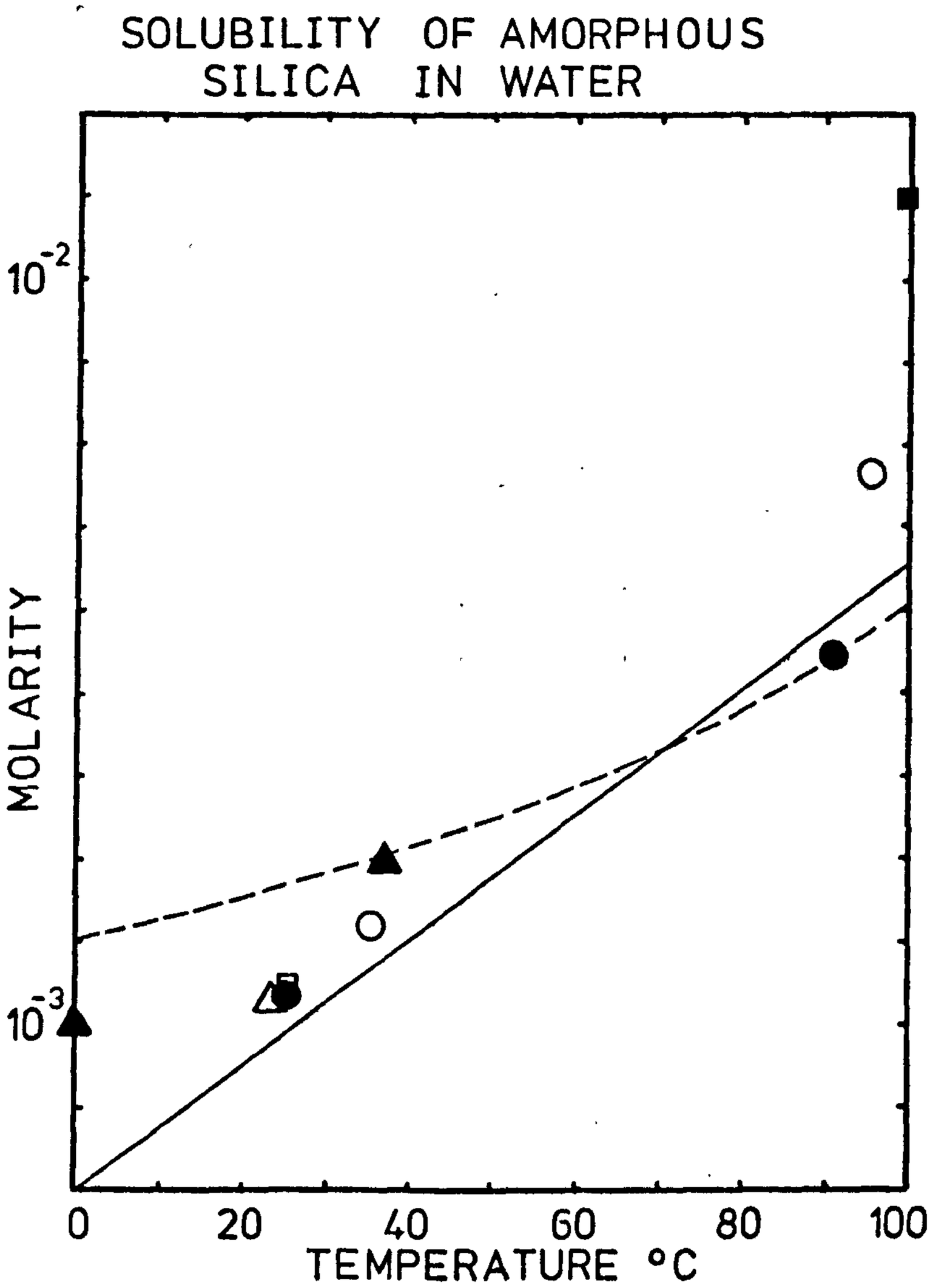
SOLUBILITY OF AMORPHOUS SILICA IN WATER
MOLARITY
10^{-2}
10^{-3}
0
20
40
60
80
100
TEMPERATURE °C
—DATA OF ALEXANDER, HESTON, ILER [243]
– – – – WITTMAN [400]
O ELMER and NORDBERG [253]
● KRAUSKOPF [238]
△ GREENBERG and PRICE [242]
▲ JOHNSTON [247]
□ ILER [244]
■ SMITH [249]

FIGURE 2-8

AQUEOUS SILICA SPECIES IN EQUILIBRIUM WITH AMORPHOUS SILICA AT 25°C [267]

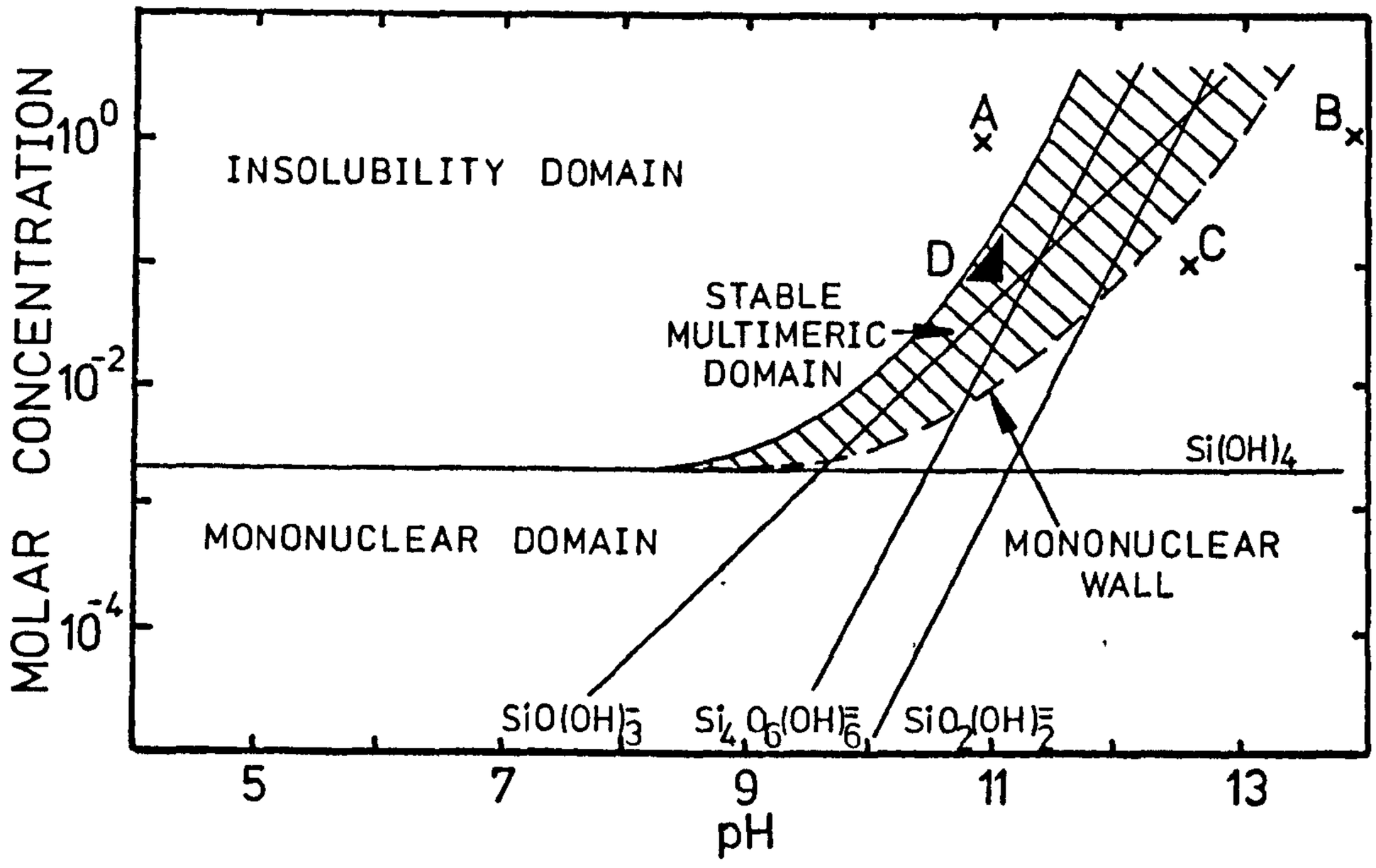

FIGURE 2-9

MONONUCLEAR WALL REPRESENTS THE LOWER CONCENTRATION LIMIT FOR THE STABILITY OF MULTINUCLEAR SILICA SPECIES

A,B DATA OF ILER [244]

C,D DATA OF DEBYE and NAUMAN [268]

FIGURE 2-10

POLYMERIZATION BEHAVIOUR OF AQUEOUS SILICA

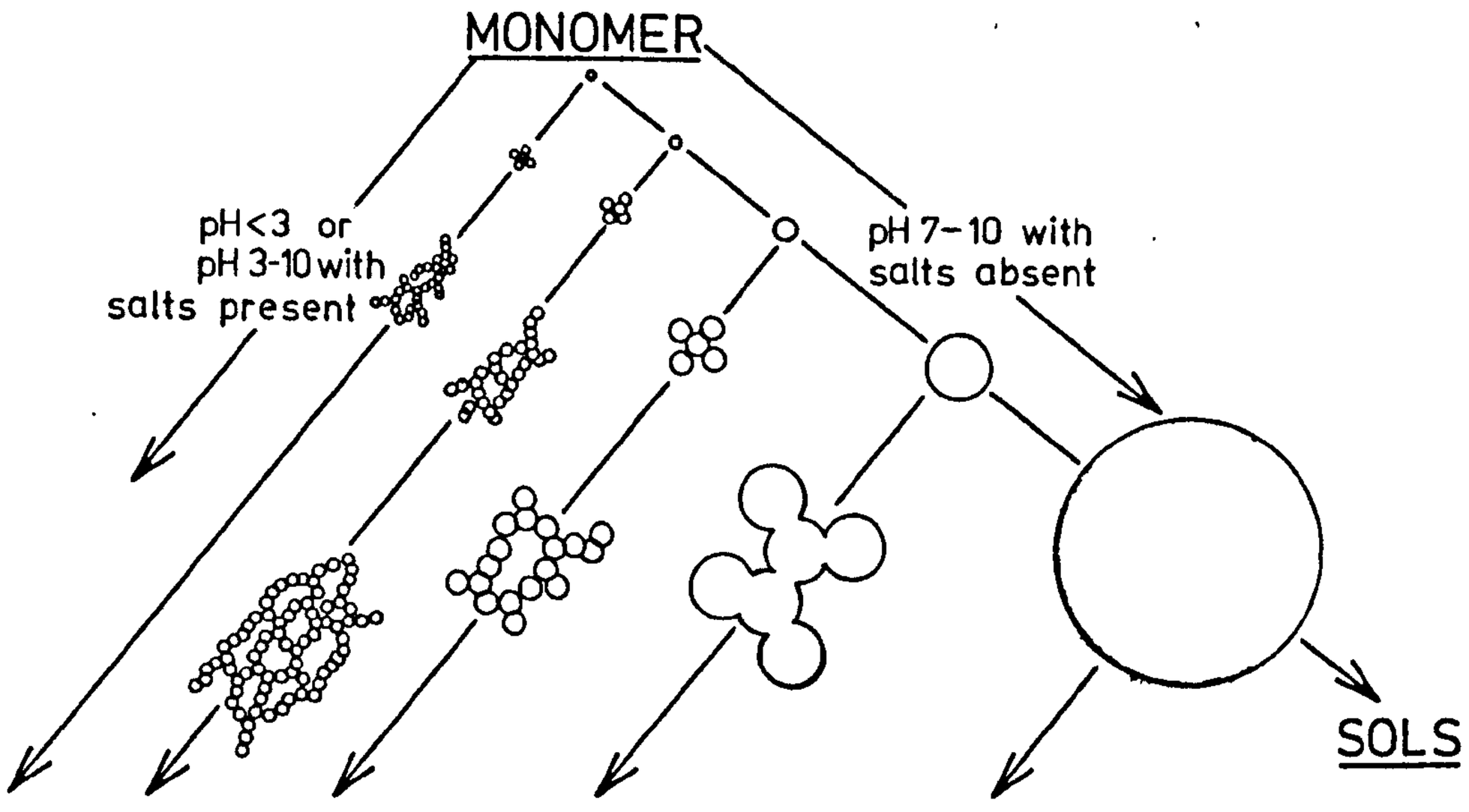

IN ACID SOLUTION OR IN PRESENCE OF FLOCCULATING SALTS, PARTICLES AGGREGATE INTO THREE DIMENSIONAL NETWORKS AND FORM GELS

IN BASIC SOLUTION PARTICLES IN SOL GROW IN SIZE WITH DECREASE IN NUMBERS

CHAPTER 3: EXPERIMENTAL MATERIALS

3 - 1 Titanium Dioxide

Three samples of titanium dioxide were used. A sample of anatase (CL/D 731) was used only in the preliminary study of the i.e.p. of titanium dioxide (Chapter 6-1) and the relevent details of its preparation and properties are given during the discussion of that study. The methods of preparation and chemical characteristics of the other two samples used, rutile CL/D 702 and commercial Rutile C are given in Table 3-1. The chemical analyses of these samples (and of the coated samples in Table 5-1) were obtained using a Phillips PW 1270 Simultaneous X-ray Fluorescence Spectrophotometer. Anatase/Rutile contents were obtained by X-ray diffraction as described elsewhere[288]. The surface areas given in Table 3-1 were determined with a Strölhein Area Meter using a single point nitrogen adsorption method (area/N_2 molecule 0.162nm^2).

The electron micrographs of the two rutiles, CL/D 702 and commercial C are given in Figures 3-1 and 3-2. All transmission electron micrographs presented in this thesis were obtained using a J.E.L. 7A electron microscope. Specimens were prepared by sprinkling the dry powder onto the microscope grid.

3 - 2 Sodium Silicate Solutions

For all the microelectrophoresis experiments and many of the "coating" experiments sodium silicate solutions were freshly prepared using a pure amorphous silica - Degussa TK800[58]. The preparation involved

TABLE 3 - 1

PHYSICAL AND CHEMICAL CHARACTERISTICS OF TITANIUM DIOXIDE SAMPLES.

RUTILE CL/D 702	
Preparation:	Hydrolysis of Liquid $TiCl_4$
	Heated in air at 450°C.
X.R.F. Analysis:	Al_2O_3 - < 0.01 wt. %
	SiO_2 - < 0.01 "
	Chloride - < 0.08 "
	Tin - < 0.002 "
	Iron - < 3 ppm.
X-ray Diffraction:	99.8% rutile
Specific Surface Area:	20 m^2/gm.
COMMERCIAL RUTILE C	
Preparation:	Hydrolysis of liquid $Ti(SO_4)_2$
	Heated in air at 800-900°C
X.R.F. Analysis:	Al_2O_3 - 0.28 wt. %
	SiO_2 - < 0.01 wt. %
	ZnO - 0.95 " "
	P_2O_5 - 0.22 " "
	Calcium - 200 ppm
	Chloride - none detected
"Total Soluble Salts"	- 0.5 wt. %
X-ray Diffraction:	99.4 % rutile
Specific Surface Area:	7 m^2/gm

fusion of the silica with A.R. sodium hydroxide and has been described elsewhere[285]. All solutions were prepared to contain 6.0g/litre of dissolved silica and to have a final pH of approximately 13. Although the above method of preparation is quantitative, the concentration of "silica" was determined independently using the molybdic acid method described by Bennett[287].

In some coating experiments "Pyramid Brand Sodium Silicate Solution, No. 1" (Crosfield Chemicals, U.K.) was used. This is a technical grade product containing 29.3 wt.% Silica (8.9 wt.% Na_2O) and a relatively high, although undisclosed, level of impurities.

3 - 3 Colloidal Dispersions

Colloidal dispersions for electrokinetic measurements were prepared by adding the finely ground powder to triply distilled water (to the required solids content) at pH approximately 8. The dispersion was agitated by magnetic stirrer for 24 hours before use in microelectrophoresis measurements.

3 - 4 Reagents

All electrolyte solutions were prepared from Analytical Reagent (A.R.) grade chemicals.

Dilute solutions of A.R. nitric acid and A.R. sodium hydroxide were used for pH control in microelectrophoresis experiments.

High purity gases were used throughout the work. Research grade (99.999%) nitrogen and argon were used for all the low temperature adsorption experiments. In all other applications "white spot" oxygen free nitrogen (99.9%) was used .

3 - 5 Water

Triply distilled water with a maximum conductivity of 0.8×10^{-6} ohm^{-1} cm^{-1} (when equilibrated with air) was used throughout the work.

The first stage distillation, to remove most of the inorganic colloidal matter from mains water, was from an all metal still. This was followed by distillation from alkaline permanganate (Pyrex still) to remove any remaining organic or oxidisable impurities, with a final third stage distillation from a Pyrex glass still. The water was stored in a Pyrex glass vessel. Polythene containers were not used as they have been shown to require conditioning before water stored in them can be used to produce reproducible electrokinetic data[286].

Ion exchange resins were not used due to the possibility of contamination by organic materials.

It is claimed that the presence of atmospheric carbon dioxide will give rise to a conductivity of 0.8×10^{-6} ohm^{-1} cm^{-1} [284]. Hence the water used is assumed to contain very little ionic impurity other than carbon dioxide.

FIGURE 3-1

Transmission Electron Micrograph
(magnification 200,000)
BASE RUTILE [CL/D702]

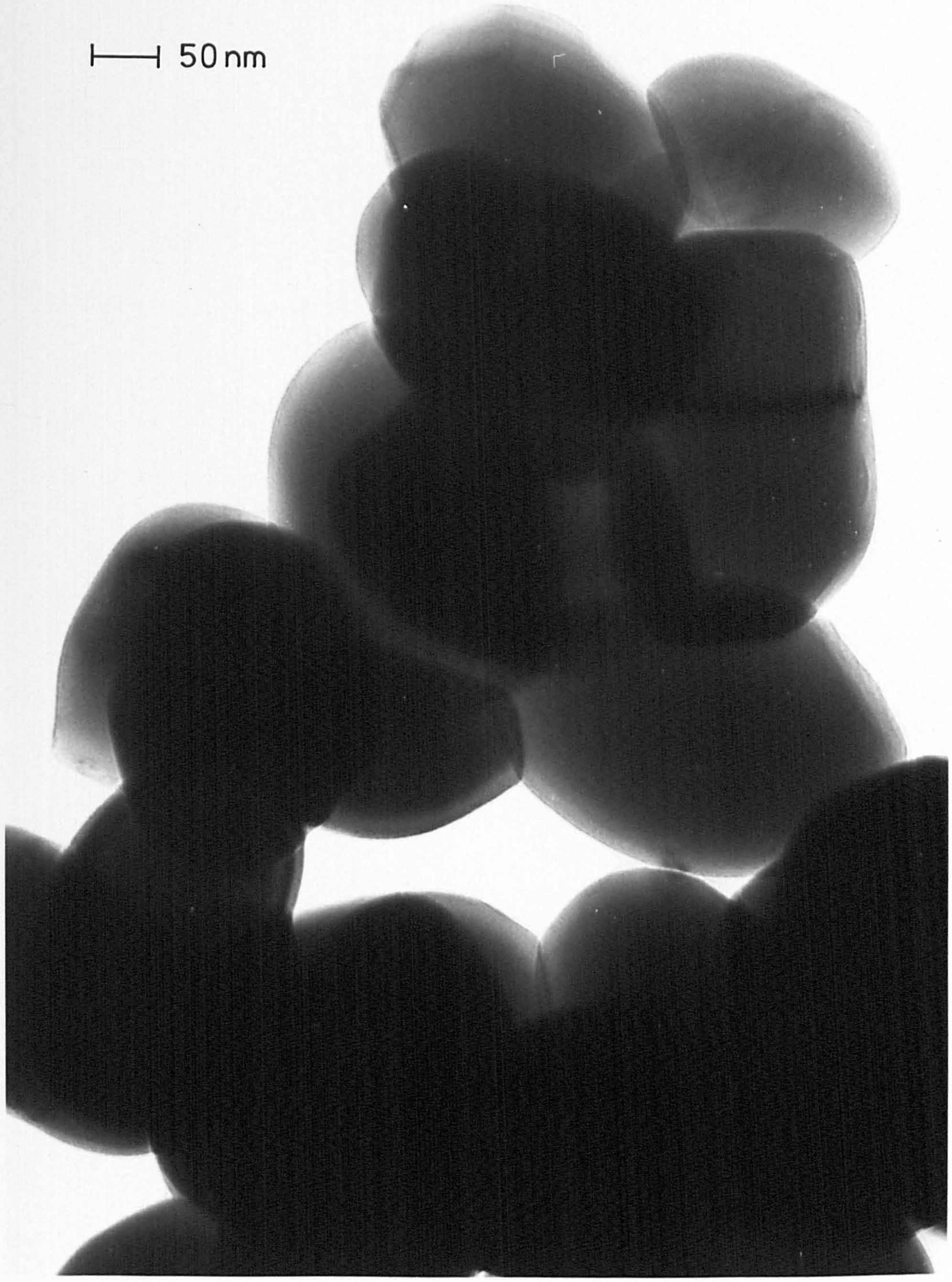

FIGURE 3-2

Transmission Electron Micrograph
(magnification 200,000)
COMMERCIAL RUTILE C

CHAPTER 4: EXPERIMENTAL METHODS

4 - 1 MICROELECTROPHORESIS

4-1-1 General Comments

Many experimental techniques can be used to investigate changes in the electrical double layer characteristics of the oxide/aqueous electrolyte interface[85,296]. In the present study the variation of electrophoretic mobility with solution pH was used to compare the electrical double layer characteristics of titanium dioxide under varying pretreatment and aqueous solution conditions. It was felt that even though attempts have been made to quantify such effects as relaxation, electrophoretic retardation, and position of shear plane[81,118,294-295], the calculation of zeta potentials contained too many uncertainties to be valuable. Hence, as it was not relevant to the present purpose, no attempt was made to calculate zeta potentials from electrophoretic mobilities.

4-1-2 Measurements of Electrophoretic Mobility

Mobilities were determined using a commercial microelectrophoresis apparatus supplied by Rank Bros. (Cambridge, U.K.). The general features of this apparatus are given by Smith[69], as is a review of the experimental and theoretical considerations required if mobility data are to be precise and accurate.

A van Gils[289] type of thin walled cylindrical glass cell was fitted with side arms to allow the dispersion under investigation to be continuously circulated through the cell via a thermostatted

equilibration vessel (25.0 ± 0.2°C). pH measurement and adjustment were made to the dispersion in this equilibration vessel (300 cm^3). To ensure that no nett transport of liquid occurred within the cell during mobility measurement the dispersion in the cell was isolated by closing a teflon tap in the circulation system. Adsorption of colloidal particles onto the cell wall will occur because of electrostatic attractions and sedimentation. Whilst both types of adsorption lead to changes in the electro-osmotic flow within the cell it is sedimentation which leads to the disruption of cell symmetry[290]. The circulation procedure served to minimize sedimentation and errors due to asymmetry in electro-osmotic flow were small.

At least 10 particles were observed at each stationary level in the cell to produce a single average mobility value. The polarity of the Pt. black electrodes was reversed between each successive observation to minimize polarization effects. The cell was immersed in a thermostat bath (25.0 ± 0.2°C) and at no time was any illumination heating of the dispersion sufficient to cause "thermal overturn"[293]. In most cases a difference of less than 10% was observed between mobilities at the upper and lower stationary levels. The velocity profile in each cell was checked periodically to ensure that laminar flow had not been disturbed by cell wall contamination. The effect described by Fukuda[144], in which the degree of velocity asymmetry is related to the p.z.c. of the glass capillary, has not been observed in this work.

Many of the sources of error in microelectrophoresis measurements have been assessed by Smith[69]. The average deviation observed in mobility measurements in the present study varied from 0.05 to 0.1 μ/sec per volt/cm.

The larger deviations occurred when mobilities were small ($< 1\ \mu$/sec per volt/cm). In some cases the deviations in small mobilities were reduced using the procedure described by Jackson and Parfitt[291].

4 - 2 WATER VAPOUR ADSORPTION

Many experimental techniques have been established for the study of water vapour adsorption on oxide surfaces. These range from use of the less precise "humidity control"[308,311-312] through mechanical balance[307,310] to the high precision volumetric[163,212,304] and electrobalance[297-298,306] techniques. New experimental techniques are constantly being developed and the recent work of Chenion and Lang[309] using radioactive tracers indicates the diversity of approach.

A gravimetric approach was used in the present work. Initially work was performed using a quartz spring balance of the McBain and Bakr type[313]. However the working sensitivity of this balance ($10\mu g$) was found to be too high and an electrobalance was used to determine all the data presented. A schematic representation of the complete water vapour adsorption apparatus is given in Figure 4-1.

4-2-1 Cahn Microbalance

Changes in sample mass were measured using a Cahn RG Electrobalance[300]. The sample and counterweights were contained in platinum buckets and suspended from the balance arms by nichrome wires. The balance was recalibrated periodically against standard analytical weights. Mass changes were registered directly onto a chart recorder

with a sensitivity of $\pm 1\mu g$.

The general theory and application of microbalances to adsorption measurements have been reviewed by Thomas[301], and the two major causes of spurious weight changes are "buoyancy" and "thermal transpiration".

(A) Buoyancy: This effect, due to different upthrusts on the two sides of the balance arm, can be calculated[160] if the temperature and volume of both sample and counterweights are known. Both hangdown tubes of the balance used were immersed (30cm) in the same thermostat bath ($25.0 \pm 0.1^{\circ}C$) and sample and counterweights were adjusted to be as close as possible to the same volume. The maximum mass change in this work caused by buoyancy effects was calculated to be $1\mu g$.

(B) Thermal Transpiration: Attempts have been made to quantify this effect[302] but precise calculation is not possible. Temperature gradients across the sample have been minimised by efficient thermostatting. Spurious weight changes of the order of $1\mu g$ may however exist at very low pressures [$(P/Ps)_{H_2O} < 0.05$]

4-2-2 Pressure Sensitive Transducer

Water vapour pressures were measured using a BELL and HOWELL pressure sensitive transducer (type 4-326). The use of pressure transducers in gas-solid adsorption work, although only recently developed, is now an established technique[297-298]. The operating principles, auxilliary apparatus and method of calibration for the transducer used in this work are as described by Baker[299]. The transducer was recalibrated periodically against a mercury manometer using water vapour and exhibited excellent linearity and no hysteresis over the

$(P/Ps)_{H_2O}$ range 0 to 1. The calibration factor of 0.561 mV/cm Hg remained constant throughout the work.

The sensitivity of pressure measurement was about ± 0.1 torr ($13 N/m^2$), that is an order of magnitude greater than manometer measurements. However, as pressure measurement was only used to calculate relative equilibrium pressure (P/Ps) (and not in Boyle's law calculations) the sensitivity of the transducer was considered adequate.

4-2-3 Sample Outgassing Procedure

Samples were outgassed in situ using a mercury diffusion pump backed by a rotary pump. If samples were to be outgassed at elevated temperatures they were prepumped at room temperature to less than 10^{-2} torr ($1 Nm^{-2}$) before a furnace was placed around the sample hangdown tube. Outgassing temperatures were controlled $\pm 2^{o}C$.

In order to obtain a pressure of less than 10^{-4} torr (10^{-2} Nm^{-2}) in the adsorption system which had been exposed to water vapour, it was necessary to outgas for periods of more than one week, such was the slow rate of desorption of water vapour from the electrobalance head. The criterion of efficient outgassing was therefore taken to be sample mass, which was recorded during outgassing. If the sample mass was constant to $\pm 4\mu g$ over a period of 4 hours the sample was considered properly outgassed. A mass change of $4\mu g$ represented approximately 0.1% of the smallest weight loss observed on outgassing. Outgassing times were normally from 16 to 20 hours and the final outgassing pressure normally less than 5×10^{-4} torr (0.07 Nm^{-2}).

4-2-4 Sample Gettering

During any sample outgassing the electrobalance "head" was always outgassed at room temperature. It was necessary therefore to prevent water desorbing from the balance onto a sample as the sample was cooled from an elevated outgassing temperature to 25°C for the adsorption isotherm measurements. The gettering procedure adopted was similar to that described by Day[218]. With the heating furnace still in position, dry nitrogen gas was added to give a pressure of 100 torr (130kN m^{-2}). The sample was then cooled to 25°C and equilibrated for 1 hour. The pressure was then reduced to 4 torr (0.5kN m^{-2}) and the mass reading of the balance taken to be the ZERO MASS READING for calculation of the adsorption isotherm. Water vapour was added to a pressure of 2 torr (0.25kN m^{-2}) and the system equilibrated a further hour. The total vapour pressure was observed to fall during this period as water vapour was adsorbed onto the balance head. The system was then pumped for 30 minutes to a residual pressure of approximately 0.1 torr (13 Nm^{-2}) and the isotherm determination continued.

4-2-5 Isotherm Determination

Addition of water vapour to the adsorption system was made via a greaseless stopcock (Springham and Co. Ltd.). The water reservoir was outgassed before each adsorption experiment. Because of the water vapour adsorption capacity of the balance head, slight adjustments of the diaphragm tap were required in order to maintain the water vapour pressure constant at any particular value. Hence the procedure adopted was to slowly admit water vapour to the required vapour pressure and then to maintain this pressure constant to less than ±0.1 torr (13Nm^{-2})

until the sample mass reading was constant to within ±2μg for a period of 30 minutes. Using this "equilibrium criterion", equilibrium times varied from approximately 30 minutes ($P/Ps_{H_2O} < 0.5$) to 1½ hours ($P/Ps_{H_2O} > 0.7$).

Because of the continual adjustment required to maintain a constant water vapour pressure, pressure measurement using a transducer connected to a digital volt meter was particularly helpful.

Desorption isotherms were recorded by slowly reducing the water vapour pressure via a diaphragm tap connecting the adsorption apparatus to the rotary vacuum pump. The same continual adjustment was required and equilibrium times were approximately the same as with adsorption isotherms.

4-2-6 Isotherm Reproducibility

The reproducibility of the water adsorption isotherms determined for oxides outgassed at elevated temperatures can be used to estimate the sum contributions of three effects:

(1) reproducibility of surface adsorption characteristics on outgassing

(2) efficiency of sample gettering

(3) reproducibility of measurement of adsorption isotherm parameters.

In as much as item (3) has been previously assessed (see sections 4-2-1 and 4-2-2) the isotherms given in Figures 4-2 and 4-3 enable some assessment of items (1) and (2).

The isotherms for a silica-coated rutile given in Figure 4-2 are typical of the reproducibility observed on most samples where adsorption

was repeated. Whilst variations in absolute adsorption capacity are small, in one case an isotherm was observed with a constant difference in adsorption capacity (approximately 0.15 mg/gm). This difference was equal to the difference in "weight loss on outgassing" for the two experiments. The parallel nature of the isotherms and the "outgassed weight" agreement suggest the following conclusions:

(A) The absolute water vapour adsorption capacity may vary due to small variations in the outgassed state of the surface. However in such cases the form of the isotherm remains unchanged.

(B) The gettering procedure has not contributed to any non-reproducibility in adsorption isotherms.

The data for pure rutile (Figure 4-3) confirm these conclusions. The differences are in good agreement with relative weight losses on outgassing. The isotherms are "parallel" and all show a "knee" at $(P/Ps)_{H_2O}$ 0.27. However, the differences in adsorption capacities are greater than those for the silica-coated rutile. This is consistent with the greater dependence of adsorption capacity on outgassing temperature for the rutile.

4 - 3 NITROGEN AND ARGON ADSORPTION CALORIMETRY

Nitrogen and argon adsorption isotherms, and the corresponding differential energies of adsorption, were determined using a volumetric adsorption apparatus in conjunction with a Tian-Calvet microcalorimeter. This adsorption system was designed and constructed at the "Centre de Recherches de Microcalorimétrie et de Thermochimie du CNRS", Marseille.

The technique involved the continuous addition of adsorptive to an outgassed sample. The recording of the equilibrium pressure in the system then enabled the adsorption isotherm to be calculated. The heat changes produced on adsorption were measured by incorporating the adsorption ampoule directly into the cell of the microcalorimeter. The general principles of the technique and its application have been briefly reported elsewhere[319-320]. However, as the technique represents a relatively new approach to the study of adsorption and adsorption thermodynamics, a detailed description of the procedure will be given in the following sections.

A schematic diagram of the adsorption apparatus is given in Figure 4-4. A description of the microcalorimeter will be given in section 4-3-1 and the remainder of the adsorption apparatus will be explained during the outline of the procedure followed in the adsorption studies (4-3-2 to 4-3-4).

4-3-1 The Microcalorimeter

A schematic representation of the microcalorimeter with an adsorption ampoule in position is shown in Figure 4-5. It can be noted that, as the entire microcalorimeter was immersed in the thermostat bath, the adsorption characteristics of the sample were unaffected by the microcalorimeter.

The microcalorimeter is termed "isothermal", after the conventions outlined by Rouquerol and Lafitte[327], in that the temperature difference between the adsorption cell and the thermostat was extremely small ($< 10^{-3}$K). Two thermopiles of the Tian-Calvet type, each containing

approximately 2000 chromel-alumel thermocouples, are mounted in the "differential arrangement"[315]. The details of construction of the thermopiles are given by Rouquerol[316]. These thermopiles provide the two basic functions of the microcalorimeter:

(i) excellent thermal contact between adsorption cell and thermostat, such that the microcalorimeter will operate under truly isothermal conditions. (In all the work reported the thermostat bath contained liquid N_2).

(ii) very sensitive measurement of the "heat flux" between adsorption cell and thermostat. The signal from the microcalorimeter in response to heat effects within the adsorption cell was amplified via an optical amplifier ('Amplispot') and registered on a chart recorder. The sensitivity of this arrangement was such that a 25μV output from the microcalorimeter produced a full scale recorder deflection. Calibration was achieved using the Joule effect[315] via a 1000 ohm resistance wound onto a sleeve surrounding the adsorption cell. Such calibrations are considered accurate to better than 1%[316,320].

The thermopiles and cells were maintained at a slight positive pressure of dry helium gas in order to maintain the level of liquid nitrogen at about the "porous floor" of the microcalorimeter. A constant rate of helium addition of approximately 3 cm^3/minute was obtained using a "copper constriction" leak similar to that described in section 4-3-3(d).

The microcalorimeter was shielded from stray electrical effects by ensuring proper earthing of both the microcalorimeter and large metal dewar. Room temperature, although not controlled, did not vary by more than a few degrees and the complete apparatus was always shielded from

direct sunlight.

The operational sensitivity of the microcalorimeter was approximately 167mm of recorder deflection per milliwatt of calorific power produced. The stability of the microcalorimeter and auxilliary instruments were such that this sensitivity was constant to ±1% over the four months duration of the work.

The microcalorimeter base line showed drifts of less than 1mm/hour - that is less than 1% of the typical experimental signals observed.

4-3-2 Sample Preparation

(a) Sample Pretreatment: The term pretreatment is used here to describe any procedures undertaken to improve the rate of transfer of heat from within the sample where it is produced, to the thermopiles of the microcalorimeter. From the form of the calibration curve (Figure 4-6) it can be seen that the response time of the microcalorimeter from time of detection to time of recorder deflection was extremely short (less than 2 seconds). However, when the adsorption of nitrogen on a powdered rutile sample was studied (Curve 1, Figure 4-8) a time lag between heat production and detection was apparent for about one hour after commencement of gas addition. As the aim of the microcalorimetry experiments was to determine the differential energies of adsorption, it was essential that quantities of heat produced by adsorption be instantly detected by the microcalorimeter. In the case of the powdered rutile sample the "nitrogen monolayer" was 70% complete before accurate differential heats of adsorption could be determined.

The "response time" of the microcalorimeter during an adsorption

isotherm depends primarily on the thermal conductivity of the sample particles and of the medium contained in the ampoule dead space volume (Vn_o). It was considered that heat transfer within the sample might be improved by increased particle-particle contact, and the rutile sample was compressed into pellets at pressures of less than 200kg/cm^2. Such pressures are relatively small, and after consideration of the results of compaction studies of various workers[321-324], it was thought unlikely that the adsorption characteristics of samples would be altered, particularly as the (P/Ps) values studied were less than 0.3. The effect of sample compaction on the microcalorimeter response time can be seen by comparing curves 1 and 3 in Figure 4-8. Although sample masses were different in the two experiments and hence the total heat produced was not the same, it can be seen that compaction has greatly reduced the response time. The problem of low thermal conductivity of the "ampoule dead space" is particularly important at the start of an isotherm where all the incoming adsorbate molecules are adsorbed onto the sample. The addition of approximately 0.3 torr (0.4kNm^{-2}) of dry helium gas to the adsorption ampoule prior to the commencement of the adsorption isotherm gave a significant reduction in the microcalorimeter "response time" (Curve 2, Figure 4-8). This technique has been reported by other workers[325] and when it was used in conjunction with sample compaction a very short response time was observed. (Curve 4, Figure 4-8).

The effects of helium addition on the subsequent adsorption behaviour of two samples are shown in Figures 4-9 and 4-10. It can be seen that any differences are very slight. Calculation of the integral energy of adsorption for these adsorption runs showed that helium addition produced less than 5% change. The combined effects of compaction and helium addition on a subsequent nitrogen isotherm are illustrated

in Figure 4-11. Again no significant differences are observed.

All samples were pretreated by compaction and helium addition before adsorption isotherms were determined.

(b) Ampoule Dead Space Volume (Vn_o): The ampoule dead space volume (see Figure 4-4) was determined at room temperature using helium gas, after each sample (2-5g) had been placed in the ampoule. The method used has been described elsewhere[299] and at least three determinations were made, the standard deviation being less than ± 0.03 cm^3. Helium was assumed to behave ideally at room temperature. Everett[185] has recently outlined four rather stringent conditions required for the above method to be strictly valid. Non-adsorption of helium is the most important of these; and using Everett's "temperature dependence test" it is considered that for all samples used no adsorption of helium occurred.

(c) Sample Outgassing: Samples were outgassed in the adsorption ampoule using an apparatus similar to that described by Rouquerol[326]. Outgassing times were from 16 to 20 hours and the final residual pressures less than 8×10^{-5}torr ($10^{-2}Nm^{-2}$). During outgassing at elevated temperatures the rate of heating of the sample was controlled such that the maximum pressure in the system was 10^{-3}torr ($10^{-1}Nm^{-2}$). Hence samples were heated slowly for approximately one hour until the desired outgassing temperature was reached.

(d) Microcalorimeter Equilibration: The microcalorimeter was "hoisted" from the dewar to allow the adsorption ampoule to be installed. The interior of the microcalorimeter was always maintained under a "flush" of dry helium whenever it was removed from the thermostat bath.

The ampoule was then "glass blown" onto the remainder of the adsorption apparatus just above tap A (Figure 4-4), and a constant feed of approximately 3 cm^3/minute of dry helium gas re-established into the microcalorimeter.

Approximately 6 hours were then required for thermal equilibrium within the microcalorimeter, as evidenced by a stable baseline signal.

4-3-3 Isotherm Preparation

(a) Apparatus Dead Space Volume (V_R): The volume between tap A (closed) and tap B (open) (Figure 4-4) was determined by difference using the technique previously described. A standard deviation of ± 0.03 cm^3 was obtained.

As tap B, a Viton A diaphragm tap , was closed during the determination of an isotherm it was necessary to make a small correction to the dead space volume as determined above. This was independently established as -0.10 cm^3, and was assumed to be constant.

(b) Addition of Helium: See section 4-3-2(a)

(c) Microcalorimeter Calibration: When a constant calorific power (W) is generated within the microcalorimeter cell, the resulting microcalorimeter output signal (Δ) can be related to W using Tian's equation[315]

$$W = A\Delta + B\frac{d\Delta}{dt} \qquad (4\text{-}1)$$

where A = principal constant of the apparatus

B = constant related to the thermal capacity of the cell contents

t = time

After a short time the microcalorimeter signal becomes constant as a steady state is achieved $\left[\frac{d\Delta}{dt} = 0\right]$ and equation (4-1) becomes $W = A\Delta$ (4-2) In all the work reported the power W was obtained by applying a voltage (V) across a 1000 ohm resistance (R) wound around the sample cell. The form of the resulting microcalorimeter signal is shown in Figure 4-6. If the current across R is I, then

$$A = \left[\frac{V.I}{\Delta(\text{Steady State})}\right]$$

Hence the calibration factor is readily measured and all microcalorimeter signals expressed in mm of recorder deflection can be converted directly into units of calorific power (mW). The microcalorimeter was recalibrated for every experiment.

(d) Rate of Addition of Gas: A slow, constant rate of addition was obtained using a metal constriction constructed from thin copper tubing (approximately 2mm I.D), as illustrated in Figure 4-15. The rate of gas flow through the constriction was independent of applied gas pressure for pressures above 3 atmospheres and the minimum applied pressure during any adsorption experiment was 3.9 atmospheres.

To measure the rate of addition of gas, a state of "dynamic equilibrium" in the apparatus was first established. This involved adding gas via the "leak" (applied pressure 4 atmospheres) whilst evacuating the system via taps I and G (Figure 4-4). The residual pressure of gas in the system was about 1 torr (130 Nm^{-2}) and several hours were allowed for equilibration. Tap B (Figure 4-4) was then closed and the rate of pressure increase in the system recorded. Gas addition was

continued up to (P/Ps) values of approximately 0.3, (i.e. the pressure range covered in adsorption experiments) before tap B was re-opened and a state of "dynamic equilibrium" re-established. The volume, V_R, is constant during this addition and the volume rate of addition (expressed at STP) is calculated from the rate of pressure increase assuming ideal gas behaviour.

Imprecision in measurement of rates of addition arising from pressure and dead space volume measurements was less than 0.3%. The rate of addition as a function of pressure was always measured before and after an adsorption experiment and found to agree within the precision of measurement. A small decrease (about 1%) in addition rate did occur as the gas pressure increased to 230 torr (30 kNm^{-2}). For isotherm calculation an average rate was used, and this may have introduced a systematic error of $\pm$0.5% into all adsorption isotherms.

4-3-4 Isotherm Determination

With the adsorption system in a state of dynamic equilibrium [see section 4-3-3(d)] adsorption was begun by closing tap B and opening tap A in rapid succession (Figure 4-4).

(a) Measurement of Pressure: Except for the determination of Vn_o and V_R for which a mercury manometer was used, all pressures were measured using a Bell and Howell Pressure transducer (type 4-326) connected to a chart recorder to give a sensitivity of 4mm/torr. The transducer characteristics were as reported elsewhere.

A recording of equilibrium pressure versus time for a typical adsorption run is included in Figure 4-7. Isotherms were measured to

(P/Ps) approximately 0.3. For nitrogen the duration of the adsorption runs were from 8 to 20 hours and for argon 8 to 15 hours depending on the sample mass used.

(b) Liquid Nitrogen Temperature: An oxygen manometer (vapour pressure thermometer) was used to measure the temperature of the liquid nitrogen in the cryostat bath. Measurements were taken at two hourly intervals during each adsorption run and an average value used for isotherm calculations. The equations of state for oxygen, nitrogen and argon have been given elsewhere[317,318]. These were used to calculate the saturated vapour pressures of nitrogen and argon liquids at the measured liquid nitrogen temperature.

(c) Microcalorimeter Signal: A typical microcalorimeter signal recorded during adsorption is shown in Figure 4-7. Calibration parameters were chosen to match as near as possible the expected experimental calorific power. Background noise and microcalorimeter instability accounted for less than 2%. For a given sample the magnitude of the microcalorimeter signal was dependent on the rate of addition of adsorbate. Preliminary experiments were performed to establish the addition rate required such that the largest heat flux encountered gave a near full scale recorder deflection. The duration of an adsorption experiment was then determined by the sample mass used.

4-3-5 Calculations

All calculations were performed using a HEWLETT PACKARD Programmable Calculator - Model 9830 A.

(a) Adsorption Isotherm:

(Using the nomenclature outlined by Everett[155])

Rate of Addition of Gas = D_o cm^3/min (expressed at STP)

At time t (mins), total volume of gas added = $D_o \times t$ cm^3 (expressed at STP)

Dead space volume of apparatus at temperature T of air thermostat = V_R cm^3

Dead space volume of ampoule at temperature T_o of liquid nitrogen = $Vn'_o = Vn_o (1 + \alpha P)$ cm^3

where Vn_o = ampoule dead space volume determined at room temperature

P = pressure of adsorptive in torr

α = non-ideality correction factor for gas at liquid nitrogen temperature[193]

$$\frac{\text{At time t (mins) total volume of adsorptive}}{} = \left(\frac{T}{P}\right)_{STP} \times \left[\frac{V_R}{T} + \frac{Vn'_o}{T_o}\right] \times P \quad cm^3 \text{ (expressed at STP)}$$

where T(STP) = 273.15K

P(STP) = 760 torr

At time t (mins),

$$\frac{\text{Total Volume of Adsorbate } V_a}{(cm^3, \text{ at STP})} = D_o t - \left(\frac{T}{P}\right)_{STP} \left[\frac{V_R}{T} + \frac{Vn'_o}{T_o}\right] \times P$$

The experimental parameters D_o, V_R, Vn_o, T and T_o were all known.

Hence the adsorption isotherm could be calculated by choosing as many points as required from the recording of equilibrium pressure versus time.

Notes: (1) It is assumed that a temperature discontinuity occurs at tap A (Figure 4-4). In practice a temperature gradient between T and T_o exists - the domain of this gradient increasing as the level of liquid nitrogen drops from just below tap A during a run. The drop was about 15cm, and at the end of a run the ampoule was submerged under about 40cm of liquid nitrogen. Additions to the dewar could not be made during a run as they contributed a thermal effect to the system which was detected by the microcalorimeter. Calculations have shown however that the above assumption leads to negligible error in the adsorption isotherm[305].

(2) As the maximum equilibrium pressures were about 230 torr (30 kNm^{-2}), the non-ideality correction to give $V'n_o$ is very small (about 0.1%) and was not normally applied.

(b) Differential Energy of Adsorption: A review of the treatment of various types of calorimetric data has recently been given by Létoquart[189]. A brief treatment of the calculations relevant to data present in this thesis has also been given by Rouquerol[319]. The basic equations for the calculation of differential energy of adsorption from the experimental data are derived as follows:*

General System: The isothermal system in which thermal changes have been produced and measured is termed "open" - in that heat, work and matter can be exchanged with the surroundings. There are considered to

---

* An alternate approach, based on the concepts of surface excess quantities has been outlined by Everett[185].

be C constituents and β phases in the system, and during an experimental transformation (e.g. addition of gas and adsorption), a quantity of heat Q, of work W, and of moles of constituent i (each possessing a molar energy ε_{ie}), Δn_i, is considered to enter the system. The variation of total internal energy, ΔE, can then be expressed as follows:

$$\Delta E = W + Q + \sum_{i=1}^{i=C} \varepsilon_{ie} \Delta n_i \qquad (4\text{-}3)$$

If the i^{th} constituent in the j^{th} phase possesses a molar energy ε_{ij}, and N_{ij} represents the number of moles of i in phase j, then:

$$\Delta E = \sum_{i=1}^{i=C} \sum_{j=1}^{j=\beta} \Delta(N_{ij} \varepsilon_{ij}) \qquad (4\text{-}4)$$

Hence from equations (4-3) and (4-4)

$$Q = \sum_{i=1}^{i=C} \sum_{j=1}^{j=\beta} \Delta(N_{ij} \varepsilon_{ij}) - \sum_{i=1}^{i=C} \varepsilon_{ie} \Delta n_i - W \qquad (4\text{-}5)$$

Adsorption System: Infinitely Small Addition of Gas

Consider a change in an adsorption system where the initial and final states are summarized in the following table.

Parameter	Initial State	Final State
Temperature	T	T
Moles adsorptive	Ng	Ng + dNg
Moles adsorbate	Na	Na + dNa
Pressure	P	P + dP
Molar energy of adsorptive	*εg	*εg
Molar energy of adsorbate	εa	εa + dεa

* It is assumed that gas molecules entering the system have the same molar energy as those at temperature T.

Substitution into the general equation (4-5) gives

$$\underline{dQex = (\varepsilon a - \varepsilon g)\, dNa + Na\, d\varepsilon a - dW} \qquad (4\text{-}6)$$

where dQex = quantity of heat received by the system.

dW = work done by molecules in the gas phase in raising the pressure.

Assuming ideal gas behaviour: $dW = RT\,(dNa + dNg)$ (4-7)

If the volume of the gas phase is Vg, then $RT\,dNg = Vg\,dP$ (4-8)

Therefore combination of equations (4-6),(4-7) and (4-8) gives

$$\underline{dQex = (\varepsilon a - \varepsilon g)dNa + Na\, d\varepsilon a - RT\, dNa - VgdP} \qquad (4\text{-}9)$$

Differentiation of equation (4-9) at constant temperature and amount adsorbed (A) gives:

$$\underline{\left(\frac{\partial Qex}{\partial Na}\right)_{T,A} = (\varepsilon a - \varepsilon g) + Na\left(\frac{\partial \varepsilon a}{\partial Na}\right)_{T,A} - RT - Vg\left(\frac{\partial P}{\partial Na}\right)_{T,A}} \qquad (4\text{-}10)$$

Having established these equations they can now be extended to an experimentally real situation.

<u>Adsorption System: Finite Addition of Gas</u>

Let the quantity of heat measured, Qex, correspond to a small addition of gas producing a variation (ΔNa) in the number of moles of gas adsorbed.

$$Qex = \int_{Na_1}^{Na_2} dQex \quad \text{where } \Delta Na = Na_2 - Na_1$$

Substitution for dQex from equation (4-9) and integration, gives

$$Qex = (\varepsilon a_2 - \varepsilon g)\, Na_2 - (\varepsilon a_1 - \varepsilon g)\, Na_1 - RT\,(Na_2 - Na_1) - Vg\,(P_2 - P_1) \qquad (4\text{-}11)$$

Equation (4-11) may be expressed as

$$Qex = \underbrace{Qint\,(2) - Qint\,(1)}_{1} - \underbrace{RT\Delta Na}_{2} - \underbrace{Vg\,(P_2 - P_1)}_{3} \qquad (4\text{-}12)$$

where term 1 represents : the increase in the integral energy of adsorption

term 2 represents : work produced by adsorbing molecules

term 3 represents : work of non-adsorbing gas molecules in producing a pressure increase.

This equation can be applied to the actual adsorption process studied.

Adsorption System : Slow, Continuous Addition of Gas

The differential energy of adsorption, q_D, may be defined as follows[319]

$$q_D = \left(\frac{\partial Qint}{\partial Na}\right)_T \qquad (4\text{-}13)$$

where the terms are as previously defined.

Equation (4-12) therefore becomes:

$$\left(\frac{\partial Qex}{\partial Na}\right)_T = q_D - RT - Vg\left(\frac{\partial P}{\partial Na}\right)_T \qquad (4\text{-}14)$$

For the use of the Tian-Calvet microcalorimeter with a continuous addition adsorption system, the microcalorimeter signal represents the thermal flux produced in the adsorption cell, i.e. $(\partial Qex/\partial t)$ (t = time)

Now: $$\left(\frac{\partial Qex}{\partial t}\right)_T = \left(\frac{\partial Qex}{\partial Na}\right)_T \times \left(\frac{\partial Na}{\partial t}\right)_T$$

if D = rate of adsorption = $\left(\partial Na/\partial t\right)$

Δ = microcalorimeter signal = $\left(\partial Qex/\partial t\right)$

then $\left(\partial Qex/\partial Na\right)_T = \Delta/D$ (4-15)

and $\left(\partial P/\partial Na\right)_T = \left(\partial P/\partial t\right)_T \Big/ D$ (4-16)

Substitution of (4-15) and (4-16) into equation (4-14) gives

$$q_D = \frac{1}{D}\left[\Delta + Vg\left(\frac{\partial P}{\partial t}\right)_T\right] + RT \qquad (4\text{-}17)$$

Equation (4-17) provides the basis for the calculation of the differential energy of adsorption from the experimental parameters D, Δ, Vg, P and t.

Notes: (1) In the derivation of equation (4-17) the "adsorption system" (volume Vg) was considered to be that volume from which thermal effects were detected. In practice this consisted of the complete sample ampoule and a short length of capillary tubing. The volume Vg was calculated from the ampoule dead space volume Vn_o. Errors in q_D arising from errors in Vg are negligible.

(2) The assumption of "equivalence of molar energy" (page 83) is valid, as molecules of gas entering the adsorption system have been equilibrated at liquid nitrogen temperature by passage through capillary tubing.

(3) In some circumstances equation (4-17) may be written in the form $\Delta = K(q_D - RT)$ where K is a constant. This is the case, for example, at the low pressure end of a type II isotherm where all the gas being admitted is adsorbed (D = constant) and the equilibrium

pressure remains very small and constant ($\partial P/\partial Na = 0$). Hence, by definition, the microcalorimeter signal is directly proportional to the "isosteric heat of adsorption"[155], a quantity which may be calculated from adsorption isotherms and is frequently used in the characterization of solid surfaces[303].

(4) Rate of Adsorption (D): This quantity was calculated directly from the volume adsorbed at any time and hence should have been in error by about 1%. However, it was observed that for rates of addition of gas of from 0.050 to 0.065 cm^3/min, when the rate of adsorption fell below 0.018 cm^3/min the errors in calculated energies of adsorption, as evidenced by a large random scatter in values, became rapidly larger. This can be seen as a combination of errors in D, and a small term Δ in comparison with the correction term $(\partial P/\partial t)$. Hence to a large extent the range of validity of the differential energy curves depended on the nature of the adsorption isotherm. However, differential energy curves were all considered to contain errors of less than 2% up to 0.85 of monolayer coverage.

4-3-6 Reproducibility

(a) Adsorption Isotherms: Figures 4-12, 4-13, and 4-14 show the reproducibility of argon and nitrogen isotherms on three different samples. Figure 4-13 represents the largest degree of non-reproducibility observed throughout the work. Hence it is concluded that with the measurements described in the previous sections, isotherms can be reproduced to better than 1%.

(b) Differential Energies of Adsorption: Differential energies

of adsorption were plotted as a function of surface coverage of adsorbate. Surface coverage was expressed as the fraction of monolayer coverage; the monolayer capacity Vm being obtained by the application of the BET equation. Therefore these plots contain the sum total of differences in sample pretreatment and isotherm determination as well as any errors in the actual measurement and calculation of thermal quantities. Figures 4-16 and 4-17 show that differential energy curves are reproducible to about 2% up to relative monolayer coverages of 0.85.

4-3-7 General Comments

The technique of continuous adsorption is based on the assumption that adsorption and the associated heat evolution take place rapidly, and that at any instant the system may be assumed to be at equilibrium. That heat evolution is rapid has been discussed and confirmed in section 4-3-2(a).

In order to confirm the equilibrium assumption and hence the absolute accuracy of the adsorption isotherms determined, some data for the adsorption of nitrogen on rutile are presented. It can be seen that a doubling of the rate of addition (Figure 4-11) of gas has given no significant change in the adsorption isotherm. In addition it can be seen that at the rate of addition of gas used througout this work the continuous adsorption isotherm is in excellent agreement with the isotherm determined by the "dose and wait" discontinuous method (Figure 4-18).

In conclusion it can be said that the technique used has enabled

the precise and accurate determination of adsorption isotherms and associated heat effects up to P/Ps values of 0.3.

4 - 4 CLEANING PROCEDURES:

(a) Glassware: All glassware was rinsed in hot concentrated A.R. nitric acid and then steamed for at least two hours before use. Steaming has been shown to be a very efficient means of cleaning glassware[328]. Chromic acid cleaning solutions were not used because of the possibility of adsorption of chromium species on the glassware.

(b) Plastics: Perspex apparatus and plastic tubing were cleaned by rinsing in 2M nitric acid and triply distilled water. The more severe procedure used with glassware has been observed to produce etching of plastics - resulting in the release of an acidic component into solutions.

(c) Microelectrophoresis Cell and Circulation System: All components were cleaned as described above. A concentrated dispersion (1g/litre) of the solid to be investigated was then pumped through the system for 1 hour. Large quantities of triply distilled water were then circulated until no suspended particles were visible under the microscope - at which time the distilled water was replaced with the dispersion under investigation. This purging was considered the most efficient method of removing impurities - particularly adsorbed particles from previous runs, and was preferred to the use of HF[329].

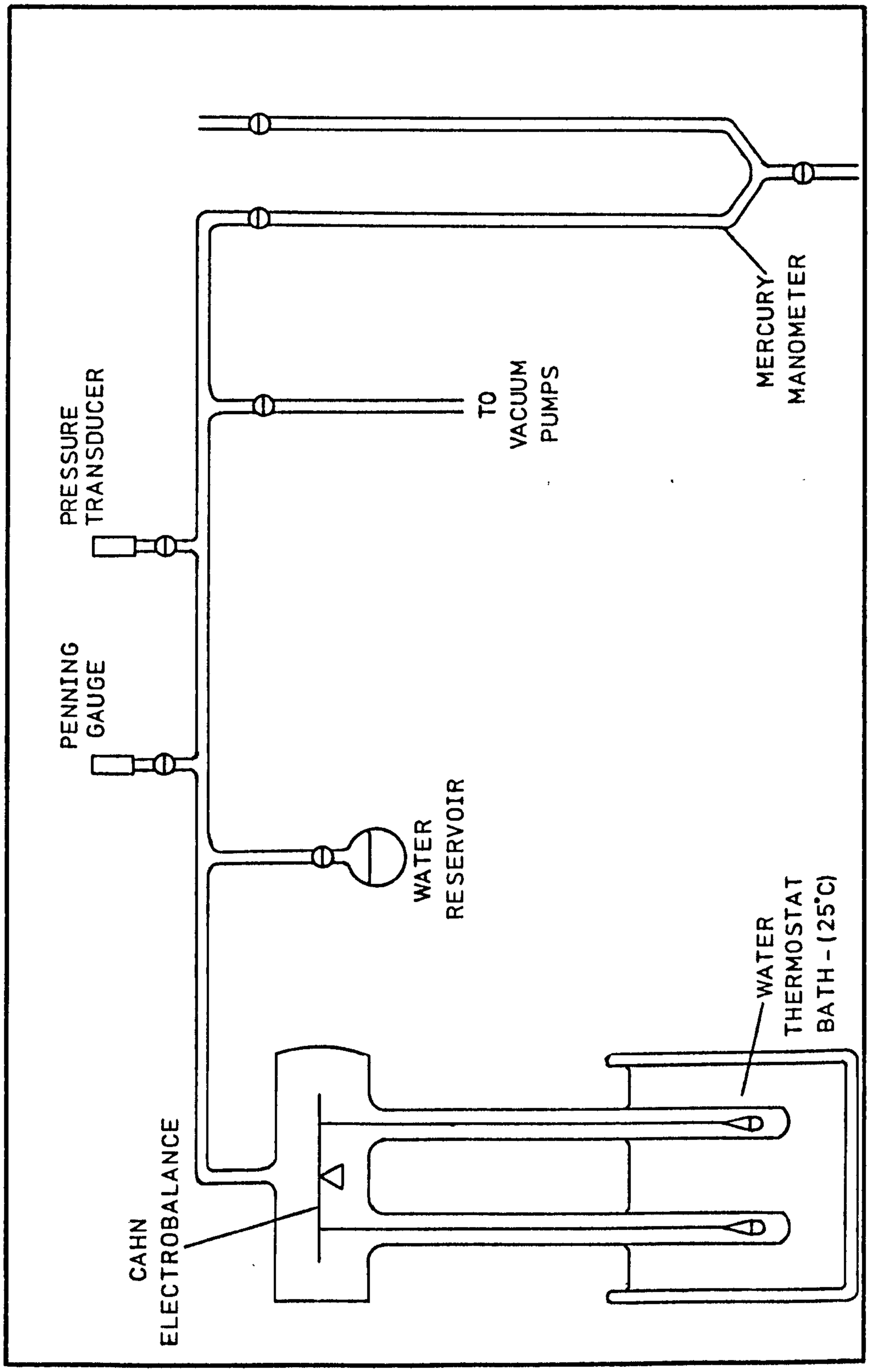
GRAVIMETRIC WATER VAPOUR ADSORPTION APPARATUS
CAHN ELECTROBALANCE
WATER THERMOSTAT BATH-(25°C)
WATER RESERVOIR
PENNING GAUGE
PRESSURE TRANSDUCER
TO VACUUM PUMPS
MERCURY MANOMETER

FIGURE 4-1

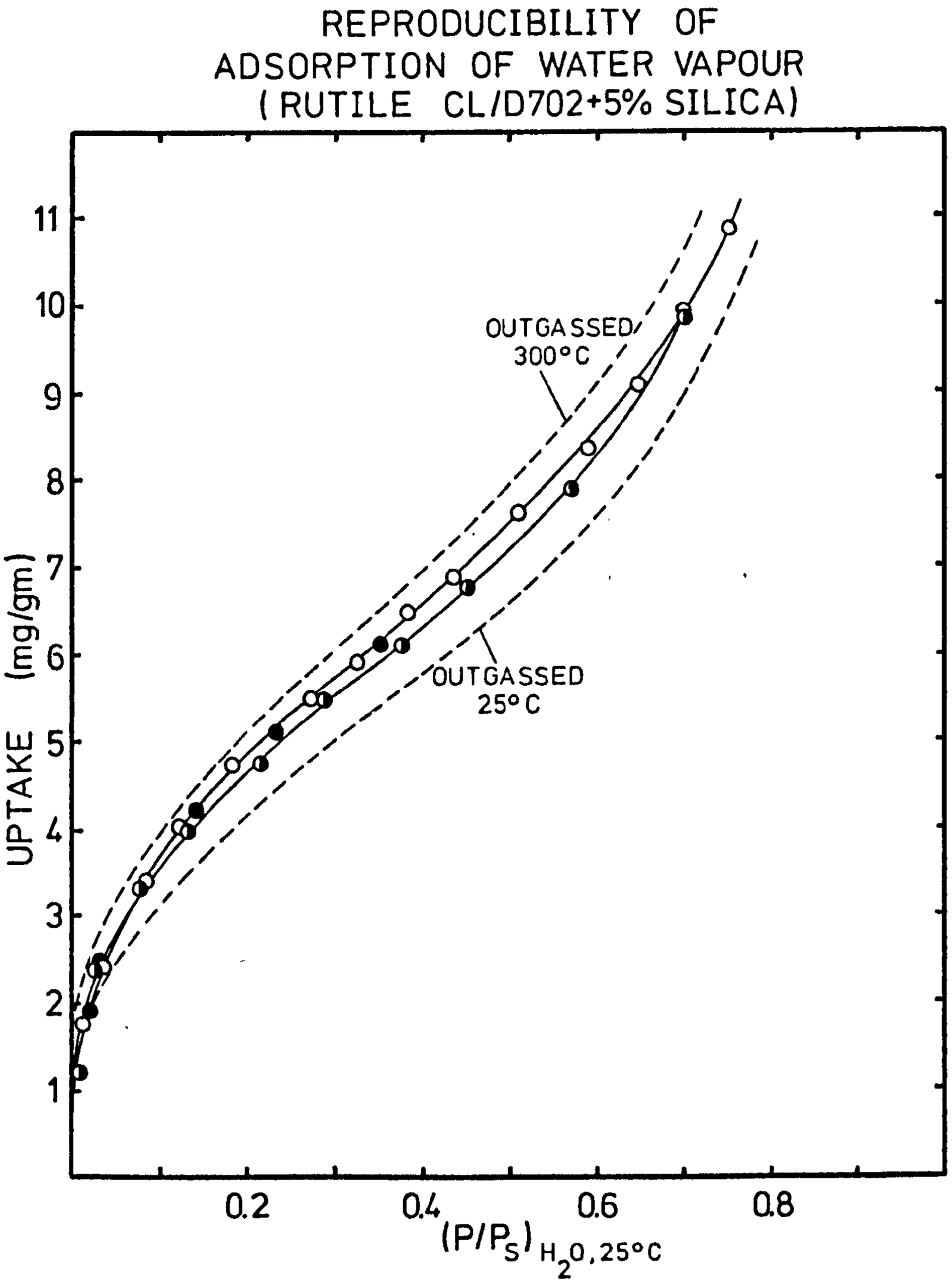
REPRODUCIBILITY OF
ADSORPTION OF WATER VAPOUR
(RUTILE CL/D702+5% SILICA)
UPTAKE (mg/gm)
11
10
9
8
7
6
5
4
3
2
1
0.2
0.4
0.6
0.8
(P/Ps) H2O, 25°C
OUTGASSED 300°C
OUTGASSED 25°C
● FIRST ADSORPTION RUN — SAMPLE OUTGASSED 200°C AND GETTERED
○ REPEAT RUN — " " "
● REPEAT ADSORPTION RUN — SAMPLE OUTGASSED 200°C BUT NOT GETTERED

FIGURE 4-2

REPRODUCIBILITY OF
ADSORPTION OF WATER VAPOUR.
(RUTILE CL/D702 - OUTGASSED 300°C)

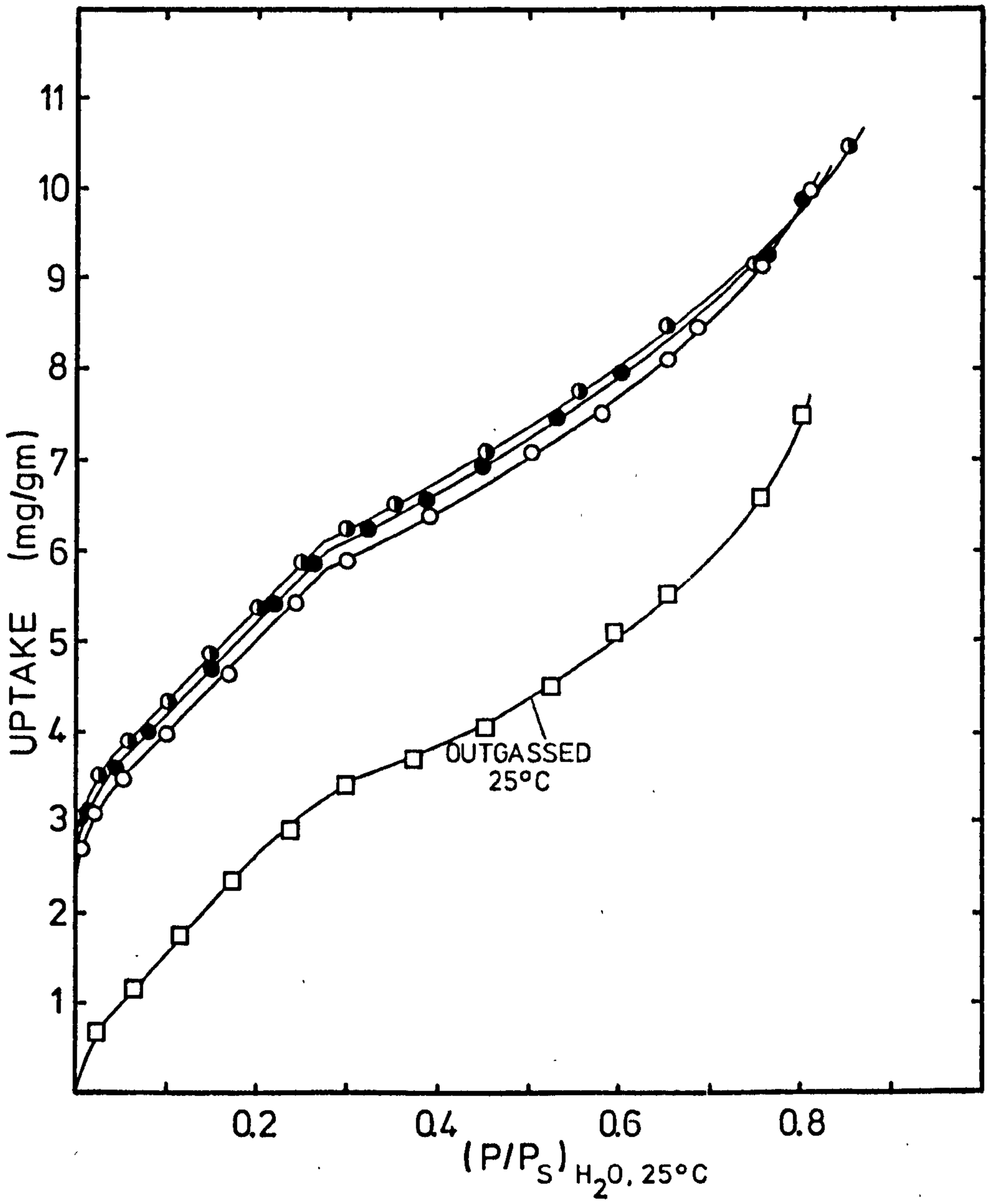

● FIRST ADSORPTION RUN
○ SECOND ADSORPTION RUN — FRESH SAMPLE
◑ THIRD ADSORPTION RUN — FRESH SAMPLE, BALANCE RECALIBRATED

FIGURE 4-3

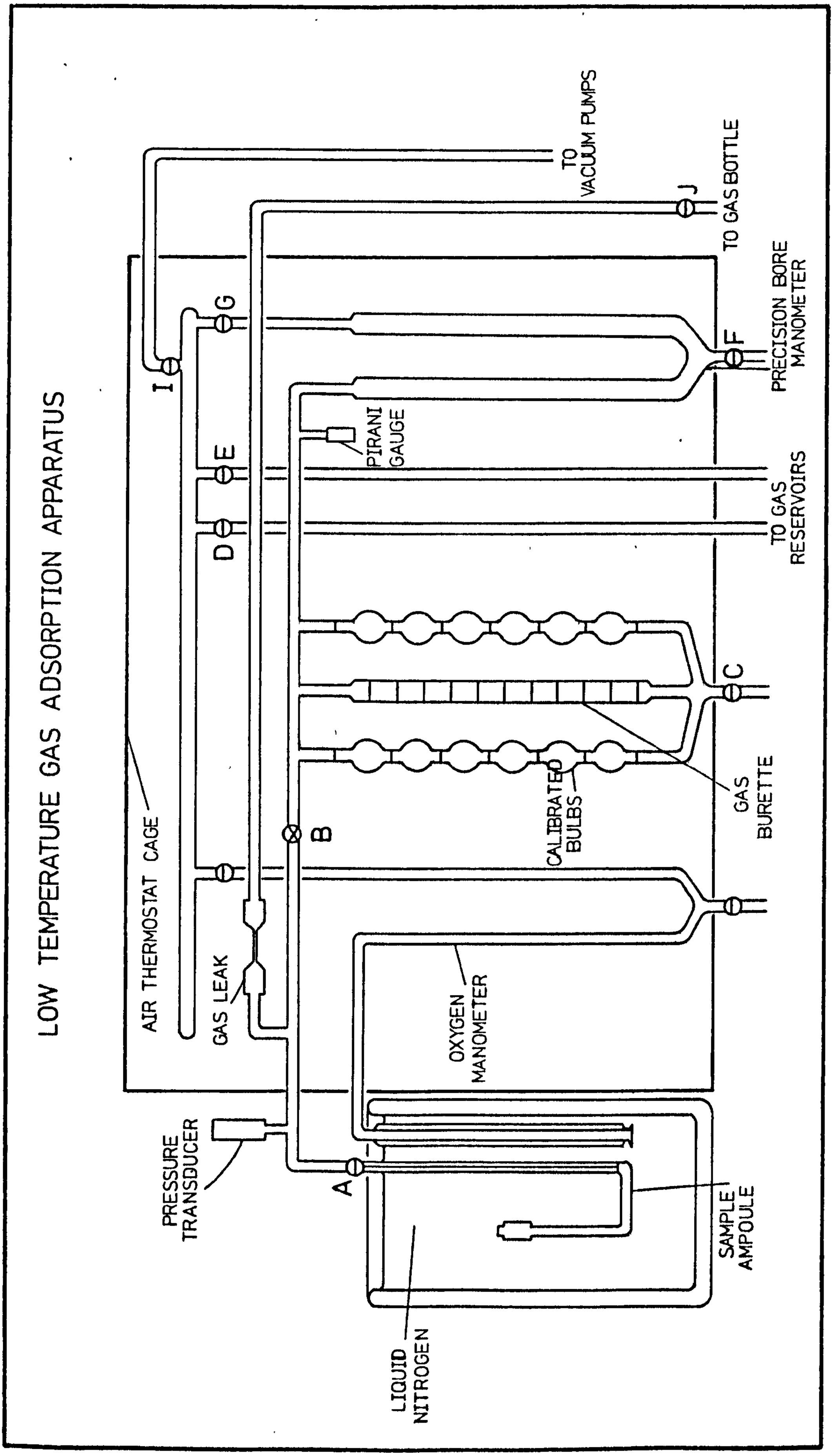
LOW TEMPERATURE GAS ADSORPTION APPARATUS
TO VACUUM PUMPS
J
TO GAS BOTTLE
PRECISION BORE MANOMETER
F
G
I
E
D
PIRANI GAUGE
TO GAS RESERVOIRS
C
GAS BURETTE
CALIBRATED BULBS
B
AIR THERMOSTAT CAGE
GAS LEAK
OXYGEN MANOMETER
PRESSURE TRANSDUCER
A
SAMPLE AMPOULE
LIQUID NITROGEN

FIGURE 4-4

TIAN-CALVET LOW TEMPERATURE MICROCALORIMETER

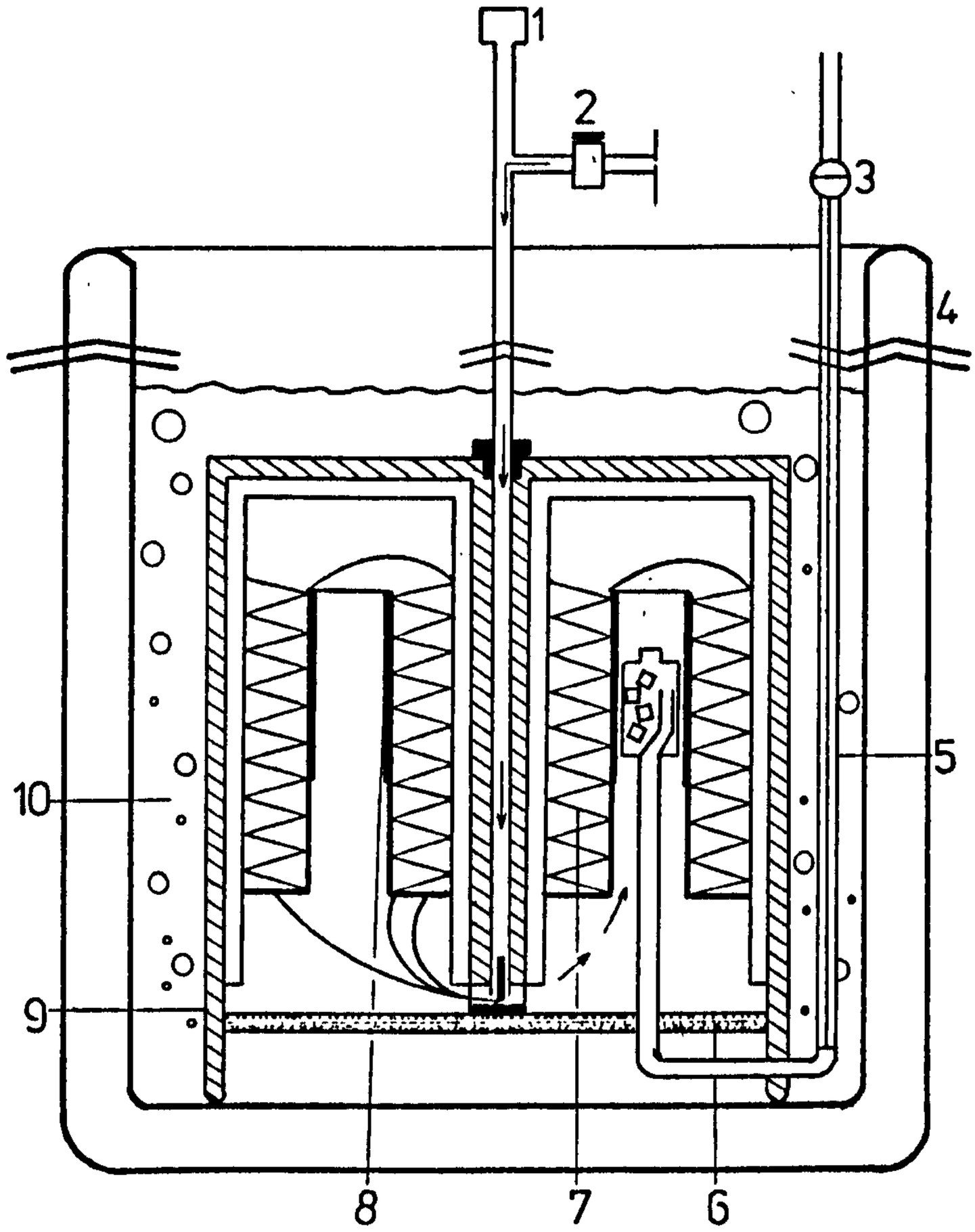

1 MICROCALORIMETER OUTPUT TO RECORDER
2 HELIUM GAS FEED CONTROL
3 GREASED STOPCOCK
4 METAL DEWAR VESSEL
5 GLASS CAPILLARY (1mm ID)
6 POROUS FLOOR
7 THERMOPILE
8 1000 OHM WIRE RESISTANCE
9 ALUMINIUM CONTAINER
10 LIQUID NITROGEN

FIGURE 4-5

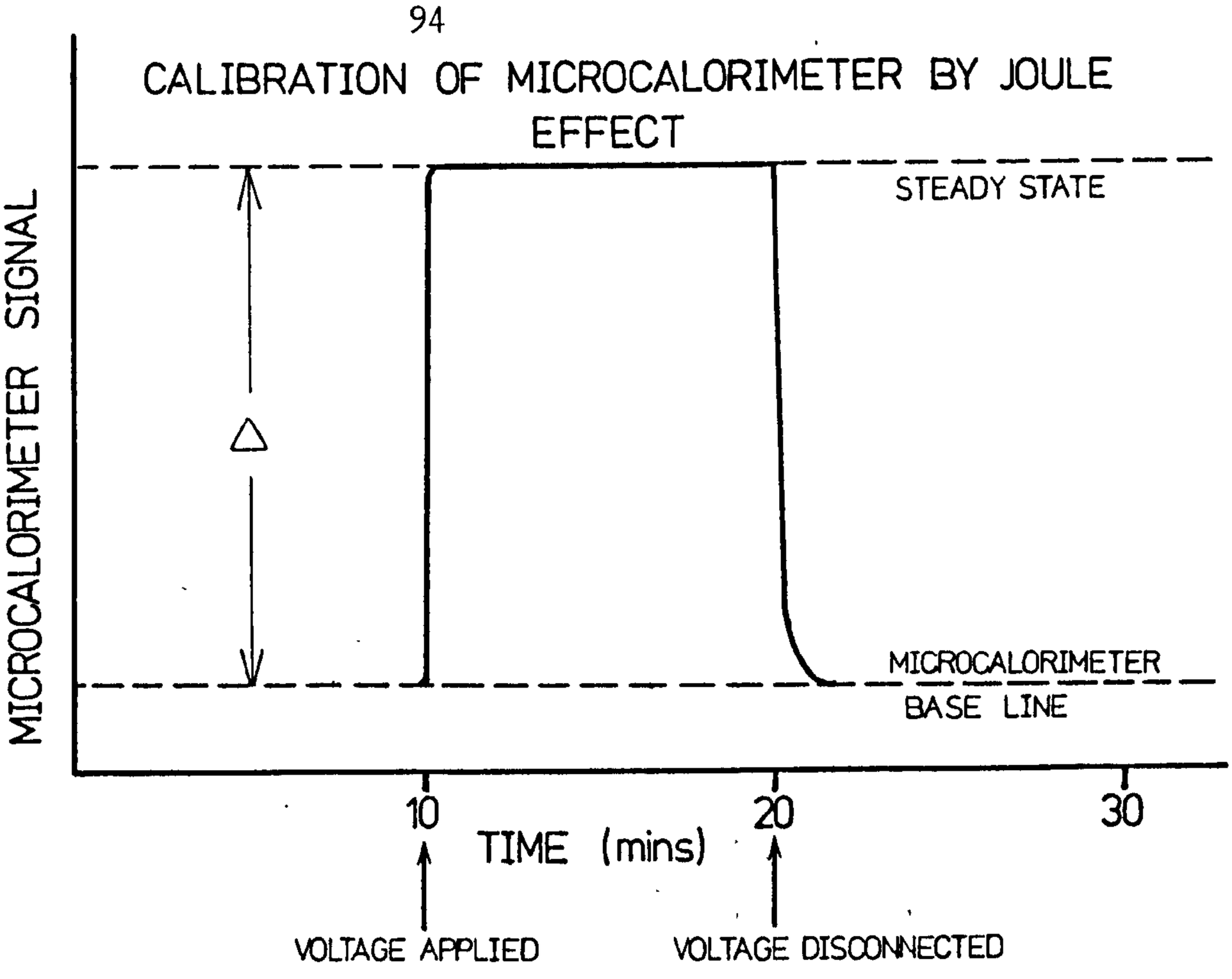

FIGURE 4-6

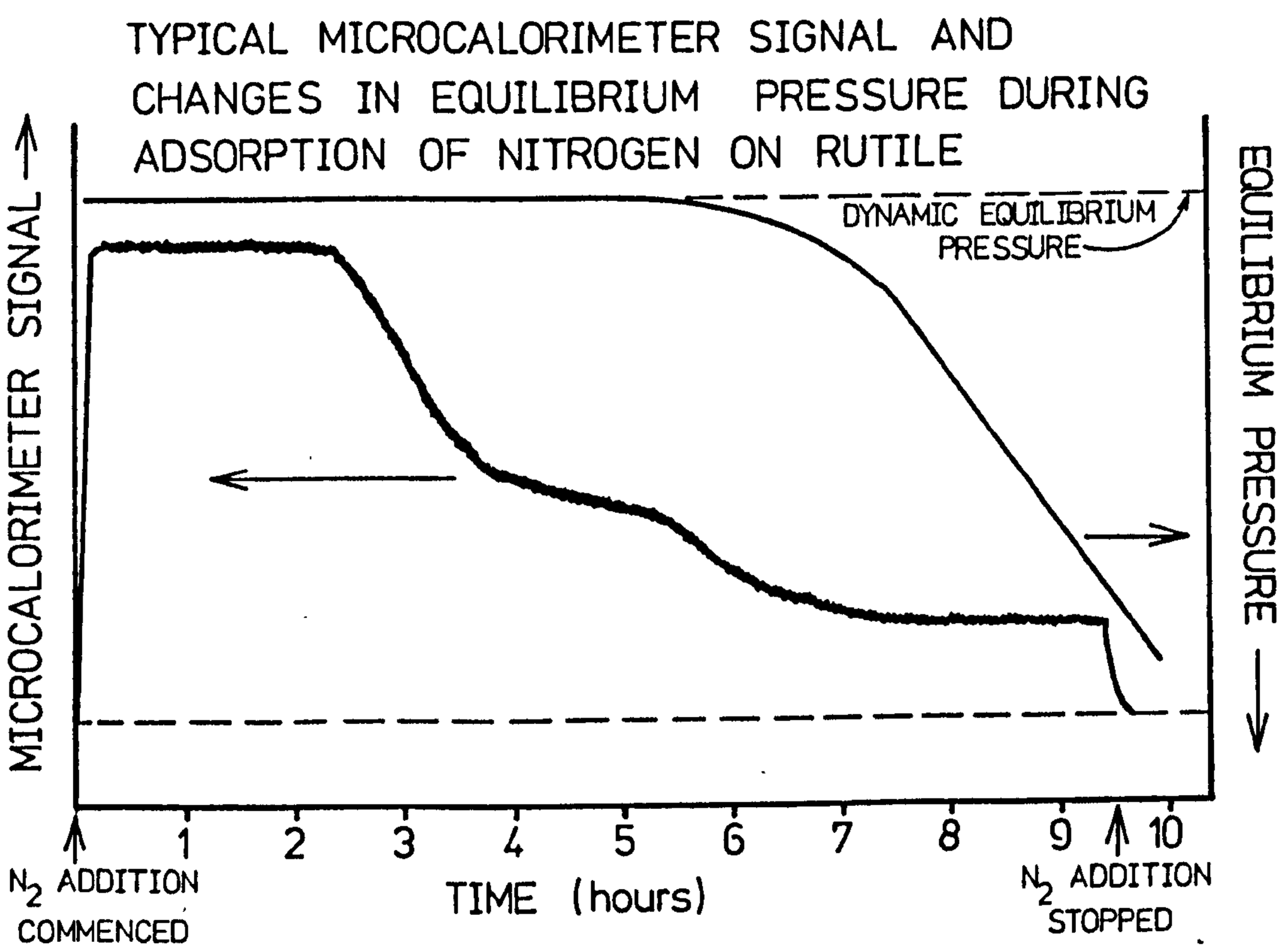

FIGURE 4-7

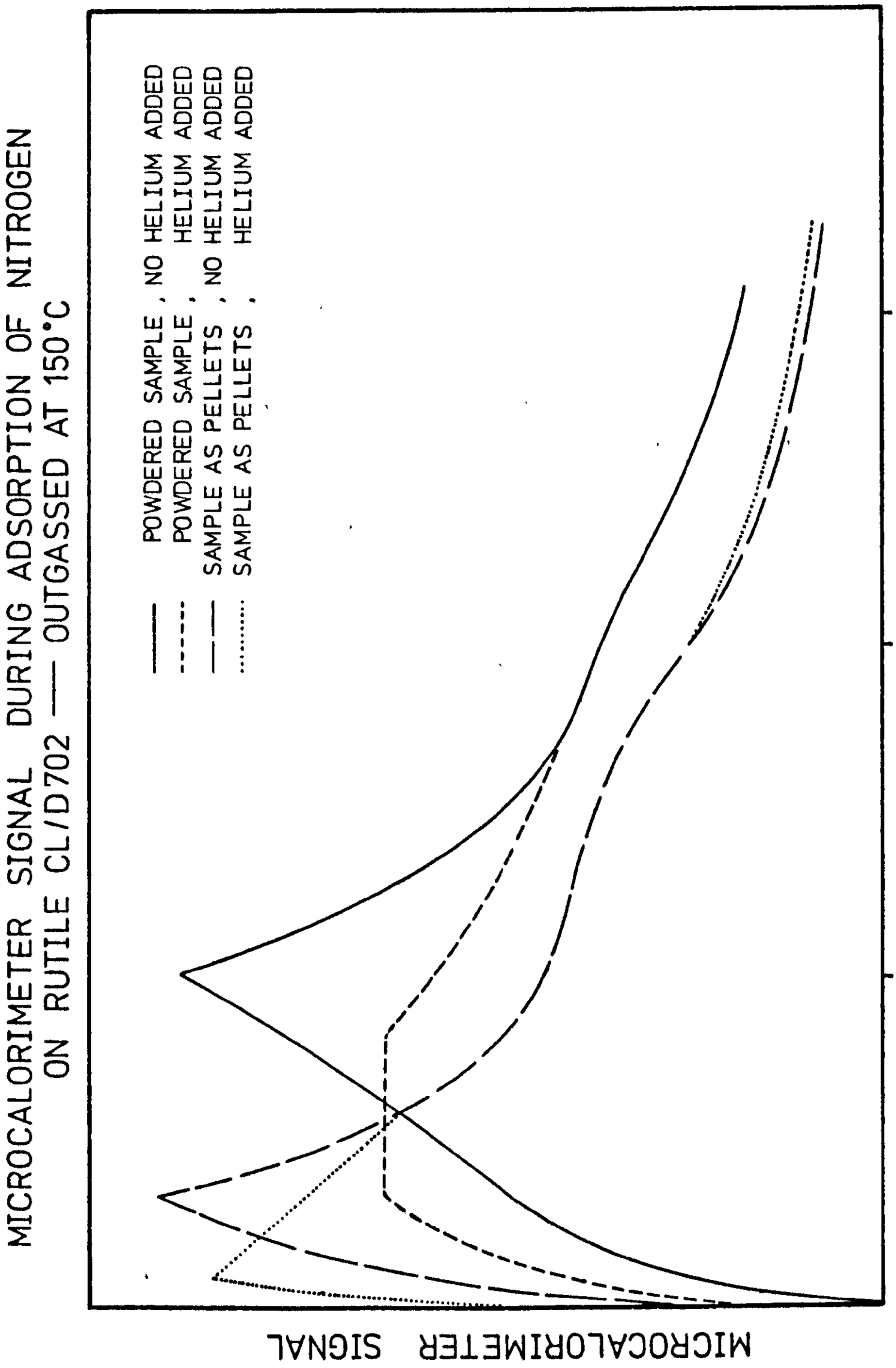
MICROCALORIMETER SIGNAL DURING ADSORPTION OF NITROGEN ON RUTILE CL/D702 — OUTGASSED AT 150°C
POWDERED SAMPLE , NO HELIUM ADDED
POWDERED SAMPLE , HELIUM ADDED
SAMPLE AS PELLETS , NO HELIUM ADDED
SAMPLE AS PELLETS , HELIUM ADDED
MICROCALORIMETER SIGNAL
TIME OF NITROGEN ADDITION (hours)
1
2
3

FIGURE 4-8

FIGURES 4-9 to 4-14
REPRODUCIBILITY OF ADSORPTION ISOTHERMS
OBTAINED BY THE
CONTINUOUS ADDITION TECHNIQUE

FIGURE 4-9

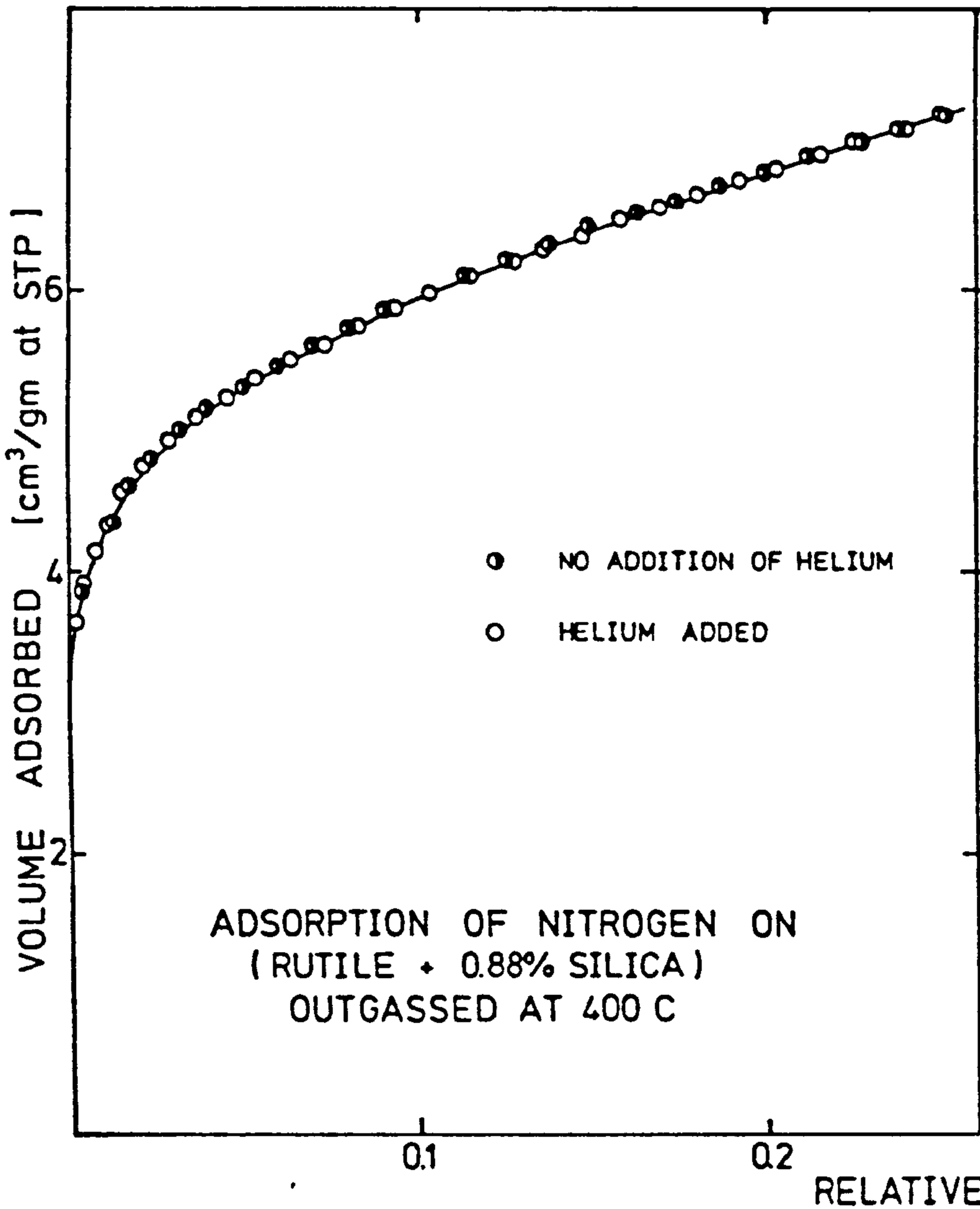

FIGURE 4-10

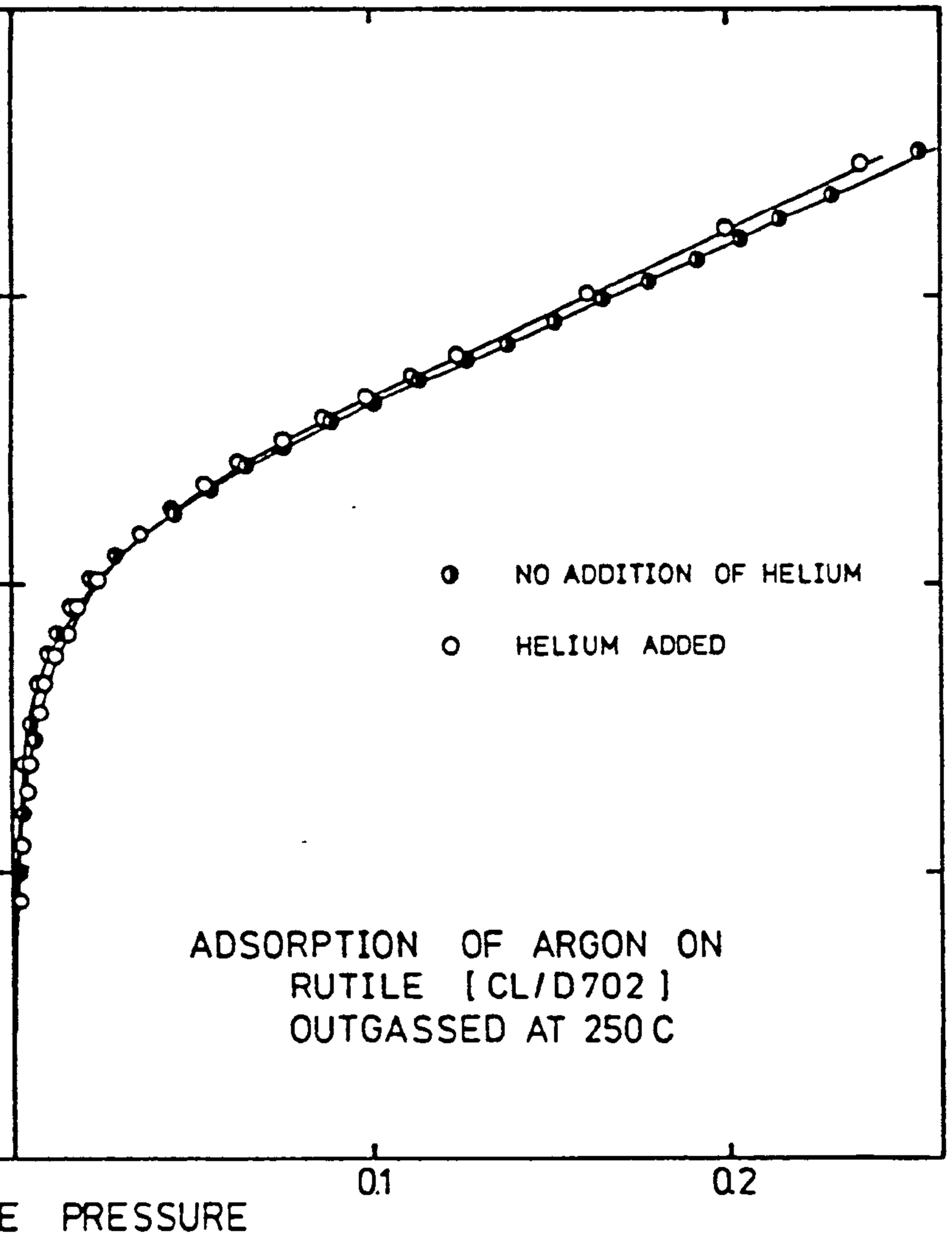

FIGURE 4-11

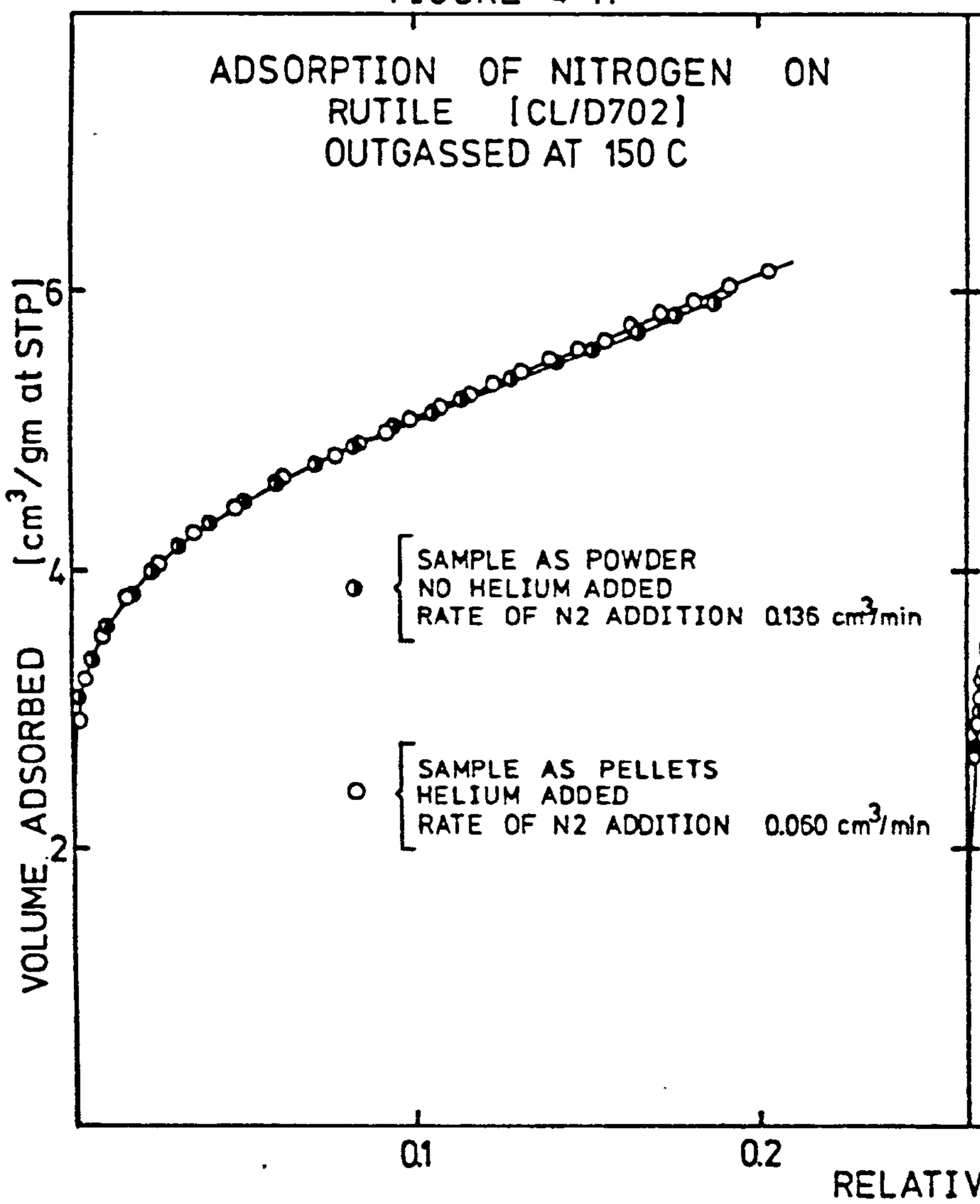

FIGURE 4-12

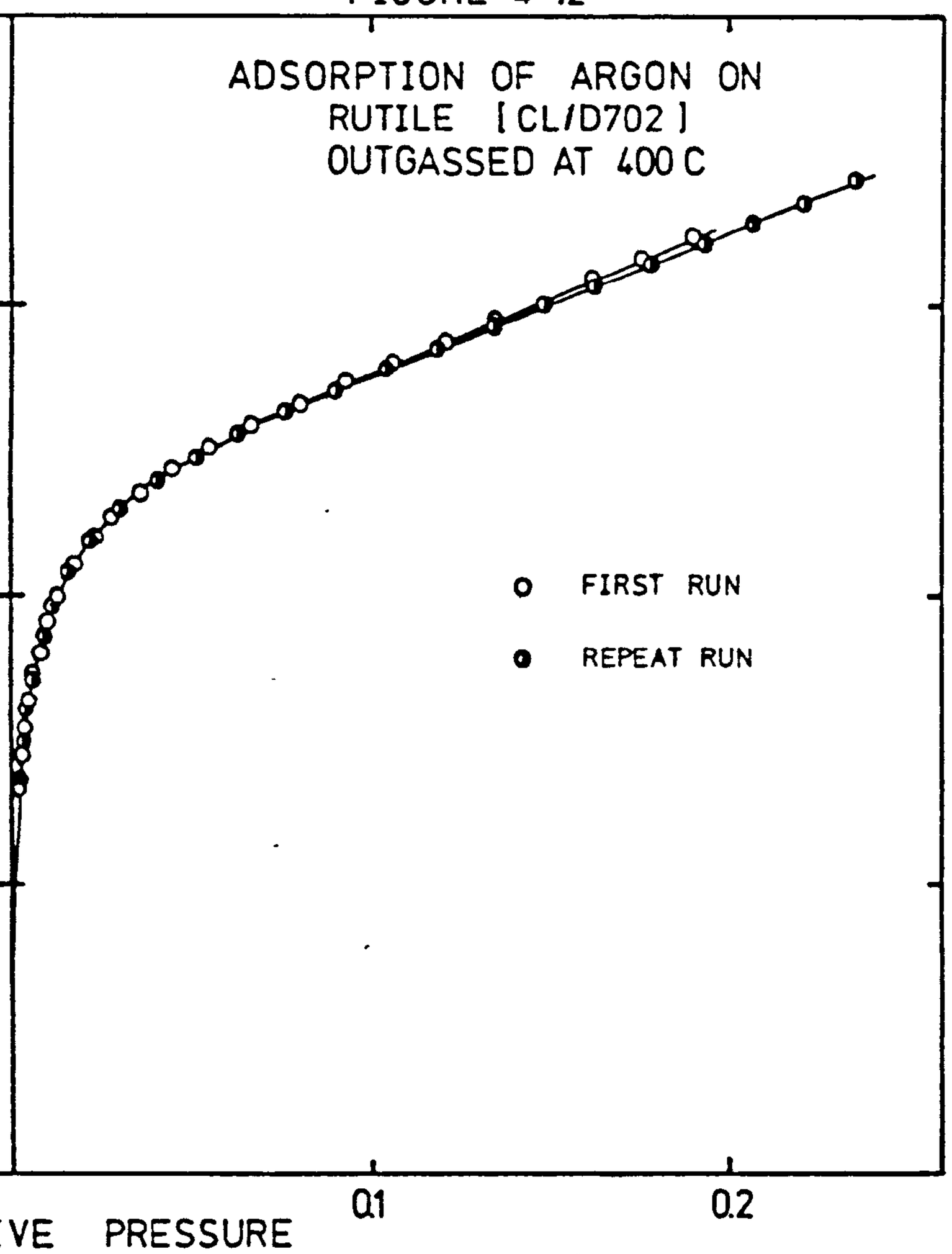

FIGURE 4-13

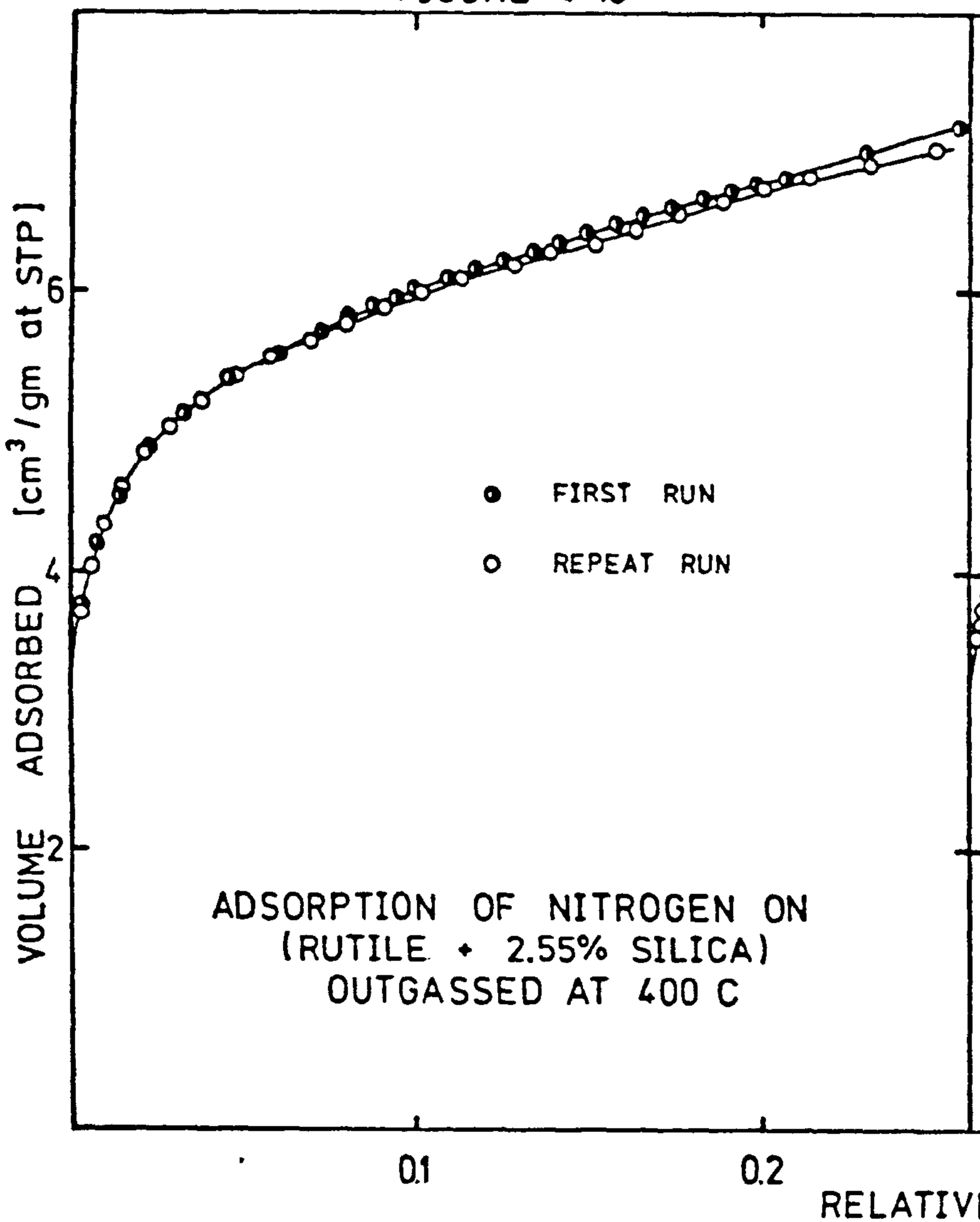

FIGURE 4-14

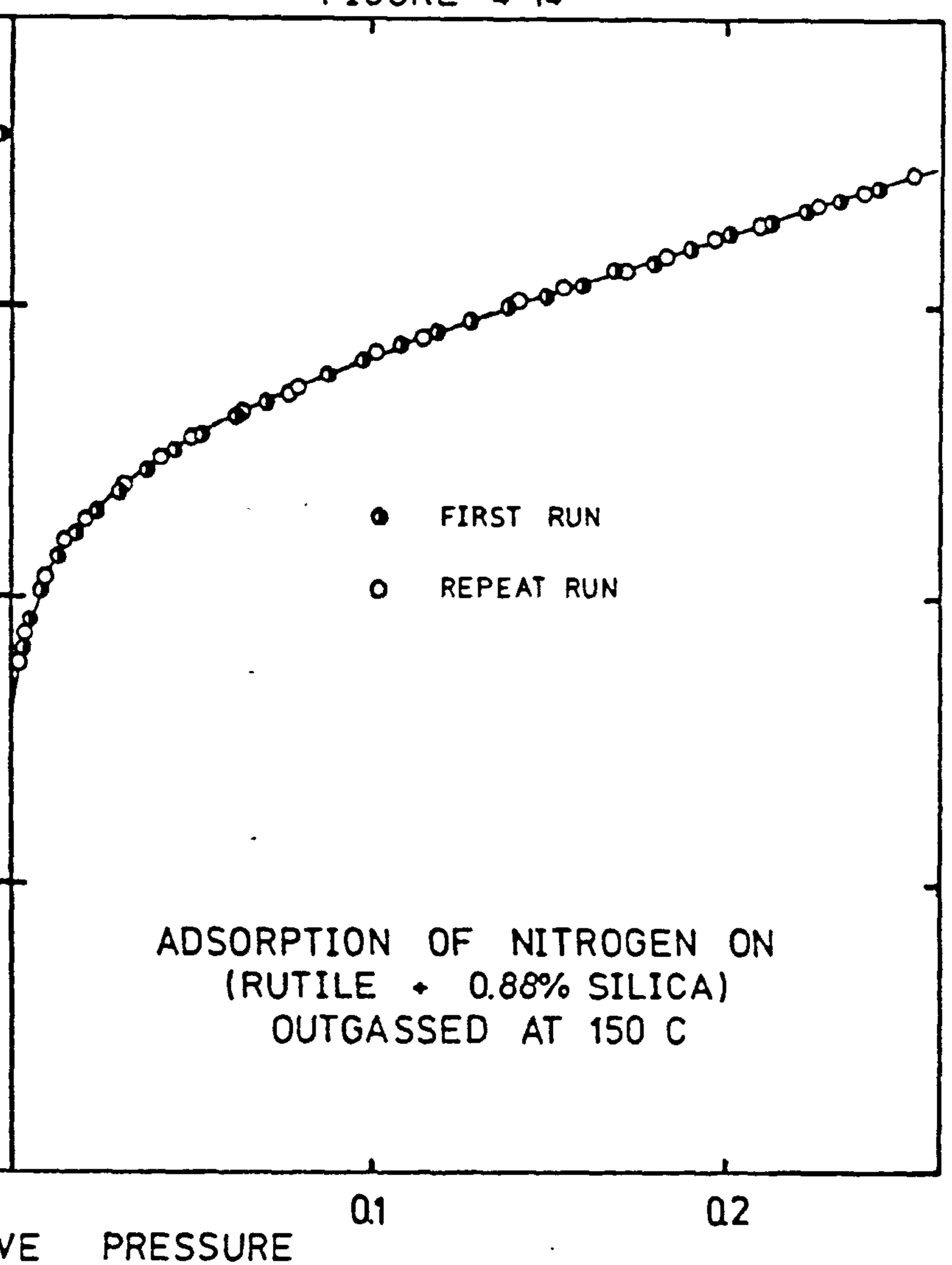

FIGURE 4-15

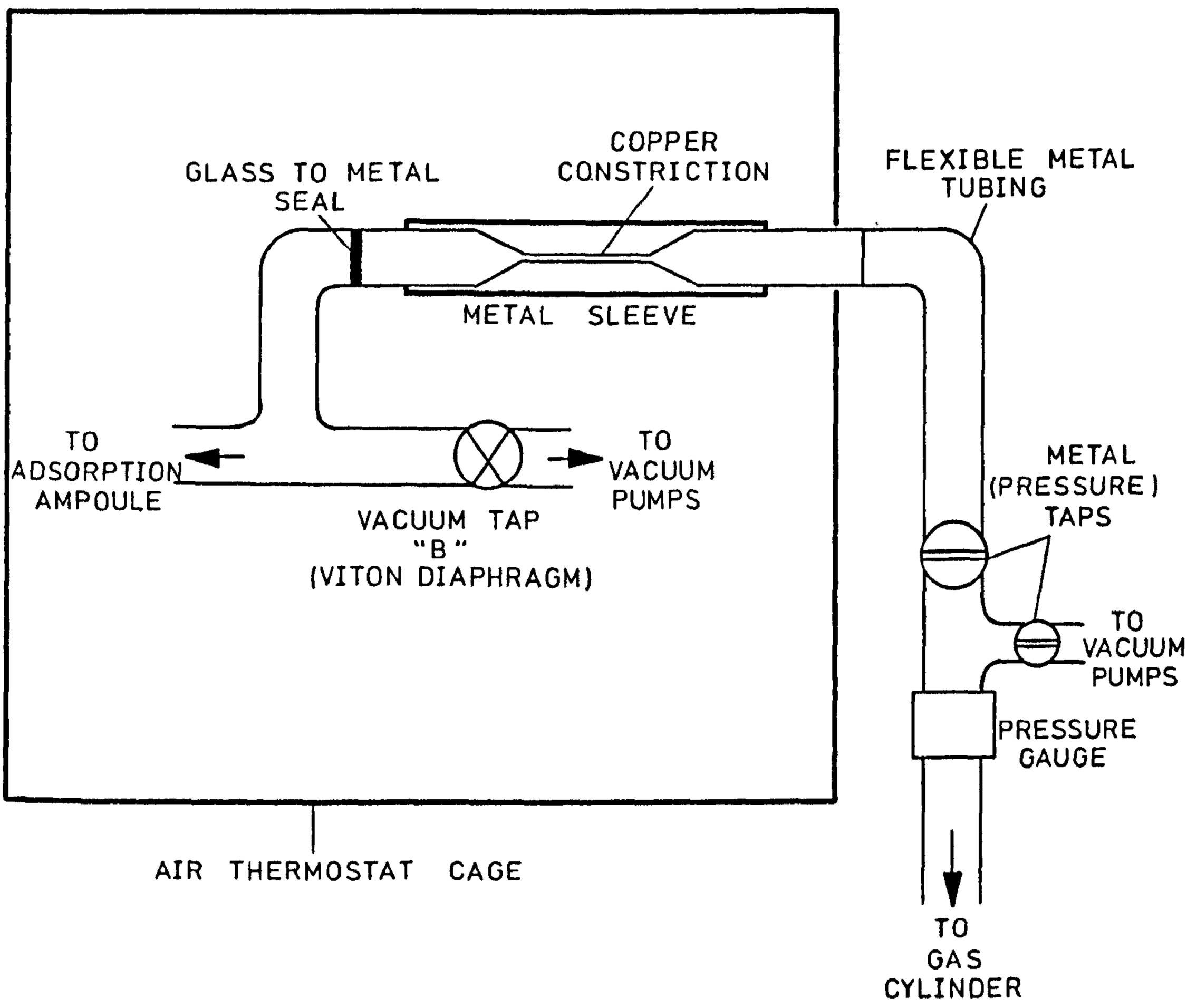

APPARATUS FOR CONTINUOUS ADDITION OF GAS

REPRODUCIBILITY OF MICROCALORIMETRY

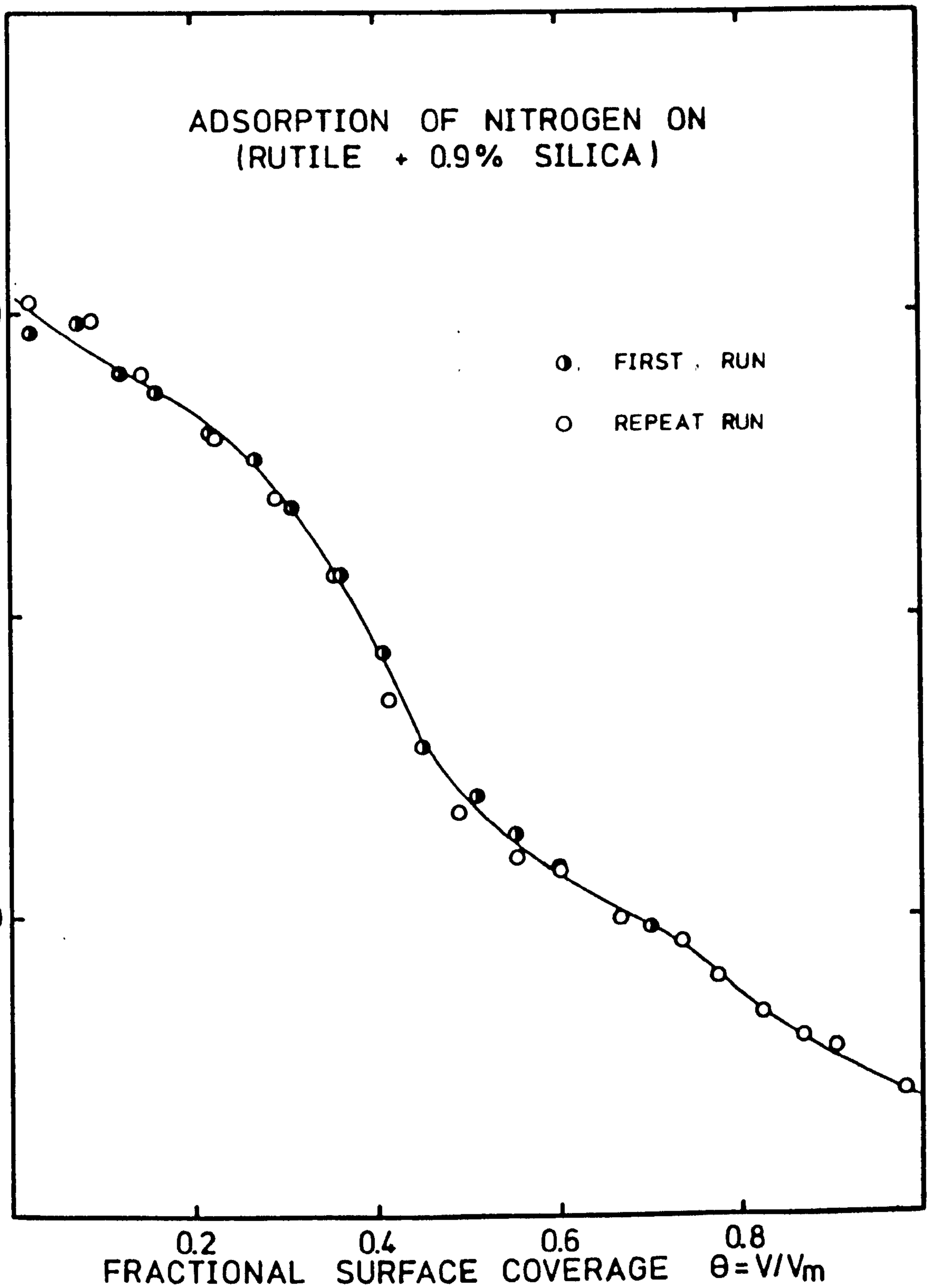

FIGURE 4-16

REPRODUCIBILITY OF MICROCALORIMETRY

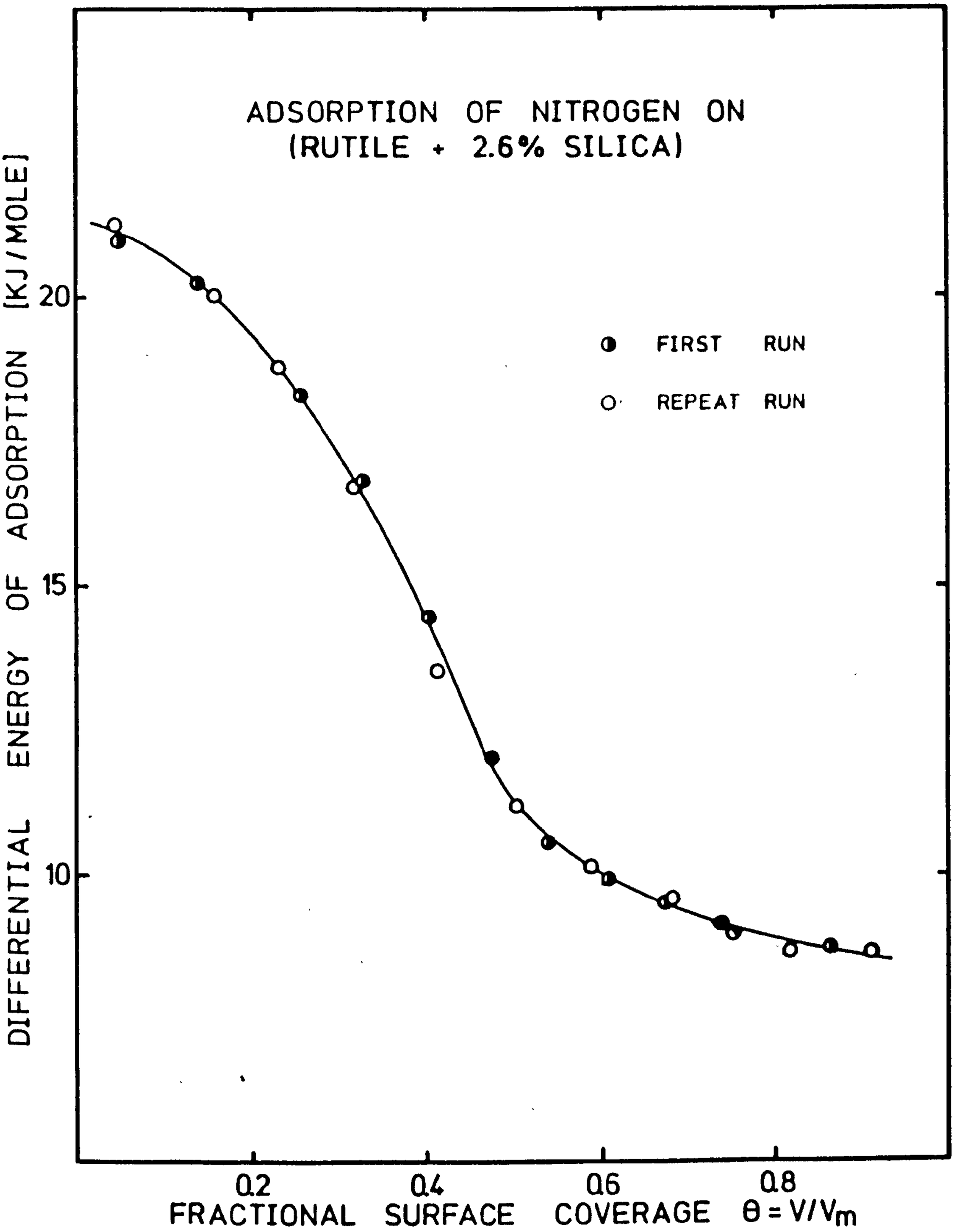

FIGURE 4-17

FIGURE 4-18

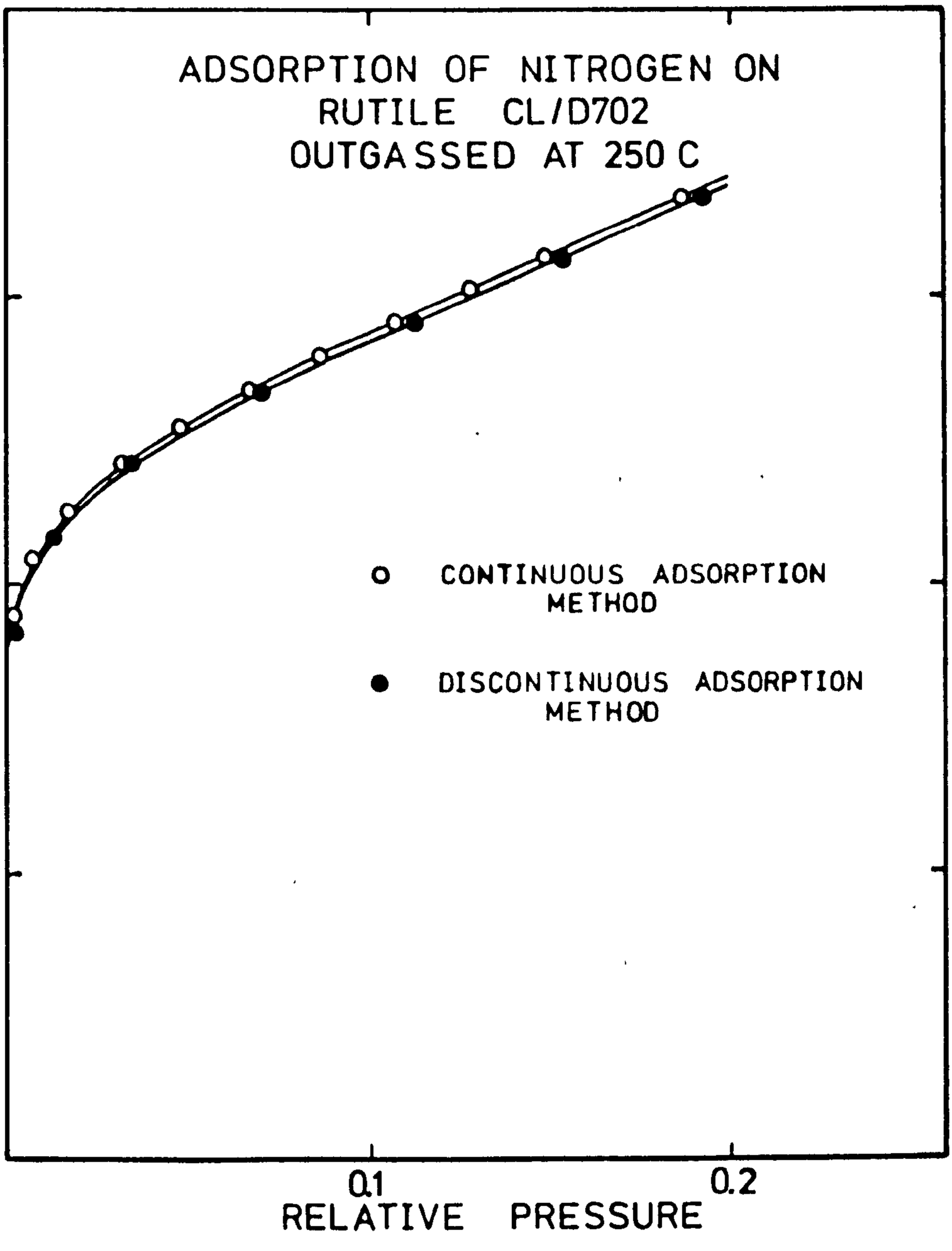
ADSORPTION OF NITROGEN ON
RUTILE CL/D702
OUTGASSED AT 250 C
VOLUME ADSORBED [cm³/gm at STP]
2
4
6
0.1
0.2
RELATIVE PRESSURE
CONTINUOUS ADSORPTION METHOD
DISCONTINUOUS ADSORPTION METHOD

CHAPTER 5: RESULTS AND DISCUSSION - I

PRELIMINARY RESULTS

5 - 1 Coating Experiments

Samples of silica-coated titanium dioxide were prepared using a method similar to that described by Iler[59] for the preparation of uniform coatings of silica on pigmentary rutile. The method involved concurrent addition of sodium silicate solution and sulphuric acid (3m) to a titanium dioxide slurry maintained at pH 10 and 90°C and vigorously stirred. Rates of addition of sodium silicate solutions varied according to their concentration, but in all preparations the silica content (as wt.% of titanium dioxide) was increased at a rate of 0.05 wt.% per minute. When addition of the required amount of sodium silicate was complete the slurry was stirred for one hour at pH 10/90°C, cooled to room temperature, filtered, washed and dried in a vacuum dessicator at room temperature. Portions of some prepared samples were redispersed in water and equilibrated for approximately half an hour at pH 7 or 2 and then filtered and dried at room temperature.

The experimental conditions and results of a number of preparations are given in Table 5-1. Several of these samples provided the basis for the characterization studies described in Chapters 6,7 and 8. Reference will be made in those Chapters to the "SAMPLE DESIGNATION" in Column 1 of Table 5-1 to denote the samples used in characterization studies. However, results obtained on silica-coated rutile samples will often be related to "the x wt.% silica sample" rather than to

TABLE 5 - 1

SUMMARY OF COATING PREPARATIONS

SAMPLE DESIGNATION	TITANIUM DIOXIDE BASE	SODIUM[a] SILICATE SOL'N	FINAL SILICA CONC'N (molar)	wt.% SILICA ADDED[b]	wt.% SILICA COATED	SAMPLE WASH pH
NF 1/2/73	RUTILE[c]	Freshly prepared and diluted (Stock Sol'n A)	1.0×10^{-1}	10.0	0.77	12.4
NF 2/2/73	CL/D702	"	"	10.0	0.59	7.0
NF 7/2/73	"	"	"	6.80	4.95	10.0
NF 8/2/73	"	"	"	6.80	4.99	7.0
NF 3/2/73	"	"	"	1.60	1.55	10.0
NF 4/2/73	"	"	"	1.60	1.35	7.0
NF 5/2/73	"	"	"	0.80	0.76	10.0
NF 6/2/73	"	"	"	0.80	0.62	7.0
NF 1/74	RUTILE	Freshly prepared and diluted (Stock Sol'n B)	2.0×10^{-2}	1.00	0.38	10.0
NF 2/74	CL/D702	"	"	1.00	0.35	7.0
NF 3/74	"	"	"	1.00	0.21	2.0
NF 4/74	"	"	"	2.00	0.52	10.0
NF 5/74	"	"	"	2.00	0.45	7.0
NF 6/74	"	"	"	2.00	0.28	2.0
NF 7/74	"	"	"	5.00	0.64	10.0
NF 8/74	"	"	"	5.00	0.48	7.0
NF 9/74	"	"	"	5.00	0.24	2.0

TABLE 5 - 1 (Cont'd)

SAMPLE DESIGNATION	TITANIUM DIOXIDE BASE	SODIUM(a) SILICATE SOL'N	FINAL SILICA CONC'N (molar)	wt.% SILICA ADDED(b)	wt.% SILICA COATED	SAMPLE WASH pH
NF 10/74	RUTILE	Stock Sol'n B aged 1 month before dilution	1.0×10^{-1}	1.90	0.83	10.0
NF 11/74	CL/D702	"	"	1.90	0.83	7.0
NF 14/74	"	"	"	1.90	0.47	10.0
NF 12/74	"	"	"	6.50	0.73	10.0
NF 11/2/73	RUTILE	COMMERCIAL	1.0×10^{-1}	1.00	0.46	7.0
NF 9/2/73	CL/D702	"	"	2.00	0.93	10.0
NF 10/2/73	"	"	"	2.00	0.82	7.0
NF 15/2/73	"	"	"	2.00	1.01	10.0
NF 16/2/73	"	"	"	2.00	0.88	7.0
NF 13/2/73	"	"	"	10.0	2.83	10.0
NF 14/2/73	"	"	"	10.0	2.55	7.0
NF 21/2/73	COMMERCIAL	COMMERCIAL	1.0×10^{-1}	1.00	0.41	10.0
NF 22/2/73	RUTILE C(c)	"	"	1.00	0.29	7.0
NF 17/2/73	"	As for NF1/2/73	"	2.00	0.65	10.0
NF 18/2/73	"	"	"	2.00	0.54	7.0
NF 19/2/73	"	COMMERCIAL	"	5.00	0.50	10.0
NF 20/2/73	"	"	"	5.00	0.44	7.0

(a) Sodium silicate solutions termed "fresh" for 2 days after preparation

(b) Wt.% Silica = (gms SiO_2/100gms TiO_2)

(c) Note: Surface Area of Rutile (CL/D702) approx 20 m^2/gm, Commercial Rutile C approx 7 m^2/gm

the "SAMPLE DESIGNATION" code.

The data in Table 5-1 show that under the conditions used the degree of coating achieved was very erratic. Changing from a pure rutile base to surface contaminated commercial rutile, or using commercial grade rather than pure sodium silicate solution had no obvious effect on the degree of coating.

Two general conclusions may be reached from the data presented in Table 5-1 with regard to the degree of coating at the two sodium silicate concentrations used:

(A) At both concentrations approximately 0.5 to 1 wt.% of silica was always incorporated onto the titanium dioxide.

(B) Higher degrees of coverage were often obtained when the final sodium silicate concentration was increased from 2.0×10^{-2} to 1.0×10^{-1}m.

From the review of solubility data for amorphous silica presented in Chapter 2-3 it can be stated that

(1) the solubility/pH curves at temperatures up to 100°C are approximately parallel

(2) the solubility at neutral pH is approximately 6×10^{-3}m at 90°C.

These facts enable the solubility/pH curve at 90°C to be drawn for amorphous silica (Figure 5-1). Also included in Figure 5-1 are the approximate "routes" with respect to pH and concentration taken by each successive addition of sodium silicate solution during a coating experiment. During each preparation the concentration of soluble silica

in the slurry is initially very low and increases during the preparation. In the case where the final concentration is 10^{-1}m the silica solution passes into the region of supersaturation where polymerization would occur. Hence at this concentration the titanium dioxide would be exposed to the sequence : monomeric - oligomeric - polymeric silica, whereas at the lower silica concentration of 2.0×10^{-2}m no polymeric silica would be expected to form. The data from coating experiments are consistent then with two types of silica - titania interaction :

(1) interaction of low molecular weight silica, most likely monomeric species, leading to the incorporation of between 0.5 and 1.0 wt.% silica.

(2) interaction of polymeric silica with titania, or polymerization of silica on the surface of titanium dioxide particles, leading to the uptake of greater amounts of silica than occurred in (1). The final concentrations of aqueous silica achieved in the coating experiments were near the polymerization line at pH 10. As was stressed in Chapter 2-3 the position of this line (Figure 5-1) is not precisely known. Small pH variations and local increases in concentration may occur during coating preparations and it is not therefore surprising that the results in Table 5-1 indicate a haphazard occurrence of polymerization leading to higher levels of silica coating.

The results in Table 5-1 indicate that for the low levels of silica of approximately 0.5 wt.% washing at pH 7 removed relatively little silica whilst washing at pH 2 removed relatively more silica, leaving only approximately 0.2 wt.% silica. This trend will be further discussed in Chapter 8.

5 - 2 Transmission Electron Micrographs

In the discussion in section 5-1 it has been assumed that the silica analysed in prepared samples exists on the surface of the titanium dioxide particles and is not the result of precipitation of silica in bulk solution. This view is reinforced by the transmission electron micrographs (magnification 2 x 10^5) of some representative samples covering the range of silica coatings obtained (Figures 5-2 to 5-5). Some approximate calculations based on the two possible extremes of form of the silica present are useful:

(A) Assume that all of the silica has polymerized in bulk solution producing spherical amorphous silica particles, (Figure 2-10). As the amount of silica is expressed from analysis as wt.% of titanium dioxide, propose that one colloidal silica particle is formed per titanium dioxide particle. Figure 3-2 shows that the base titanium dioxide particles may be reasonably well approximated by cylindrical rods of 40 x 200 nm. Given these dimensions the diameter of each hypothetical colloidal silica particle corresponding to a given wt.% silica analysis can be calculated. Some representative values are given in the following table:

Wt.% silica	Diameter of Colloidal Particle
0.5	18 nm.
1.0	20 nm.
2.5	30 nm.
5.0	35 nm.

(B) Assuming that the cylindrical rods of titanium dioxide are covered with a uniform surface coating of amorphous silica, the coating thickness corresponding to a given wt.% silica can be calculated. Some values are given in the table below.

Wt.% silica	Thickness of Coating
0.5	0.5 nm.
1.0	1.0 nm.
2.5	2.5 nm.
5.0	5.0 nm.

The limit of resolution of the electron microscope used was of the order of 2 nm. The micrographs of 2.6 and 5.0 wt.% silica-coated titanium dioxide (Figures 5-4 and 5-5) show a uniform surface coating of the order of thickness given by the calculations (B) above. This correlation indicates that although the microscope only shows coatings on surfaces parallel to the electron beam it may be assumed that the particle surfaces are uniformly covered. Uniform surface coatings corresponding to weight % silica less than 2, according to the calculations in (B) above, would not be clearly resolved by the electron microscope. Indeed for the sample containing 0.6 wt.% silica no coating is apparent (Figure 5-2) whilst the slight coating seen on the sample with 1.4 wt.% silica (Figure 5-3) may be real or due to anomalous beam effects. If, on the other hand, the silica in these latter samples had been present as colloidal particles, then the calculations (A) indicate that these particles ought to be clearly visible at the magnification of 2×10^5. For the samples which have been exposed to silica (Figures 5-2 to 5-5) there are no more particles of the dimensions

indicated in the calculations (A) than are present in the sample of pure rutile base (Figure 3-2).

The electron micrographs therefore provide evidence that during the preparations described in section 5-1 the formation of polymeric silica is associated with the growth of a coating on the surface of titanium dioxide particles.

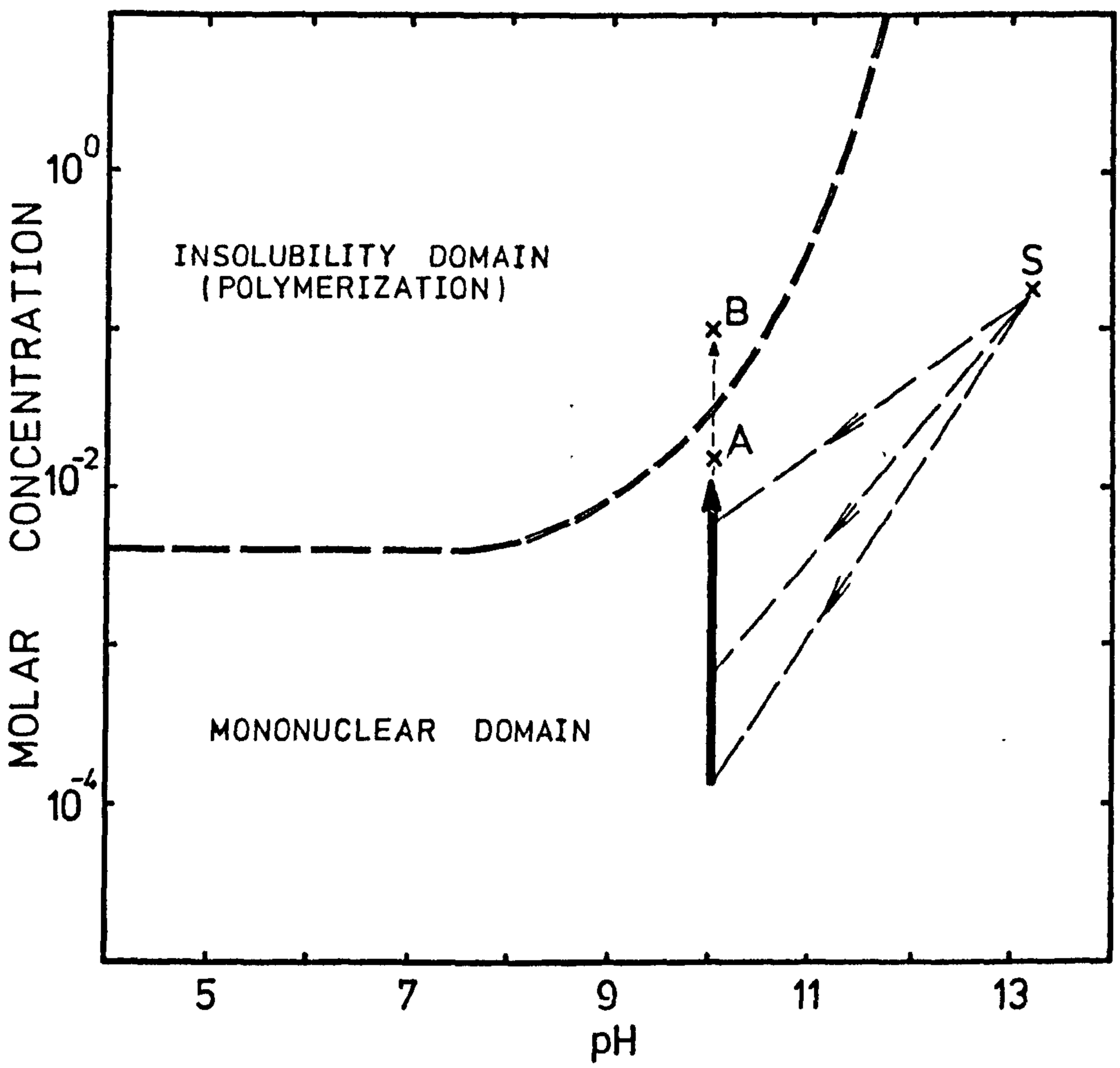
AQUEOUS SILICA SPECIES AT 90°C
MOLAR CONCENTRATION
10^{0}
10^{-2}
10^{-4}
INSOLUBILITY DOMAIN
(POLYMERIZATION)
MONONUCLEAR DOMAIN
B
A
S
5
7
9
11
13
pH
——APPROXIMATE CONCENTRATION ABOVE WHICH POLYMERIZATION WILL OCCUR AT 90° C
CONCENTRATION AND pH OF:
S ——— ADDED SODIUM SILICATE SOLUTION
A,B ——— COATING SOLUTION AFTER ADDITION OF SODIUM SILICATE SOLUTION (A=2×10⁻² m, B=10⁻¹ m)
CHANGE IN CONCENTRATION OF SILICA IN COATING SOLUTION DURING COATING EXPERIMENT

FIGURE 5-1

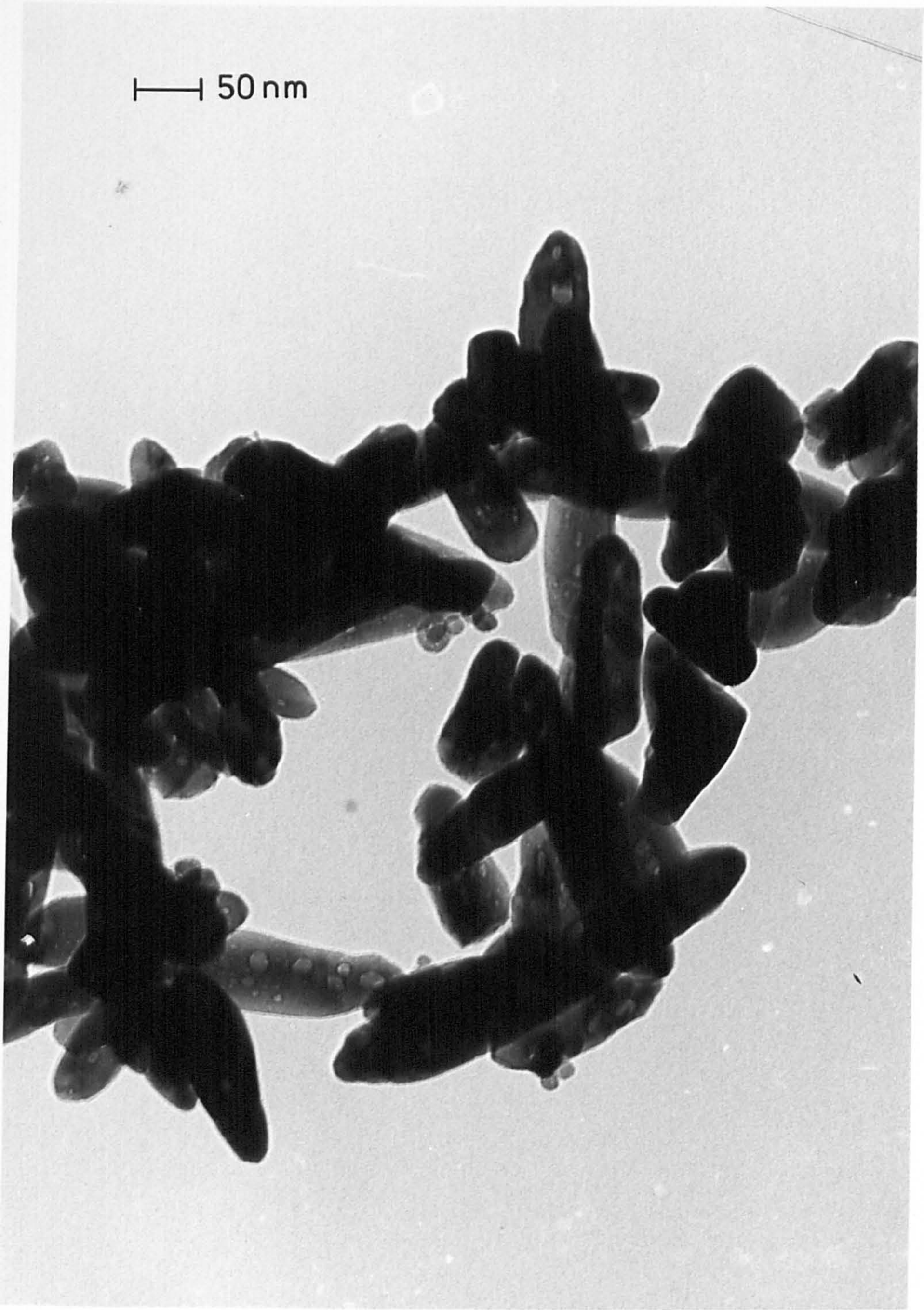

FIGURE 5-2

Transmission Electron Micrograph
(magnification 200,000)
(BASE RUTILE + 0.6 WT% SILICA)

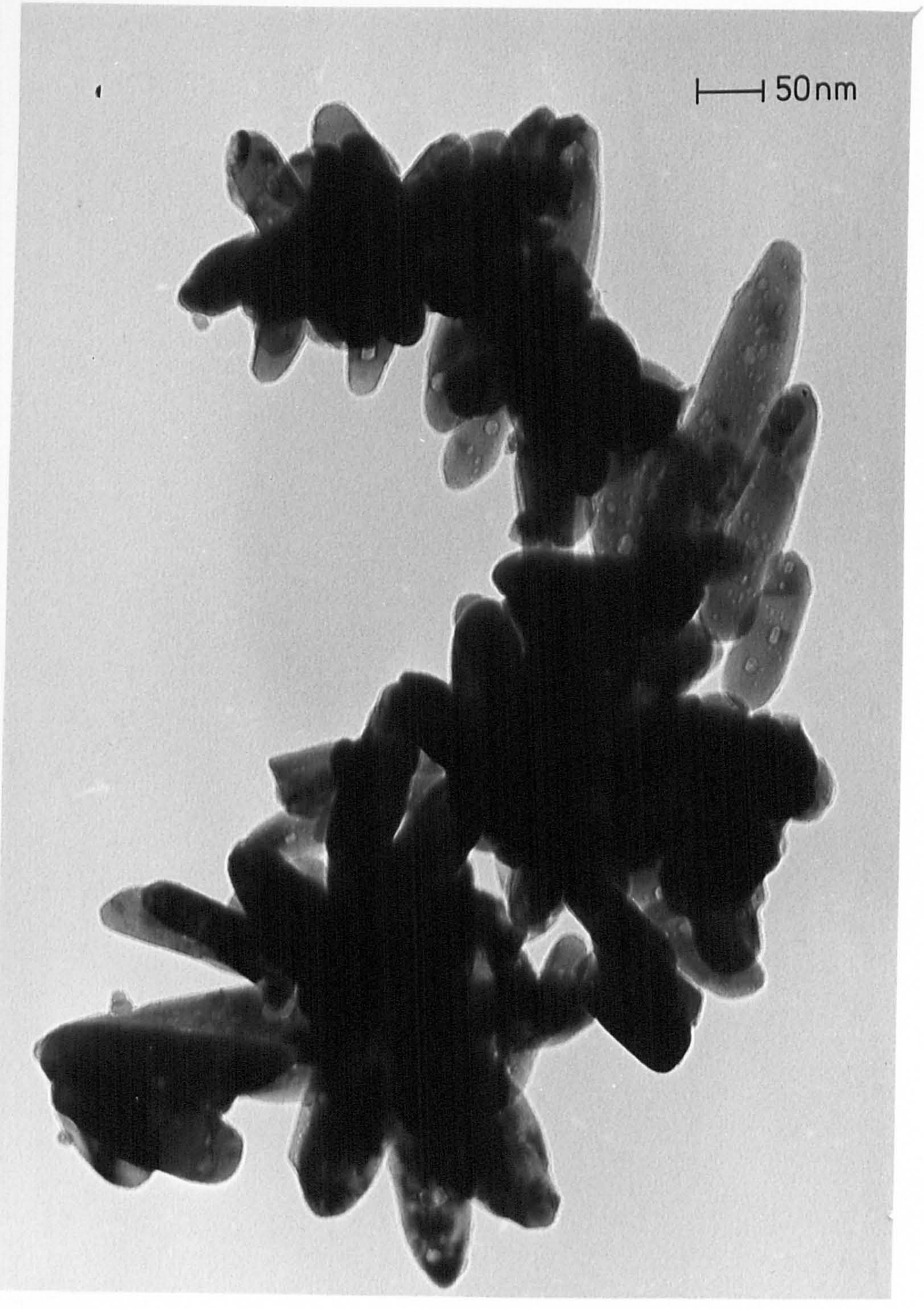

FIGURE 5-3

Transmission Electron Micrograph
(magnification 200,000)
(BASE RUTILE + 1.4 WT% SILICA)

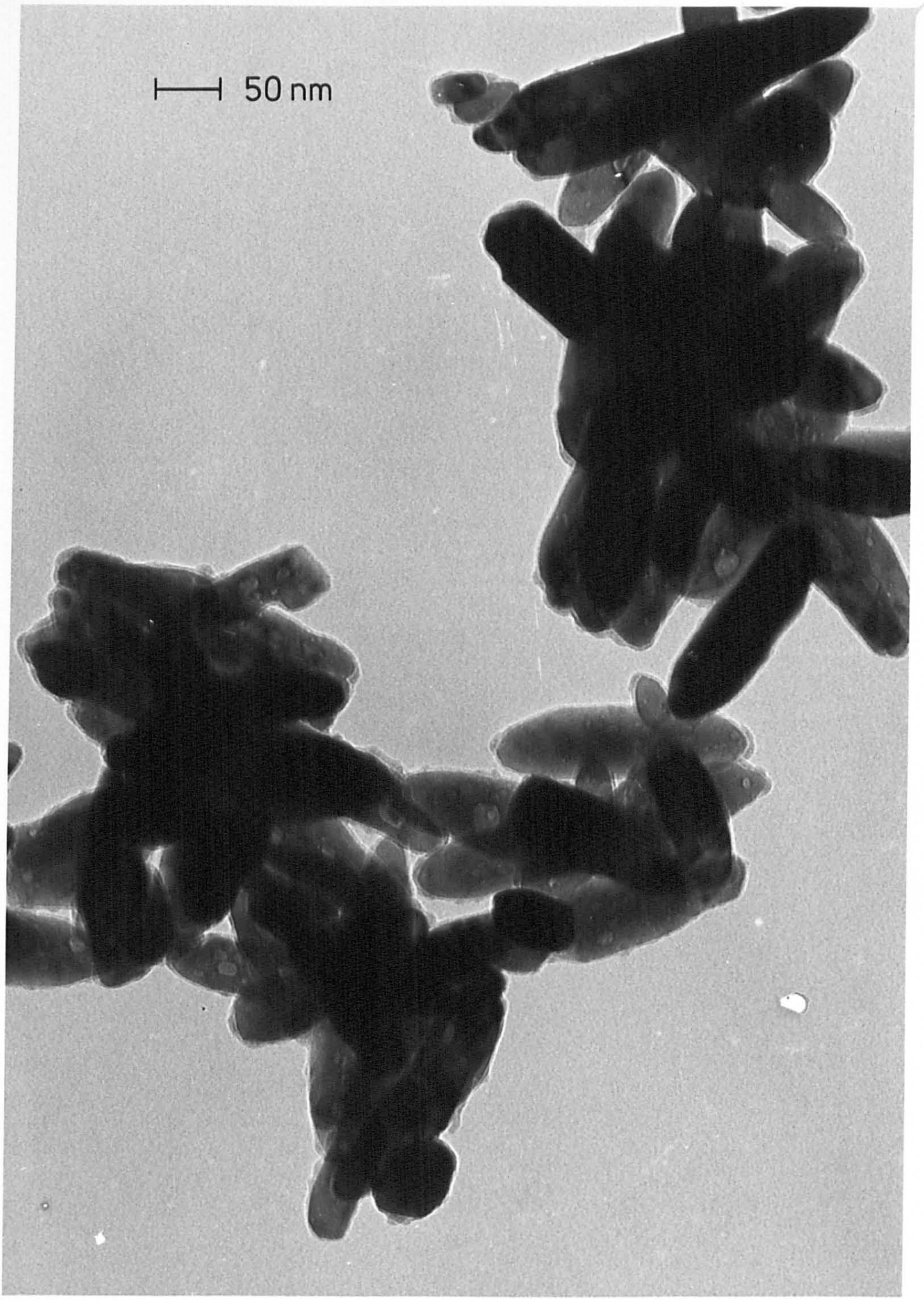

FIGURE 5-4

Transmission Electron Micrograph
(magnification 200,000)
(BASE RUTILE + 2.6 WT% SILICA)

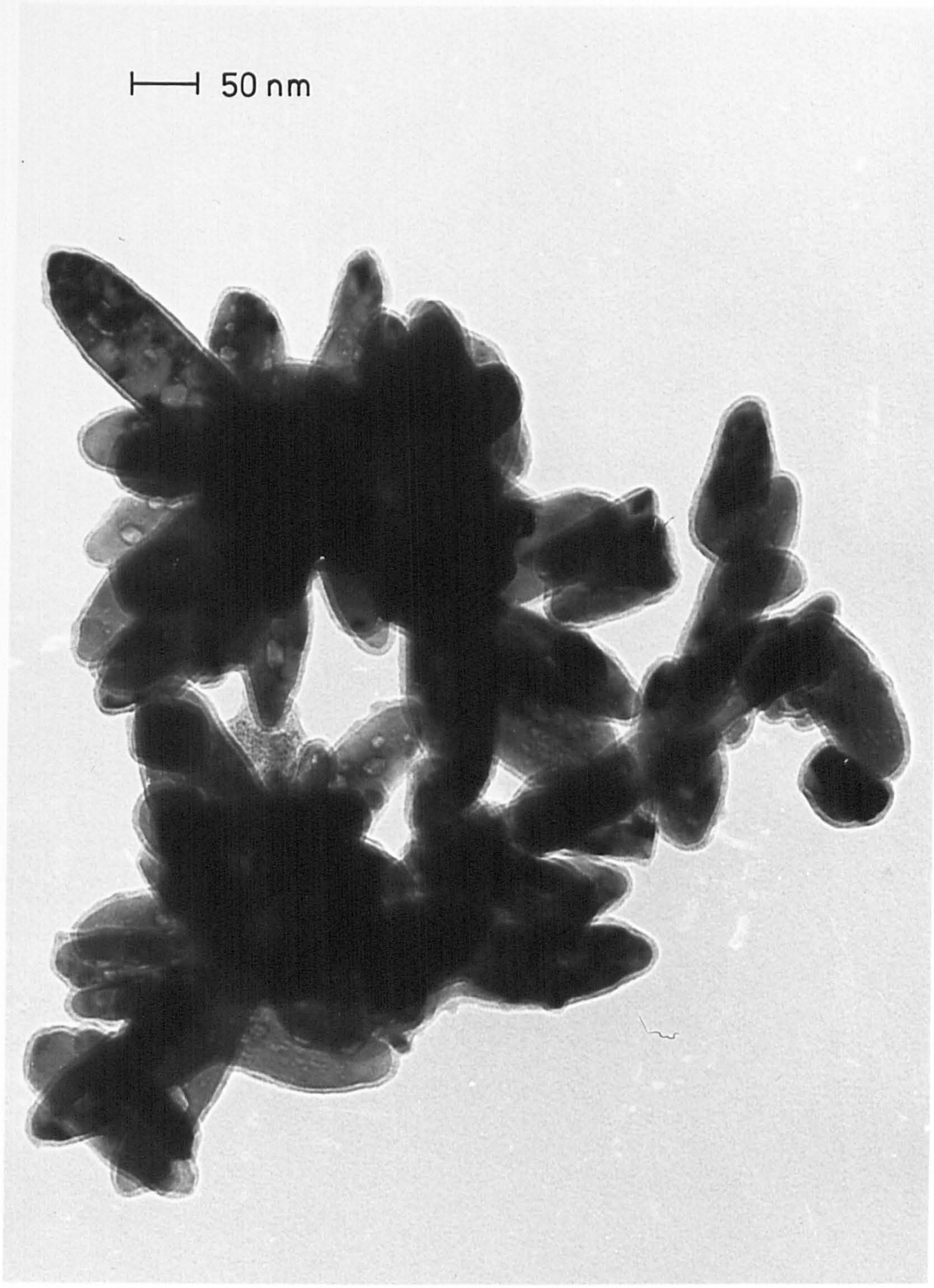

FIGURE 5-5

Transmission Electron Micrograph
(magnification 200,000)
(BASE RUTILE + 5.0 WT% SILICA)

CHAPTER 6: RESULTS AND DISCUSSION -- II

ELECTROKINETIC STUDIES

The technique of microelectrophoresis has been used for investigating the nature of silica-coated rutile surfaces and the interactions between aqueous silica species and colloidal titanium dioxide particles. In the discussion of results many of the concepts of electrical double layer theory and of the nature of silica in aqueous solution, previously outlined in Chapters 2-1 and 2-3 respectively, will be utilised.

A brief preliminary study of the electrokinetic properties of the titanium dioxide samples used in the present work is included as Section 1 of this Chapter.

6 - 1 The i.e.p. of Titanium Dioxide

For a given metal oxide the main factors which can change its isoelectric point are[330]:

(1) surface contamination,

(2) surface structure - including surface defects,

(3) surface hydration/dehydration.

Numerous studies[121,143-144,330-332] have shown that all three factors can lead to changes in the i.e.p. of titanium dioxide. Although a clear distinction cannot always be made between the above effects[144], the wide range of values (pH 3.5 to 7.2) reported in the literature for the i.e.p. of titanium dioxide[333] emphasizes the need for carefully

controlled experimental conditions in any study of its electrokinetic properties.

In order, therefore, to use electrophoretic mobility to assess the nature of silica coatings and coating processes on titanium dioxide (section 6-2) it was necessary that the electrokinetic properties of the samples used be well characterized and reproducible. The two samples of titanium dioxide, pure rutile CL/D702 and a commercial rutile (Rutile C), have been characterized electrokinetically and some relevant data are given in Table 6-1. Both samples gave stable i.e.p. values, the pure rutile only after extensive ageing. The electrophoretic mobility curves giving i.e.p. values of 5.5 and 4.3 for CL/D702 and Rutile C respectively will be used in further work.

In order to relate the i.e.p. values in Table 6-1 to surface properties of the samples, it will be assumed here that surface charge is acquired by dissociation of surface hydroxyl groups and that the electrical double layer at the titanium dioxide/indifferent electrolyte interface may be described by a Grahame type of model (Chapter 2-1). Therefore (1) the total double layer potential $\psi(0)$ is controlled by solution pH and at constant ionic strength the electrophoretic mobility changes in direct relation to changes in $\psi(0)$, and (2) the magnitude of $\psi(0)$ is controlled by the acid/base character of surface hydroxyl groups. This model is appropriate to these samples as only comparisons between similar non-porous surfaces are involved.

The purity of the rutile CL/D702 is indicated by the very small shift in i.e.p. after soxhlet washing and heat treatment, a cleaning

TABLE 6 - 1

ISO-ELECTRIC POINTS OF TITANIUM DIOXIDE SAMPLES

SAMPLE	SUCCESSIVE TREATMENTS	i.e.p.
PURE RUTILE CL/D702	As received, approximately one month after preparation.	4.8
	After 12 successive soxhlet wash/heat at 450°C treatments[143]	5.0
	After acid leaching by vigorous stirring in boiling 10% HNO_3[110] for 1 week, followed by soxhlet washing for 1 week.	5.0
	Aged in air for 6 months.	5.5
	Aged in air for 12 months.	5.5
	Heated in air at 850°C/24 hours.	4.8
ANATASE CL/D731	As received.	6.0
	Heated in air at 850°C/24 hours.	4.6
	Aged in air for 6 months.	3.6
	Aged in air for 12 months.	3.5
	Acid leached/soxhlet washed as described above.	4.8
COMMERCIAL RUTILE - C	As received, approximately one month after preparation.	4.3
	Soxhlet washed in water for 1 week.	4.3
	Acid leached/soxhlet washed as described above.	4.8
	Aged in air for 6 months.	4.3

procedure designed to remove both bulk and surface chloride[143]. Rutile C, on the other hand, shows an increase in i.e.p. after vigorous cleaning[110] and the i.e.p. of 4.8 is more likely to be that of the clean surface. Rutile CL/D702 had been heated in air at 450°C during preparation, Rutile C at 850°C. It can be seen from Table 6-1 that heating of fully aged rutile CL/D702 at 850°C has lowered its i.e.p. from 5.5 to 4.8. Further information on the effect of heat treatment on the i.e.p. of titanium dioxide can be obtained from the results for anatase CL/D731 given in Table 6-1. This sample was prepared by the hydrolysis of titanyl sulphate. The only significant impurities in this sample were 0.05 wt.% sulphate (expressed as SO_3) and 0.01 wt.% of K_2O. The sample also contained 0.3 wt.% of the rutile form of titanium dioxide. As prepared, anatase CL/D731 gave an i.e.p. of 6.0. Such a value is slightly lower than most values in the literature for anatase[144,332,352-354], (up to 0.6 pH units lower) which probably indicates the presence of anionic sulphate[332] on the surface of CL/D731. Heating in the temperature range 800 to 1100°C has been reported to result in conversion of anatase to rutile[355-356]. When CL/D731 was heated in air at 850°C for 24 hours an 86% conversion to rutile was achieved and the i.e.p. was lowered from 6.0 to 4.6. Such a lowering of i.e.p. on conversion of anatase to rutile has been previously observed[144,332] although in some studies[144] changes have not been interpreted in terms of phase transition. After ageing in air for 6 months the i.e.p. of the 86% rutile sample had dropped to 3.6 and appeared stable at this value for a further 6 months. The fully aged sample when thoroughly surface cleaned gave an i.e.p. of 4.8. It appears that the drop in i.e.p. on ageing in air was due to the slow

diffusion of anionic impurities from the bulk of the titanium dioxide particle to the surface.

The data for the three titanium dioxide samples given in Table 6-1 indicate that heating of titanium dioxide at 850°C causes an irreversible lowering of its isoelectric point to 4.8. Heating at 450°C may cause a lowering of i.e.p. but these surfaces slowly change to give an equilibrium value of approximately 5.5. It is known that titanium dioxide surfaces heated at 450 to 850°C will undergo

(i) reduction, in a non-oxidising atmosphere or in the presence of surface impurities[341]. Bérubé and de Bruyn have shown[121] however, that heat treatment under controlled non-reducing conditions does not affect the changes observed in surface charge properties due to that heat treatment,

(ii) dehydroxylation and dehydration[304,334-337] and

(iii) structural change. Although titanium dioxide surfaces contain defects at lower temperatures[339], heating from 450 to 850°C would greatly increase their number[12]. The slow upward drift of i.e.p. for CL/D702 would be consistent with slow rehydration and rehydroxylation of the surface. These processes have been shown to be irreversible in the gas phase, at least after 450°C outgassing[214,306,338] and although they have been claimed to be fully reversible in the liquid phase[306] there is some evidence from heats of immersion studies that they may be very slow [340,357]. The non-reversible lowering of i.e.p at 850°C is most likely due to permanent structural change in the surface region and probably some distance into the bulk particle. The change is sufficient to give a significantly different environment for

the surface hydroxyl groups formed on rehydration[331], and hence a different i.e.p.[330]. Such changes would be consistent with recently proposed models for the structure of titanium dioxide surfaces in which the nature of hydrating species depends on the nature of the surface crystal plane[162-163].

6 - 2 Silica-Coated Rutile

The electrophoretic mobility/pH curves for silica-coated titanium dioxide samples NF 6/2/73, NF 4/2/73, NF 14/2/73 and NF 8/2/73, along with that of the titanium dioxide base (rutile CL/D702) are given in Figures 6-1 to 6-4. These samples are those for which electron micrographs are shown in Chapter 5 and they contain 0.6, 1.4, 2.6 and 5.0 wt.% silica respectively. All of these mobility curves were obtained using dispersions containing 0.1gm/litre of solid and at constant ionic strength of 10^{-2}m KNO_3. Potassium nitrate has been shown not to specifically adsorb onto titanium dioxide[143,144], (an INDIFFERENT electrolyte). Each dispersion was equilibrated at pH 8 to 9 for 24 hours prior to commencement of mobility measurements. At least one hour was allowed for equilibrium at each pH value; the dispersion was left overnight at low pH (<3) before the "increasing pH" run was commenced. In no run was sufficient acid or base added to significantly change the total ionic strength of the electrolyte solution.

The mobility/pH curves show two marked patterns of behaviour depending on the pH history of the dispersion.

(i) Decreasing pH run: On initial lowering of pH from about 8 all samples gave smooth mobility/pH curves with the i.e.p. lower for

samples containing more silica. Values for the i.e.p. of amorphous silica reported in the literature[330,342] cover the pH range 1.0 to 3.0. The mobility curve given by the 5.0 wt.% silica sample is therefore consistent with a surface behaving similarly to amorphous silica.

Parks[147] has shown that for mixed oxide surfaces the i.e.p. would be a weighted average of the i.e.p. values of the various components. Parks' concepts would therefore indicate that the increasing of wt.% silica from 0.6 to 5.0 in the samples studied corresponded to a gradual covering of the titanium dioxide surface with silica. The model of Parks is inappropriate for the system studied in the present work for the following reasons:

(A) It assumes that patches on the surface behave as pure components, i.e. mixed oxides are formed in which surface groups, such as hydroxyls, experience forces from within the particle equivalent to those on the surface of a one component particle. This is unlikely to be so on surfaces containing a thin coating of one component on a particle of another component.

(B) The i.e.p. of the 5.0 wt.% silica sample (3.0) is on the high end of reported values for amorphous silica; lower i.e.p. values have also been reported for silica-coated rutile[50]. Parks' model would therefore predict that the 5.0 wt.% sample consisted largely of silanol groups with some areas of bare titanium dioxide surface. In order that this be the case, and that this sample gives the appearance of having a uniform surface coating as it does under the electron microscope, it must be proposed that Ti-OH groups exist under the amorphous silica network and are accessible to protons and hydroxyl ions in order to contribute to the charge behaviour of the particle.

The existence of Ti-OH groups in such an environment is thought unlikely.

An alternative approach which is similar to the above model but more realistic and consistent with the mobility data is as follows. It is proposed that a gel layer type of model (see Chapter 2-1) is applicable to the coated rutile/electrolyte interface.

Over the pH range 3 to 8 the solubility of amorphous silica will be small and it is reasonable to propose "surface" charge in the silica-coated rutile samples is generated by the dissociation of silanol groups. These samples were prepared at pH 10 and 90°C and neutralised to pH 7. Polymerization of silica under these conditions in the absence of titanium dioxide would be expected to give colloidal particles containing few internal hydroxyl groups. There is no evidence in electron micrographs (Chapter 5-2) for the formation of colloidal silica in bulk solution in the presence of titanium dioxide particles, and it appears that the patterns established for the polymerization of silica in bulk solution may have been changed. It is then possible that the coating structure contains some internal hydroxyl groups which are accessible to aqueous hydrogen and hydroxyl ions and therefore contribute to the "total surface charge" of the particle. Similarly penetration of counter ions into the coating may occur leading to smaller mobilities if the electrokinetic shear plane were located at the coating/electrolyte boundary. This model would predict that even though the sample with 5.0 wt.% silica had a uniform surface coating of silica, the dissociation behaviour of some silanol groups would be greatly affected by the field of the underlying titanium

dioxide structure. The isoelectric point would therefore be at a slightly higher pH than that of pure amorphous silica. The data in Figures 6-2, 6-3 and 6-4 show that the i.e.p. is lowered only slightly when the wt.% silica increases from 1.4 to 5.0. This would be consistent with a number of silanol groups in close proximity to the titanium dioxide particle and, as the wt.% silica increases, more silanol groups being added and having dissociation characteristics less affected by the titanium dioxide. The i.e.p. of the sample containing 0.6 wt.% silica is only 0.3 pH units below that of the base rutile whilst that of the 1.4 wt.% sample is 2 pH units lower. This would indicate that the dissociation of surface groups on the 0.6 wt.% silica sample was very much more influenced by the underlying titanium dioxide particle. In view of the small differences observed in increasing silica content from 1.4 to 2.5 wt.% it is more likely that the 0.6 wt.% sample contains only a partial coating of silica and some Ti-OH groups are also present on the surface. This is not surprising bearing in mind the calculations in Chapter 5-2 which showed that if this sample contained a completely covered rutile surface the coating would only be around 0.5nm in thickness.

(ii) Increasing pH run: All four of the silica-coated rutile samples gave "increasing pH" mobility curves which deviate from the "decreasing pH" curves over the pH range 4 to 5. In the case of the 0.6 and 1.4 wt.% silica samples the mobility curves are similar at pH greater than 5 with values of i.e.p. of 5.4 and 5.2 respectively. These are close to that of the base rutile itself (5.5). The 2.6 and 5.0 wt.% silica samples showed less irreversibility with respect to pH and gave an "increasing pH" i.e.p. of less than 3.5.

Further evidence of the irreversible nature of the mobility curves is given in Figures 6-5 and 6-6. Dispersions for these runs contained 0.1gm/litre of sample and 10^{-2}m KNO_3. Figure 6-5 shows that 3 weeks soaking in water at pH 7 of the sample containing 5.0 wt.% silica produced little change in subsequent mobility/pH behaviour. Soaking of this sample at pH 2 resulted in an upward shift of i.e.p. to 4.0. The sample did not show any irreversibility in mobility as a function of pH during the electrophoresis experiment. The results of ageing of the sample with 1.4 wt.% silica in water vapour and liquid water at pH 7 are more complex. Whilst both ageing processes resulted in an upward shift in i.e.p. of approximately one unit, the "decreasing pH" curve showed a marked point of inflection at pH 4.5 for the sample aged in water vapour. During ageing in water vapour nothing was removed from the sample. However, after ageing in liquid water samples were filtered and dried at room temperature prior to being redispersed in electrolyte for mobility measurements. Any silica dissolved during ageing was not present in the subsequent microelectrophoresis experiment. From the data in Figures 6-5 and 6-6 it can be concluded that (a) changes in the double layer of the 5.0 wt.% silica sample occurred at pH 2 but not pH 7, (b) ageing of the 1.4 wt.% sample is similar in liquid water at pH 7 and water vapour, and (c) changes occurring over the pH region 4 to 5 are closely associated with a change in the nature of the silica present in the sample.

Before discussing the nature of ageing at pH about 2 and the subsequent changes in the nature of the silica at pH 4 to 5, it will be useful to consider the mobility data in Figures 6-7 to 6-10. The

mobility/pH curves given in these figures are for titanium dioxide in the presence of dilute solutions of sodium silicate. (The solution will henceforth be termed "aqueous silica" as the form of silica varies with solution pH). The reasons why more concentrated solutions could not be used were two fold:

(a) as it was intended to try and detect changes in the double layer due to interactions of silica with the titanium dioxide surface which would perhaps be small, measured mobilities should be reasonably large. This requires as low a total ionic strength as practical.

(b) silica solutions involve acid/base equilibria and concentrated solutions would require large amounts of added acid and base to change solution pH. Hence a high concentration of indifferent electrolyte would be needed to ensure a constant total ionic strength.

A compromise between (a) and (b) was achieved using 10^{-2}m KNO_3 and 1.2×10^{-5}m or 1.0×10^{-4}m aqueous silica. Additions of acid and base during mobility/pH runs were measured, and based on the data of Hunter[118], the maximum change in mobility due to change in total ionic strength over a "decreased pH — increased pH" cycle was 0.25 mobility units. This variation agrees with the variations in final mobility values shown in Figure 6-10 at the end of the pH cycles undertaken. Clearly none of the abrupt changes in mobility seen in Figures 6-7 to 6-10 are due to changes in ionic strength. The weight % silica present in the system was varied by using one of the two silica solutions and changing the solids content of the dispersion from 0.02 to 0.1gm/litre.

The mobility/pH curves for pure rutile CL/D702 in two different silica solutions and at various silica/titania ratios are given in

Figures 6-7 and 6-8. These data show that an i.e.p. of from 5.5 to 2.5 can be obtained indicating substantial interaction of silica from solution with the titanium dioxide surface over the pH range 9.0 to 2.5. When the experimental i.e p. is plotted as a function of the wt.% silica present a reasonable correlation is obtained with the i.e.p. of samples with known wt.% silica coatings (Figure 6-11). A relatively large degree of scatter occurred, probably due to inaccuracies in the effective % solids contents of dispersions due to particles adhering to the walls of the equilibration vessel and circulation tubing. All mobility curves in Figures 6-7 and 6-8 show a marked inflection at pH 4 to 5 indicating a change in the double layer yielding a lower i.e.p. The more carefully controlled experiments (Figure 6-8) showed that a marked change in mobility also occurred at pH 7.5. This change at pH 7.5 led to a lower i.e.p. in the 1.0 wt.% silica systems but not in the 0.5 wt.% silica system.

The mobility curves in Figures 6-9 and 6-10 show that regardless of the nature of the "decreasing pH" curve in the presence of aqueous silica, all silica is removed from the inner region of the rutile/ electrolyte double layer during the "increasing pH" run over the pH range 4 to 5. Included in Figure 6-10 is a mobility curve obtained by Wiseman[49] using a similar system to those in the present work but with a very much higher silica concentration. As would be expected from double layer theory Wiseman obtained much smaller mobilities than reported in the present work. Wiseman did not observe any abrupt changes in mobility but did obtain an apparent i.e.p. of less than 2. The remainder of the data in Figure 6-10 show that the patterns of behaviour in Figures 6-7 to 6-9 for pure rutile CL/D702 are also

observed when a rutile pigment base (made via the sulphate process) is used instead.

The mobility data presented in Figures 6-1 to 6-10 indicate that three regions of pH are significant with regard to interactions between aqueous silica species and colloidal titanium dioxide particles:

(A) pH 7 to 8: It is known that in supersaturated aqueous solutions of silica polymerization to give relatively dense colloidal particles will occur rapidly in slightly alkaline solutions. For these particles to influence the electrokinetic behaviour of titanium dioxide particles in the same solution, they must be absorbed into the inner regions of the electrical double layer and be well attached so as not to be displaced under the conditions of shear in an electrophoresis experiment. The aqueous silica solutions used in the microelectrophoresis experiments reported in the present work were much too dilute to be in a supersaturated condition at any pH. At pH 7 to 8 both titanium dioxide and colloidal silica particles would be negatively charged. Hence a sufficient number of attachments between these particles to strongly connect them is electrostatically unfavourable.

It is more likely that the adsorbing species at pH 7 to 8 are monomeric — $Si(OH)_4$ and $SiO(OH)_3^-$. The equilibrium diagram for aqueous silica (Figure 2-9) shows that at a concentration of approximately 10^{-4}m the predominant silica species changes from $SiO(OH)_3^-$ to $Si(OH)_4$ over the pH range 8 to 7. An hydroxylated rutile surface would contain $Ti\text{-}O^-$ surface sites at pH 7 to 8 and electrostatic interactions

would favour adsorption of the uncharged $Si(OH)_4$ species at these sites. The nature of the surface species formed cannot be deduced from the present work, but infra-red studies[143,343] have shown that surface $Ti-O-Si(OH)_3$ species can be produced by interaction of titanium dioxide with silicon tetrachloride in the gas phase, followed by hydrolysis. It seems likely that similar species would be formed by adsorption of $Si(OH)_4$ from the liquid phase. Parfitt et al[143] have determined electrophoretic mobilities of titanium dioxide containing the $Ti-O-Si(OH)_3$ surface species and observed that substantial numbers of these species may be present without lowering the measured i.e.p. of the surface. This observation is consistent with the present work (Figure 6-8). Parfitt[143] explains this qualitatively by saying that the remaining rutile hydroxyl groups are sufficient to dominate the surface charge. It is a little surprising, however, that no downward shift at all is observed in the i.e.p. especially as Parfitt[143] shows an i.e.p. reduced from 6 to 2.5, due he claims to a more extensive surface coverage of silanol groups.

For the adsorption of monomeric silica species to cause a lowering of the i.e.p. of a rutile surface whose charge is generated by the dissociation of surface hydroxyl groups, it is necessary that:

(i) monomers adsorb as charged species in excess of that required by electrostatic interactions (Figure 2-3).

The 1 : 1 interaction giving $Ti-O-Si(OH)_3$ surface species would not fulfill this requirement.

(ii) the surface silanol groups dissociate. This implies dissociation of the OH groups in $Ti-O-Si(OH)_3$.

(iii) the monomers adsorb onto specific types of surface site on titanium dioxide, thus altering not only the number of Ti-OH or other surface groups but also the average dissociation behaviour of the surface. Such specific site adsorption has been suggested for the adsorption of silica onto fluorites[349].

No distinction between (ii) and (iii) for the adsorption of $Si(OH)_4$ can be made from the data presented in this Chapter. However, the fact that initial adsorption of monomeric silica does not lower the i.e.p. of the rutile whilst subsequent adsorption does (Figure 6-8), is an indication that initial adsorption may occur onto a "non-charge contributing" part of the rutile surface. It should be noted that discussion above concerning the adsorption of silica at pH 7 to 8 does not preclude the possibility of some form of silica already being present on the surface at higher pH.

(B) pH 4 to 5: There appear to be three possible processes which would explain the marked mobility changes at pH 4 to 5 in the "decreasing pH" curves of Figures 6-7, 6-8 and 6-9:

(i) enhanced adsorption of monomeric silica due to increasing positive charge on the titanium dioxide surface. The facts that a solid with a significantly lower i.e.p. still gave changes over pH 4 - 5 (Figure 6-10), and that the ageing experiments indicate that the change at pH 4-5 corresponds to a change in the nature of the adsorbed silica, would tend to rule out this increased adsorption of monomer. Other investigations[344-346] have shown that on substrates such as alumina and geothite adsorption of monomeric silica decreases at pH less than 5. Parfitt et al[143] have shown that in systems where monomeric silica has been preadsorbed onto rutile, in the subsequent

electrophoresis experiment abrupt changes from a smooth mobility curve do occur at pH 4-5. In this work no additional silica was present to give enhanced adsorption of silica at this pH. There is substantial evidence therefore, both from the present and previous investigations, that enhanced adsorption of monomeric silica does not occur at pH 4 to 5.

(ii) in systems where no change in the amount of silica present is possible the abrupt changes at pH 4 to 5 may indicate a flattening out of adsorbed silica to give greater effective coverage of the rutile surface. This flattening out might occur in response to the electrostatic attraction between a positive rutile surface and adsorbed anionic silica. However, for the reasons given in (A) above this mechanism appears unlikely in the present work.

(iii) polymerization of silica at the solid/liquid interface may be occurring with preadsorbed monomeric species acting as "anchors" holding the polymeric silica onto the titanium dioxide surface. At the concentrations used for the microelectrophoresis runs in Figures 6-7 to 6-10 all soluble silica should be monomeric (Figure 2-9). However it has been shown[347-348] that the conditions of precipitation of metal hydroxides can be drastically altered in the vicinity of colloidal particle surfaces. The shapes of the mobility curves in Figures 6-7 to 6-10 are very similar to those reported by James and Healy[347(b)] for the precipitation of metal hydroxides onto titanium dioxide. It seems likely then that changes over the pH range 4-5, both on decreasing and increasing pH runs, could be caused by surface catalyzed polymerization of silica. The formation of polymeric silica in bulk solution at pH 4-5 followed by its adsorption due to

electrostatic attraction, a mechanism put forward by Fuerstenau[350] for silica adsorption onto calcite, is believed unlikely for reasons outlined in (A) above.

(C) pH less than 3: Studies of the polymerization-depolymerization behaviour of silica (Chapter 2-3) have shown that the former process is catalysed by hydroxyl ions and is slowest at pH slightly less than 2. Numerous studies on co-precipitated titanium dioxide-silica samples[62,351] indicate that the surfaces of these mixed oxides contain very acidic sites which are centred on the structural unit (Ti-O-Si). Similarly, adsorption of monomeric silica via Si-O links is low in acid solution[345-346]. The evidence is therefore, that Si-O bonds, particularly if the unit (Si-O-Ti) is involved, would show a tendency to break in strongly acid solutions.

With the concepts proposed in sections (A), (B) and (C) above a rational explanation can be made of the "increasing pH" mobility curves in Figures 6-1 to 6-10.

Prepared silica-coated samples: Exposure of these samples to very low pH results in the breaking of (Ti-O-Si) bonds, where these bonds are accessible to aqueous hydrogen ions. In the case of the fully silica-coated sample (5.0 wt.%) relatively short ageing at low pH as in the microelectrophoresis experiments, leads to little change in subsequent higher pH double layer characteristics. The three dimensional polymer network remains surrounding the titanium dioxide particle and controls its electrokinetic behaviour. Prolonged exposure of this sample to pH 2 in the ageing experiment appears to have resulted in slight depolymerization in the coating giving perhaps more internal hydroxyl groups closer to the titanium dioxide core as evidenced by a slightly increased i.e.p.. With the lower silica content

samples (0.6 and 1.4 wt.%) the "decreasing pH" mobility curves indicated thin penetrable coatings, and breaking of Si-O bonds would give disruption of the silica coating. Raising the pH to 4-5 would promote polymerization of the silica in the vicinity of the surface. However, adsorbed monomer "anchors" would no longer be present and as the titanium dioxide becomes negatively charged the polymeric silica would be repelled from the titanium dioxide surface. Hence the observed i.e.p. is very similar to that of the base rutile.

Rutile in Aqueous Silica: The concepts outlined for the prepared samples apply to these systems with one basic difference. The preparations of the coated rutile samples were carried out under conditions likely to produce substantially cross linked polymers with relatively few uncondensed internal Si-OH groups (neutralized to pH 7). However, in the microelectrophoresis experiments in aqueous silica solutions, silica polymerization occurred at low pH (4 to 5) and in the presence of preadsorbed monomer. The coatings formed would be expected, therefore, to be much more open polymeric structures readily penetrated by hydrogen and hydroxyl ions. Exposure to low pH will result in Si-O bond breakage at the surface and subsequent raising of pH sees the silica removed at pH 4-5 regardless of the level of silica adsorbed during the decreasing pH run.

FIGURES 6-1 to 6-10
ELECTROPHORETIC MOBILITY VERSUS pH CURVES

[10^{-2}m KNO_3 and 0.1 gm/litre of SAMPLE unless otherwise stated.]

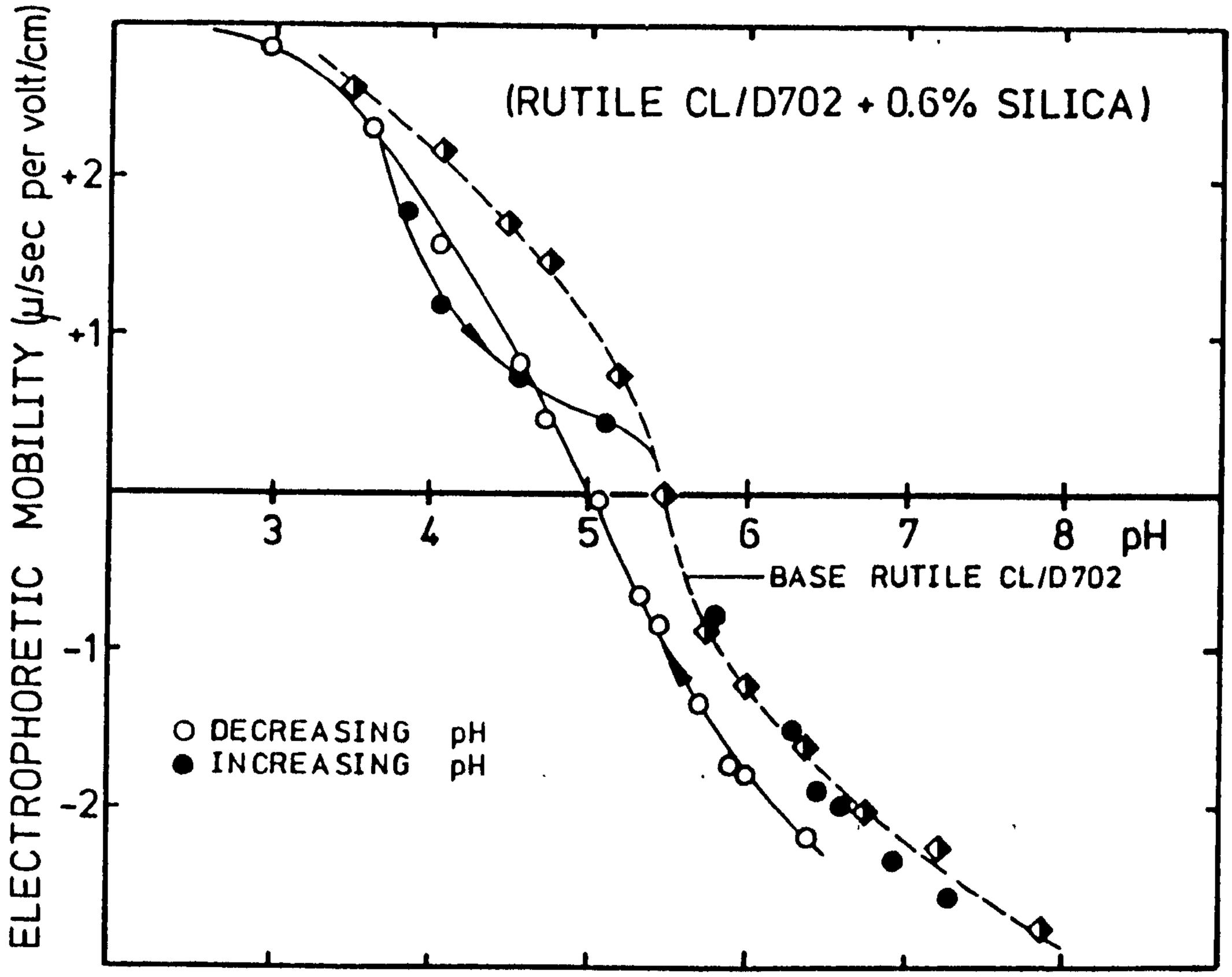

FIGURE 6-1

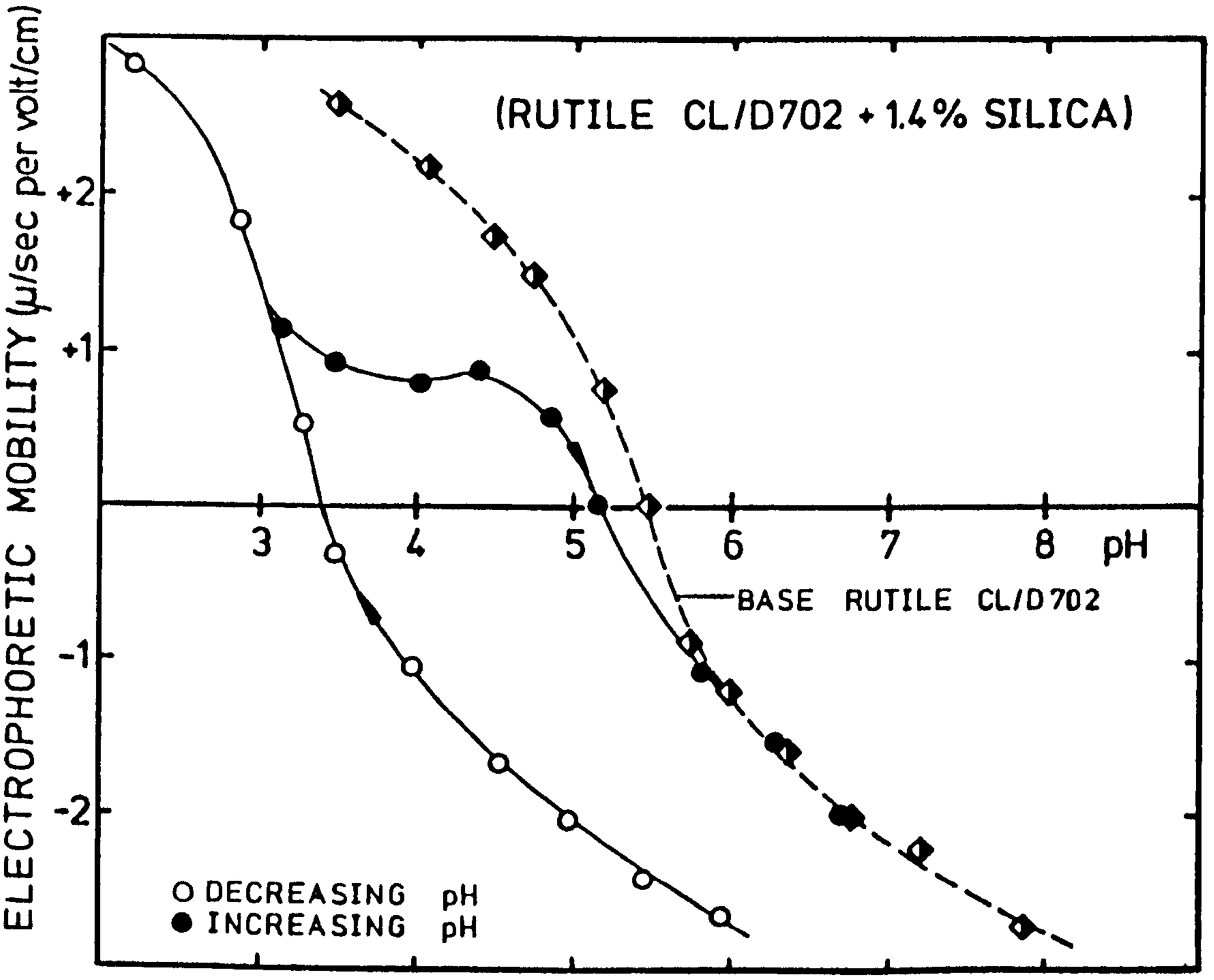

FIGURE 6-2

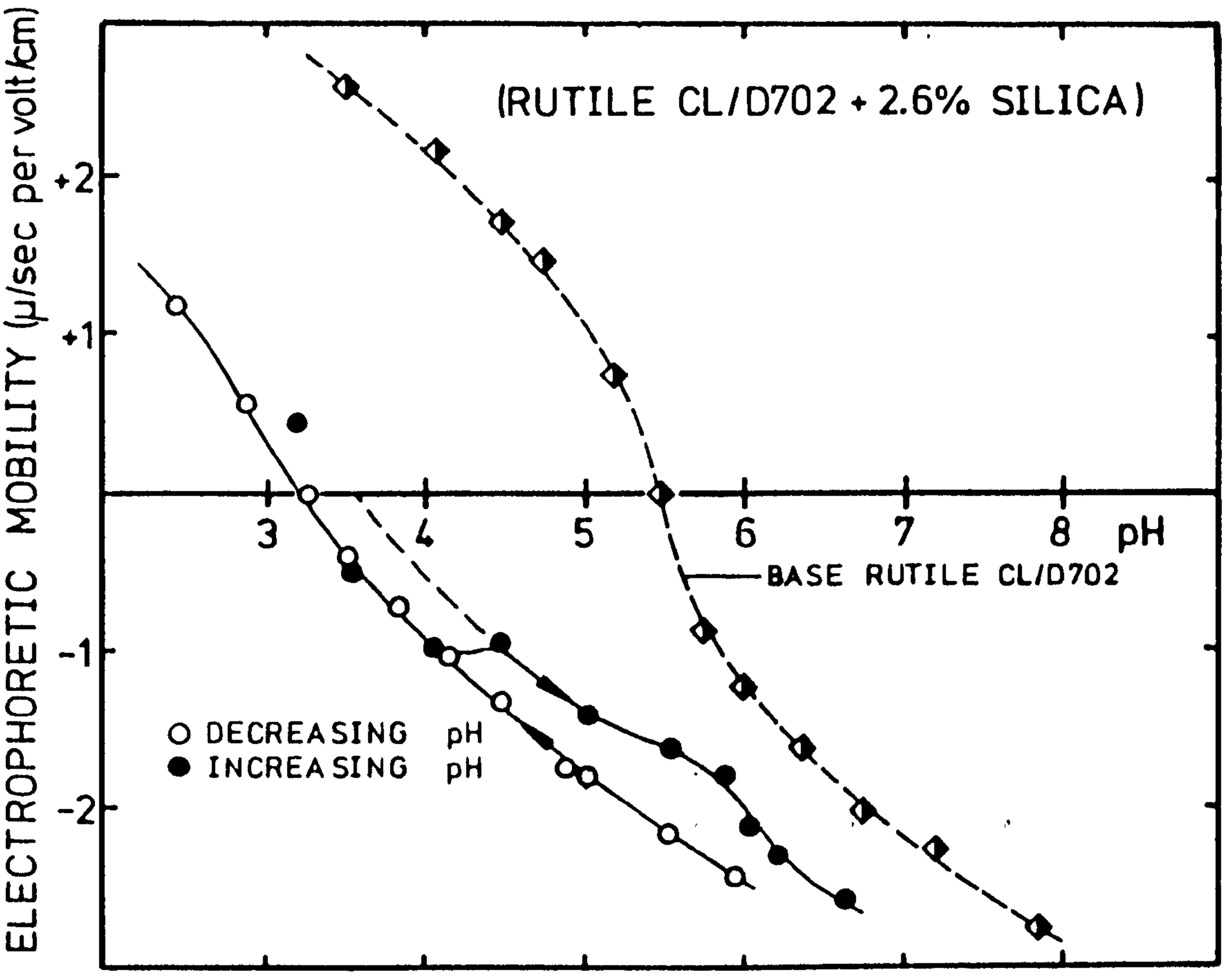

FIGURE 6-3

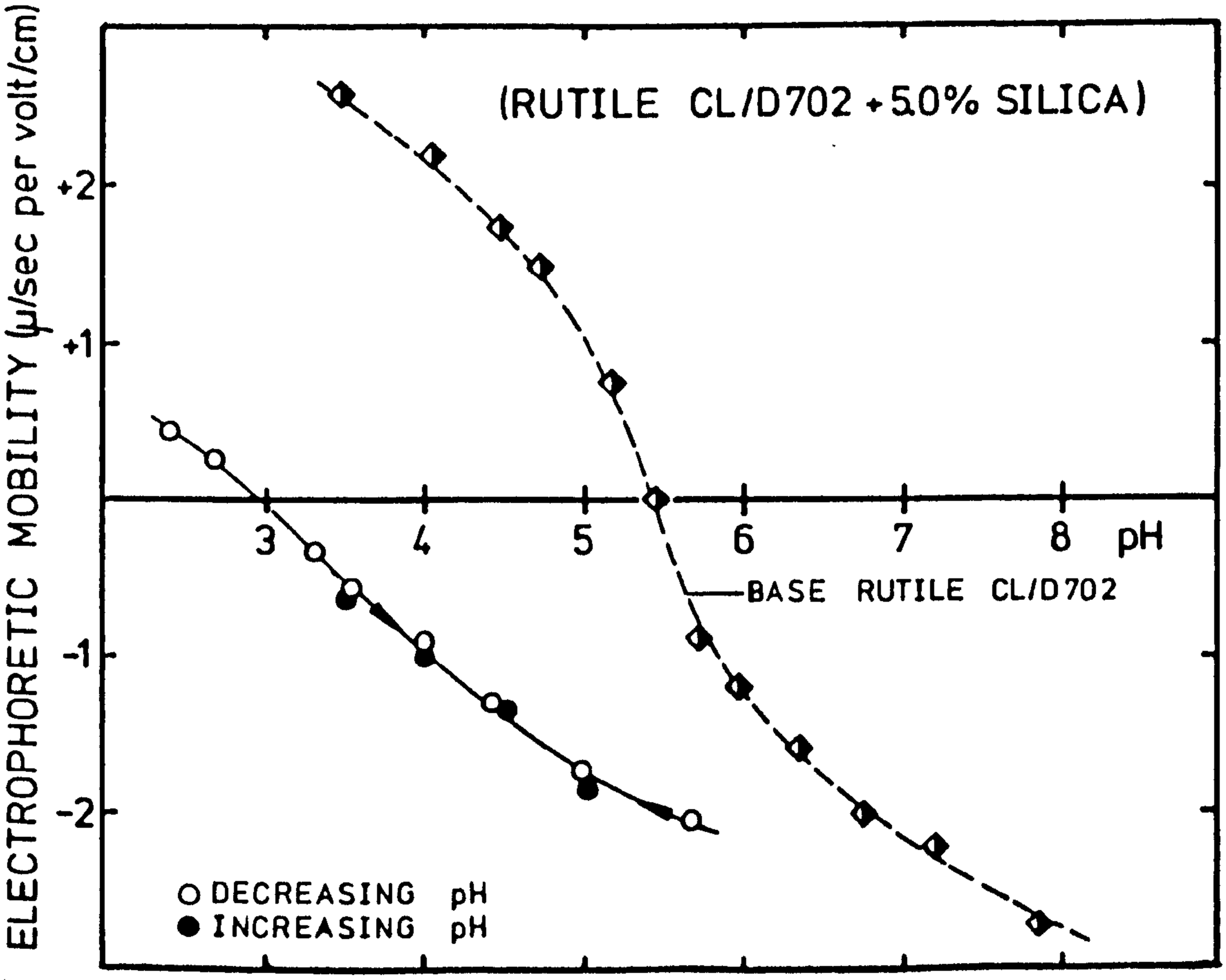

FIGURE 6-4

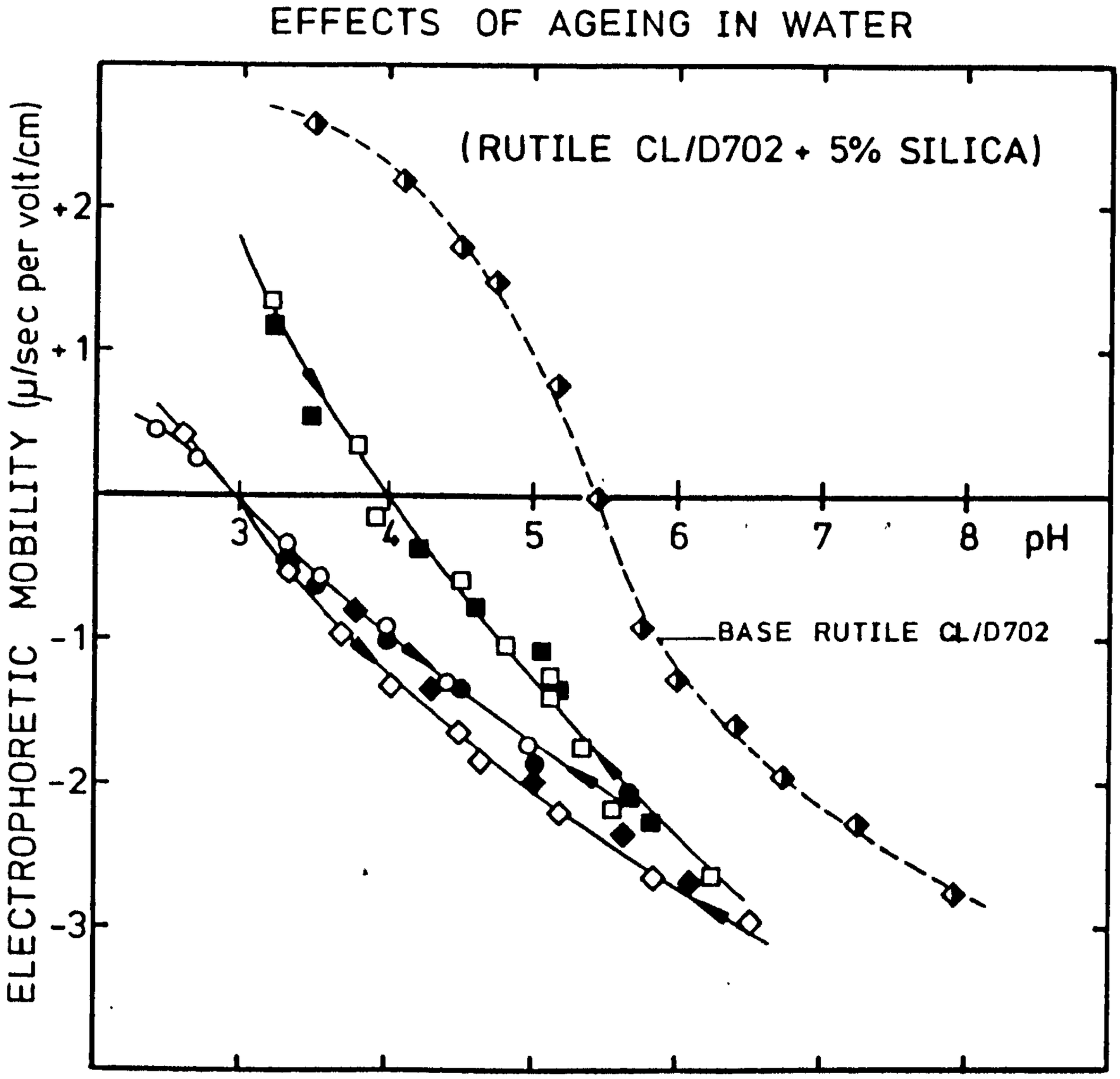
EFFECTS OF AGEING IN WATER
(RUTILE CL/D702 + 5% SILICA)
BASE RUTILE CL/D702
ELECTROPHORETIC MOBILITY (μ/sec per volt/cm)
+2
+1
-1
-2
-3
3
4
5
6
7
8
pH
OPEN SYMBOLS -DECREASING pH
CLOSED SYMBOLS-INCREASING pH
O ● SAMPLE AS PREPARED
SAMPLE AFTER 3 WEEKS AGEING IN LIQUID WATER:
◇ ◆ AT pH 7
□ ■ AT pH 2

FIGURE 6-5

(RUTILE CL/D702 + 1.4% SILICA)

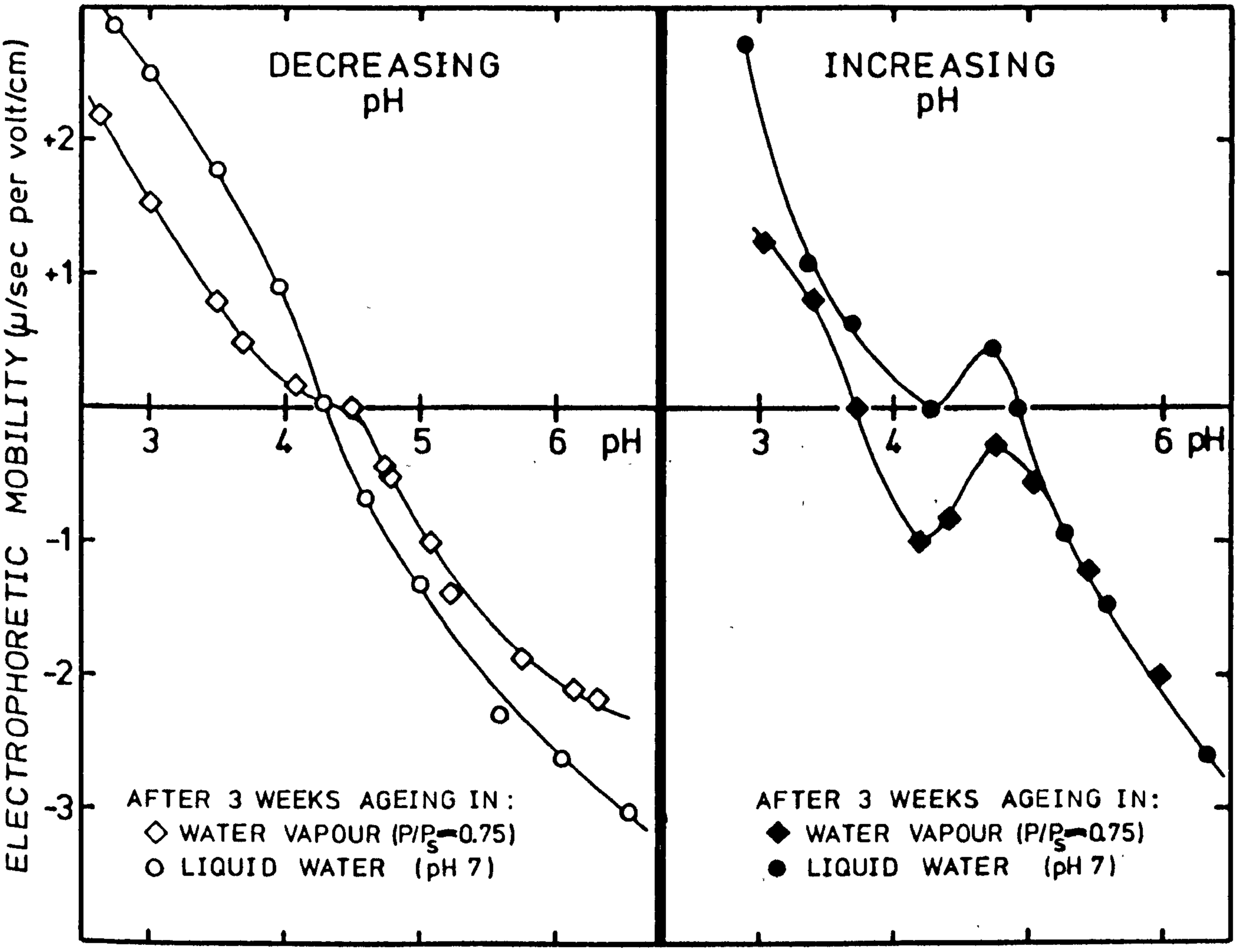

EFFECTS OF AGEING IN WATER

FIGURE 6-6

FIGURE 6-7

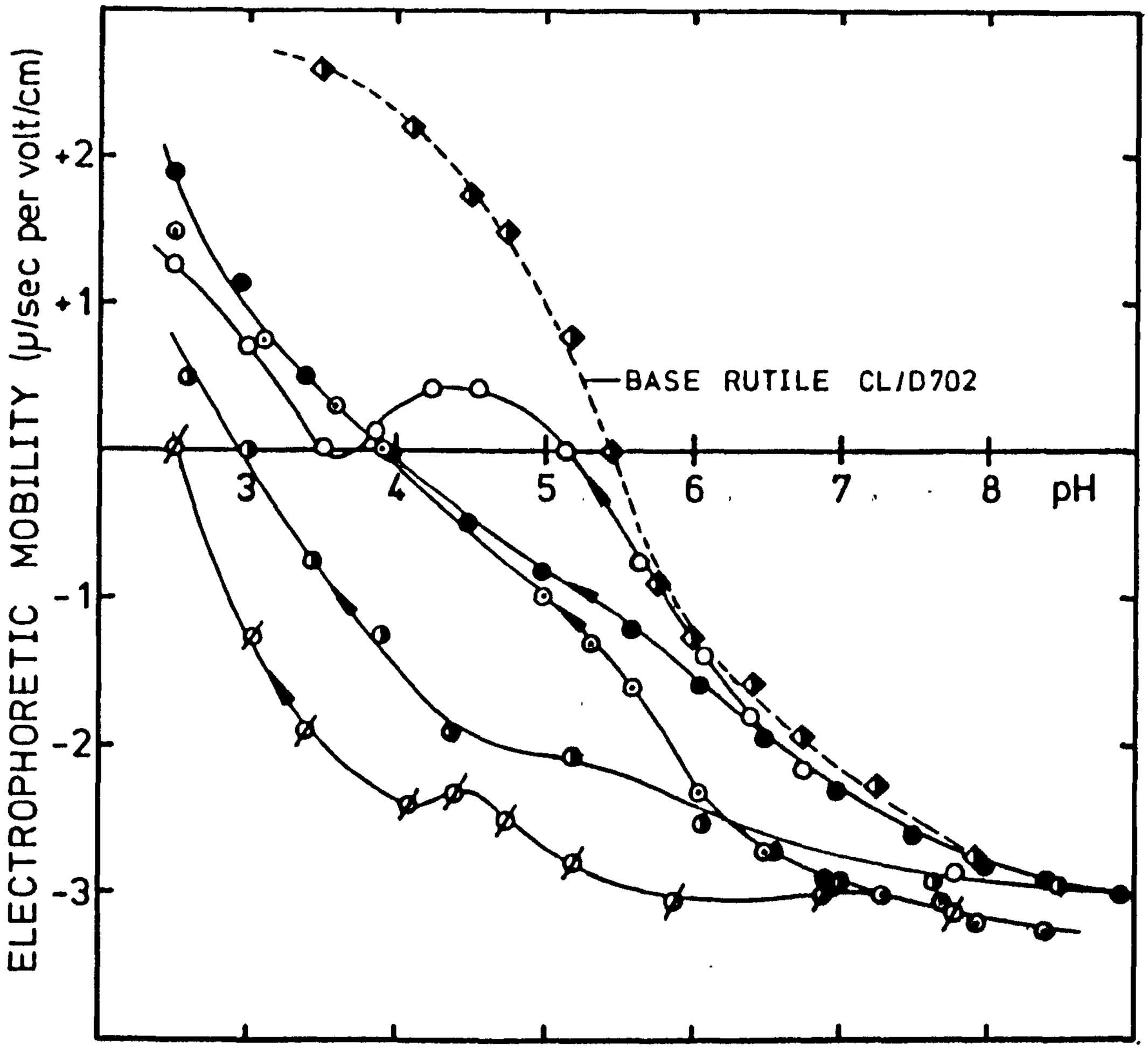

ALL RUNS 0.02 gm/litre RUTILE CL/D702

○ ◑ 1.0×10^{-4}m AQUEOUS SILICA

● ⌀ ⊙ 1.2×10^{-5}m AQUEOUS SILICA

— BASE RUTILE IN SODIUM SILICATE SOLUTIONS

FIGURE 6-8

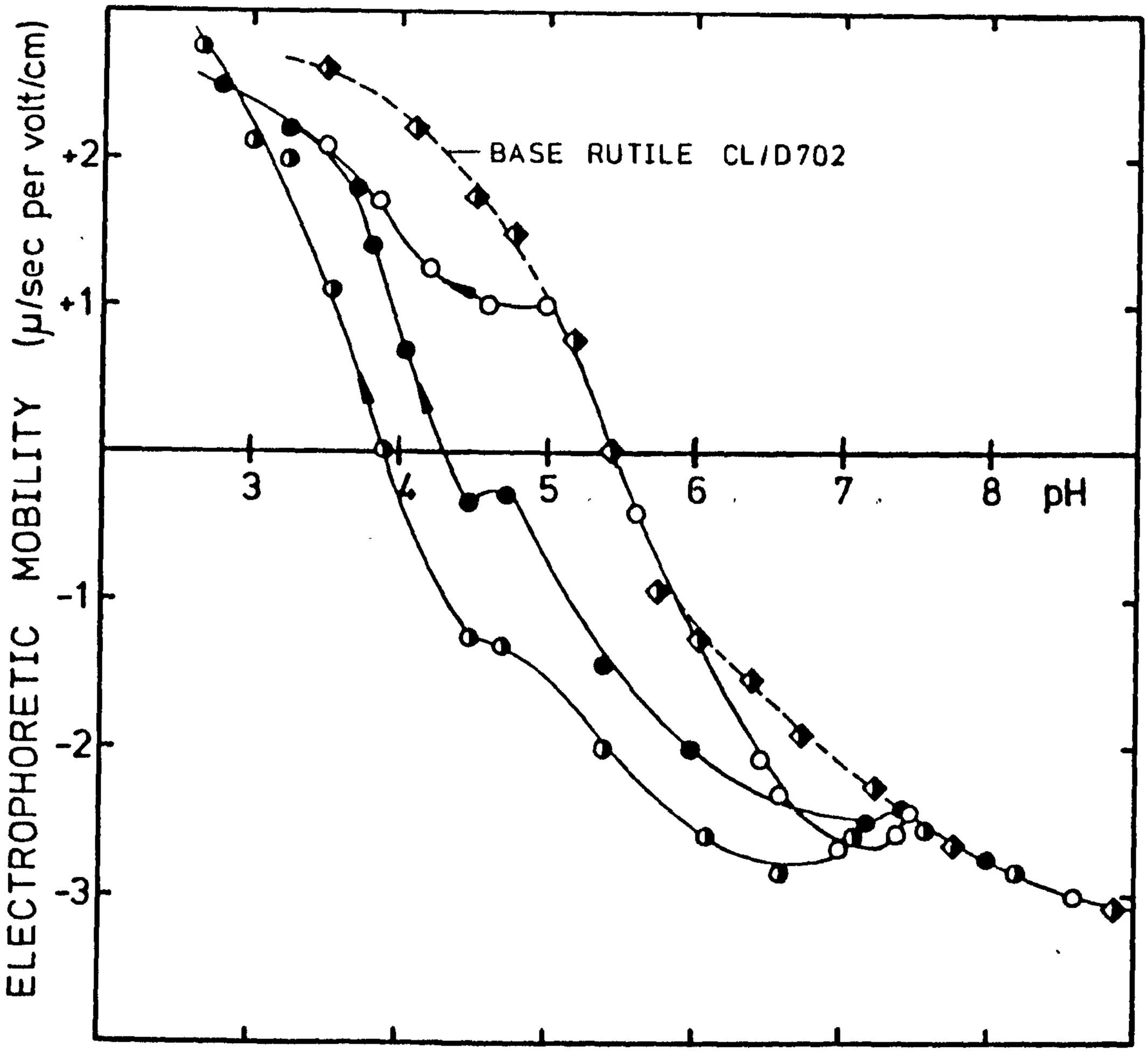

○ 0.1 gm/litre RUTILE CL/D702 — 1.2×10^{-5}m AQUEOUS SILICA

● ● 0.05 gm/litre RUTILE CL/D702 — 1.2×10^{-5}m AQUEOUS SILICA

— BASE RUTILE IN SODIUM SILICATE SOLUTIONS

FIGURE 6-9

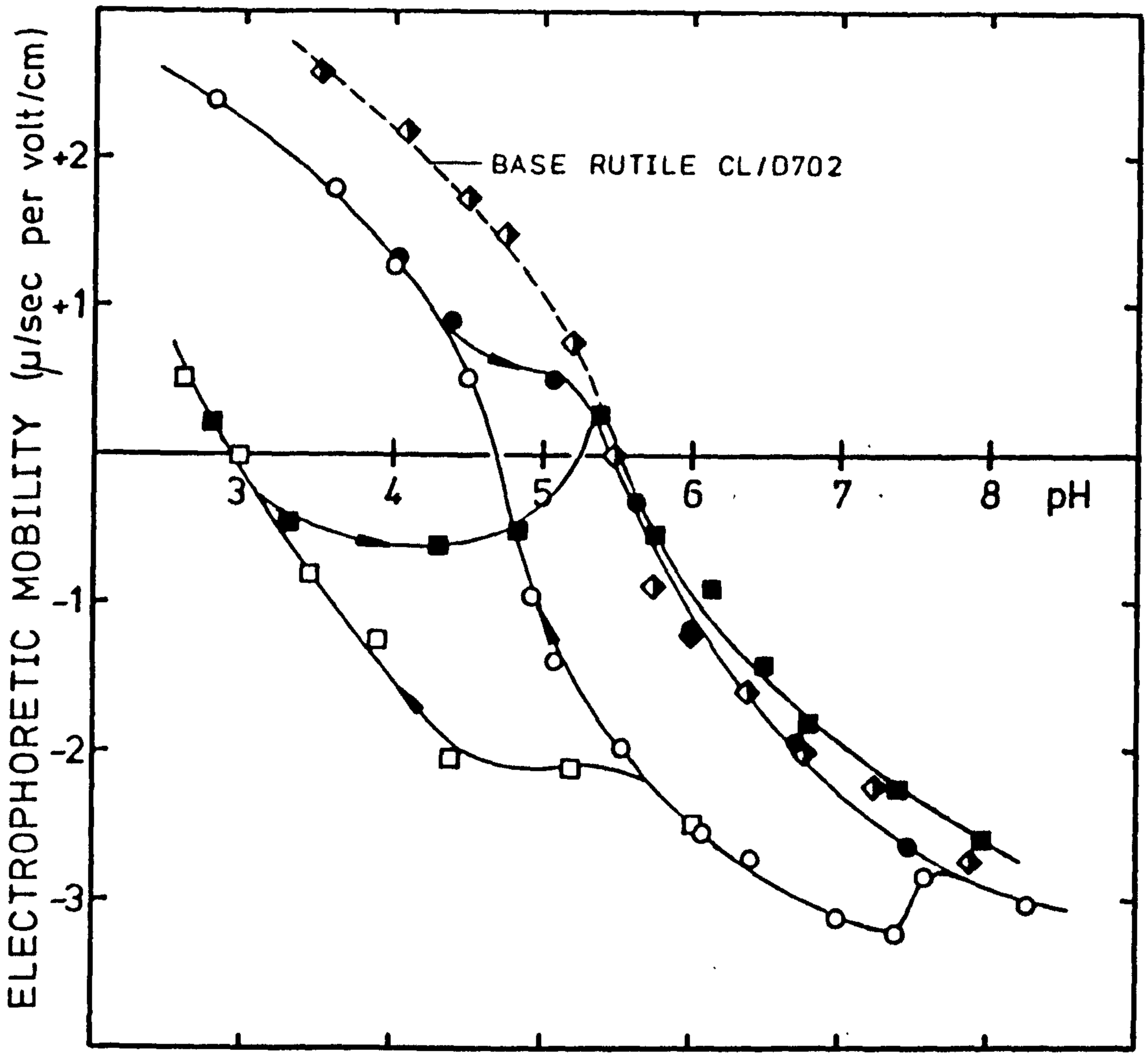

OPEN SYMBOLS - DECREASING pH
CLOSED SYMBOLS - INCREASING pH

○ ● 0.1 gm/litre RUTILE CL/D702 — 1.0×10^{-4}m AQUEOUS SILICA
□ ■ 0.02 gm/litre RUTILE CL/D702 — 1.0×10^{-4}m AQUEOUS SILICA

— BASE RUTILE IN SODIUM SILICATE SOLUTIONS

FIGURE 6-10

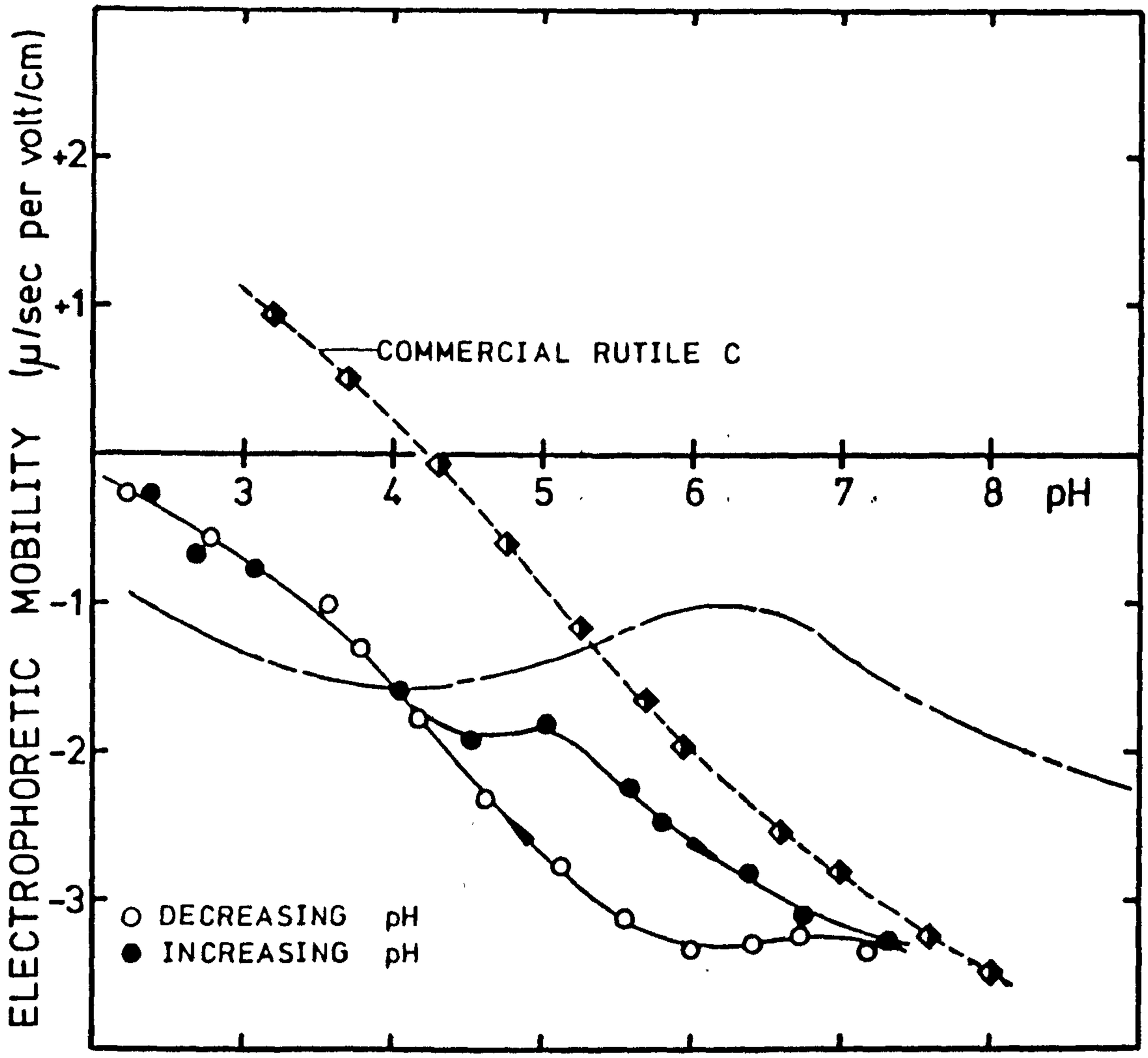

● O 0.1 gm/litre RUTILE C — 1.0×10^{-4} m AQUEOUS SILICA

— COMMERCIAL RUTILE IN SODIUM SILICATE SOLUTIONS

FIGURE 6-11

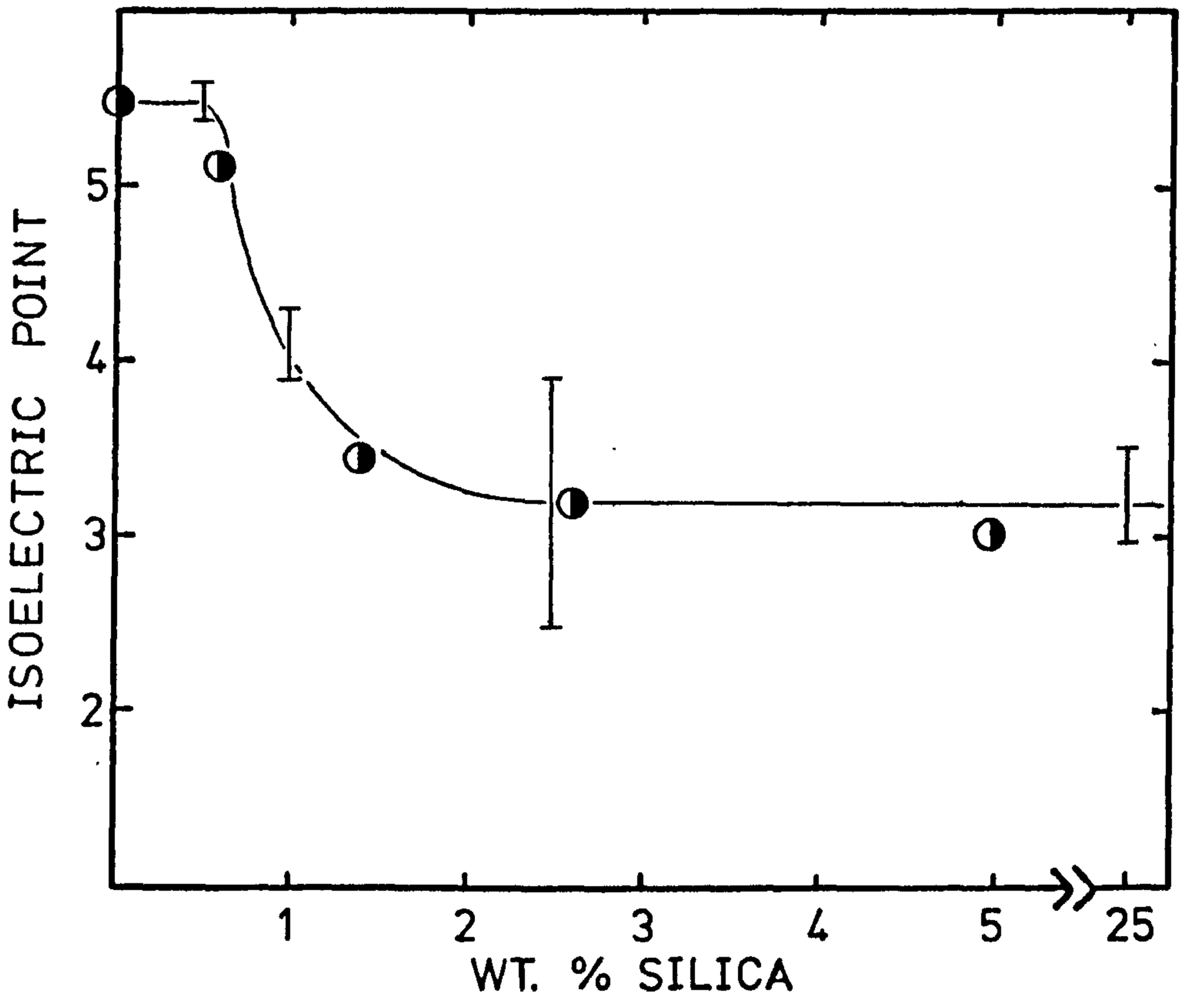

SUMMARY OF ISOELECTRIC POINT DATA

CHAPTER 7: RESULTS AND DISCUSSION III

NITROGEN AND ARGON ADSORPTION ON SILICA-COATED RUTILE

The adsorption of nitrogen and argon on rutile and some silica-coated rutile samples has been investigated by measuring adsorption isotherms and differential energies of adsorption. After a brief preliminary adsorption study (Chapter 7-1) it was decided to use sample outgassing conditions which might expose differences between the adsorption characteristics of titanium dioxide and silica (Chapter 7-1). The adsorption isotherms and the calorimetric data are discussed in Chapters 7-2 and 7-3 respectively.

7 - 1 Outgassing Temperature

The study of surfaces using gas adsorption requires the removal, under well defined conditions, of residual gases on the surface. The physical and chemical nature of titania and silica surfaces are of course closely associated with their degree of hydration and hydroxylation which can be changed by outgassing at ambient temperatures and above. Several workers have shown that outgassing above room temperature can lead to significant changes in the texture of coated pigments[45-46,55] prepared by methods similar to those used in the present work. As a result it has been recommended that if studies of the texture of silica coatings are to be undertaken then high outgassing temperatures should be avoided.

Figures 7-1, 7-2 and 7-3 give the nitrogen adsorption isotherms for three samples: rutile CL/D702 ("base rutile"), rutile + 1.4 wt.% silica (NF 4/2/73) and rutile +5.0 wt.% silica (NF 8/2/73), after

each was outgassed for 24 hours at room temperature (approx. 20°C) to a residual pressure of 10^{-4} torr (0.01 N/m^2). These isotherms (and that of argon in Figure 7-3) were determined using a conventional volumetric adsorption apparatus which is similar to that described elsewhere[358]. The results of BET and FHH analyses of the isotherms are summarized in Table 7-1.

The base rutile gave a type II adsorption isotherm[171] and a narrow type B[360] hysteresis loop on desorption which closed at P/Ps 0.4. The BET C constant of 73 is low compared with values reported for rutile outgassed at higher temperatures[214,359]. However, Day[214] has shown that the C constant for nitrogen adsorption on rutile is reduced as water is presorbed on the surface. The low C constant for the base rutile is consistent then with more residual water on the surface after outgassing at room temperature than would occur on outgassing at 100°C. This remaining physisorbed water would tend to reduce the effective polarity of the surface towards an incoming nitrogen molecule, which might explain the low value[231] of 1.8 for the slope of the FHH plot. The FHH plot on this sample showed no evidence of microporosity but did indicate the onset of capillary condensation at P/Ps > 0.8. When the isotherm is plotted in a reduced form (Figure 7-4) and compared with suggested standard isotherms for nitrogen adsorption[359,361] good agreement is obtained at relative pressures below 0.5. This agreement, taken in conjunction with the FHH data, provides good evidence that the base rutile outgassed at 25°C contained no significant microporosity. The curves in Figure 7-4 do show that substantially more capillary condensation has occurred on the base rutile than on the suggested

TABLE 7 - 1

SUMMARY OF BET AND FHH ANALYSES OF ADSORPTION ISOTHERMS ON RUTILE AND SILICA-COATED RUTILE AFTER OUTGASSING AT ROOM TEMPERATURE

SYSTEM	BET ANALYSIS				FHH ANALYSIS		
	Vm cm^3/gm)	$S_{BET}^{(a)}(m^2/gm)$	C	LINEARITY RANGE P/Ps	SLOPE	LINEARITY RANGE P/Ps	COMMENTS
Adsorption N_2 on Rutile (CL/D 702)	4.59	20.0	73	0.04 - 0.37	1.8	0.4 - 0.8	Slight capillary cond'n at P/Ps > 0.8. Only slight deviation from linearity at P/Ps < 0.4.
Adsorption N_2 on Rutile + 1.4 wt.% Silica (NF 4/2/73)	5.15	22.3	(b)	0.10 - 0.38	APPROX 2.2	-	Plot generally curved with evidence of capillary condensation at P/Ps > 0.4
Adsorption N_2 on Rutile + 5.0 wt.% Silica (NF 8/2/73)	5.92	25.7	APPROX 240	0.03 - 0.30	2.2	0.1 - 0.75	Capillary condensation at P/Ps > 0.7
Adsorption Argon on Rutile + 5.0 wt.% Silica	5.51	20.4	40	0.02 - 0.30	-	-	-

(a) Using cross sectional areas of 0.138 nm^2 for argon and 0.162 nm^2 for nitrogen.

(b) BET plot linear but gave a negative intercept.

standard samples. The shape of the adsorption - desorption isotherm given by the base rutile is normally associated with capillary condensation between plate-like particles or in open slit-shaped capillaries[160]. The electron micrograph of the base rutile (Figure 3-1) showed that it consisted of rod shaped particles with an axial ratio of approximately 5 : 1. Capillary condensation would appear to have occurred in the long narrow spaces between particles lying in close proximity to one another.

The two silica-coated rutile samples both gave type II adsorption isotherms after outgassing at room temperature. On desorption, hysteresis loops were obtained which did not close until the relative pressure was less than 0.01. BET analyses showed that the BET surface area increased from 20.0 to 25.7 m^2/gm with the incorporation of 5.0 wt.% silica onto the surface of the base rutile. Reliable C constants could not be obtained for the silica-coated rutile samples. The FHH plots on these samples indicate capillary condensation in the multilayer region of the isotherm. The slopes of the FHH plots again indicate low energy (non-polar) surfaces.

The peculiar feature of nitrogen adsorption on the two coated samples is the presence of low pressure hysteresis[176]. Figure 7-3 shows that adsorption of argon on the 5.0 wt.% silica sample, after a nitrogen adsorption - desorption run, was fully reversible. Nitrogen adsorption involves only physisorption processes and a basis for the cause of low pressure hysteresis during physisorption has been given by Bailey and co-workers[384] as "the irreversible intercalation of adsorbate in pore structures of molecular dimensions leading to inelastic distortion of the solid". Barrer[363] observed low pressure

hysteresis during adsorption studies on montmorillonite and proposed the following adsorption/desorption scheme:

(1) above a certain threshold pressure, adsorbate molecules penetrate between montmorillonite lamellae giving swelling and separation of lamellae.

(2) due to the increased separation of lamellae - capillary condensate is removed at high relative pressure during desorption - interlamellar forces are less and desorption of interlamellar adsorptive occurs at lower relative pressures than adsorption.

Hence a wide hysteresis loop is observed - the form of which depends on the strength of interlamellar forces[363]. Barrer observed hysteresis loops for polar vapours similar in shape to those reported in Figures 7-2 and 7-3. In the case of the silica-coated rutiles it is possible that two types of penetration/structural change processes have occurred during nitrogen adsorption.

(A) Some siloxane bonds may have formed between particles, especially during the compaction of a wet filter cake during filtration, resulting in interparticle space being inaccessible to nitrogen until high relative pressures are reached. Interparticle siloxane bonds would probably be strained and easily broken when liquid nitrogen penetrates interparticle spaces.

(B) Coating structures may be such that nitrogen penetrates into spaces within the coating at high relative pressure and is not readily removed when the pressure is reduced. Such entry within the coating may result in some permanent structural change.

The present data do not allow distinction to be made between processes (A) and (B). The reversible adsorption of argon shown in Figure 7-3 may mean that (i) nitrogen adsorption has caused a permanent structural change or (ii) that argon near saturation pressure at 77K forms a solid which does not undergo a penetration process.

The discussion of the isotherms in Figures 7-1, 7-2 and 7-3 serves to indicate some difficulties in characterizing the texture of silica coatings after outgassing at room temperature. It was decided therefore to concentrate on studying the extent of rutile coverage with silica and the location of silica on partially coated rutile surfaces and to choose the appropriate outgassing temperatures. It was first necessary to review the information available in the literature on the states of hydration and hydroxylation of silica and titania after outgassing at various temperatures.

The surface hydration of titanium dioxide has been extensively studied using infra-red spectroscopy[336-338,365-368], gas adsorption[304,334,364] and immersion calorimetry[357,368]. Fully hydrated titanium dioxide surfaces have been shown to contain (i) hydroxyl groups, (ii) molecular water co-ordinately bound to lattice ions and (iii) molecular water hydrogen bonded to hydroxyl groups or ligand water molecules. Although the temperatures at which surface species are removed under vacuum vary from sample to sample[369] some general trends have been established. Hydrogen bonded molecular water can normally be removed at room temperature. Conditions for the removal of ligand water have not been well defined although it is generally agreed that co-ordinated water

molecules whether bound to titanium cations or more weakly to oxide anions[163], are more easily removed than surface hydroxyl groups. The lower temperature limit for the removal of ligand water has been put at about 150°C[306,338], less than 200°C[162] and greater than 200°C[365], whilst many have claimed all ligand water molecules are removed below 300 to 350°C[163,337,366]. The removal of surface hydroxyl groups depends on their location on the surface[162] and their degree of mutual hydrogen bonding[365]. There is much evidence to suggest that surface hydroxyls are progressively removed on outgassing over the temperature range 200 to 400°C[162,306,338,365]. The upper limit is however very uncertain as some workers have claimed that from 10[304] to 40%[336] of the total surface water, in the form of hydroxyl groups, remains at 450°C. In summary it can be said that ligand water is (i) removed from titanium dioxide surfaces at approximately 150°C and (ii) completely removed before surface dehydroxylation is complete.

As with titanium dioxide the hydration of amorphous silica has been extensively studied[370-383]. There are two significant differences in the nature of hydrated silica surfaces compared to titanium dioxide:

(A) Amorphous silica surfaces contain hydrogen bonded molecular water and hydroxyl groups. The latter may be geminal or vicinal groups[383,385] and exist free of mutual interactions[372] (type A[370]) or be hydrogen bonded[372] (type B[370]). However, no evidence has been found of water molecules being co-ordinately bound to lattice ions in amorphous silicas.

(B) As well as containing <u>surface</u> hydroxyl groups in the sense of being external to a crystalline surface, amorphous silicas may also

contain internal or so called "intraglobular"[372] hydroxyl groups. Amorphous silicas have been shown to lose weight on outgassing over the temperature range 25 to 1100°C[380-381,385].

Some workers have claimed[377-378] that all water adsorbed on silica in molecular form can be removed at room temperature whilst others claim temperatures as high as 250 to 350°C are required[373,379]. Two studies giving reasonable agreement are those of Klier[376], using adsorption and spectroscopic techniques, and Kondo[375] using differential thermal analysis and infra-red spectroscopy. Both studies give good evidence for the removal of adsorbed molecular water on outgassing at 150 to 170°C. Most evidence seems to suggest, therefore, that most of the water molecules adsorbed on amorphous silica but not undergoing mutual hydrogen bonding are removed on outgassing from 25 to 105°C[371,386], and that all molecular water is removed below about 150°C. Hydroxyl groups are removed from amorphous silicas between outgassing temperatures of 180°C[371] and 1100°C[374]. Koberstein[382] claims 40% are removed below 400°C and 75% below 800°C. Hockey[383] claims 50% removal below 300°C, and Cornier[374] gives the same % removal below 500°C. In general, interacting hydroxyl groups (H bonded) are most easily removed, say below 500°C[370] whilst isolated hydroxyls remain at much higher temperatures[379]. The conditions for removal of internal hydroxyl groups have been shown to vary greatly for different samples[370-371,374]. In summary it can be said that water attached to amorphous silica by hydrogen bonds can be removed on outgassing from ambient temperature to about 150°C whilst hydroxyl groups can be progressively removed between 180 and 1100°C.

Thus both silica and titania lose water on outgassing between ambient temperatures and approximately 400°C and for the studies described in the following sections of this Chapter the outgassing range actually used was 150 to 400°C. For the water sorption studies described in Chapter 8 the outgassing range 25 to 300°C was used.

7 - 2 Adsorption Isotherms

The base rutile and three silica-coated rutile samples have been studied and the adsorption isotherms at 77.5K, and up to relative pressures of 0.25, are given in Figures 7-5 to 7-8. These isotherms were determined using the continuous addition technique (Chapter 4-3) and the adsorption points plotted in Figures 7-5 to 7-8 were those calculated from the continuously recorded experimental parameters.

The sample containing 2.6 wt.% silica (NF 14/2/73) was chosen as one which microscopic and electrokinetic studies have shown to consist of particles of rutile completely covered by a coating of silica. The two other samples containing 0.6 and 0.9 wt.% silica (NF 6/2/73 and NF 16/2/73) were likely to consist of partially covered rutile particles and represented the amount of silica always deposited onto the rutile particles (Chapter 5).

The results of the BET analyses of the adsorption isotherms are summarized in Table 7-2. In general the region of linearity of the BET plots did not extend above (P/Ps) 0.25. This relative pressure is below the more often reported upper limit of 0.35 but many examples of restricted linear regions in BET plots have also been reported.[160] The linearity of the BET plots within the ranges stipulated in Table 7-2

TABLE 7 - 2

SUMMARY OF BET ANALYSES OF NITROGEN AND ARGON ADSORPTION ISOTHERMS ON RUTILE AND SILICA-COATED RUTILE

SAMPLE	T(°C) OUTGAS	ADSORPTION OF ARGON				ADSORPTION OF NITROGEN			
		Vm(cm^3/gm	C	LINEARITY RANGE P/Ps	$S^{(a)}_{BET}$(m^2/gm)	Vm(cm^3/gm)	C	LINEARITY RANGE P/Ps	$S^{(a)}_{BET}$ (m^2/gm)
BASE RUTILE	150	4.98	74	0.04 - 0.20	18.5	5.07	82	0.06 - 0.20	22.0
(CL/D702)	250	5.50	63	0.06 - 0.25	20.4	5.75	83	0.07 - 0.20	25.0
"	400	5.56	82	0.05 - 0.20	20.6	5.74	116	0.06 - 0.25	25.0
RUTILE + 0.6 wt.%	150	5.35	59	0.05 - 0.20	19.8	5.45[b]	-	-	23.8
SILICA	250	-	-	-	-	5.80	-	-	25.3
(NF 6/2/73)	400	5.51	73	0.04 - 0.21	20.4	5.80	-	-	25.3
RUTILE + 0.9 wt.%	150	5.22	59	0.05 - 0.25	19.4	5.27	301	0.07 - 0.25	22.9
SILICA	250	5.41	58	0.05 - 0.20	20.1	5.39	199	0.04 - 0.18	23.4
(NF 16/2/73)	400	5.50	65	0.04 - 0.26	20.4	5.61	178	0.04 - 0.20	24.4
RUTILE + 2.6 wt.%	150	5.57	53	0.04 - 0.22	20.7	5.36	283	0.05 - 0.15	23.3
SILICA	250	5.70	53	0.07 - 0.25	21.1	5.37	(c)	0.05 - 0.18	23.3
(NF 14/2/73)	400	5.62	61	0.05 - 0.22	20.8	5.61	238	0.07 - 0.20	24.4

(a) Using cross sectional area of 0.138 nm^2 for argon and 0.162 nm^2 for nitrogen.

(b) BET plots were not satisfactory for nitrogen adsorption on this sample. These are Point B monolayer capacities.

(c) BET plot linear but gave a negative intercept.

enable monolayer capacities to be estimated to 0.1 cm^3/gm whilst errors in BET C constants are more likely to be approximately ±5%.

(A) Base Rutile: Adsorption capacities for both nitrogen and argon were increased when the outgassing temperature was raised from 150 to 250 to 400°C. For nitrogen adsorption the isotherms for the 150 and 400°C outgassed samples were approximately parallel at relative pressures above ~0.02, whilst the isotherm for the 400°C outgassed sample approached that for the 250°C sample at higher (P/Ps) values. The slightly sharper knee after outgassing at 400°C is reflected in an increased C constant. For all three outgassing temperatures the value of C was higher for nitrogen adsorption than for argon adsorption. This is consistent with nitrogen being able to undergo additional specific interactions with the surface field on account of its quadrupole moment[168-169]. The enhanced adsorption capacity on increasing the outgassing temperature from 150 to 250°C is not accompanied by an increased C constant but does, in contrast to the effect of raising the outgassing temperature to 400°C, give an increased BET monolayer capacity. For the adsorption of nitrogen and argon on the base rutile BET plots were not linear below about 80% monolayer coverage. Therefore, as stressed in Chapter 2-2, the BET C constant may not give a reliable estimate of adsorption interactions below such coverages. As adsorption of a vapour on an energetically heterogeneous surface would be expected to occur on the most active surface sites at lowest relative pressures[387], the BET C constants for the base rutile (Table 7-2) are unlikely therefore to be reliable

guides to the extent of surface heterogeneity after various outgassing treatments. Hence the adsorption isotherms and the BET analyses do not allow distinction between an increase in surface area, or more localised adsorption (on high energy sites) occurring when the outgassing temperature was raised from 150 to 250°C.

(B) Rutile + 2.6 wt.% Silica: The nitrogen and argon isotherms for this sample outgassed at 150, 250 and 400°C (Figure 7-8) show marked differences to those for the base rutile. The BET monolayer capacity for argon shows little change over the outgassing range 150 to 400°C. The monolayer capacity for nitrogen is constant on outgassing from 150 to 250°C but does show a small increase between 250 and 400°C. The C constants for nitrogen adsorption are much larger on the 2.6 wt.% silica sample than on the base rutile indicating that average adsorption interaction energies over the BET range are significantly increased. The interactions are of a specific nature as values of C for nitrogen are much larger than those for argon.

(C) Rutile + 0.9 wt.% Silica: The analyses of the adsorption isotherms for the 0.9 wt.% silica sample show that this sample is behaving very similarly to the 2.6 wt.% silica sample. Nitrogen monolayer capacities and C constants are similar for both these samples. In particular both show BET C constants which are reduced as outgassing temperatures are increased from 150 to 400°C. Argon monolayer capacities are slightly less for the 0.9 wt.% sample compared with the 2.6 wt.% sample, but for both samples argon C constants are much less than nitrogen C constants.

(D) Rutile + 0.6 wt.% Silica: The adsorption isotherms for this sample were more difficult to interpret because the BET plots

for nitrogen adsorption were slightly curved over the whole (P/Ps) range studied. If straight lines of best fit were used negative intercepts were obtained and nitrogen BET monolayer capacities were unrealistic. For nitrogen adsorption, monolayer capacities were estimated from the Point B on the isotherms (See Figure 2-6). The argon and nitrogen monolayer capacities for the 0.6 wt.% silica sample were very similar to those of the base rutile except after outgassing at 150°C. One possible reason for the increased monolayer capacity at this temperature is that the 0.6 wt.% silica sample contains some microporosity. This is also possible for the other silica-coated rutile samples studied. Unfortunately it has not been possible for these samples to apply the usual methods of micropore analysis, such as that using α_s[388], since no suitable standard isotherms[362,388] are available. In any case the α_s (or the t[361]) method of analysis cannot clearly distinguish between the presence of micropores and high energy surface sites[214,218]. On the other hand the measurement of nitrogen and argon adsorption energies does enable such a distinction and results of such measurements are discussed in the following section (7-3).

A possible explanation for the apparent breakdown of the BET equation for nitrogen adsorption on the 0.6 wt.% silica sample lies with the "compensating errors" concept outlined in Chapter 2-2. The deposition of a small amount of silica onto the rutile surface, perhaps selectively in a surface energy sense, may have been sufficient to upset the balance between surface heterogeneity and lateral adsorbate-adsorbate interactions, a balance responsible for the

applicability of the BET model for nitrogen adsorption on rutile.

In summary then it is clear that the analyses of argon and nitrogen adsorption isotherms show significant differences between the base rutile and the 2.6 wt.% silica-coated rutile. The partially coated (0.9 wt.% silica) rutile sample gave similar adsorption isotherm characteristics to the more heavily coated rutile surface whilst analysis of the 0.6 wt.% silica sample is inconclusive. More detailed discussion of the interactions of nitrogen and argon with all four samples is given in the following section.

7 - 3 Differential Energies of Adsorption

Differential energies of adsorption of argon and nitrogen were determined concurrently with the adsorption isotherms shown in Figures 7-5 to 7-8 and are presented in Figures 7-9 to 7-21. The differential energies of adsorption are plotted as a function of surface coverage θ (= V/Vm) as has been done with other calorimetric data reported in the literature[219,325,389-390]. The choice of θ as a measure of surface coverage has been criticised[362] because it involves evaluation of the BET monolayer capacity Vm. However, the alternative parameter, relative pressure[362], is not appropriate in the present study as many of the significant changes in adsorption energies occur at equilibrium (P/Ps) values which are very close to zero. Any probable errors in the values of Vm will not significantly alter the conclusions drawn from the calorimetric data. Included in Figures 7-12, 7-13 and 7-15 are the results of some previously reported calorimetric studies of the adsorption of argon and nitrogen on rutile[219,325,389-390], recalculated where necessary as the

corresponding differential energy of adsorption (see Chapter 2-2). Precise conditions of sample pretreatment were not always given in these other studies. The data in Figures 7-12, 7-13 and 7-15 show that the results obtained in the present study are in substantial agreement with those reported in the literature.

All the differential energy curves given in Figures 7-9 to 7-21 have the same general shape: the differential energy of adsorption (q_D) decreases with increasing surface coverage (θ). Such behaviour is consistent with adsorption on an energetically heterogeneous surface in order of decreasing surface site energy. Methods have been derived to calculate site energy distribution functions [$F(U_o)$] for heterogeneous surfaces based on this "ordered filling" approach and ignoring adsorbate-adsorbate interactions[220]. In these treatments heterogeneous surfaces are assumed to consist of homotattic patches[391]. Adsorption on each patch follows a postulated isotherm equation, represented by $\prod(P, U_o)$, and the total adsorption equation is obtained by adding adsorption from all patches: $\Omega = \int F(U_o)\prod(P, U_o)\, dU_o$. Some attempts to solve this equation and obtain a site energy distribution for titanium dioxide have recently been summarized by House and Jaycock[235] and by Rudzinski and Jaroniec[236]. Several very different distributions have been obtained from the one set of experimental data[220]. It was decided therefore, not to attempt to calculate site energy distributions from the calorimetric data presented in Figures 7-9 to 7-21. Nevertheless some general conclusions from a theoretical treatment by Ross and Olivier[392] will be useful. These workers showed that if the

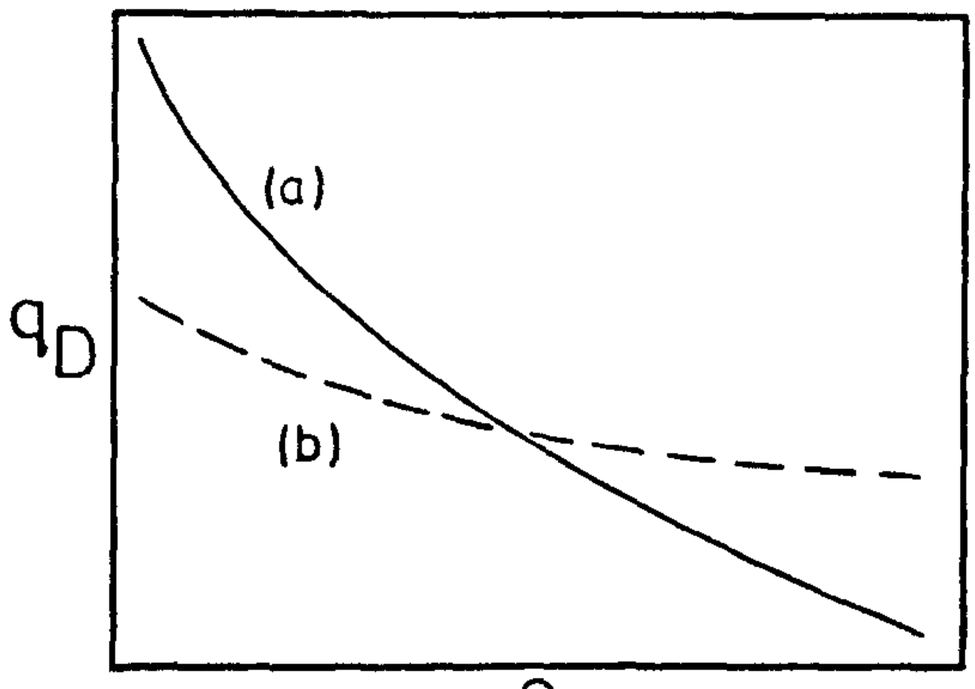

FIGURE (i)

distribution of site energies is Gaussian then the change in q_D against θ curves from type (a) to (b) (See Figure (i) opposite) represents a change to a much narrower distribution of interaction energies whilst the median interaction energy remains unchanged.

(A) Adsorption on Rutile: Inspection of the curves of q_D versus θ for argon and nitrogen adsorption on rutile (Figures 7-15 and 7-19) shows that:

(i) relatively large increases in q_D occur at less than half monolayer coverage when outgassing temperature is increased from 150 to 250°C. A smaller additional increase occurs when outgassing temperature is raised to 400°C.

(ii) the increases described in (i) are much larger for nitrogen than for argon.

(iii) q_D values for nitrogen are larger than for argon at low values of θ but not at θ greater than 0.60 to 0.75.

(iv) q_D values for both nitrogen and argon approach the values of the energy of liquefaction of the adsorbate at θ values close to 1. This seems to provide good reason for using the saturation vapour pressure of supercooled liquid argon, rather than solid argon, when calculating relative pressures for representing isotherms of argon on rutile.

The observation in (ii) provides evidence that the large values

for q_D (nitrogen) at low values of θ are not to be ascribed solely to the enhancement of dispersion forces in micropores. Such enhancement would depend primarily on the ratio of molecular diameter to pore width, and as nitrogen and argon molecules are approximately the same size[204] enhancement should occur for both adsorbates. The θ values noted in (i) are consistent with the conclusions from the BET analysis discussed in section 7-2. The changes in q_D between 150 and 250°C outgassing occur at low coverages and are not reflected in the BET C constant. Between 250 and 400°C changes in q_D do occur at larger values of θ, and are beginning to be detected by the BET analysis in terms of an increased C constant. The nitrogen calorimetry data on rutile emphasize yet again the limitations of the BET C constant. The q_D versus θ curves for rutile, and the BET analyses, indicate very strong specific interaction of nitrogen with the rutile surface. This interaction appears to involve a small proportion of high energy sites, at least up to an outgassing temperature of 250°C. From the discussion in section 7-1 a rutile surface outgassed at 150°C would be substantially free of hydrogen bonded molecular water and would consist of ligand water molecules and surface hydroxyl groups. Various models[162-163,394] for titanium dioxide have proposed that 40 to 50% of the surface consists of ligand water molecules. The difference between the q_D curves for argon and nitrogen after outgassing at 150°C is reflecting the specific interaction[393] of the nitrogen quadrupole[168-169] primarily with surface hydroxyl groups. Outgassing between 150 and 400°C may remove both ligand water molecules, exposing cations, and hydroxyl

groups from the titanium dioxide surface. Cations in zeolites have been shown[395] to react very strongly with nitrogen and it has been suggested[158] that the potential energy of interaction is minimised when the nitrogen molecule is orientated "end-on" to a surface cation. Dehydroxylation on the other hand would give a reduced specific interaction with nitrogen. The curves of q_D versus θ represent the sum effect of cation exposure and dehydroxylation. It appears then that increases of q_D at θ less than 0.5 (i.e. 50% coverage) represent the removal of ligand water and the exposure of surface cations. These increases occur primarily over the 150 to 250°C range, corresponding to the increase in BET monolayer capacity (section 7-2), and 50% of the surface agrees very well with the models for titanium dioxide. Because removal of ligand water and surface hydroxyl groups would give opposing changes in q_D, the increases after outgassing from 250 to 400°C cannot be used as evidence that dehydroxylation has not occurred. The constancy of the BET monolayer capacity may indicate that no further localisation occurs over this range of outgassing temperature. That the removal of ligand water molecules from the rutile surface gives a very marked increase in the surface field strength is further indicated by the increases in q_D for argon adsorption. It is possible that these increases are indicating a small amount of microporosity in the sample which is not accessible to argon until the removal of ligand water between 150 to 250°C. However the argon isotherm shapes do not indicate <u>increased</u> microporosity (section 7-2). An alternate explanation is an increased ϕ_P interaction for argon due to strong surface field/induced dipole interactions. The polarizabilities of

argon and nitrogen are approximately the same[168,325] and ϕ_p terms are usually considered small. However, the strong surface field of rutile may well lead to a significant contribution from this type of interaction for both argon and nitrogen.

The adsorption isotherms and calorimetric data show therefore, that any model for the adsorption of argon and nitrogen on rutile must take account of localised adsorption on high energy surface sites. The changes in BET monolayer capacity between outgassing at 150 and 250°C do not reflect a change in surface area. It would not be meaningful to calculate the change in BET monolayer capacity due to the localisation of one nitrogen molecule per exposed cation, due to the unknown extent of localisation occurring on surface hydroxyl groups. However, the cation density figures given in the models of Munuera[163] and Hockey[162] would predict an increase in monolayer capacity, as observed, due to localised adsorption. The apparent localised adsorption of argon on rutile means that argon surface areas cannot be confidently calculated using $0.138nm^2$ per argon atom, and hence argon surface areas cannot be used to estimate the degree of localisation of nitrogen adsorbed on rutile.

(B) Adsorption on Silica-Coated Rutile: The differential energy of adsorption curves for all three silica-coated rutile samples are markedly different from those obtained for the base rutile. The coated samples gave curves which indicate that their surfaces are more energetically homogeneous than that of the base rutile. This is most evident for nitrogen adsorption after outgassing at 250 and 400°C (Figures 7-10, 7-11). The form of these curves shows why the C constants were larger for nitrogen adsorption on the coated samples than on the rutile base. Even though the rutile contained some high

energy sites after outgassing at 250 and 400°C, in the BET region the differential energies of adsorption of nitrogen were greater for the silica-coated samples. The coated samples also gave a different pattern of behaviour with increasing outgassing temperature. For nitrogen adsorption (Figures 7-16, 7-17, 7-18) q_D values were slightly increased on outgassing at 250°C whilst subsequent outgassing at 400°C gave lower q_D values over a large part of monolayer formation. This change between 250 and 400°C is also reflected in a reduced C constant (Table 7-2).

q_D values for nitrogen on coated samples are larger than corresponding values for argon, indicating, as with rutile, that specific surface field-quadrupole interactions are occurring during nitrogen adsorption. The argon differential energy curves for the coated samples (Figures 7-12 to 7-14 and 7-19 to 7-21) show little evidence of enhanced values due to micropores[158] as observed in reported studies on microporous silicas[398-399].

The q_D (argon) curve for rutile shows much larger changes on outgassing from 150 to 400°C than do the corresponding curves for the silica containing samples. Titanium dioxide lattices are more compact than those of silica[382] and hence dispersion interactions would be larger for titanium dioxide. In contrast to this the adsorption studies discussed in section 7-1 did indicate that some adsorption space within silica coatings might be accessible under some conditions. Such penetration might be expected to give enhanced dispersion interactions. It cannot, therefore, be concluded that the enhancement in q_D (argon) for rutile compared with silica-coated rutile is due to different dispersion interactions or specific interactions

between argon and rutile.

The q_D (nitrogen) curves provide much evidence for the nature of the interaction of nitrogen with coated samples and for the location of silica on the rutile surface in the partially coated samples. For all three coated samples the specific interaction of nitrogen with a portion of the surface containing very high energy sites, as found for rutile, is not observed (Figures 7-10 and 7-11). This implies that the interaction of silica with the surface of rutile has either completely covered ligand water molecules, or replaced them, with species that are not removed on outgassing at up to 400°C. For the 2.6 wt.% silica sample all previous discussion has indicated a uniform coating of silica with Si-OH, not Ti-OH, groups accessible to nitrogen. The lowering of q_D (nitrogen) on outgassing from 250 to 400°C is consistent with slight dehydroxylation, as other studies on pure amorphous silicas[396-397] have shown that complete dehydroxylation (at approximately 1000°C) results in the same q_D curve being obtained for argon and nitrogen.

A feature seen only in the q_D (nitrogen) curves for the 2.6 wt.% silica sample was an apparent discontinuity at $\theta = 0.56$. This effect, although relatively small, was well reproduced after outgassing at 150 and 250°C but was not observed after outgassing at 400°C (Figure 7-18). The reason for the discontinuity is unknown, but its disappearance at 400°C may indicate a change in the type of hydroxyls accessible to nitrogen. The increase in outgassing temperature from 250 to 400°C was accompanied by a slight increase in BET monolayer capacity (Table 7-2), and it is possible that additional hydroxyl groups within the coating have become accessible

to nitrogen.

All the nitrogen and argon adsorption data for the 2.6 wt.% silica sample are consistent, therefore, with it having a uniform coating of amorphous silica thick enough to shield any specific effects of the underlying titanium dioxide particle. A completely hydroxylated silica surface, which is more open than that of titania[382], has meant that for this sample specific interactions of nitrogen are greater than for the base rutile when the latter does not possess exposed cation sites (Figure 7-9). For the fully coated sample adsorption of nitrogen would not be localised to the same extent as on high energy rutile and BET monolayer capacities are more meaningful. Comparisons with the low energy rutile surface (outgassed 150°C) show that some volume within the surface coating may be accessible to argon and nitrogen at all outgassing temperatures investigated.

The calorimetric data indicate that for <u>both</u> the low silica content samples the high energy sites characteristic of rutile are not exposed on outgassing at 250°C. However, although at all three outgassing temperatures used the interaction of nitrogen on the <u>most</u> active sites (i.e. at $\theta = 0.02$) was the same for all three silica containing samples (Figures 7-9, 7-10, 7-11), the nature of the q_D versus θ curves does indicate that the lower silica content samples have more energetically heterogeneous surfaces. The pattern is very clear after outgassing at 250 and 400°C. <u>An</u> explanation for this behaviour would be that the 0.6 and 0.9 wt.% silica samples have both Si-OH and Ti-OH surface species.

In summary, the calorimetric data have shown clear differences between the samples studied, confirming and extending the information obtained from isotherm analyses. The outgassing conditions were chosen to this end, and although some information on coating structure has been obtained a full study of surface textures has not been undertaken.

FIGURES 7-1 to 7-8
NITROGEN AND ARGON ADSORPTION ISOTHERMS

FIGURE 7-1

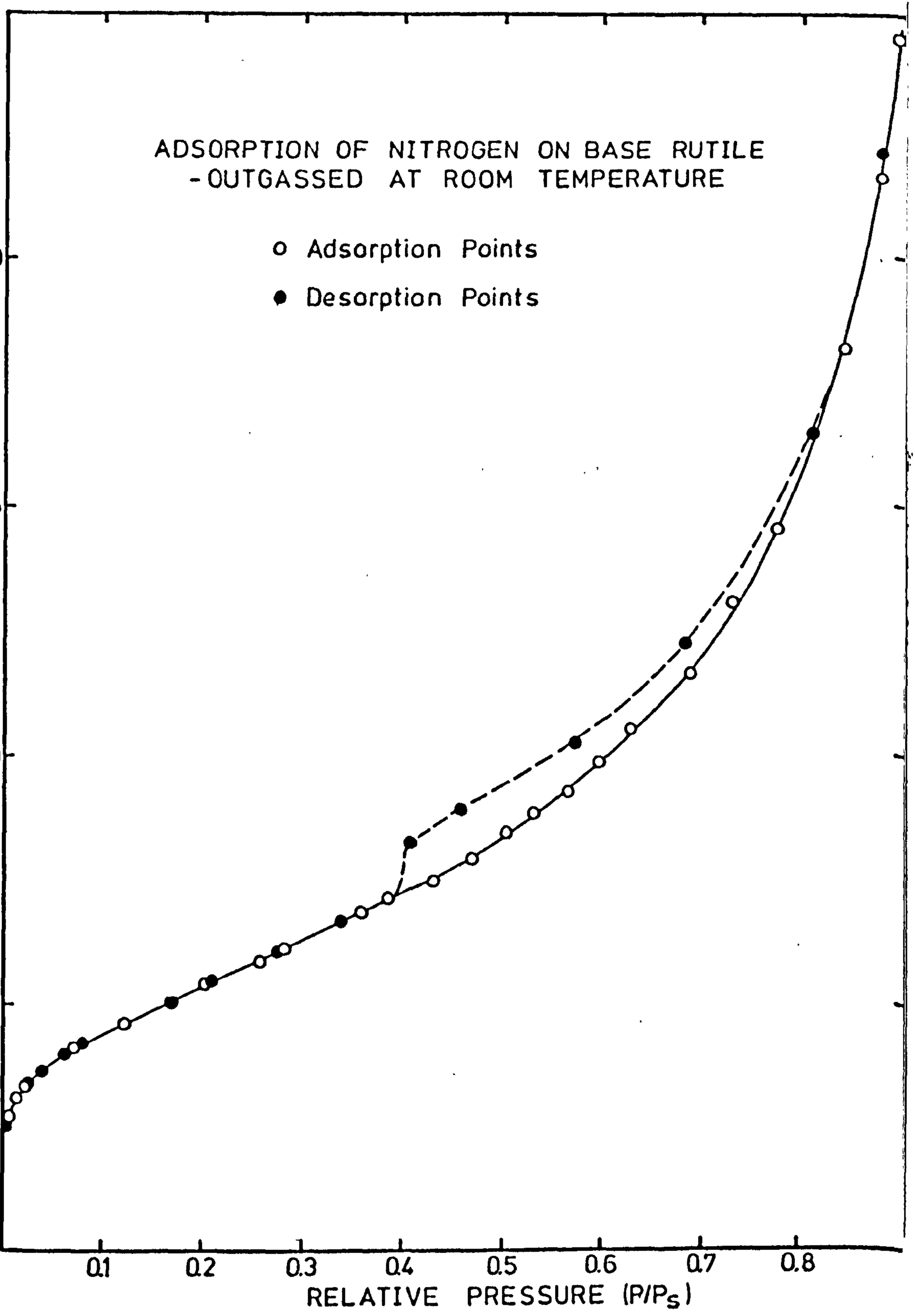
ADSORPTION OF NITROGEN ON BASE RUTILE
-OUTGASSED AT ROOM TEMPERATURE
o Adsorption Points
● Desorption Points
AMOUNT ADSORBED (cm³/gm, STP)
5
10
15
20
0.1
0.2
0.3
0.4
0.5
0.6
0.7
0.8
RELATIVE PRESSURE (P/Ps)

FIGURE 7-2

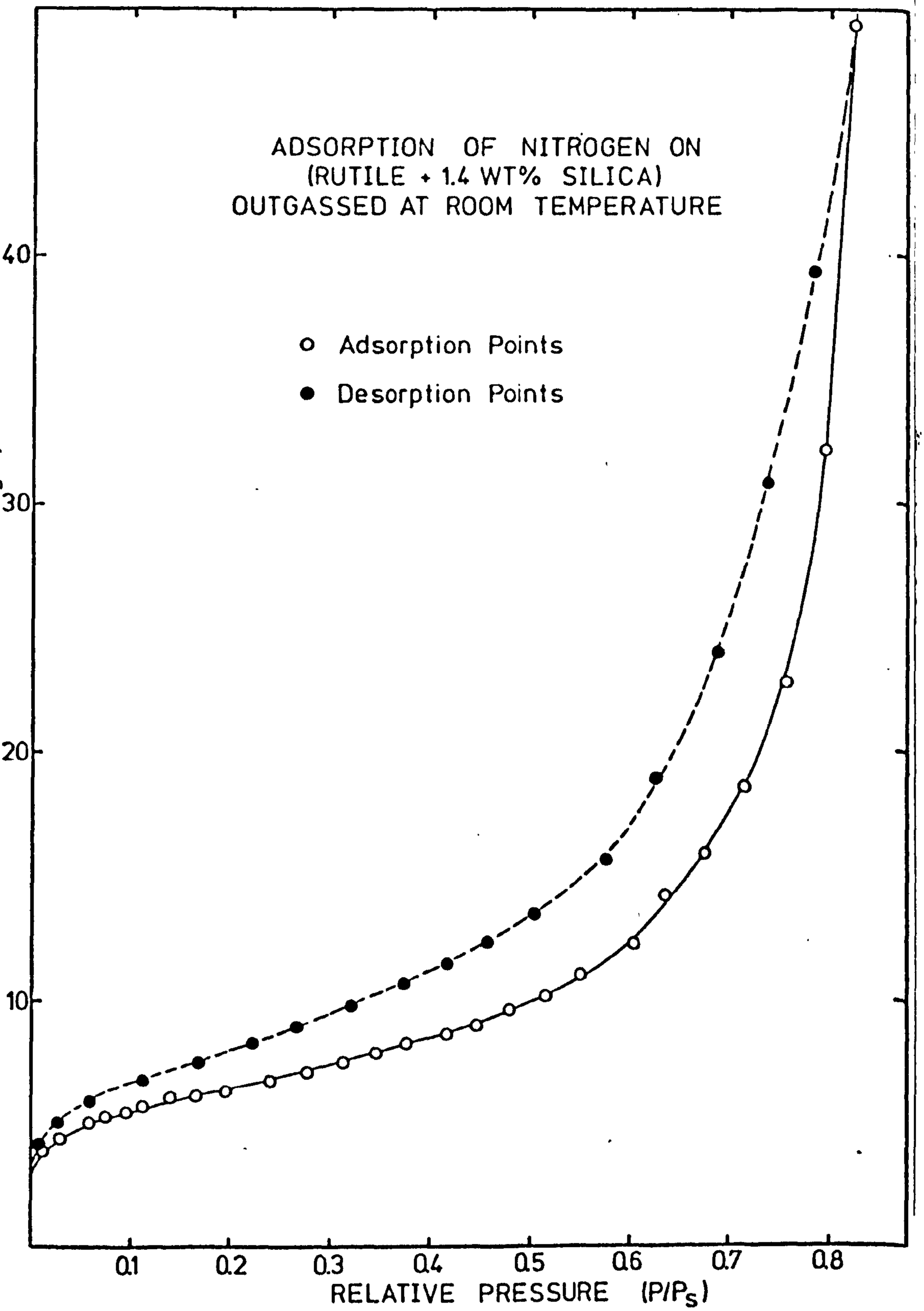
ADSORPTION OF NITROGEN ON
(RUTILE + 1.4 WT% SILICA)
OUTGASSED AT ROOM TEMPERATURE
o Adsorption Points
● Desorption Points
AMOUNT ADSORBED (cm³/gm, STP)
40
30
20
10
0.1
0.2
0.3
0.4
0.5
0.6
0.7
0.8
RELATIVE PRESSURE (P/Ps)

FIGURE 7-3

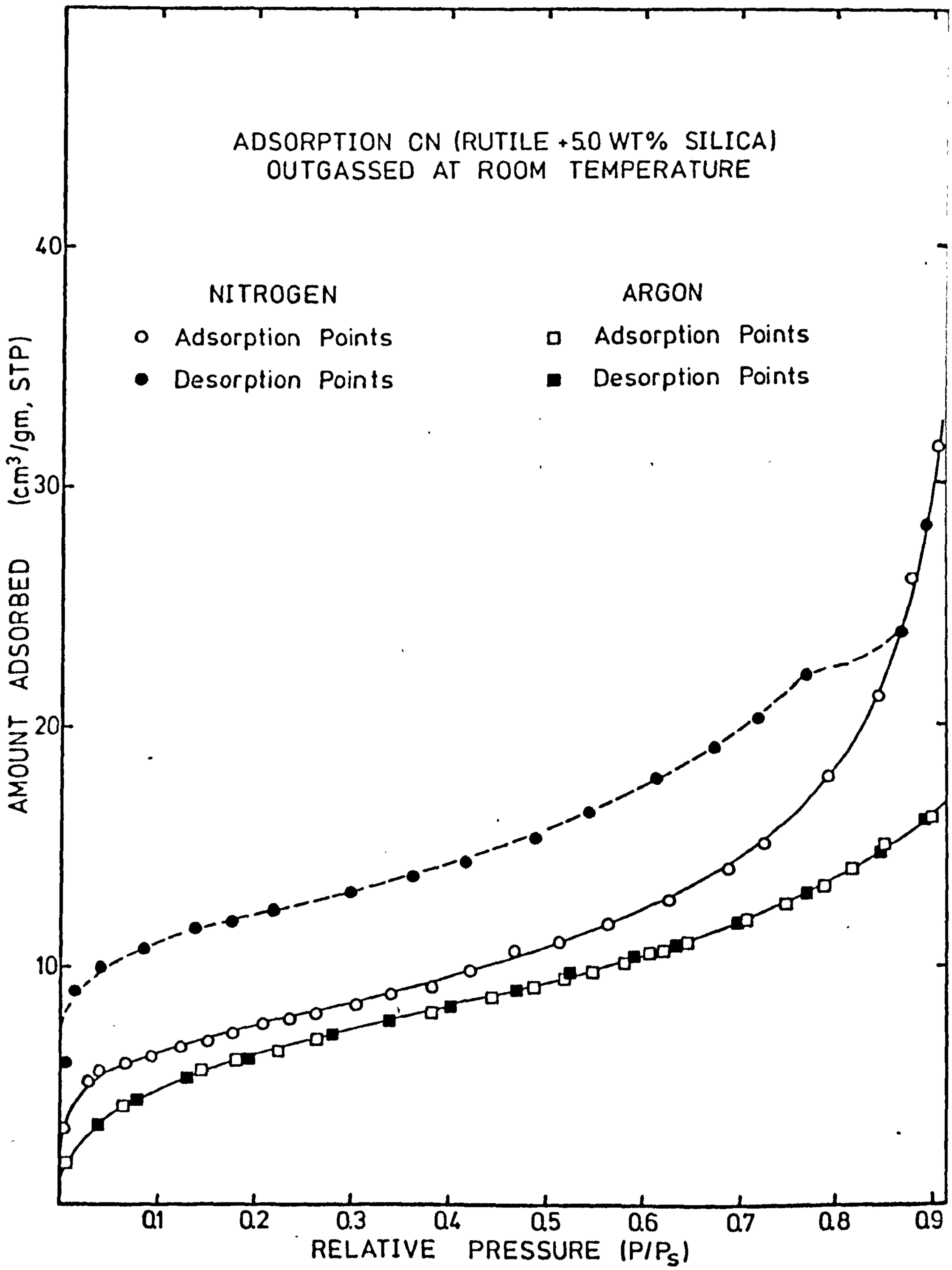
ADSORPTION ON (RUTILE + 5.0 WT% SILICA)
OUTGASSED AT ROOM TEMPERATURE
NITROGEN
Adsorption Points
Desorption Points
ARGON
Adsorption Points
Desorption Points
AMOUNT ADSORBED (cm³/gm, STP)
40
30
20
10
0.1
0.2
0.3
0.4
0.5
0.6
0.7
0.8
0.9
RELATIVE PRESSURE (P/Ps)

FIGURE 7-4

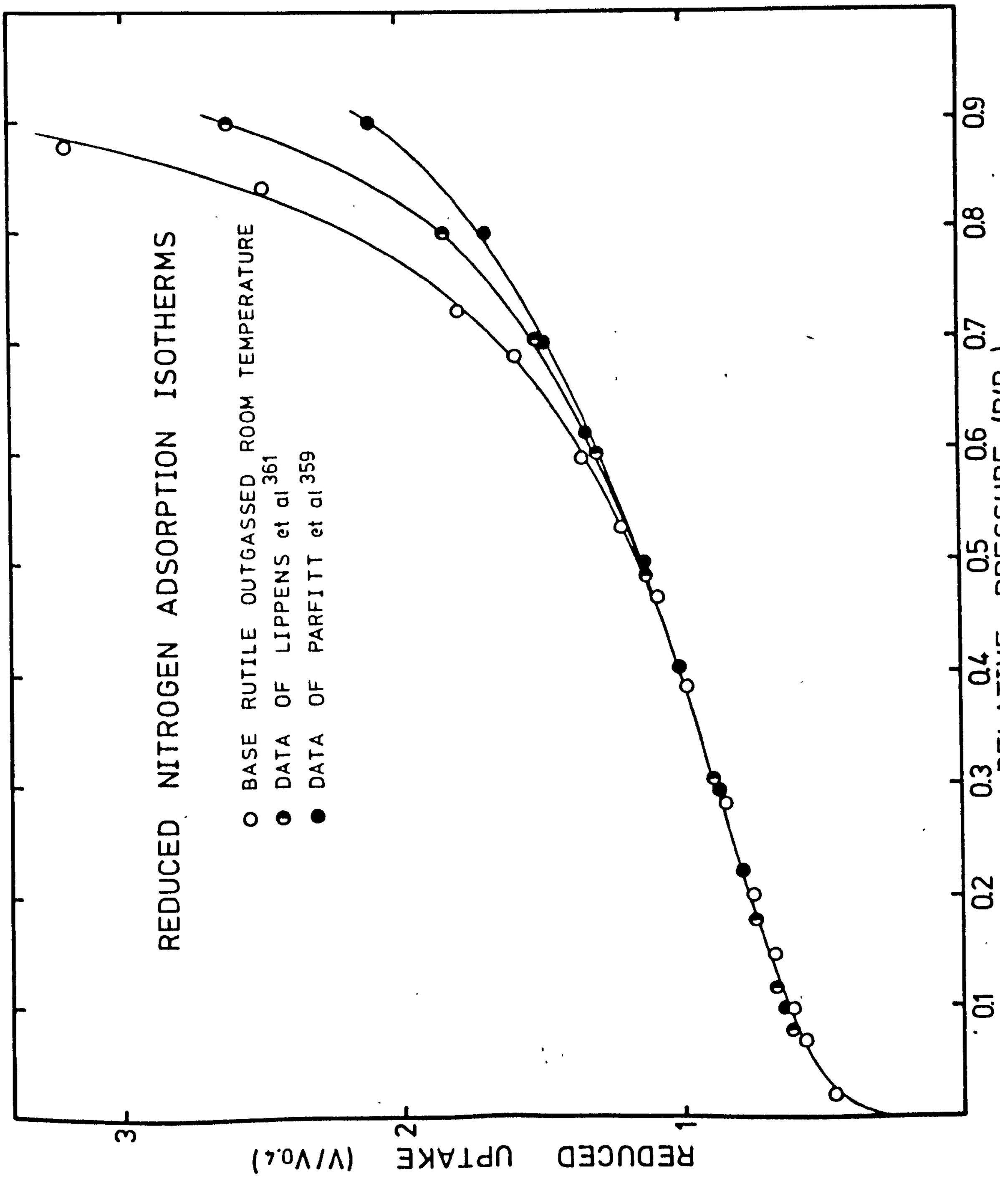
REDUCED NITROGEN ADSORPTION ISOTHERMS
O BASE RUTILE OUTGASSED ROOM TEMPERATURE
● DATA OF LIPPENS et al[361]
● DATA OF PARFITT et al[359]
REDUCED UPTAKE (V/V0.1)
RELATIVE PRESSURE (P/Pe)
1
2
3
0.1
0.2
0.3
0.4
0.5
0.6
0.7
0.8
0.9

FIGURE 7-5

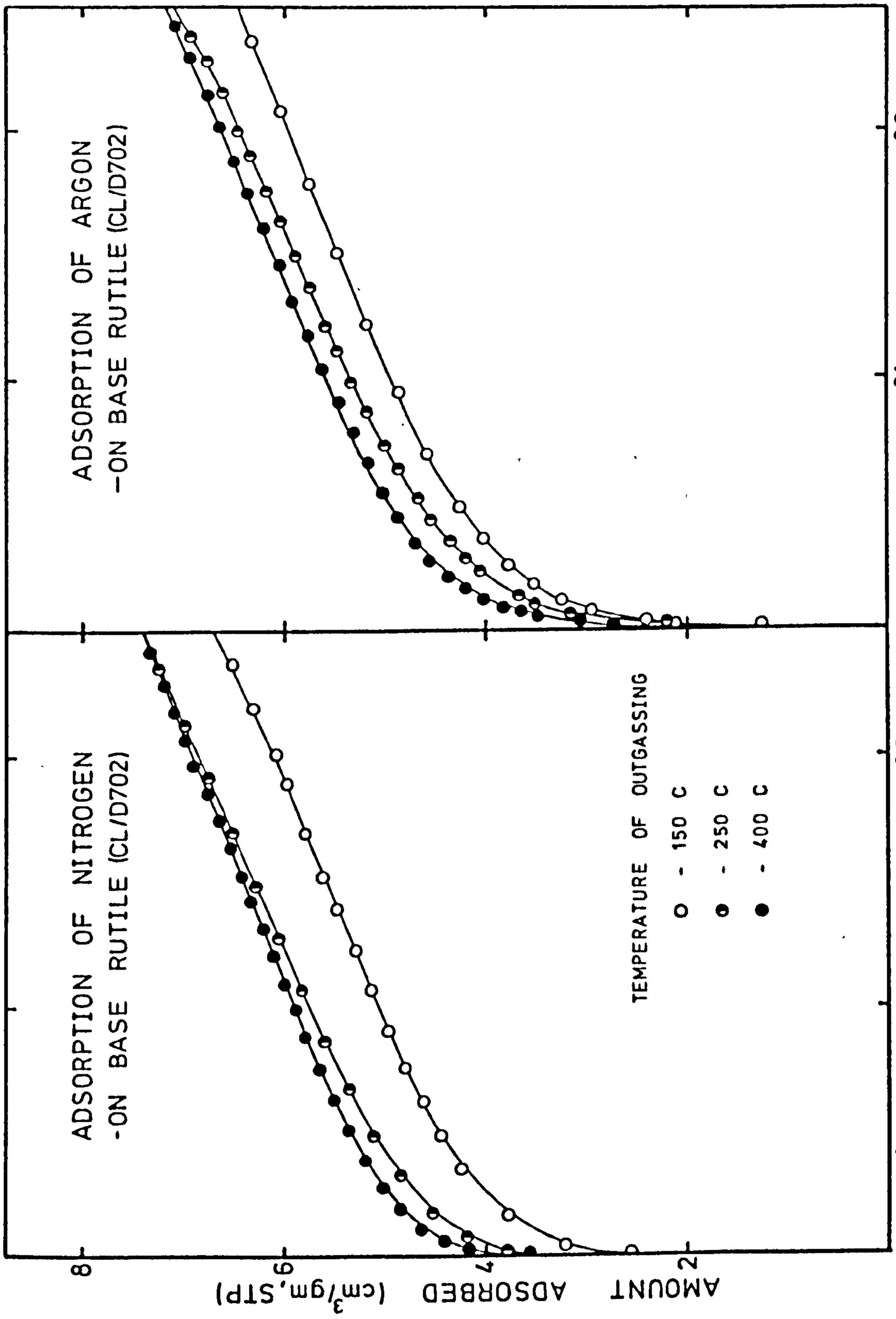
ADSORPTION OF NITROGEN -ON BASE RUTILE (CL/D702)
ADSORPTION OF ARGON -ON BASE RUTILE (CL/D702)
TEMPERATURE OF OUTGASSING
O - 150 C
● - 250 C
● - 400 C
AMOUNT ADSORBED (cm³/gm,STP)
RELATIVE PRESSURE (P/Ps)
0.1
0.2
2
4
6
8

FIGURE 7-6

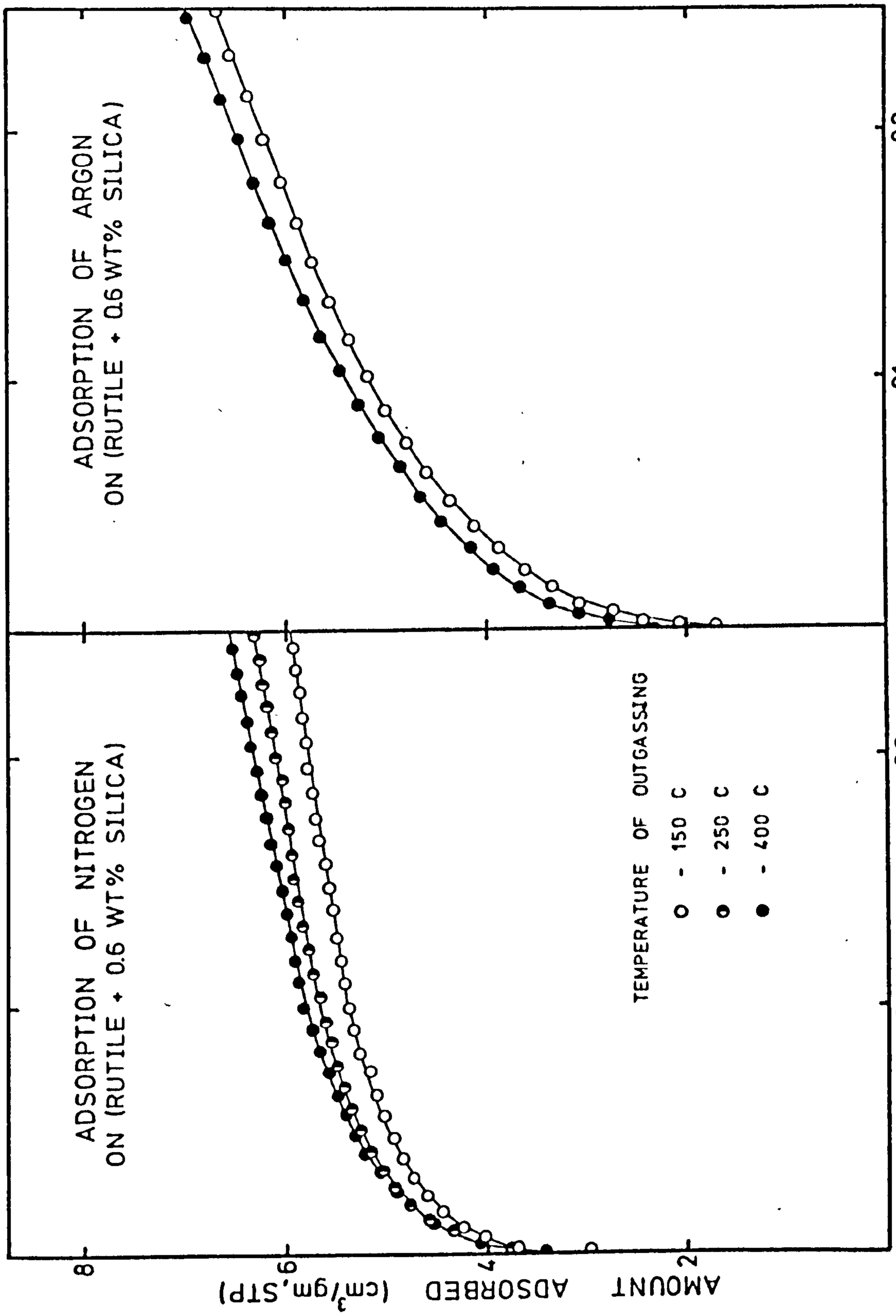
ADSORPTION OF NITROGEN ON (RUTILE + 0.6 WT% SILICA)
ADSORPTION OF ARGON ON (RUTILE + 0.6 WT% SILICA)
TEMPERATURE OF OUTGASSING
○ - 150 C
◎ - 250 C
● - 400 C
AMOUNT ADSORBED (cm³/gm,STP)
RELATIVE PRESSURE (P/Ps)
0.1
0.2
0.1
0.2
2
4
6
8

FIGURE 7-7

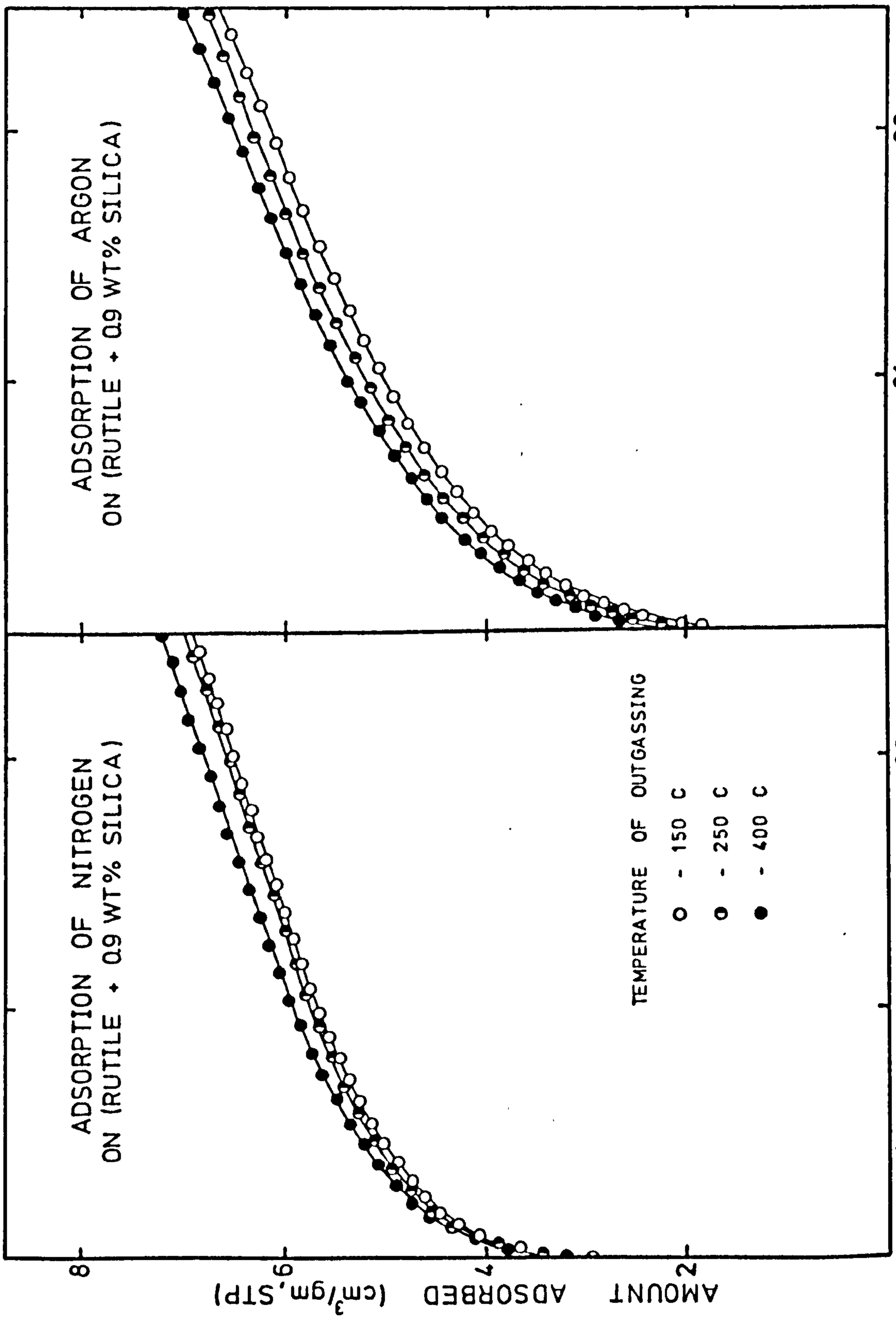
ADSORPTION OF ARGON
ON (RUTILE + 0.9 WT% SILICA)
ADSORPTION OF NITROGEN
ON (RUTILE + 0.9 WT% SILICA)
TEMPERATURE OF OUTGASSING
○ - 150 C
⊖ - 250 C
● - 400 C
AMOUNT ADSORBED (cm³/gm,STP)
PRESSURE (P/P₀)
0.1
0.2
0.1
0.2
8
9
7
2

FIGURE 7-8

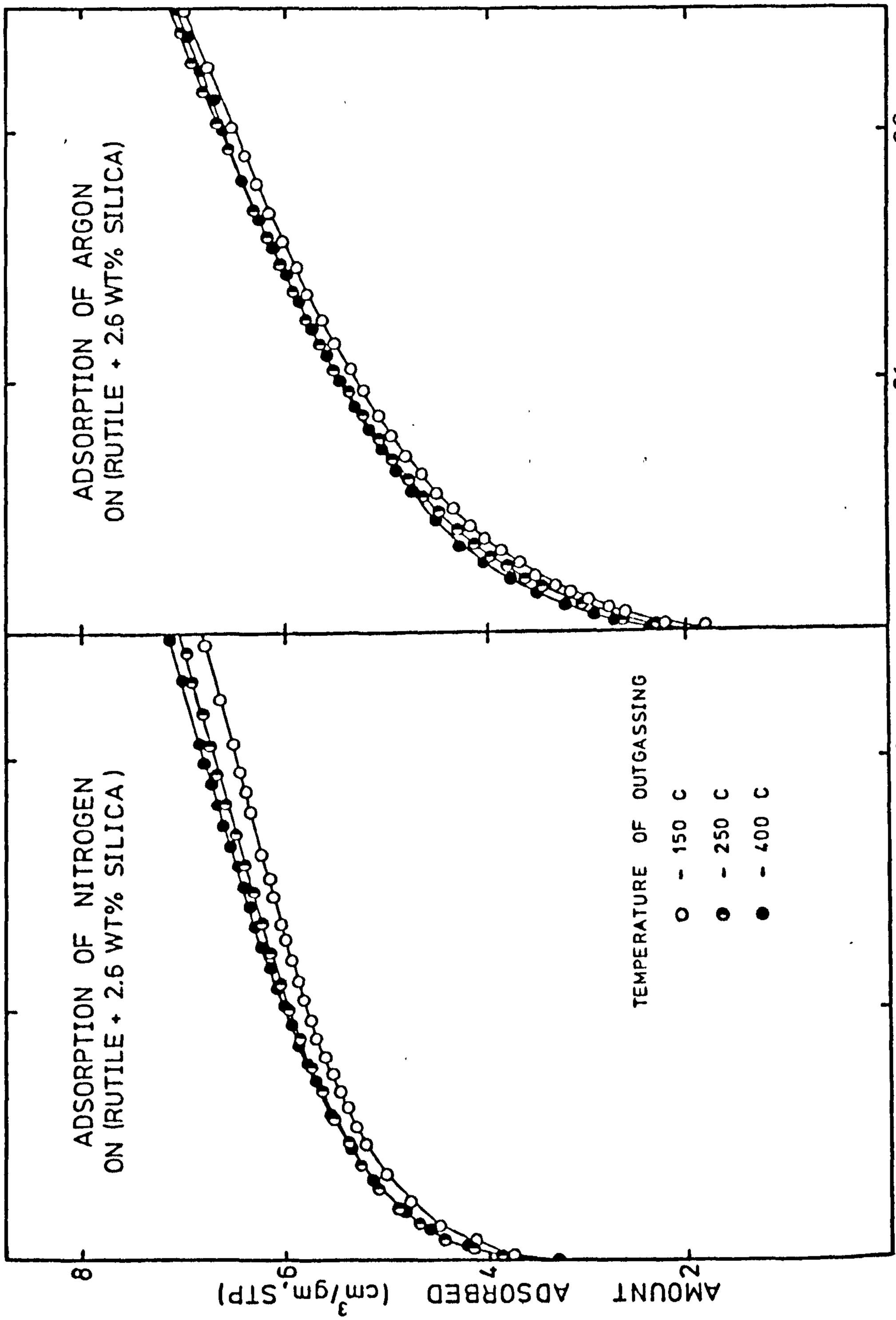
ADSORPTION OF ARGON
ON (RUTILE + 2.6 WT% SILICA)
ADSORPTION OF NITROGEN
ON (RUTILE + 2.6 WT% SILICA)
TEMPERATURE OF OUTGASSING
○ - 150 C
◐ - 250 C
● - 400 C
AMOUNT ADSORBED (cm³/gm, STP)
RELATIVE PRESSURE (P/Ps)
0.1
0.2
2
4
6
8

FIGURES 7-9 to 7-21
CURVES OF DIFFERENTIAL ENERGY OF ADSORPTION VERSUS SURFACE COVERAGE OF ADSORBATE

FIGURE 7-9

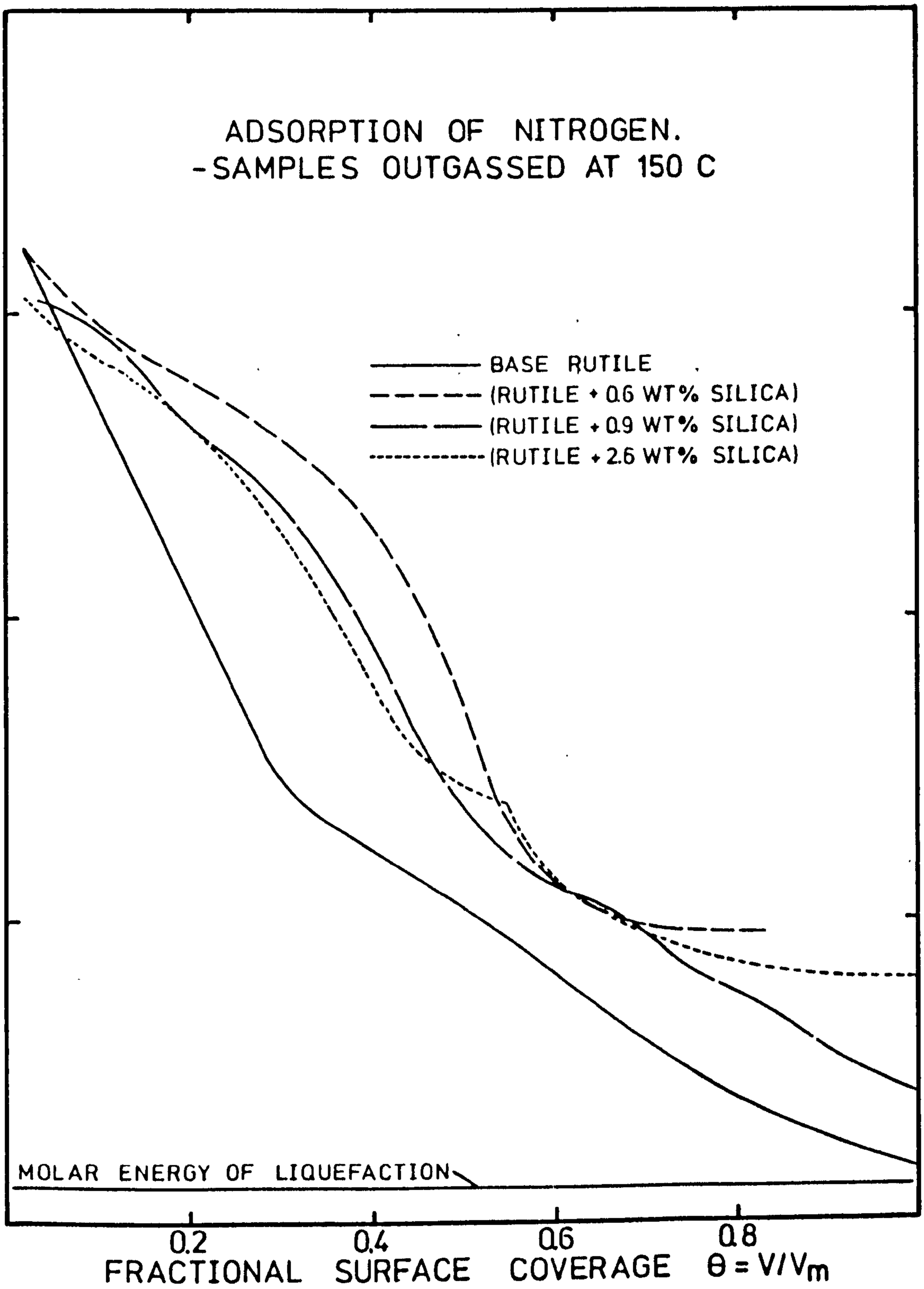
ADSORPTION OF NITROGEN.
-SAMPLES OUTGASSED AT 150 C
DIFFERENTIAL ENERGY OF ADSORPTION [KJ/MOLE]
20
15
10
BASE RUTILE
(RUTILE + 0.6 WT% SILICA)
(RUTILE + 0.9 WT% SILICA)
(RUTILE + 2.6 WT% SILICA)
MOLAR ENERGY OF LIQUEFACTION
0.2
0.4
0.6
0.8
FRACTIONAL SURFACE COVERAGE θ = V/Vm

FIGURE 7-10

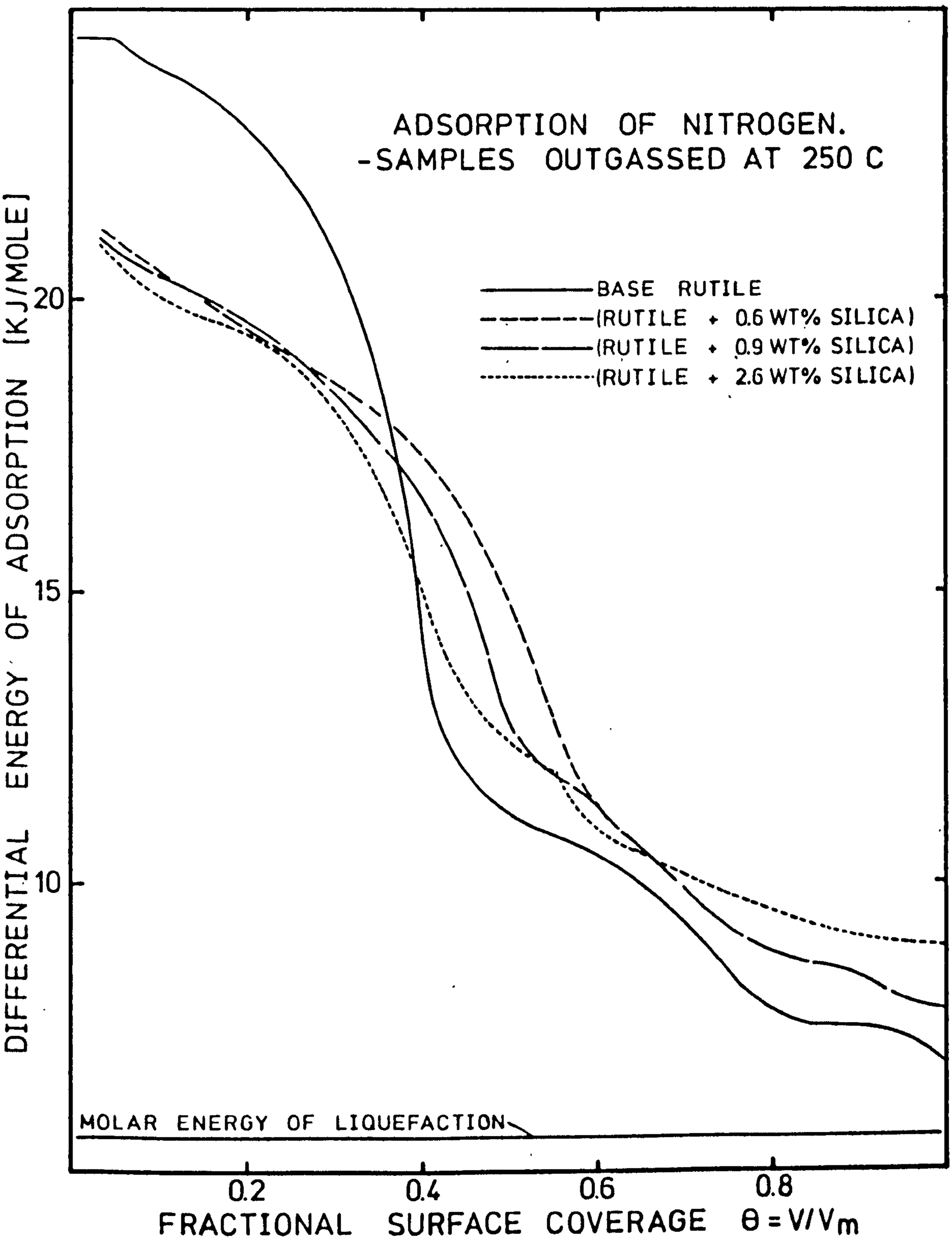
ADSORPTION OF NITROGEN.
-SAMPLES OUTGASSED AT 250 C
BASE RUTILE
(RUTILE + 0.6 WT% SILICA)
(RUTILE + 0.9 WT% SILICA)
(RUTILE + 2.6 WT% SILICA)
DIFFERENTIAL ENERGY OF ADSORPTION (KJ/MOLE)
20
15
10
MOLAR ENERGY OF LIQUEFACTION
0.2
0.4
0.6
0.8
FRACTIONAL SURFACE COVERAGE θ = V/Vm

FIGURE 7-11

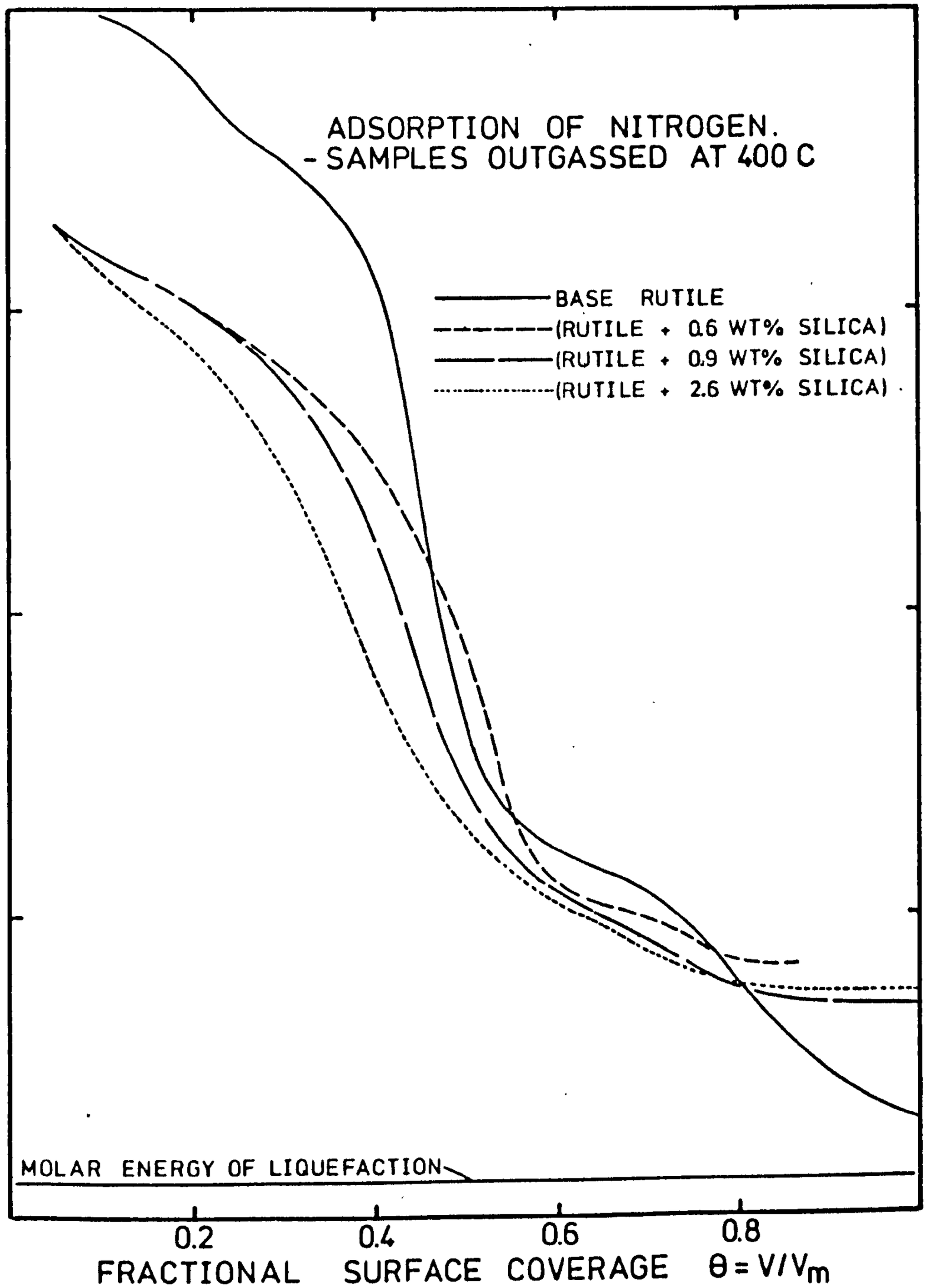
ADSORPTION OF NITROGEN.
- SAMPLES OUTGASSED AT 400 C
BASE RUTILE
(RUTILE + 0.6 WT% SILICA)
(RUTILE + 0.9 WT% SILICA)
(RUTILE + 2.6 WT% SILICA)
DIFFERENTIAL ENERGY OF ADSORPTION [KJ/MOLE]
20
15
10
MOLAR ENERGY OF LIQUEFACTION
0.2
0.4
0.6
0.8
FRACTIONAL SURFACE COVERAGE θ = V/Vm

FIGURE 7-12

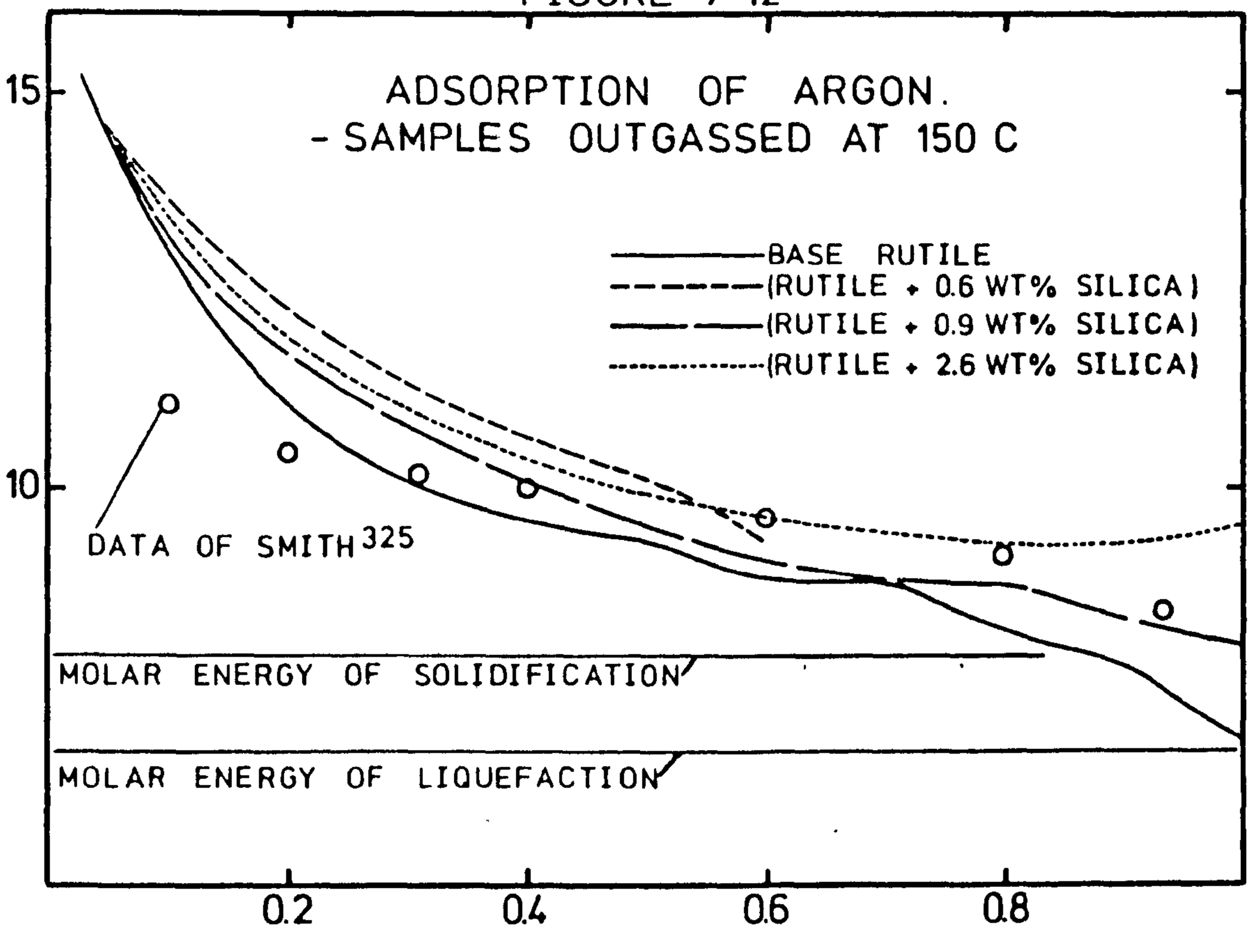

FIGURE 7-13

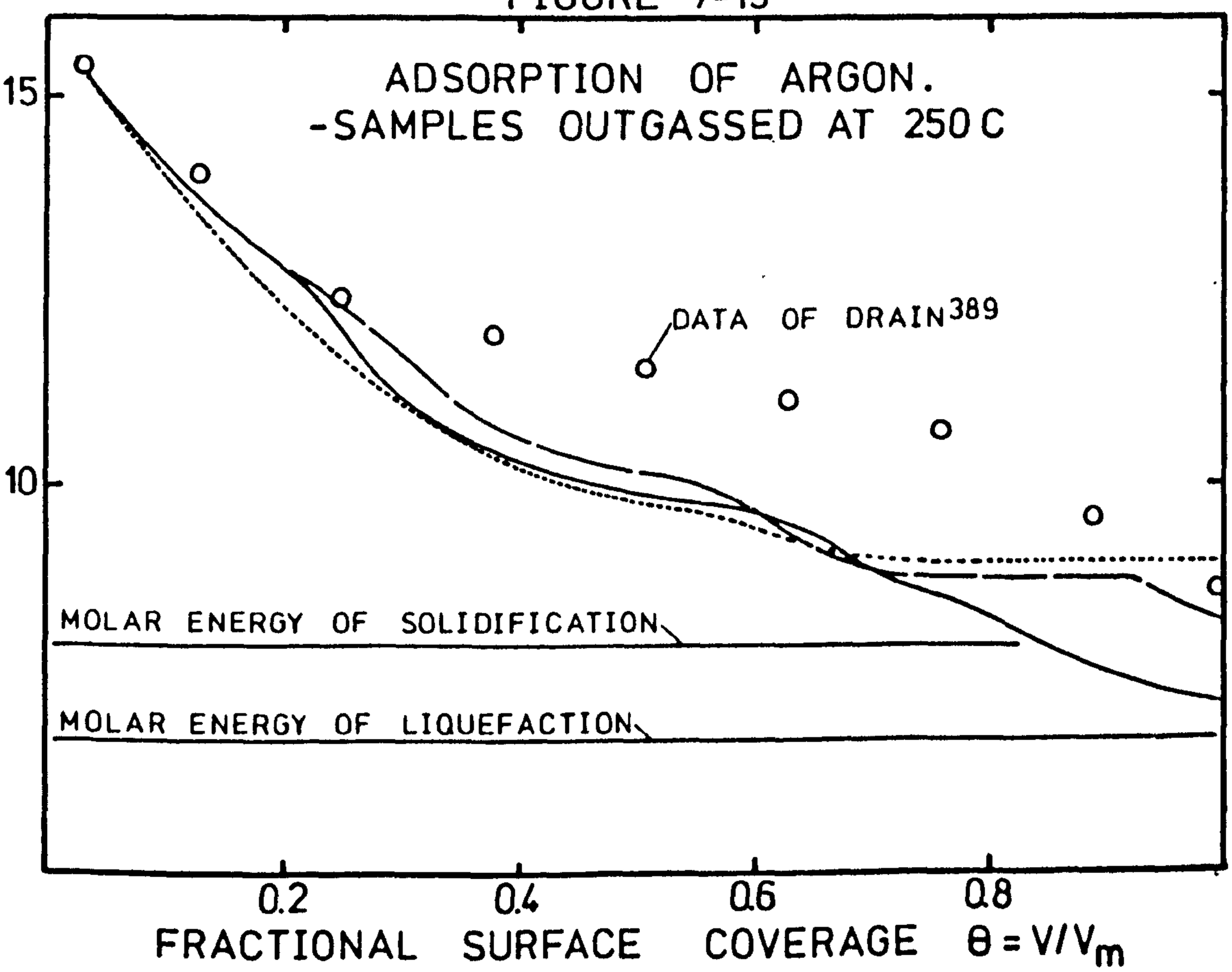

FIGURE 7-14

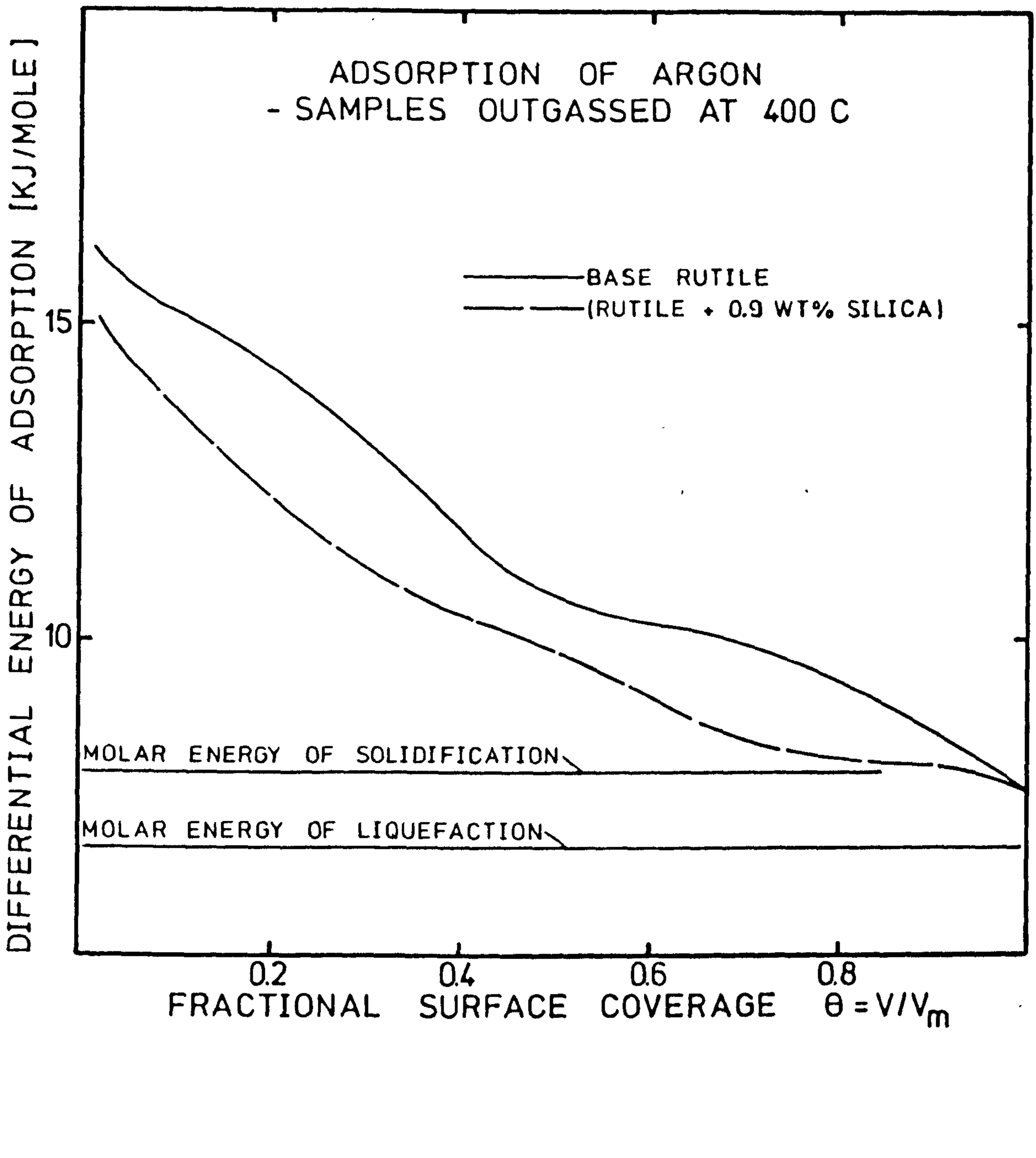
ADSORPTION OF ARGON
- SAMPLES OUTGASSED AT 400 C
BASE RUTILE
(RUTILE + 0.9 WT% SILICA)
DIFFERENTIAL ENERGY OF ADSORPTION [KJ/MOLE]
15
10
MOLAR ENERGY OF SOLIDIFICATION
MOLAR ENERGY OF LIQUEFACTION
0.2
0.4
0.6
0.8
FRACTIONAL SURFACE COVERAGE θ = V/Vm

FIGURE 7-15

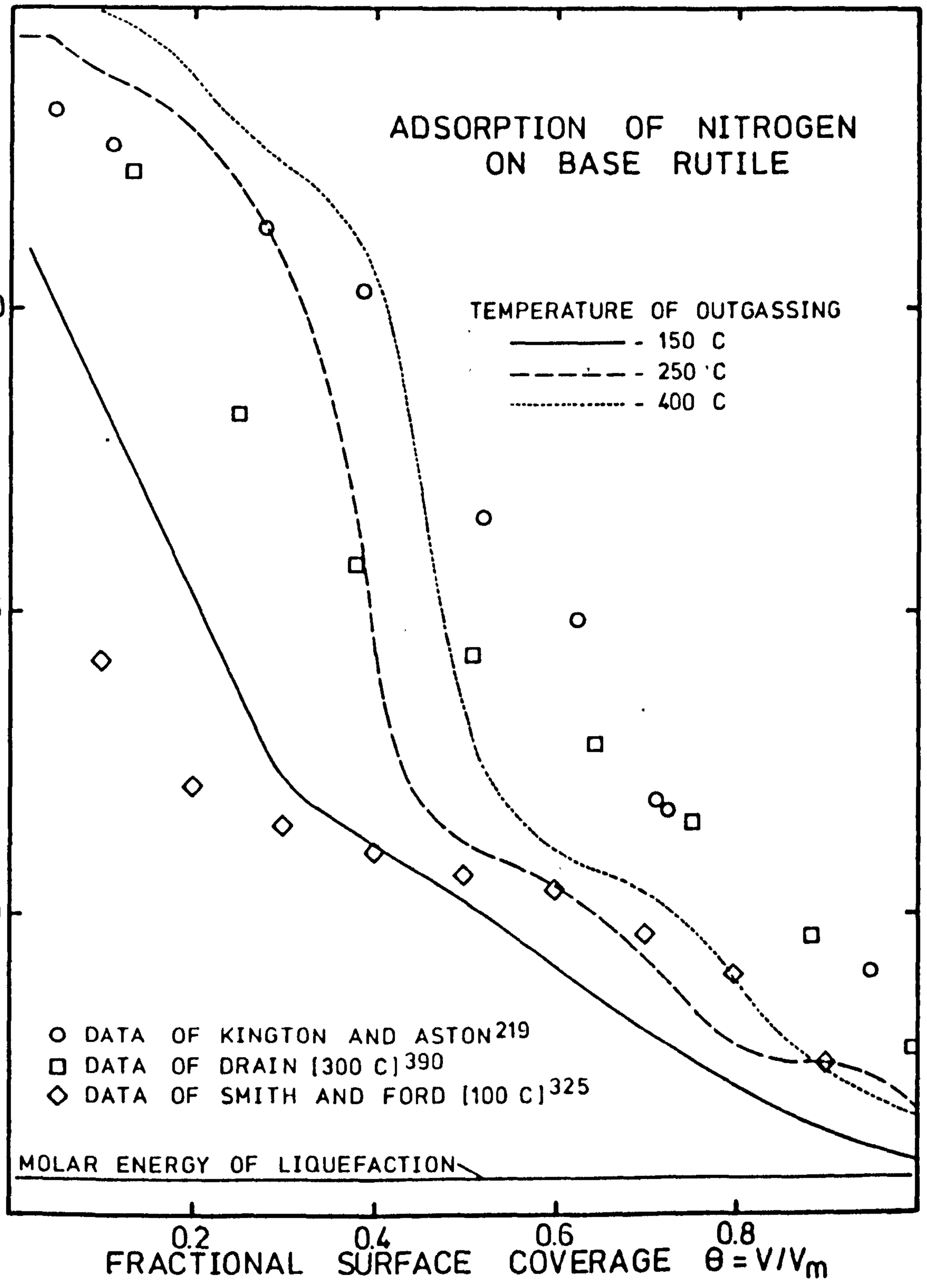
ADSORPTION OF NITROGEN
ON BASE RUTILE
TEMPERATURE OF OUTGASSING
150 C
250 C
400 C
DIFFERENTIAL ENERGY OF ADSORPTION [KJ/MOLE]
20
15
10
DATA OF KINGTON AND ASTON 219
DATA OF DRAIN [300 C] 390
DATA OF SMITH AND FORD [100 C] 325
MOLAR ENERGY OF LIQUEFACTION
0.2
0.4
0.6
0.8
FRACTIONAL SURFACE COVERAGE θ = V/Vm

FIGURE 7-16

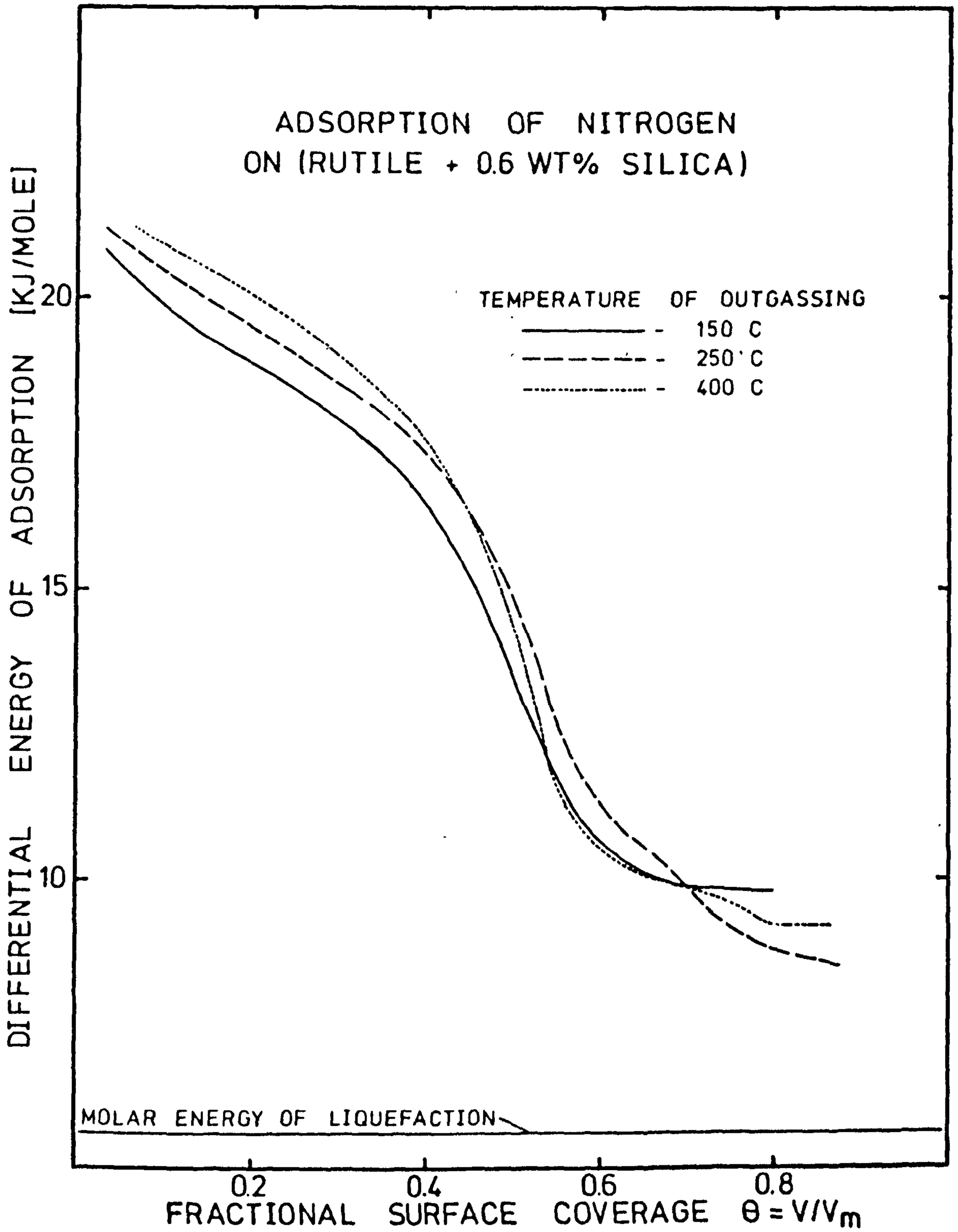
ADSORPTION OF NITROGEN
ON (RUTILE + 0.6 WT% SILICA)
TEMPERATURE OF OUTGASSING
150 C
250 C
400 C
DIFFERENTIAL ENERGY OF ADSORPTION (KJ/MOLE)
20
15
10
MOLAR ENERGY OF LIQUEFACTION
0.2
0.4
0.6
0.8
FRACTIONAL SURFACE COVERAGE θ = V/Vm

FIGURE 7-17

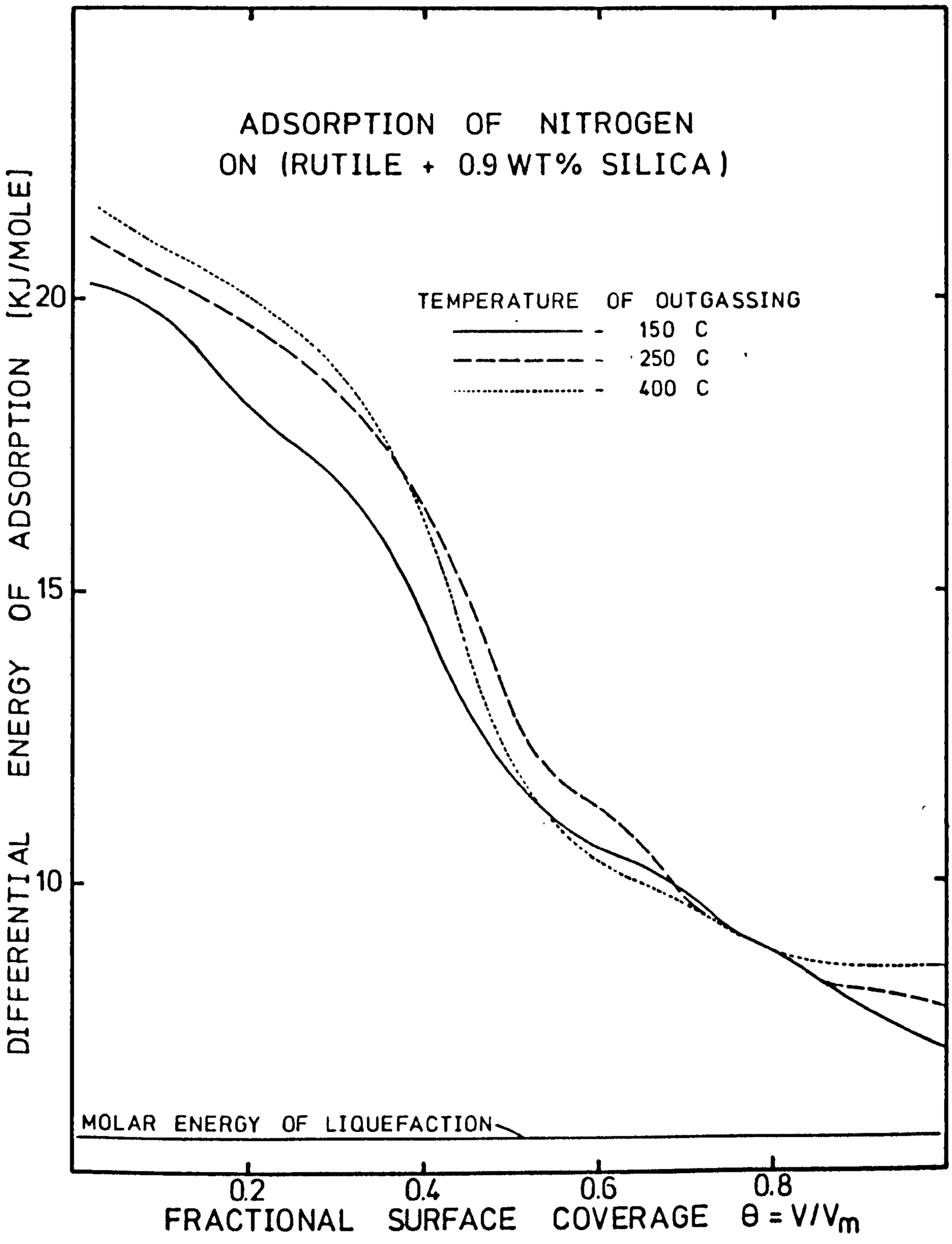
ADSORPTION OF NITROGEN
ON (RUTILE + 0.9 WT% SILICA)
TEMPERATURE OF OUTGASSING
150 C
250 C
400 C
DIFFERENTIAL ENERGY OF ADSORPTION [KJ/MOLE]
20
15
10
MOLAR ENERGY OF LIQUEFACTION
0.2
0.4
0.6
0.8
FRACTIONAL SURFACE COVERAGE θ = V/Vm

FIGURE 7-18

ADSORPTION OF NITROGEN
ON (RUTILE + 2.6 WT% SILICA)
TEMPERATURE OF OUTGASSING
150 C
250 C
400 C
DIFFERENTIAL ENERGY OF ADSORPTION [KJ/MOLE]
20
15
10
MOLAR ENERGY OF LIQUEFACTION
0.2
0.4
0.6
0.8
FRACTIONAL SURFACE COVERAGE θ = V/Vm

FIGURE 7-19

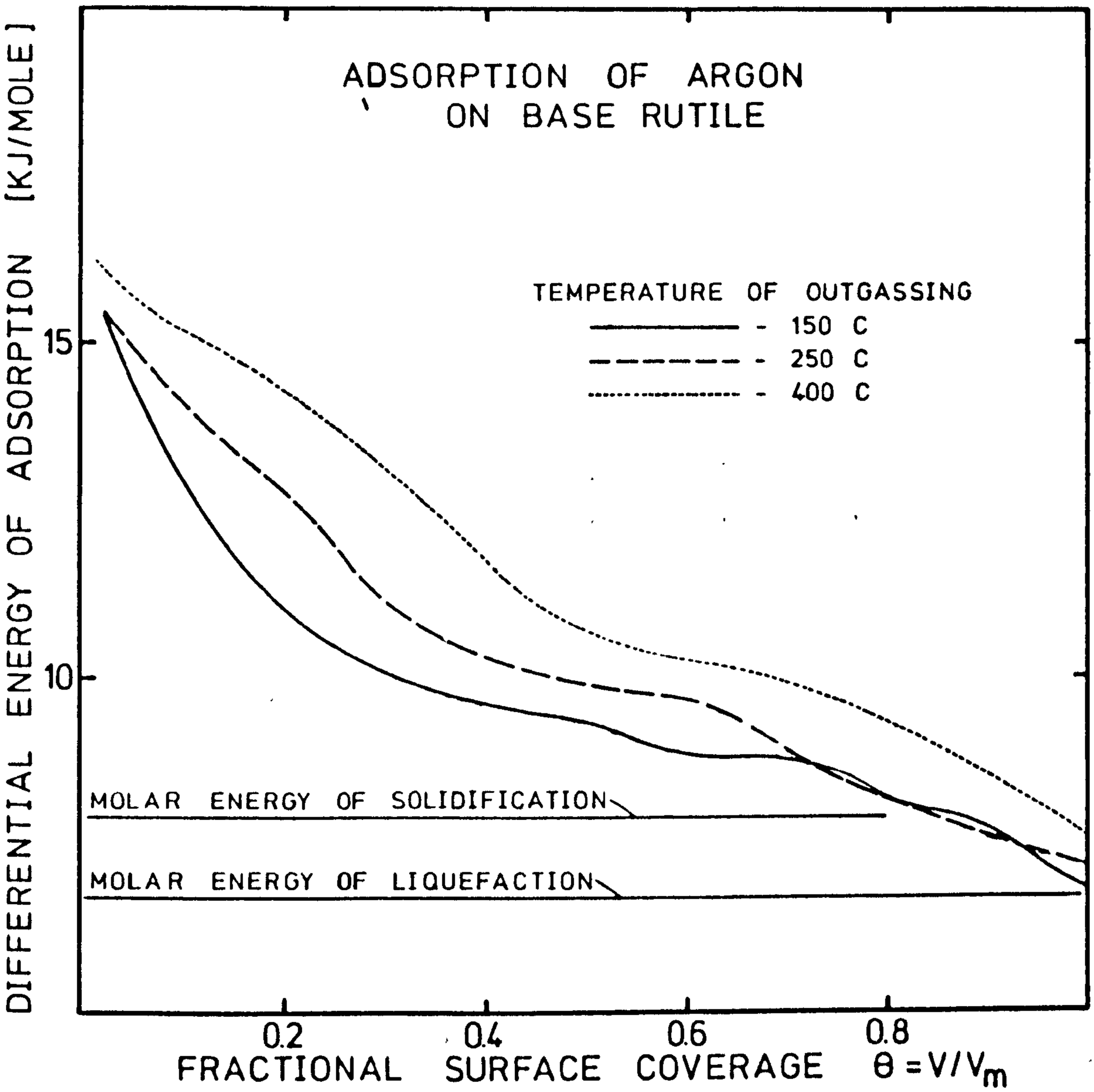
ADSORPTION OF ARGON
ON BASE RUTILE
TEMPERATURE OF OUTGASSING
150 C
250 C
400 C
DIFFERENTIAL ENERGY OF ADSORPTION [KJ/MOLE]
15
10
MOLAR ENERGY OF SOLIDIFICATION
MOLAR ENERGY OF LIQUEFACTION
0.2
0.4
0.6
0.8
FRACTIONAL SURFACE COVERAGE θ = V/Vm

FIGURE 7-20

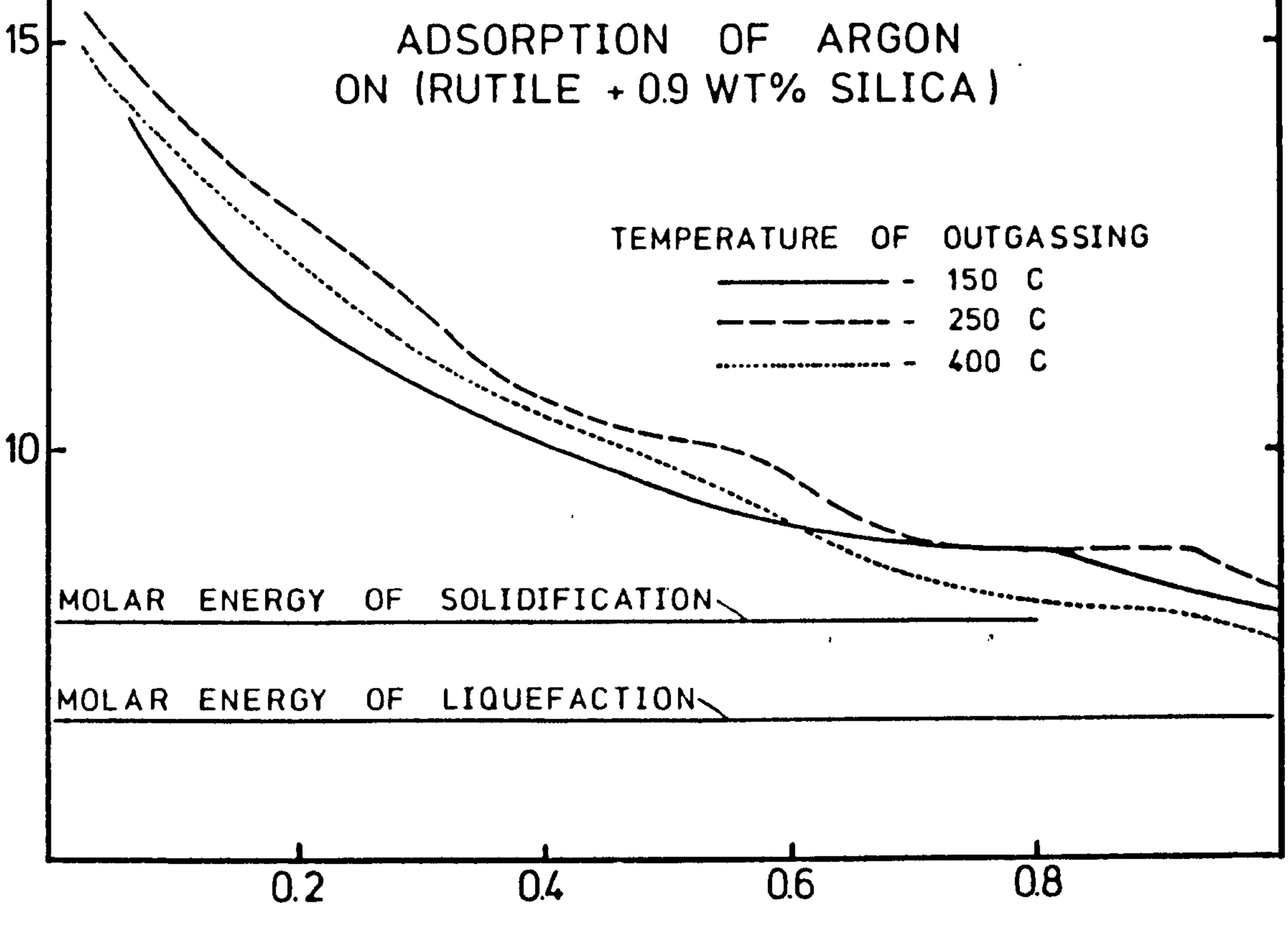

FIGURE 7-21

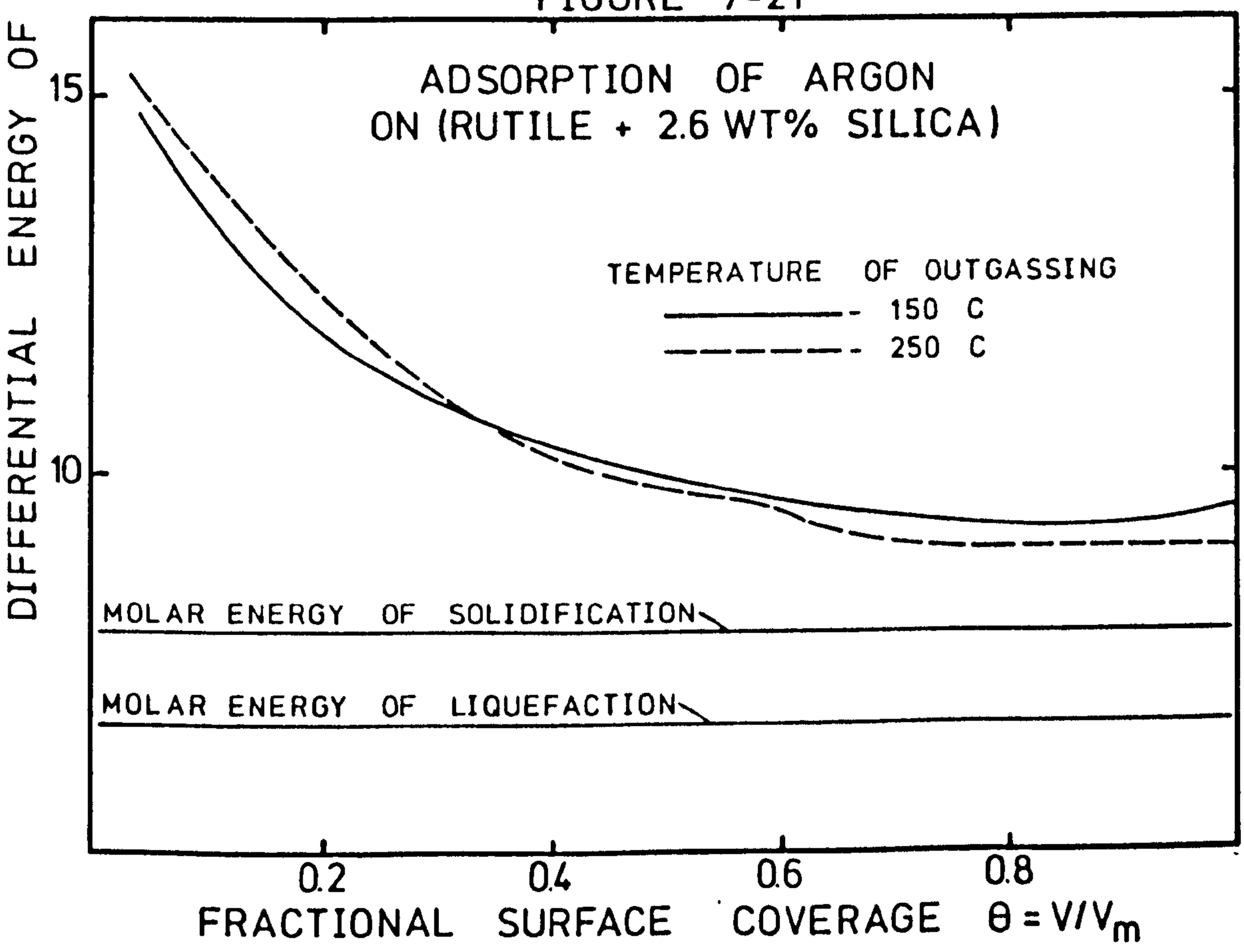

CHAPTER 8: RESULTS AND DISCUSSION - IV

WATER SORPTION ON SILICA-COATED RUTILE

8 - 1 Water Sorption versus Silica Coverage

The water vapour adsorption isotherms at 25°C for the base rutile and for rutile + 0.6, 1.4, 2.6 and 5.0 wt.% silica are given in Figures 8-1 to 8-7. The silica coatings on the latter four samples were prepared at pH 10 but each sample was neutralized to pH 7 after preparation. Samples were outgassed at 25, 100, 150 and 300°C prior to isotherm determination. Water vapour uptakes are expressed per gm. of adsorbent as has been done by other workers[214,218,364]. It was not considered necessary to express water vapour uptakes on a unit surface area basis using the BET nitrogen surface area. This procedure, as used for example by Zettlemoyer et al[213], may be suspect for the present data due to the apparent inapplicability of the BET equation to some adsorption data for rutile (See reference 214 and Chapter 7). Water vapour uptakes for all water adsorption data presented in this Chapter are expressed relative to the zero mass reading of the electrobalance after each outgassing treatment. Sample mass was taken as mass after drying at room temperature. Some samples, when left in water vapour (at P/Ps ~ 0.8) overnight prior to the desorption run, gave slight negative hysteresis (reduced uptake on desorption compared with adsorption). These small effects will be discussed in some detail in Chapter 8-2 and such desorption isotherms are not included in Figures 8-1 to 8-7. Three samples, rutile + 1.4, 2.6 and 5.0 wt.% silica gave positive hysteresis after outgassing at

300°C. These hysteresis loops did not close on pumping at 25°C and are shown in Figures 8-4, 8-5 and 8-6.

(A) Adsorption on Rutile: The adsorption isotherms for the initial sequence of outgassing, isotherms (1) to (4) in Figure 8-1, show that adsorption capacity increased when outgassing temperature was raised from 25 to 300°C. These isotherms are nearly parallel for $0.02 < (P/Ps) < 0.4$ (Figure 8-2), as has been previously reported[212,304,334] for water sorption on rutile, indicating that increased outgassing temperature has led to enhanced adsorption at low relative pressures (< 0.02). The isotherms were Type II[171] after outgassing at 25, 100 and 150°C but after outgassing at 300°C were linear in the range $0.03 < (P/Ps) < 0.27$ and exhibited normal type II multilayer adsorption at higher relative pressures (isotherms (4) and (6), Figures 8-1 and 8-2). The second "knee" in the isotherm at (P/Ps) approximately 0.25 has previously been reported for water adsorption on rutile[163,212,214,234] and similar behaviour has also been observed with zinc oxide[199]. However, there does not appear to be an explanation in the literature for the appearance of the second knee in some investigations and not in others[304,334], or for the changes represented in Figure 8-1. Dawson[212] has explained the linear portion of the water isotherm in terms of a continuous condensation process building up a close packed monolayer which is preceded and initiated by the localised adsorption of water onto an outgassed rutile surface. Dawson showed that the linear section of the isotherm was not observed for some small particle size rutiles and explained this by concluding, as have other workers[162-163], that the adsorption characteristics of rutile are linked with the lattice

geometry of exposed crystal surfaces. It would appear reasonable to propose that the non-appearance of the second knee in isotherms (1), (2) and (3) of Figures 8-1 and 8-2 is due to either surface impurities or surface structural characteristics preventing the ordered formation of a monolayer of water. It can be seen from Figure 8-1 that prolonged ageing of the base rutile in water at pH 7 has resulted in a less distinct second knee being observed in subsequent water isotherms (isotherms (5) and (7), Figure 8-1). The sample of rutile used in the present work has given (i) lower nitrogen BET C constants (Tables 7-1, 7-2) and (ii) different conditions for the applicability of the BET equation to water vapour adsorption (Table 8-1), than similar samples used in other adsorption studies[214,359]. The adsorption data confirm the conclusions of studies using other techniques, such as electrokinetics (Chapter 6-1), that the surface chemistry of titanium dioxide is dependent on sample origin and pretreatment.

The base rutile outgassed at 25°C will contain surface water in two forms — molecular water bound by co-ordinate bonds to lattice ions and chemisorbed water in the form of hydroxyl groups[211]. Outgassing at 300°C will remove ligand water molecules and may result in some dehydroxylation. It has recently been concluded[218] that (at least after 300°C outgassing) both processes are reversed on exposure to water vapour at ambient temperature. Isotherms (4) and (6) in Figure 8-1 indicate that rehydration occurs at low relative pressures (< 0.02). If the position of the second knee in isotherm (4) is taken to represent the completed water monolayer[212,214,218] then the amount of water removed from the base rutile between 25 and 300°C

TABLE 8 - 1

DATA FROM WATER ADSORPTION ISOTHERMS ON SOME SILICA-COATED RUTILE SAMPLES

Sample	T(°C) OUTGAS	BET ANALYSIS				FHH ANALYSIS	
		Vm(mg/gm)	$S_{BET}(m^2/gm)$	C	Linearity Range P/Ps	Slope	Linearity Range P/Ps
BASE RUTILE	25	2.8	9.9	24	0.06 - 0.29	2.8	0.5 - 0.8
(CL/D702)	100	3.2	11.4	23	0.06 - 0.29	4.3	0.4 - 0.8
"	150	3.7	13.1	43	0.06 - 0.29	6.2	0.4 - 0.8
"	300	BET 6.0 from second "knee"	PLOT	NON	LINEAR	3.4	0.4 - 0.8
RUTILE + 0.6	25	2.7	9.6	62	0.02 - 0.13	2.2	0.2 - 0.7
wt.% SILICA		3.0	10.6	48	0.13 - 0.25		
(NF 6/2/73)	100	3.1	11.0	43	0.04 - 0.29	-	Plot Non Linear
"	150	3.2	11.4	39	0.04 - 0.29	2.1	0.25 - 0.9
"	300	4.2	14.9	67	0.02 - 0.18	2.3	0.2 - 0.4
		3.4	12.1	-	0.18 - 0.33	2.2	0.5 - 0.8
RUTILE + 1.4	25	3.3	11.7	22	0.07 - 0.29	1.9	0.3 - 0.8
wt.% SILICA	100	3.3	11.7	24	0.07 - 0.29	1.9	0.2 - 0.8
(NF 4/2/73)	150	3.7	13.1	37	0.07 - 0.29	2.1	0.4 - 0.8
"	300	4.0	14.2	49	0·07 - 0.29	2.0	0.2 - 0.7

TABLE 8 - 1 (Cont'd)

Sample	T(°C) OUTGAS	BET ANALYSIS				FHH ANALYSIS	
		Vm(mg/gm)	$S_{BET}(m^2/gm)$	C	Linearity Range P/Ps	Slope	Linearity Range P/Ps
RUTILE + 2.6	25	3.2	11.4	24	0.08 - 0.29	2.1	0.4 - 0.7
wt.% SILICA	100	3.3	11.7	28	0.08 - 0.29	1.9	0.2 - 0.75
(NF 14/2/73)	150	3.5	12.4	40	0.08 - 0.29	1.9	0.2 - 0.75
"	300	3.7	13.1	39	0.08 - 0.29	2.0	0.2 - 0.8
RUTILE + 5.0	25	3.7	13.1	30	0.08 - 0.30	2.1	0.3 - 0.8
wt.% SILICA	100	4.1	14.5	18	0.08 - 0.30	2.2	0.4 - 0.8
(NF 8/2/73)	150	4.2	14.9	21	0.08 - 0.30	2.2	0.3 - 0.7
"	300	4.8	17.0	21	0.08 - 0.30	2.3	0.3 - 0.7

corresponds to approximately 40% of the water monolayer. This agrees with the estimated part of the surface containing ligand water molecules[162,163,394] and may indicate that little dehydroxylation occurred on outgassing at 300°C.

Frenkel-Halsey-Hill analysis of the multilayer region of water adsorption on rutile (Table 8-1) reveals the highly polar nature of the rutile surface. After outgassing at 25°C a value of 2.8 is obtained for the slope of the FHH plot, a value slightly higher than those obtained by Harkins and Jura[234] and Zettlemoyer[231] for an hydrophilic oxide. For the rutile surface outgassed at 100, 150 and 300°C FHH slopes of greater than 3 are obtained which are consistent with high energy surfaces but may also indicate the inapplicability of the FHH model of adsorption to the surfaces formed under these outgassing conditions.

(B) Adsorption on Silica-Coated Rutile

(i) Rutile + 1.4, 2.6 and 5.0 wt.% Silica: These samples gave Type II adsorption isotherms and only showed significant hysteresis after outgassing at 300°C (Figures 8-4, 8-5, 8-6). BET plots were linear from (P/Ps) 0.08 to 0.29 and BET C constants tended to increase with increasing outgassing temperature (Table 8-1). The FHH plots were linear over substantial regions of multilayer adsorption with slopes of around 2.0 for the 1.4 and 2.6 wt.% silica samples and around 2.2 for the 5.0 wt.% silica sample. These FHH slopes are significantly different from those obtained with the base rutile and a little less than the 2.5 figure given by Zettlemoyer[231] for an hydrophilic oxide.

All three samples gave increased water adsorption capacity with increased outgassing temperature although there does not appear to be a consistent pattern of increase from sample to sample. The BET monolayer capacities given in Table 8-1 show that approximately 20% of the water monolayer was removed from these three coated samples between outgassing at 25 and 300°C. This compares with the 40% figure obtained for the base rutile. Using the molecular cross sectional area of 0.106nm^2 for water, the BET surface areas for all three coated samples (Table 8-1) were much less than corresponding nitrogen BET surface areas (Table 7-1). This is consistent with results of some other studies on amorphous silicas[200,205-206,380] but the opposite to results obtained by Zettlemoyer[213] for silica-coated rutile. Zettlemoyer prepared coatings approximately 0.6nm thick by a method similar to that used in the present work, but may not have neutralised samples to pH 7 after preparation. Clearly the coatings prepared by Zettlemoyer were more porous to water than those represented by Figures 8-4, 8-5 and 8-6; and further discussion of this point will be given in Chapter 8-3.

Because of the type II form of the water isotherms obtained for the 1.4, 2.6 and 5.0 wt.% silica samples the BET equation should be a consistent method of estimating monolayer capacities[380]. The 5.0 wt.% silica sample is the only one to show any significant increase in water monolayer capacity over that of the base rutile. This may indicate some volume within the coating that is accessible to water vapour.

Outgassing of amorphous silica at a temperature below 150°C has

been shown to remove physisorbed water whilst dehydroxylation may occur above 180°C (Chapter 7-1). According to some workers water adsorption capacities for amorphous silica increase on outgassing from 25 to 110°C[380] although differences may be small up to 200°C[200]. This indicates that physisorbed water is readily replaced on exposure to water vapour. Rehydroxylation, however, may be a slow process and may not occur during the water isotherm determination. Hence dehydroxylation may result in reduced water adsorption capacity[205]. The water isotherms for the 1.4, 2.6 and 5.0 wt.% silica samples are consistent with dehydration occurring at outgassing temperatures less than 150°C which is readily reversed on exposure to water vapour. The low pressure hysteresis observed after outgassing at 300°C may indicate either (a) activated entry of water into some type of pore structure or (b) outgassing at 300°C has removed some hydroxyl groups which are not replaced until the sample is exposed to water vapour pressures approaching saturation[205,380,383].

(ii) Rutile + 0.6 wt.% Silica: The water isotherms for this sample (Figure 8-3) were generally sigmoid in shape but there is slight evidence of a second knee at (P/Ps) about 0.25 after outgassing at 25, 100 and 150°C. When the water isotherms for the base rutile and the four silica-coated rutiles (after outgassing at 300°C) are plotted together (Figure 8-7) two distinct patterns are evident:

(a) the silica-coated rutile samples all show similar adsorption behaviour in the multilayer region (i.e. parallel isotherms). The behaviour on rutile is markedly different.

(b) the 0.6 wt.% silica sample shows different adsorption behaviour from the other silica coated rutiles at (P/Ps) below 0.4.

In order to compare isotherm shapes some isotherms have been replotted in a reduced form in Figures 8-8 and 8-9. In these isotherms the water uptake at any relative pressure is expressed relative to the water uptake at P/Ps = 0.4,$(W/W_{0.4})$, and this ratio plotted as a function of (P/Ps). The reduced isotherms confirm the non silica-like behaviour of the 0.6 wt.% silica sample for water adsorption in the sub-monolayer to monolayer region and the silica-like behaviour in the multilayer regions.

Sub-monolayer to monolayer adsorption: BET analyses of water isotherms on the 0.6 wt.% silica sample show that the BET model does not apply to the 25 and 300°C outgassed surfaces (Table 8-1). However, BET analyses indicate that substantially less of the water monolayer (about 20%) was removed from the 0.6 wt.% silica sample on outgassing over the temperature range 25 to 300°C than was removed from the base rutile (about 40%). This would indicate that fewer ligand water molecules are present on the 0.6 wt.% silica sample. This sample gives no evidence of hysteresis after outgassing at 300°C which may be due to either

(a) a thin coating containing no cracks or pores and hence giving no activated entry of water molecules, or

(b) no irreversible dehydroxylation occurring on outgassing at 300°C. This would imply that any silanol groups on the surface would be present in patches such that any dehydroxylation is readily reversed on exposure to water vapour.

The build up of the adsorbed monolayer of physisorbed water on the surface of the 0.6 wt.% silica sample (Figure 8-3) shows evidence

of a second "knee" which may indicate[212] that the spacing of surface groups is similar to that on the base rutile. This is consistent with the formation of 1 : 1 Ti-O-$Si(OH)_3$ groups on the particle surface.

Multilayer adsorption: FHH analyses (Table 8-1) suggest that multilayer adsorption of water on the 0.6 wt.% silica sample occurs in response to longer range interactions than were operative during multilayer adsorption of water on rutile. This again implies that the high energy portion of the rutile surface which would be exposed after outgassing at above 150°C, the cation sites, has been effectively masked by the incorporation of the 0.6 wt.% of silica on to the rutile surface.

8 - 2 Ageing in Water Vapour

The four silica-coated rutile samples discussed in Chapter 8-1 were aged for varying periods in water vapour at near saturation pressure (P/Ps 0.8) and at 25°C. After ageing, samples were outgassed at 25°C and water vapour adsorption isotherms determined at 25°C. These isotherms are given in Figures 8-10 to 8-13. Included in Figures 8-11 and 8-13 are two desorption isotherms determined directly after ageing — that is without prior outgassing at 25°C. These desorption isotherms illustrate the "negative hysteresis" mentioned in Chapter 8-1.

The effect of ageing for all four silica-coated rutiles was to reduce the subsequent water sorption capacity. From the data on the 1.4 wt.% silica sample (Figure 8-11) prior outgassing at 300°C had little effect on changes brought about by ageing. These changes

vary greatly from sample to sample. The samples were not aged for the same periods of time but some qualitative comparisons between them can be obtained by applying the BET and FHH analyses to the adsorption isotherms of each sample in its most aged state. (Isotherms marked (I) in Figures 8-10 to 8-13). These isotherms correspond to samples aged for at least one week and the BET monolayer capacities and FHH slopes are summarized in Table 8-2. Also included in Table 8-2

TABLE 8 - 2

DATA FROM WATER VAPOUR ADSORPTION ISOTHERMS.
SAMPLES AGED IN WATER VAPOUR (P/Ps 0.8) AND
OUTGASSED AT 25°C PRIOR TO ISOTHERM DETERMINATION

SAMPLE	BEFORE AGEING		AFTER AGEING	
	Vm(BET)mg/gm	FHH SLOPE	Vm(BET)mg/gm	FHH SLOPE
BASE RUTILE CL/D702	2.8	2.8	3.0(a)	2.8
RUTILE + 0.6wt.% SILICA (NF 6/2/73)	APPROX.2.8(b)	2.2	2.8	2.1
RUTILE + 1.4wt.% SILICA (NF 4/2/73)	3.3	1.9	2.0	2.7
RUTILE + 2.6wt.% SILICA (NF 14/2/73)	3.2	2.1	2.3	2.0
RUTILE + 5.0wt.% SILICA (NF 8/2/73)	3.7	2.1	3.3	2.1

(a) Base Rutile aged in liquid water at pH 7 for 3 weeks prior to drying at room temperature.

(b) See Table 8-1

are the analyses of isotherms obtained on the base rutile before and after ageing in liquid water at pH 7 for 3 weeks (isotherms (1) and (7), Figure 8-1). Whilst the comparison between ageing in liquid and vapour may not be strictly valid it would be expected, and was indeed indicated in the electrokinetic studies (Chapter 6-2), that the two ageing processes would give similar results.

The base rutile shows no significant change in either BET monolayer capacity or FHH slope due to ageing in liquid water. The slight increase in Vm after ageing may reflect the difficulty in applying the BET model to the isotherm when it shows evidence of the second "knee" in the BET region. The FHH plots for the base rutile were only linear at (P/Ps) > 0.5, and the lack of change of FHH slope is consistent with the isotherms (1) and (7) in Figure 8-1 being parallel at such pressures. Clearly the BET and FHH methods of analysis do not reflect the crossover of the isotherms (1) and (7) at (P/Ps) 0.35, and the cause of this behaviour is not known.

The isotherms for the 0.6 wt.% silica sample (Figure 8-10) show that ageing has very little effect, and this is confirmed by the BET and FHH data in Table 8-2. The 1.4, 2.6 and 5.0 wt.% silica samples all show a marked reduction in BET monolayer capacity after ageing and the 1.4 wt.% silica sample alone out of all five samples shows a change in the FHH slope as a result of ageing. The effect of ageing on the 1.4, 2.6 and 5.0 wt.% silica samples has been to reduce the amount of physisorbed water which forms the adsorbed water monolayer. The monolayer capacities for the first two of these samples are less than that of the base rutile and therefore the

removal of accessible volume within the surface coatings cannot be the sole consequence of ageing. The mechanism of physisorption of water onto silica has recently been described by Prigogine and Fripiat[248] and the primary attachment stems from the formation of hydrogen bonds between water molecules and surface hydroxyl groups. Hence at low coverages water is believed to adsorb as localised clusters, with bridging between clusters occurring at higher coverages to give a continuous network of adsorbed water molecules. It seems that the reduced monolayer capacities after ageing indicate that fewer hydroxyl groups were present to promote the localised adsorption of water molecules. Although the samples were aged in a water vapour atmosphere at (P/Ps) approximately 0.8 it is likely that liquid water has condensed on the samples in surface cracks or capillaries. From the discussion in Chapter 2-3 silanol groups are rapidly condensed to form siloxane bonds at around neutral pH and it appears likely that the process initiated by ageing of the silica-coated samples is polymerization. This polymerization may occur within the coating as well as on its external surface, although the data in Table 8-1 indicated that very little volume within the coatings was accessible to water. Condensation of external surface Si-OH groups would not be expected to change the multilayer adsorption of water provided this condensation did not effect the "rutile covering ability" of the silica. Hence the data in Table 8-2 are consistent with the 2.6 and 5.0 wt.% silica samples consisting of uniform coatings many "silica layers" thick. The 1.4 wt.% silica sample has however shown changes in multilayer adsorption after ageing which are consistent with exposure of the underlying rutile surface. This would indicate

that the 1.4 wt.% silica sample contains a thin layer of silica prior to ageing which "rolls up" into polymer and exposes bare rutile surface. The calculated thickness of the silica layer on this sample, 1.4nm (Chapter 5-2), compares well with the 2.0nm thickness that Zettlemoyer[213] found was necessary to mask rutile behaviour in heat of immersion experiments.

The apparent stability of the 0.6 wt.% silica sample to ageing in water vapour, and the similarity between multilayer water adsorption on all silica-coated samples prior to ageing, indicate that (a) the 0.6 wt.% silica sample consists largely of Ti-OH groups that do not mutually condense and (b) the silica species covering the high energy part of the rutile surface are sufficiently strongly anchored so as not to be removed during ageing. It should, however, be noted that the multilayer adsorption of water on the 1.4 wt.% silica sample was also largely unaffected by only one week's ageing in water vapour.

8 - 3 Effects of Pre-Equilibration pH

It was shown in Chapter 8-2 that ageing in water vapour produced significant changes in the water sorption characteristics of silica-coated rutile samples which were prepared at pH 10 but neutralised to pH 7 immediately after preparation. It was also noted that samples prepared by Zettlemoyer[213] at pH 10 were more porous to water vapour than those neutralised to pH 7. In addition, both the preparative work (Table 5-1) and the electrokinetic studies (Chapter 6) indicate that at pH 2 silica coatings undergo depolymerization which

may result in the removal of silica from the particle.

Two samples (base rutile + 0.6 and 5.0 wt.% silica) were pre-equilibrated in liquid water at pH 10, 7 and 2 for up to three weeks and then dried in a vacuum dessicator at room temperature. Water adsorption isotherms were determined at 25°C after outgassing at 25 and 300°C. The isotherms are given in Figures 8-14 to 8-21. Although some obvious effects of pre-equilibration pH on water sorption are evident from the isotherms it is useful to characterize the isotherms in terms of BET monolayer capacities and slopes of FHH plots — and these data are given in Table 8-3.

(A) Rutile + 5.0 wt.% Silica: Water isotherms on this sample were all basically of sigmoid shape over the sometimes limited (P/Ps) range studied and showed hysteresis loops after outgassing at 300°C which did not close on pumping at 25°C (Figure 8-16). BET monolayer capacities were slightly less after the final outgassing at 25°C than after the initial outgassing at 25°C, and this effect is further illustrated by the isotherms themselves (Figure 8-13). It was concluded in Chapter 4-2 that water uptakes, especially after outgassing at 25°C, were difficult to reproduce to within a few per cent. If the reduced uptakes shown in Figure 8-18 are real they would indicate that complete rehydroxylation of the 5.0 wt.% silica sample did not occur during isotherm determination after outgassing at 300°C.

The most marked effect of pre-equilibration pH on water sorption occurred between pH 10 and 7. The BET monolayer capacity dropped significantly when the sample was neutralised from pH 10 to pH 7 and

TABLE 8 - 3

DATA FROM WATER VAPOUR ADSORPTION ISOTHERMS OBTAINED ON SILICA-COATED RUTILE PRE-EQUILIBRATED AT VARIOUS pH VALUES PRIOR TO OUTGASSING.

SAMPLE	DESIGNATION TABLE 5-1	Wt.% SILICA	TREATMENT	T (°C) OUTGASSING	Vm(BET) mg/gm	FHH SLOPE
1	NF 5/2/73	0.8	Prepared at pH 10	25 (Initial)	*	1.4
2	NF 6/2/73	0.6	(1) neutralised to pH 7 at preparation	"	APPROX 2.8	2.2
3	-	-	(1) neutralised to pH 7 after 12 months	"	*	2.1
4	-	-	(3) acidified to pH 2	"	*	2.2
1				300	4.3	1.7
2				"	*	2.3
3				"	4.3	2.6
4				"	*	3.0
1				25 (Final)	3.4	*
2				"	*	*
3				"	2.9	2.3
4				"	3.3	2.3
5	NF 7/2/73	5.0	Prepared at pH 10	25 (Initial)	5.1	1.5
6	NF 8/2/73	5.0	(5) neutralised to pH 7 at preparation	"	3.7	2.2
7	-	-	(5) neutralised to pH 7 after 12 months	"	3.9	2.8
8	-	-	(7) re-equilibrated at pH 10	"	3.8	2.4
9	-	-	(5) acidified to pH 2	"	4.0	*

TABLE 8 - 3 (Cont'd)

SAMPLE	DESIGNATION TABLE 5-1	Wt.% SILICA	TREATMENT	T (°C) OUTGASSING	Vm(BET) mg/gm	FHH SLOPE
5				300	6.4	1.5
6				"	4.8	2.3
7				"	4.9	3.0
8				"	4.6	3.0
9				"	5.1	*
5				25 (Final)	5.0	1.5
6				"	†	†
7				"	3.7	2.5
8				"	3.6	2.5
9				"	3.8	*

* BET or FHH plots were non-linear for these adsorption isotherms.

† Data not obtained.

showed a very slight increase following pre-equilibration at pH 2. The FHH analyses showed a good deal of variation between all the samples although a consistent value for the FHH slope (1.5) was obtained for the sample prepared at pH 10. This value was significantly lower than those given by the 5.0 wt.% silica sample after pre-equilibration at pH 7 or 2. The FHH plots for water sorption on this sample prepared at pH 10 are given in Figure 8-19. These plots are linear between (P/Ps) 0.2 and 0.6 showing no upward deviation due to capillary condensation. The low value for the slope of the FHH plot may, however, indicate the presence of very small capillaries as was suggested by Pierce[228]. The FHH slopes for the water sorption on this sample after all other pH pre-treatments are much nearer the 2.5 figure given by Zettlemoyer[231] for hydrophilic silica. The evidence is, therefore, that neutralisation of the fully silica-coated sample has resulted in the removal of adsorption volume from within the surface coating. The likely cause would be polymerization of silica both within and at the surface of the silica coating. The majority of the siloxane bonds formed would be inaccessible to water molecules whilst those near the surface of the coating would be relatively strain free, hence the non-reversibility of the changes initiated by the drop in pH when the pH is readjusted to 10 (Figures 8-14 to 8-17). Zettlemoyer[213] also found evidence of "minute capillaries" in silica coatings prepared at pH 10 which he showed were accessible to water but not to nitrogen. This would

indicate that these "minute capillaries" were of "micropore" dimensions[155]. It was not possible to calculate total pore volumes from the isotherms presented in this section and it is not known whether the reduction in micropore volume obtained in the 5.0 wt.% silica sample was accompanied by an increase in the size of "bulk holes", as suggested by Dollimore[277] for commercial silica gels soaked in water. The large increase in nitrogen surface area observed by Dollimore on decreasing the pH from 11 to 7 does not appear consistent with the results obtained in the present work.

The small increase in monolayer capacity when the pre-equilibration pH was lowered from 7 to 2 would indicate slight depolymerization, although the effect on this sample is barely significant. Marked reductions in water monolayer capacity on silica gels on increasing the pH from 3.5 to 5.0 have been recorded by Sing[202].

(B) Rutile + 0.6 wt.% Silica: Water sorption isotherms for this sample following varying pretreatments are given in Figures 8-20 and 8-21. All the isotherms were fully reversible after outgassing at both 25°C and 300°C. Following preparation at pH 10 this sample gave a smooth sigmoid shaped isotherm. However, after pre-equilibration at pH 7 and 2 some isotherms showed a second "knee" at (P/Ps) approximately 0.25. As a result monolayer analysis using the BET equation is not appropriate for some isotherms (Table 8-3). Nevertheless, from those isotherms for which a BET monolayer capacity could be calculated it appears that the water monolayer capacity on the 0.6 wt.% silica sample was not significantly affected by different values of pre-equilibration pH. FHH analyses of the isotherms indicate similar multilayer

adsorption characteristics to those observed on the 5.0 wt.% silica sample.

From the isotherms in Figures 8-20 and 8-21 it can be seen that whilst neutralisation from pH 10 to 7 reduces water uptake at (P/Ps) above 0.1 - 0.2, pre-equilibration at pH 2 reversed this trend and gave adsorption isotherms very similar to those of the base rutile. The slight variations between the pH 2 sample and the base rutile may indicate that a small amount of silica remains on the surface, and this is consistent with the chemical analyses given in Table 5-1.

In summary then it appears that treatment at pH 2 will depolymerize silica from the rutile surface as suggested in Chapter 6 and that removal of part of the 0.6 wt.% of silica on this sample is sufficient to restore some of the water sorption characteristics of the base rutile.

FIGURES 8-1 to 8-21
WATER SORPTION ISOTHERMS

FIGURE 8-1

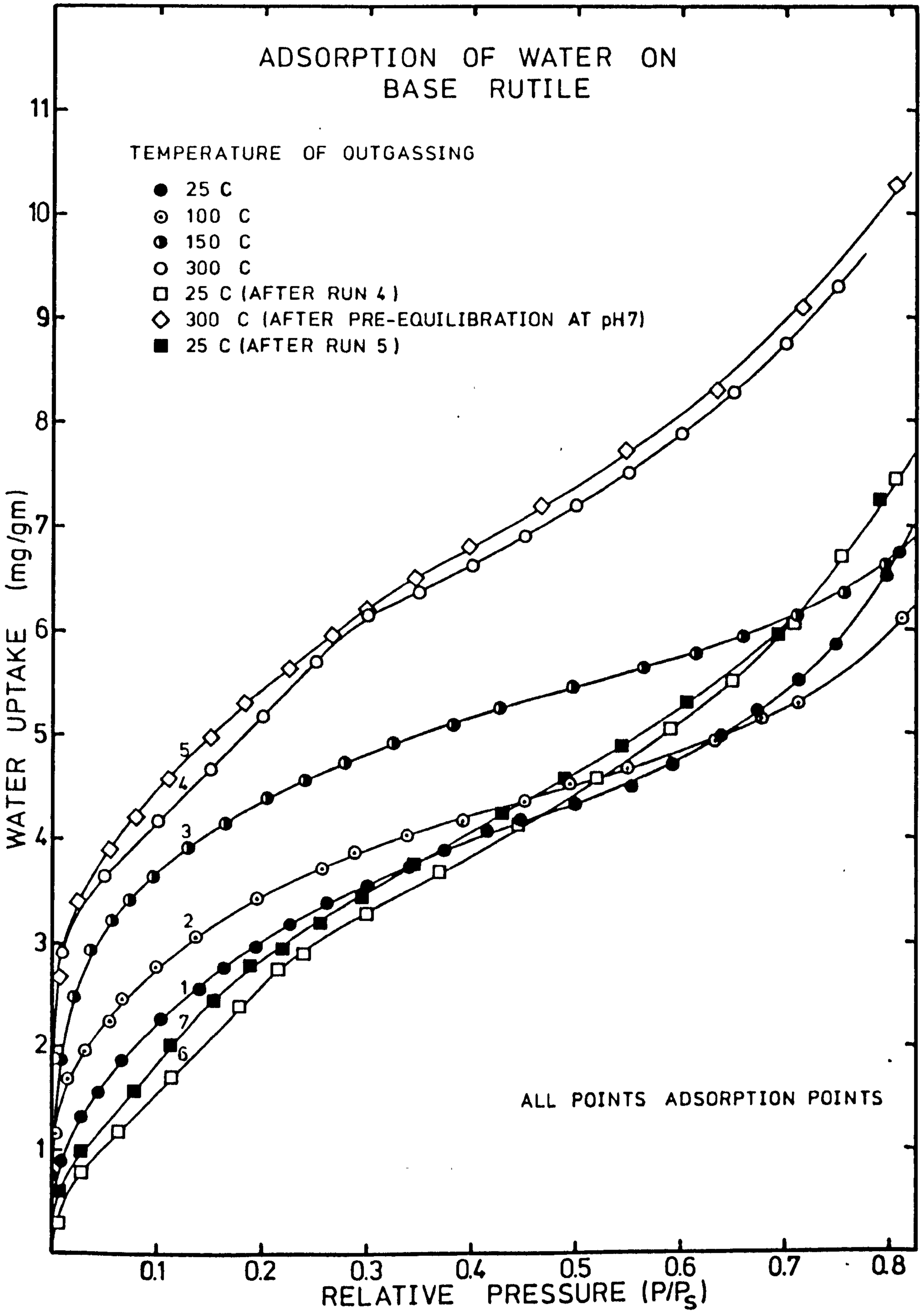
ADSORPTION OF WATER ON
BASE RUTILE
TEMPERATURE OF OUTGASSING
25 C
100 C
150 C
300 C
25 C (AFTER RUN 4)
300 C (AFTER PRE-EQUILIBRATION AT pH7)
25 C (AFTER RUN 5)
WATER UPTAKE (mg/gm)
RELATIVE PRESSURE (P/Ps)
ALL POINTS ADSORPTION POINTS
1
2
3
4
5
6
7

FIGURE 8-2

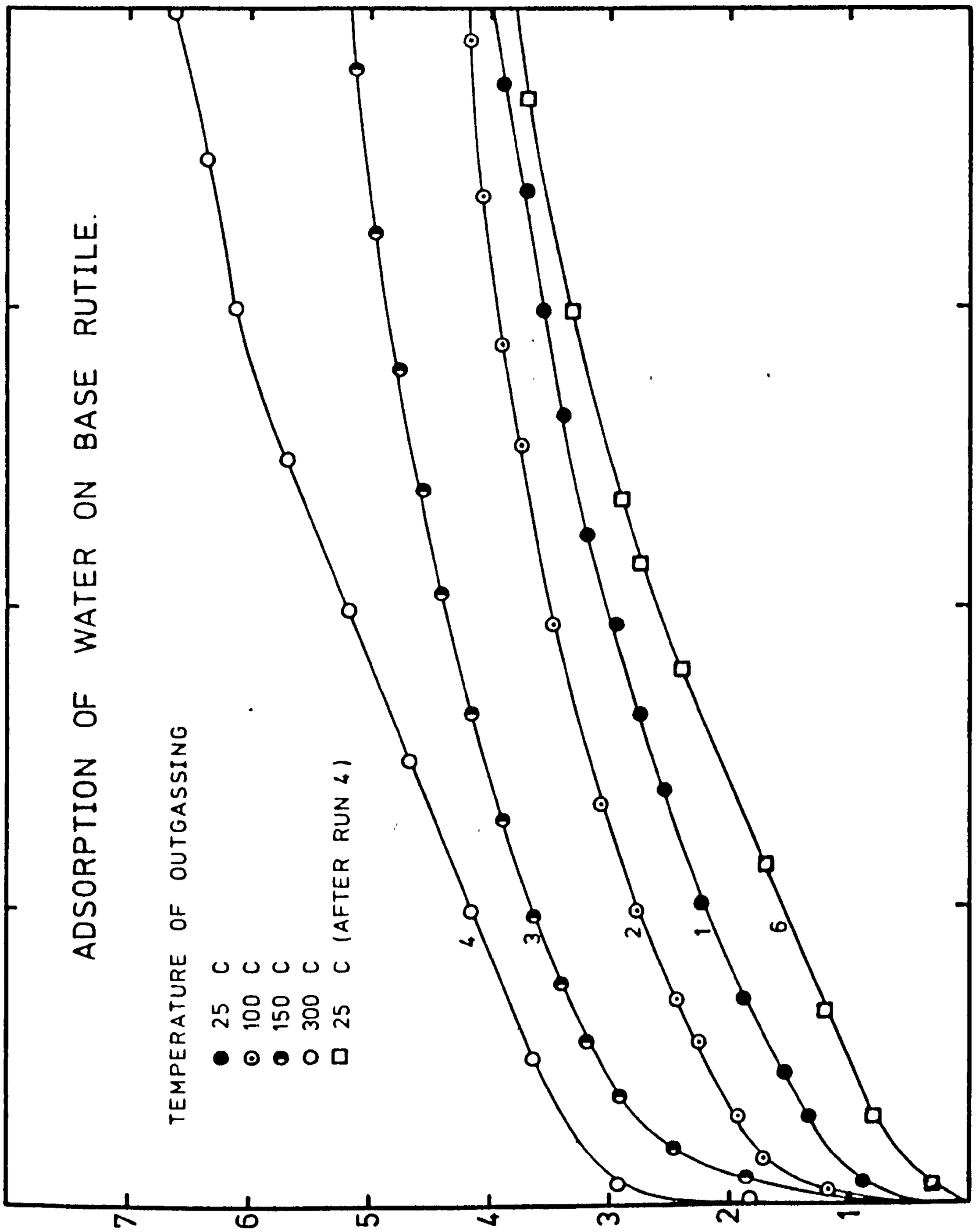
ADSORPTION OF WATER ON BASE RUTILE.
TEMPERATURE OF OUTGASSING
25 C
100 C
150 C
300 C
25 C (AFTER RUN 4)
4
3
2
1
6
0.1
0.2
Q3
RELATIVE PRESSURE (P/Ps)
WATER UPTAKE (mg/gm)
7
6
5
4
3
2
1

FIGURE 8-3

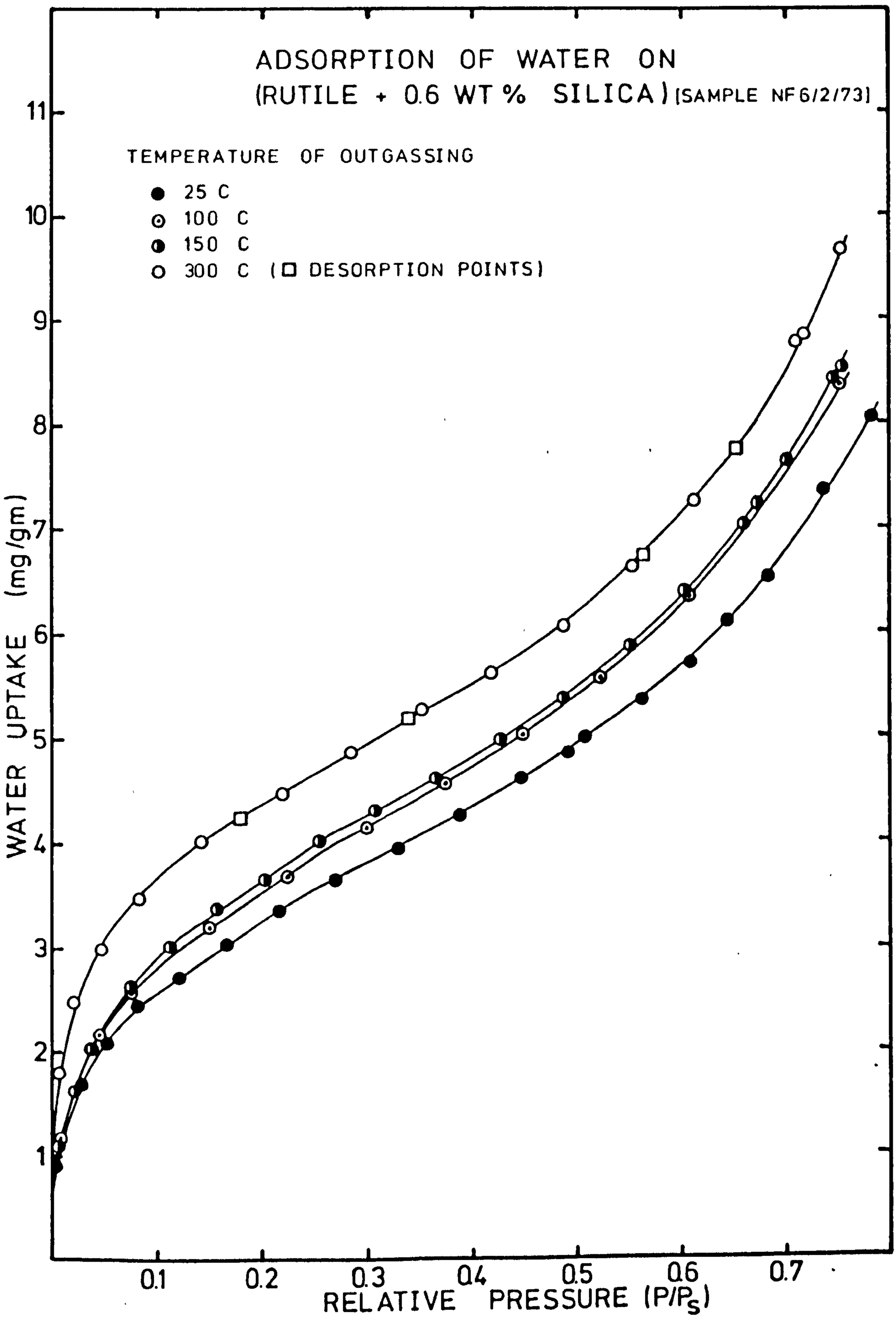
ADSORPTION OF WATER ON
(RUTILE + 0.6 WT % SILICA) [SAMPLE NF 6/2/73]
TEMPERATURE OF OUTGASSING
25 C
100 C
150 C
300 C (□ DESORPTION POINTS)
WATER UPTAKE (mg/gm)
RELATIVE PRESSURE (P/Ps)
1
2
3
4
5
6
7
8
9
10
11
0.1
0.2
0.3
0.4
0.5
0.6
0.7

FIGURE 8-4

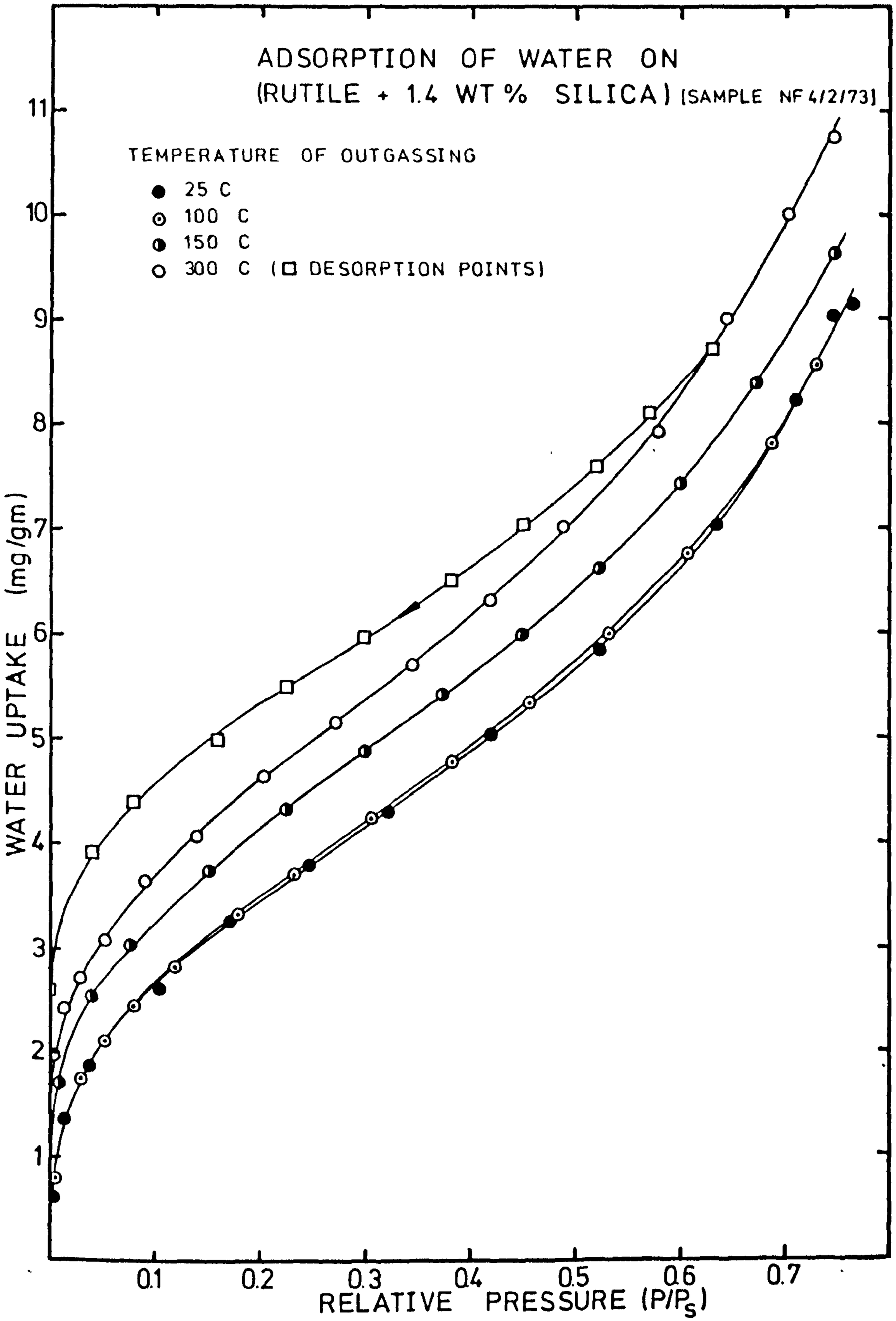
ADSORPTION OF WATER ON
(RUTILE + 1.4 WT % SILICA) (SAMPLE NF 4/2/73)
TEMPERATURE OF OUTGASSING
25 C
100 C
150 C
300 C (□ DESORPTION POINTS)
WATER UPTAKE (mg/gm)
RELATIVE PRESSURE (P/Ps)
1
2
3
4
5
6
7
8
9
10
11
0.1
0.2
0.3
0.4
0.5
0.6
0.7

FIGURE 8-5

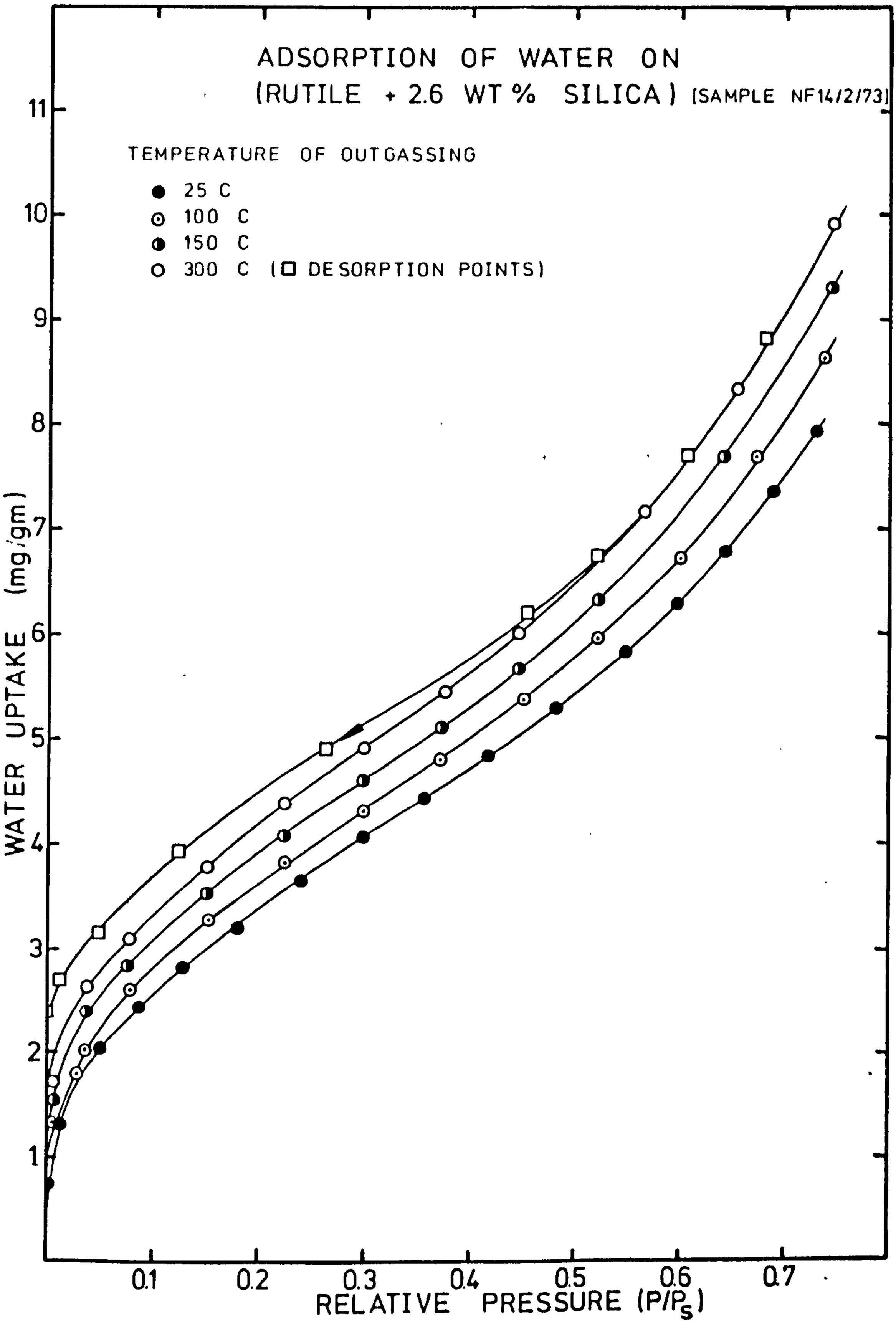
ADSORPTION OF WATER ON
(RUTILE + 2.6 WT % SILICA) (SAMPLE NF14/2/73)
TEMPERATURE OF OUTGASSING
● 25 C
⊙ 100 C
◐ 150 C
○ 300 C (□ DESORPTION POINTS)
WATER UPTAKE (mg/gm)
RELATIVE PRESSURE (P/Ps)
11
10
9
8
7
6
5
4
3
2
1
0.1
0.2
0.3
0.4
0.5
0.6
0.7

FIGURE 8-6

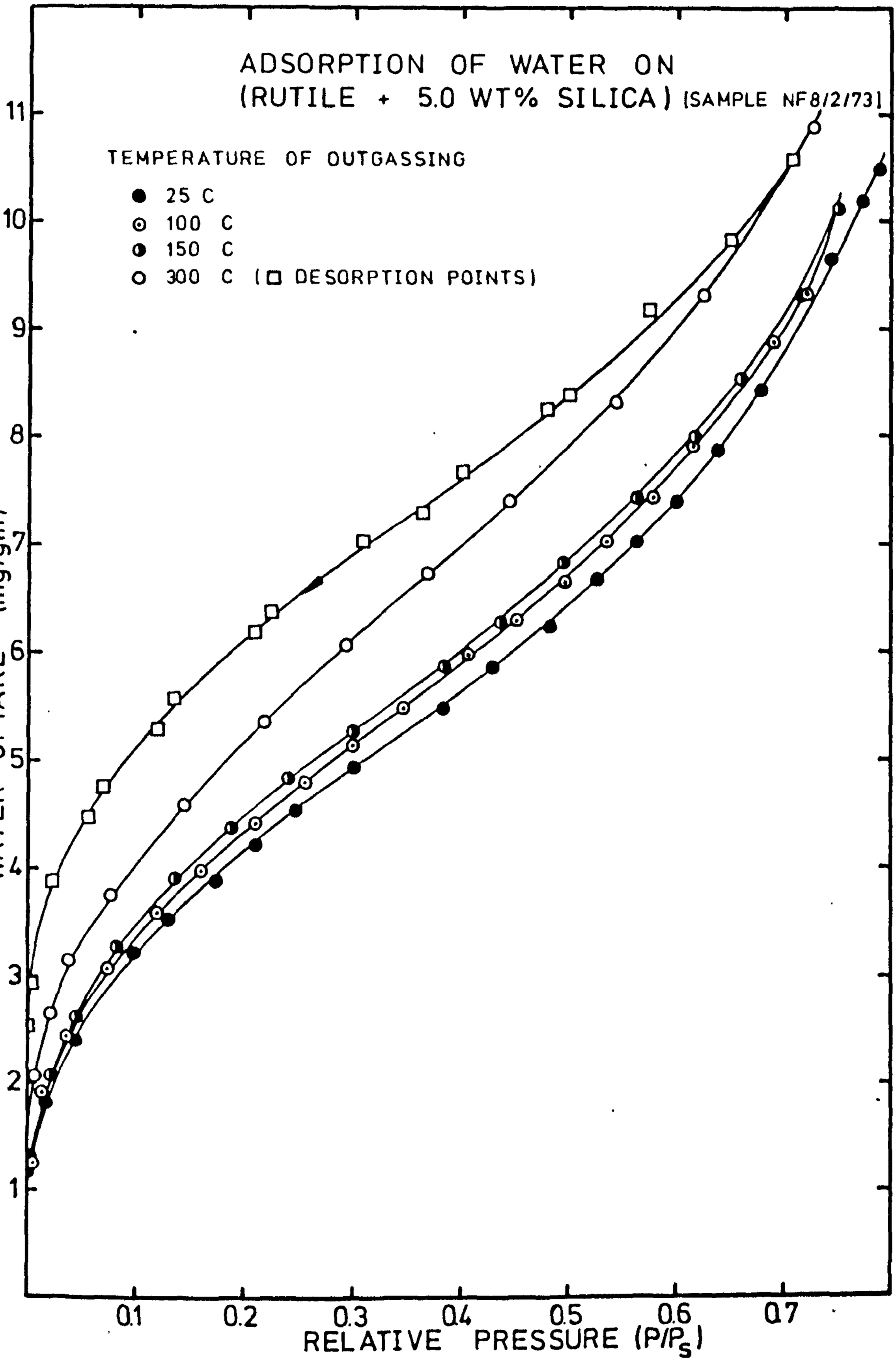
ADSORPTION OF WATER ON
(RUTILE + 5.0 WT% SILICA) [SAMPLE NF8/2/73]
TEMPERATURE OF OUTGASSING
25 C
100 C
150 C
300 C (□ DESORPTION POINTS)
WATER UPTAKE (mg/gm)
RELATIVE PRESSURE (P/Ps)
1
2
3
4
5
6
7
8
9
10
11
0.1
0.2
0.3
0.4
0.5
0.6
0.7

FIGURE 8-7

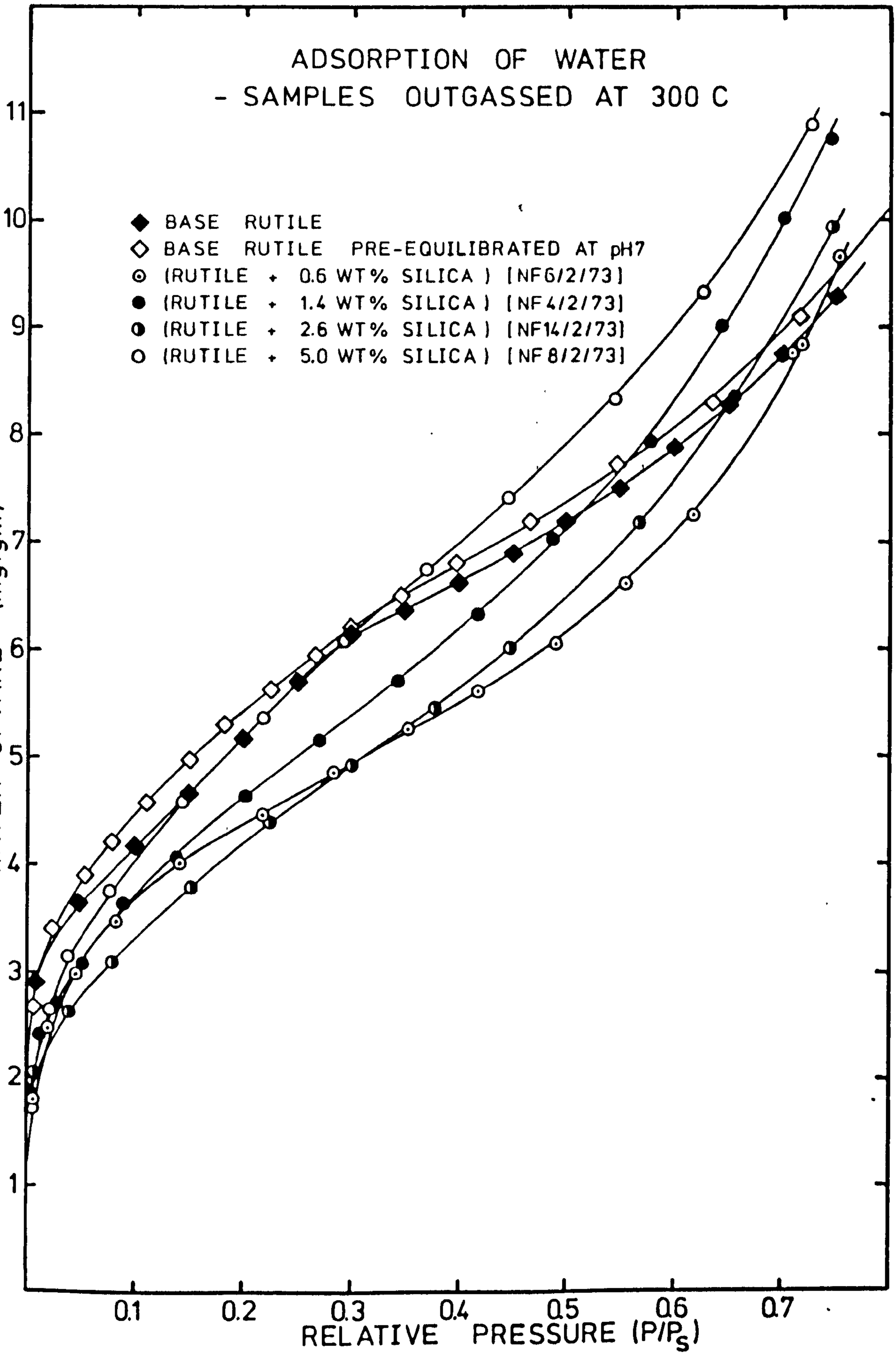
ADSORPTION OF WATER
- SAMPLES OUTGASSED AT 300 C
◆ BASE RUTILE
◇ BASE RUTILE PRE-EQUILIBRATED AT pH7
⊙ (RUTILE + 0.6 WT% SILICA) [NF6/2/73]
● (RUTILE + 1.4 WT% SILICA) [NF4/2/73]
◑ (RUTILE + 2.6 WT% SILICA) [NF14/2/73]
○ (RUTILE + 5.0 WT% SILICA) [NF8/2/73]
WATER UPTAKE (mg/gm)
11
10
9
8
7
6
5
4
3
2
1
0.1
0.2
0.3
0.4
0.5
0.6
0.7
RELATIVE PRESSURE (P/Ps)

FIGURE 8-8

REDUCED ADSORPTION ISOTHERMS

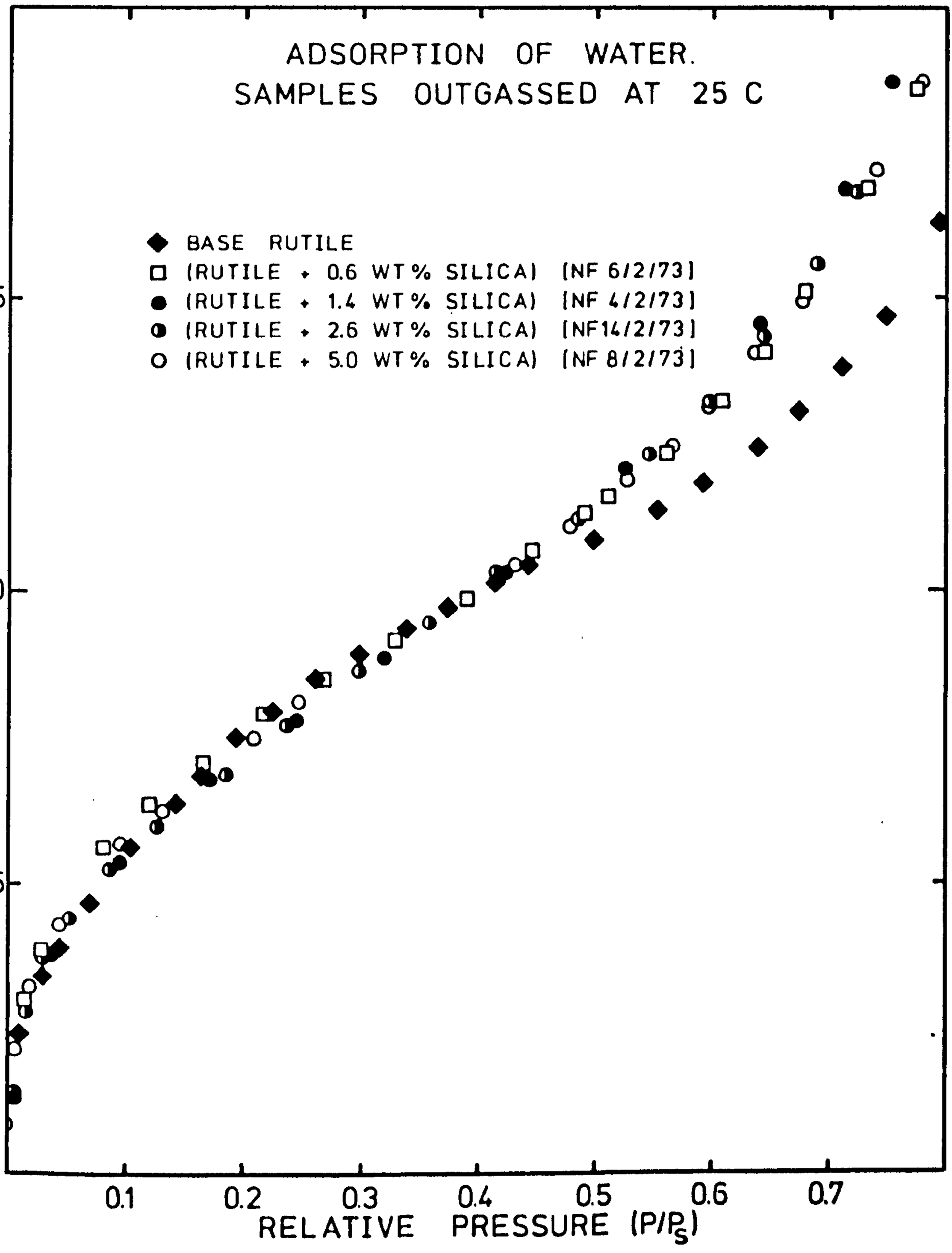

FIGURE 8-9

REDUCED ADSORPTION ISOTHERMS

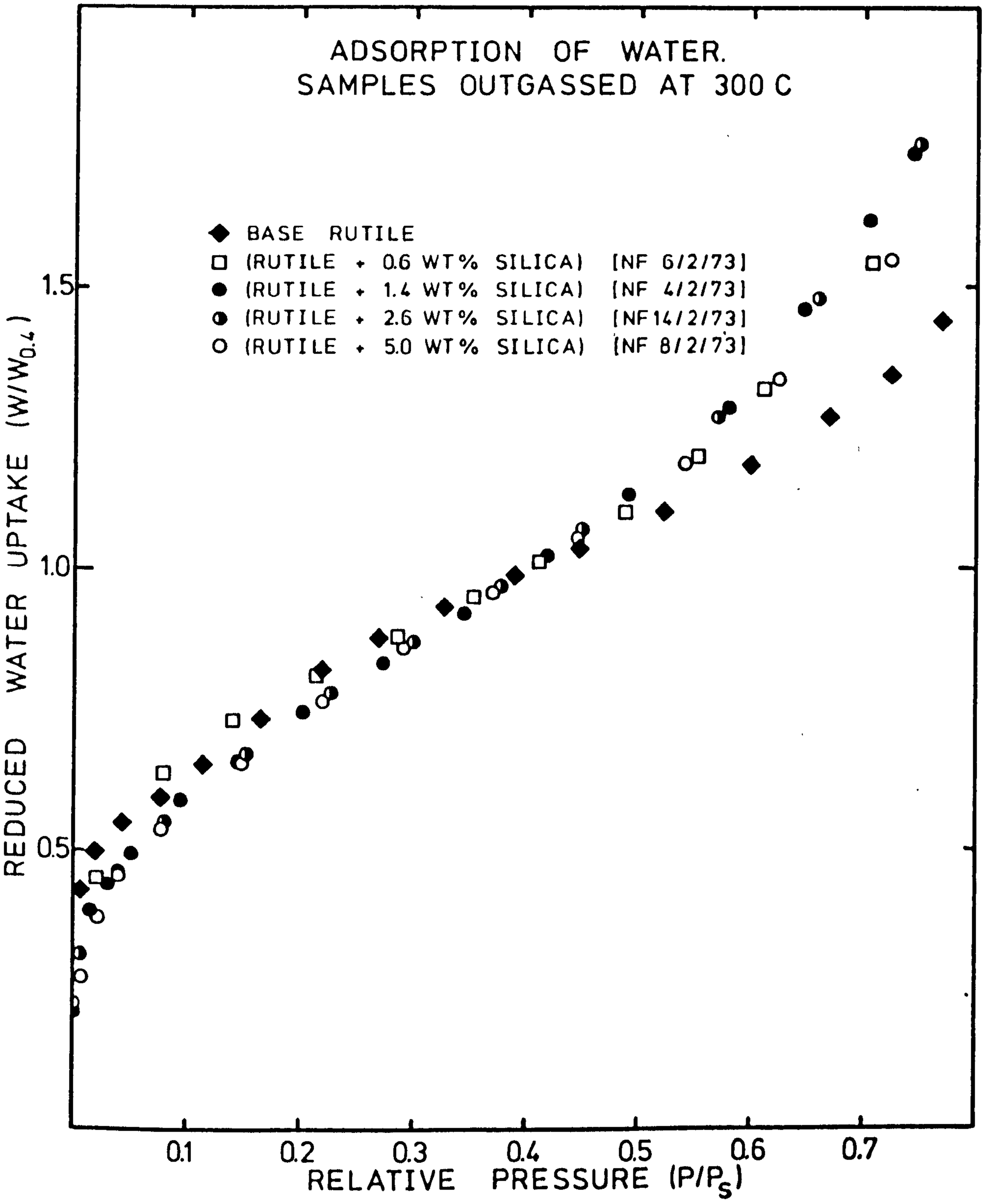

FIGURE 8-10

AGEING IN WATER VAPOUR

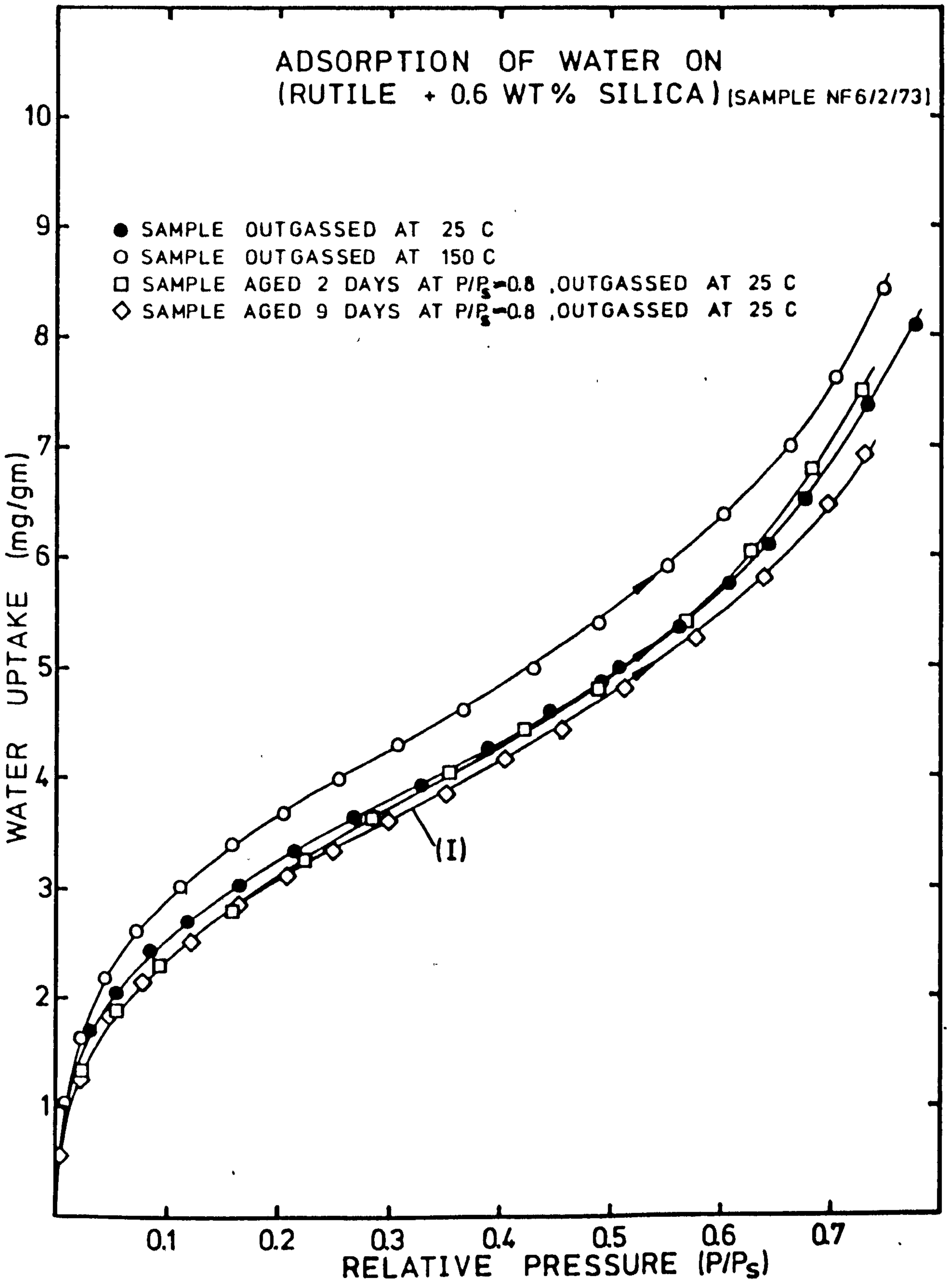

FIGURE 8-11

AGEING IN WATER VAPOUR

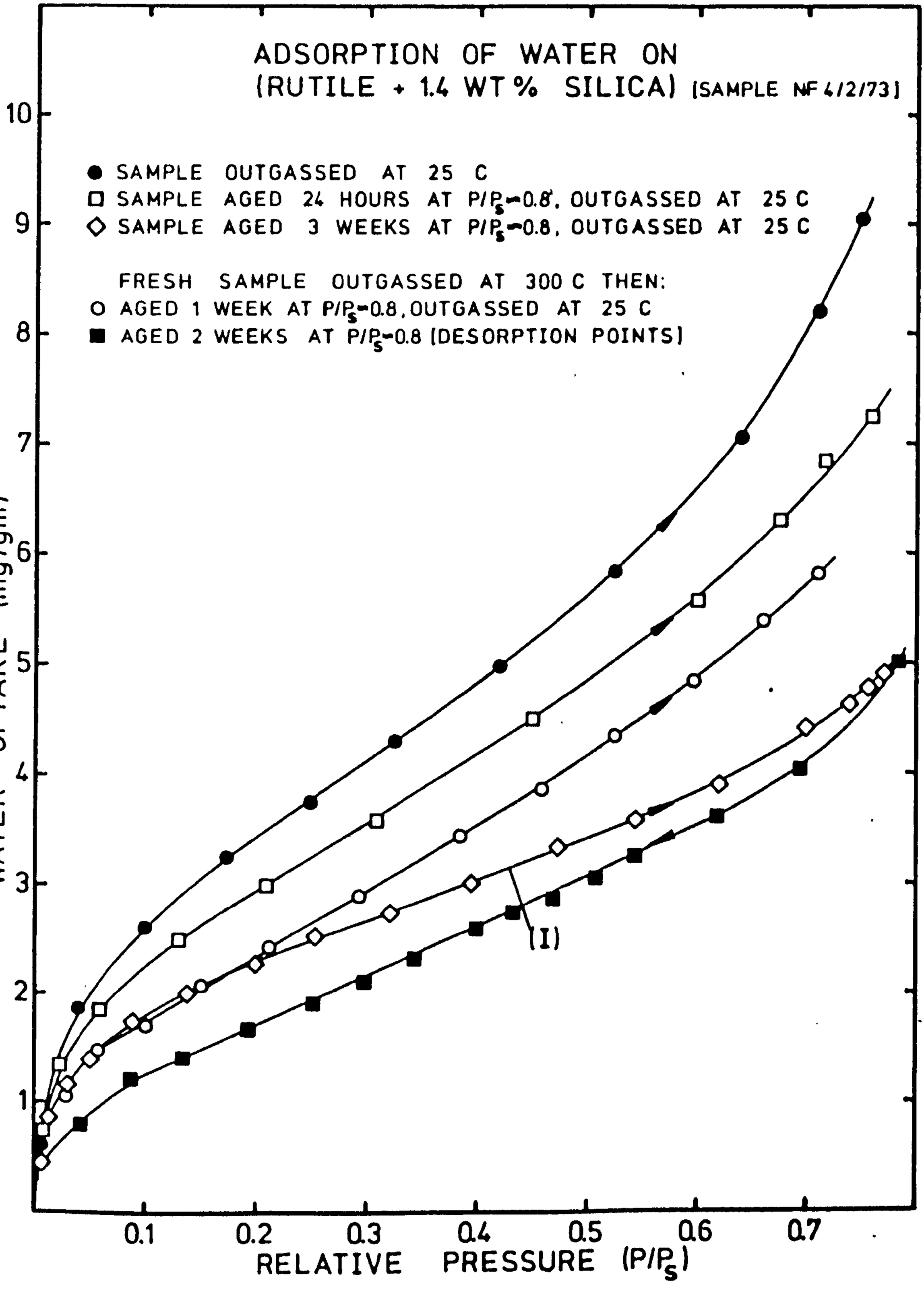

FIGURE 8-12

AGEING IN WATER VAPOUR

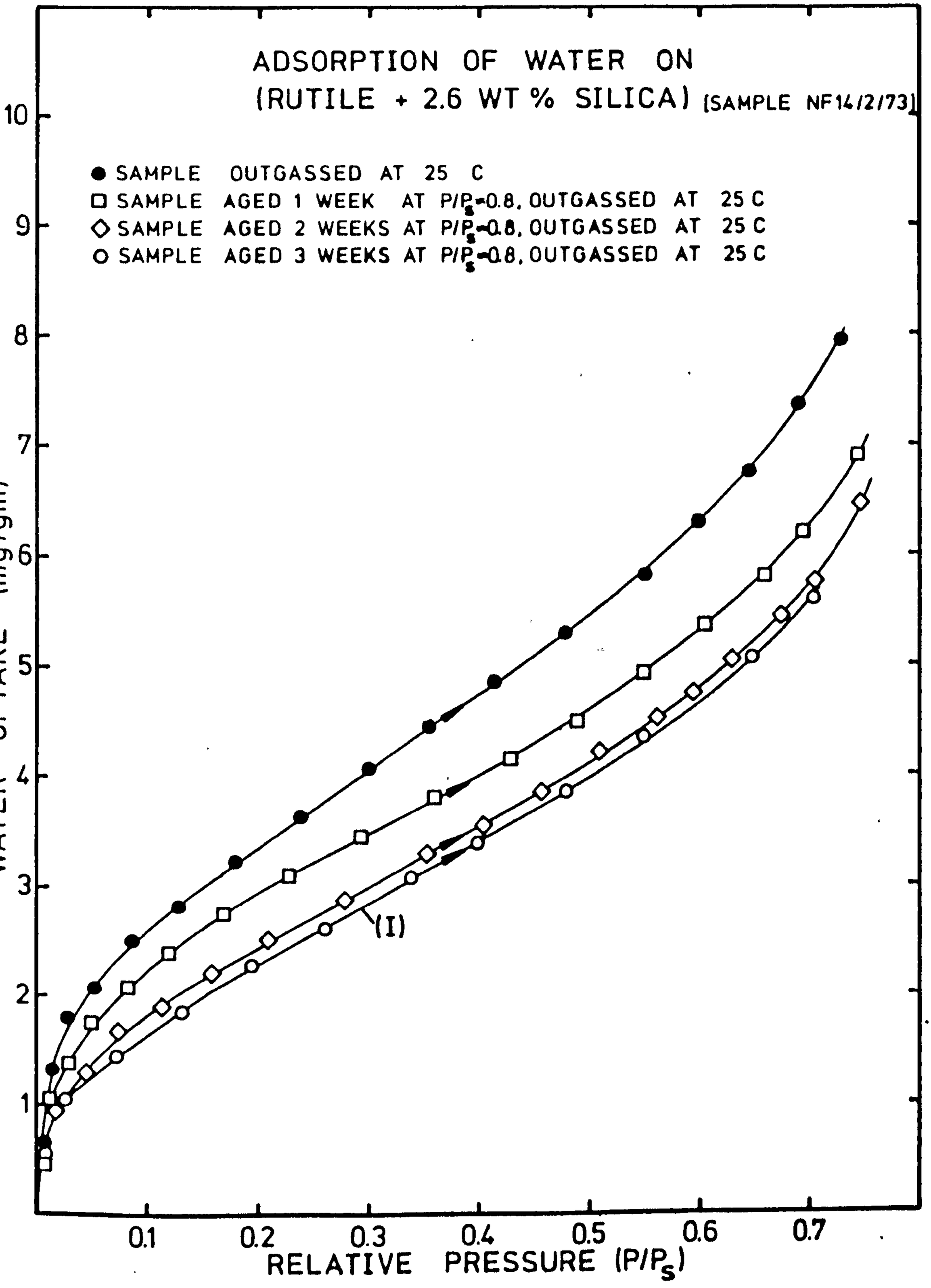

FIGURE 8-13

AGEING IN WATER VAPOUR

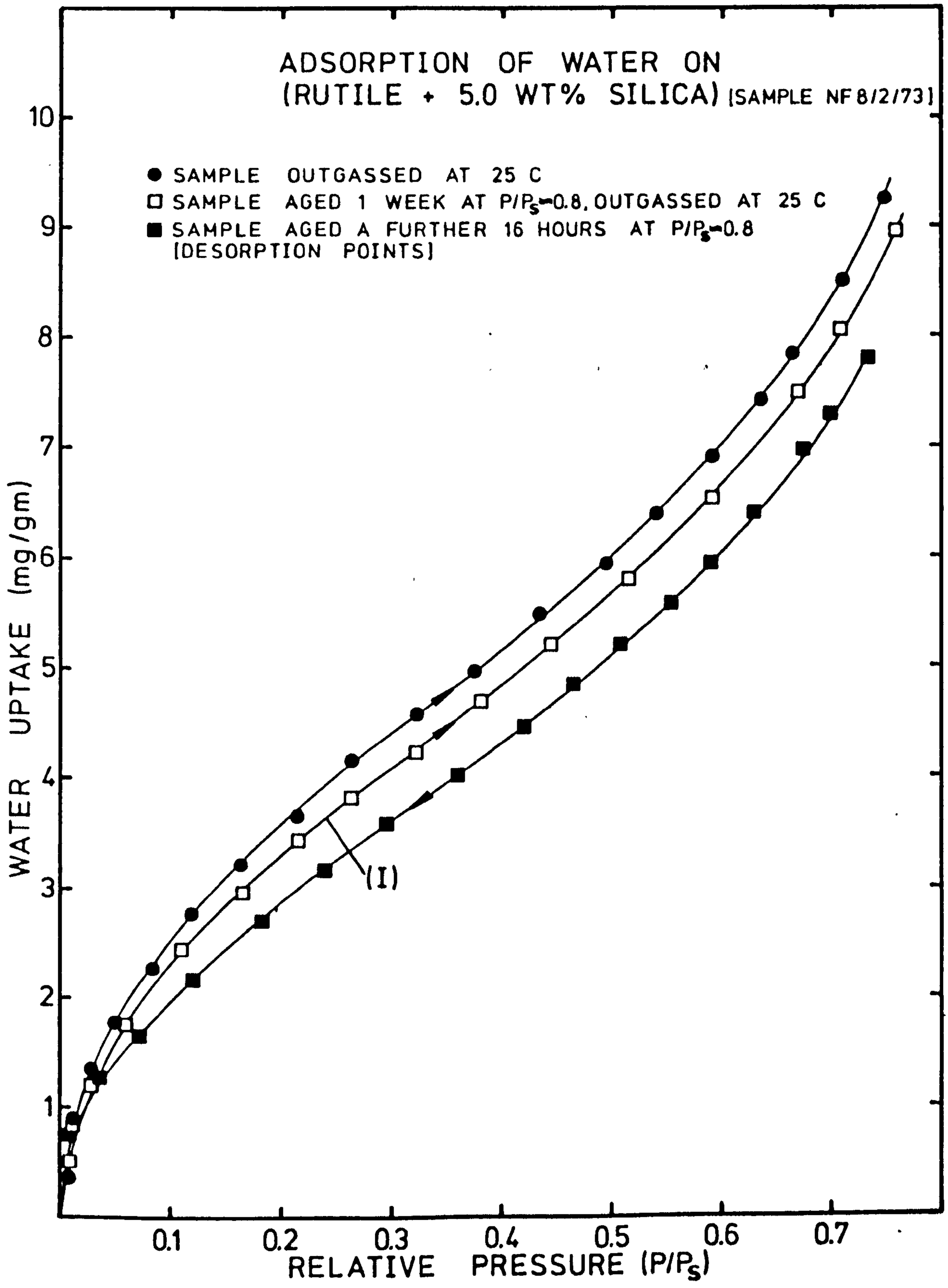

FIGURE 8-14

EFFECTS OF PRE-EQUILIBRATION pH

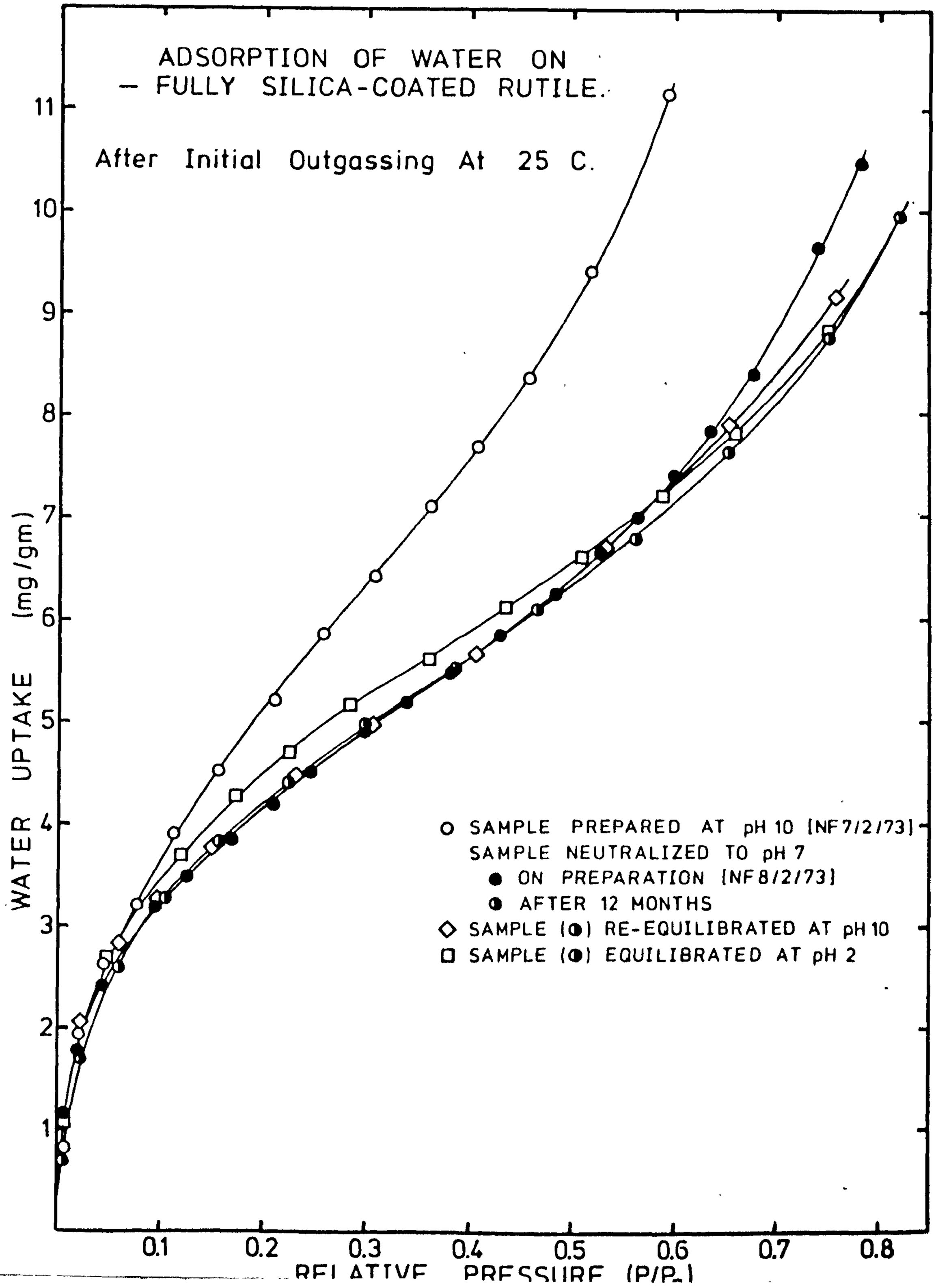

FIGURE 8-15

EFFECTS OF PRE-EQUILIBRATION pH

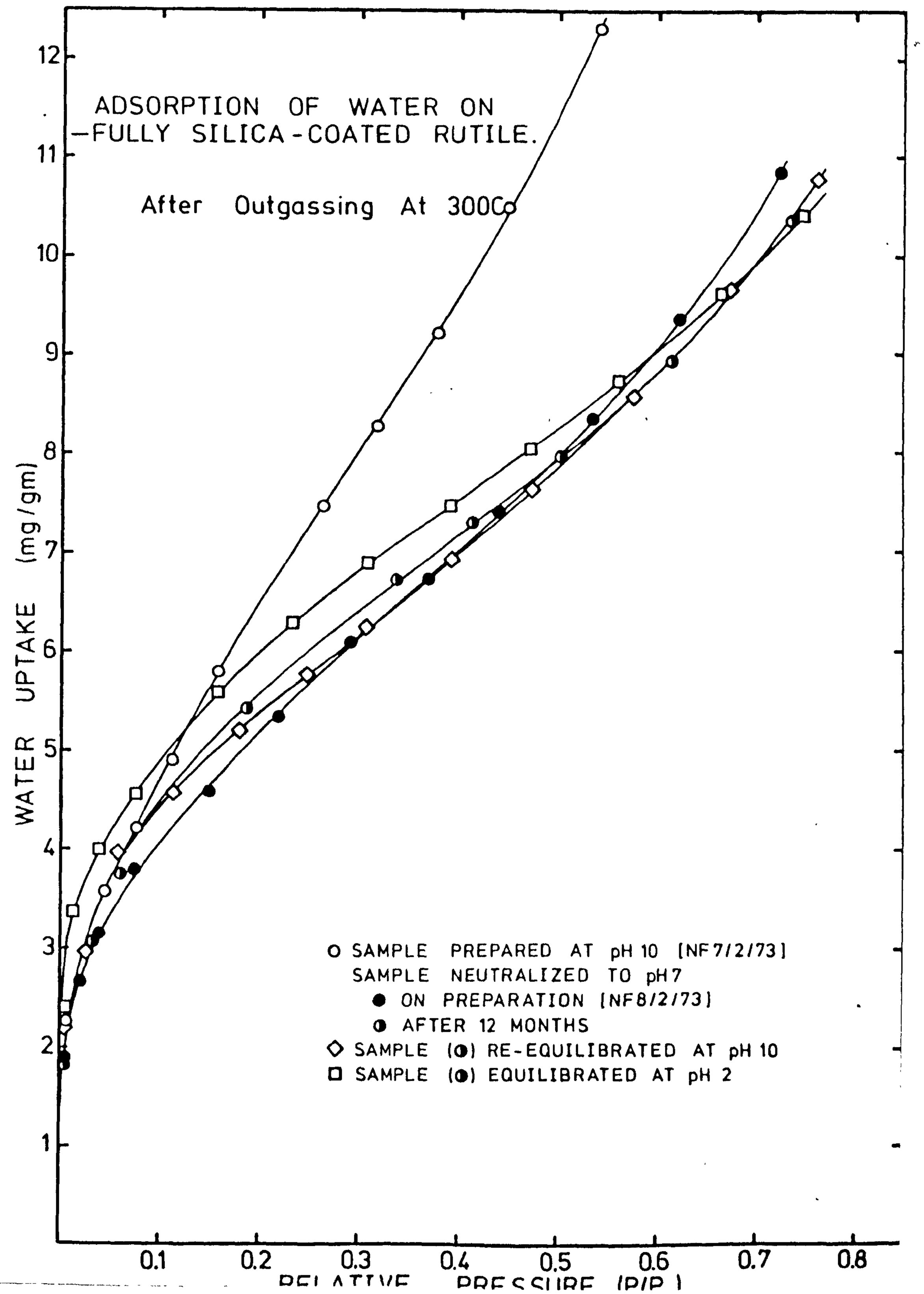

FIGURE 8-16

EFFECTS OF PRE-EQUILIBRATION pH

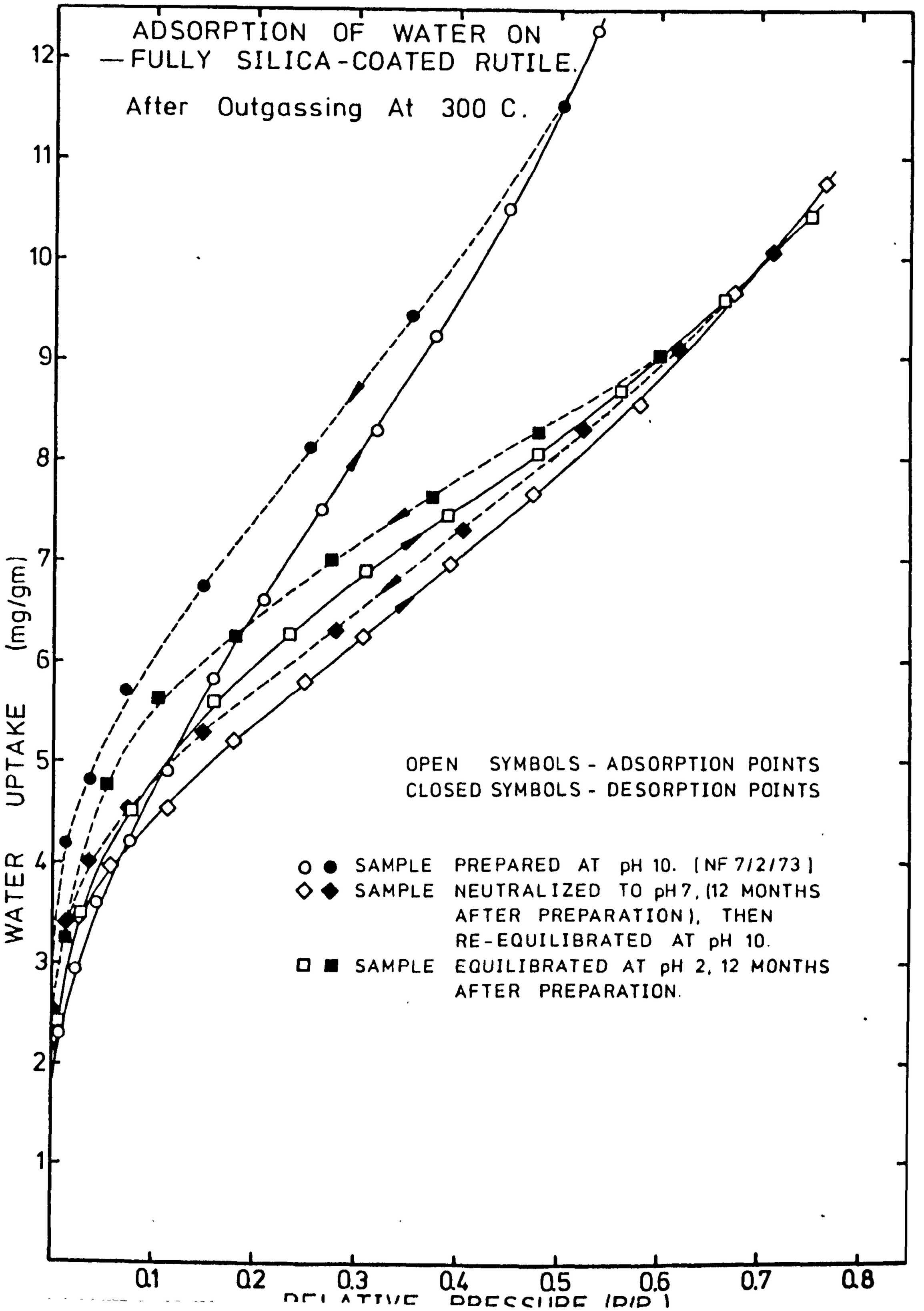

FIGURE 8-17

EFFECTS OF PRE-EQUILIBRATION pH

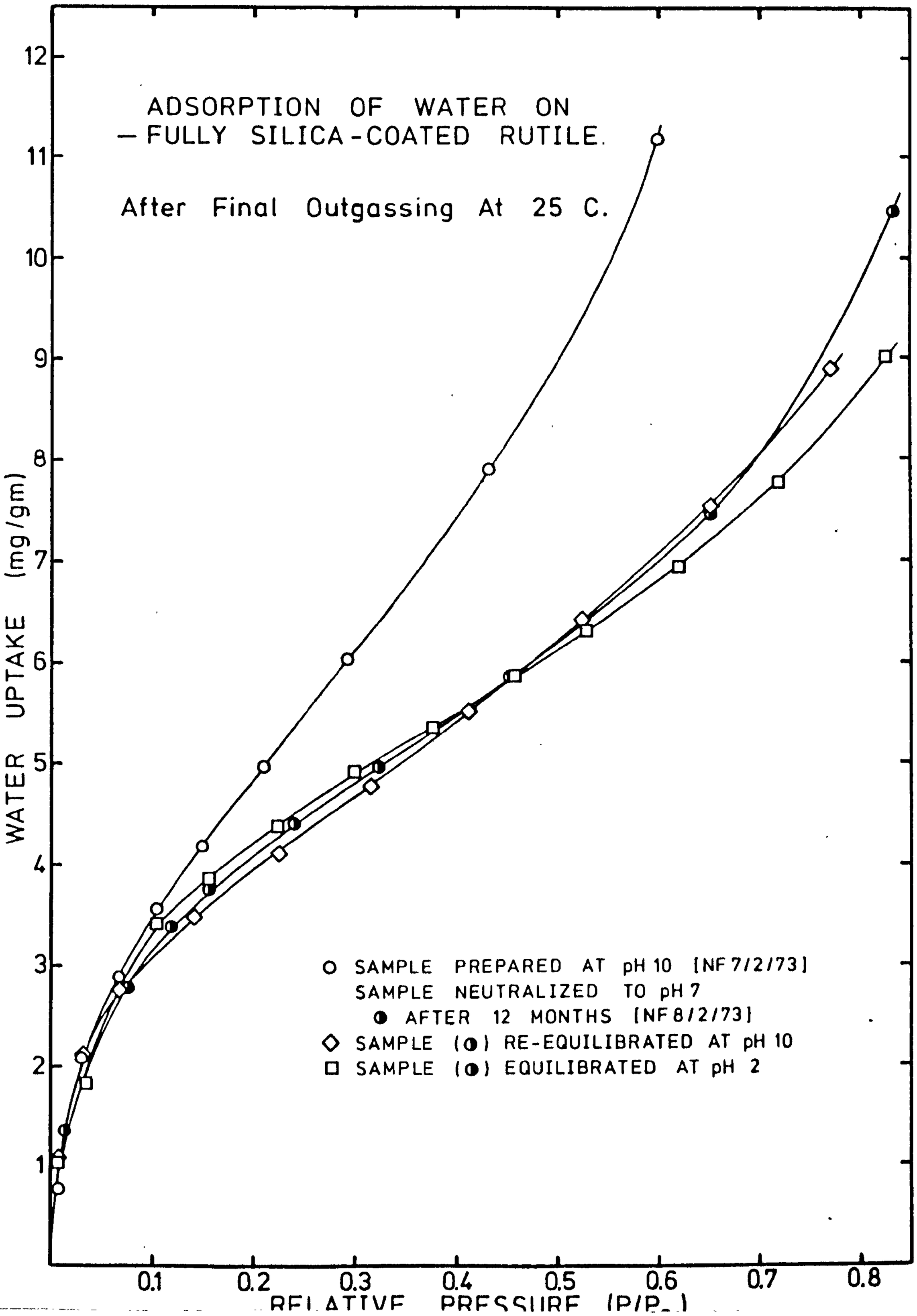

FIGURE 8-18

EFFECTS OF PRE-EQUILIBRATION pH

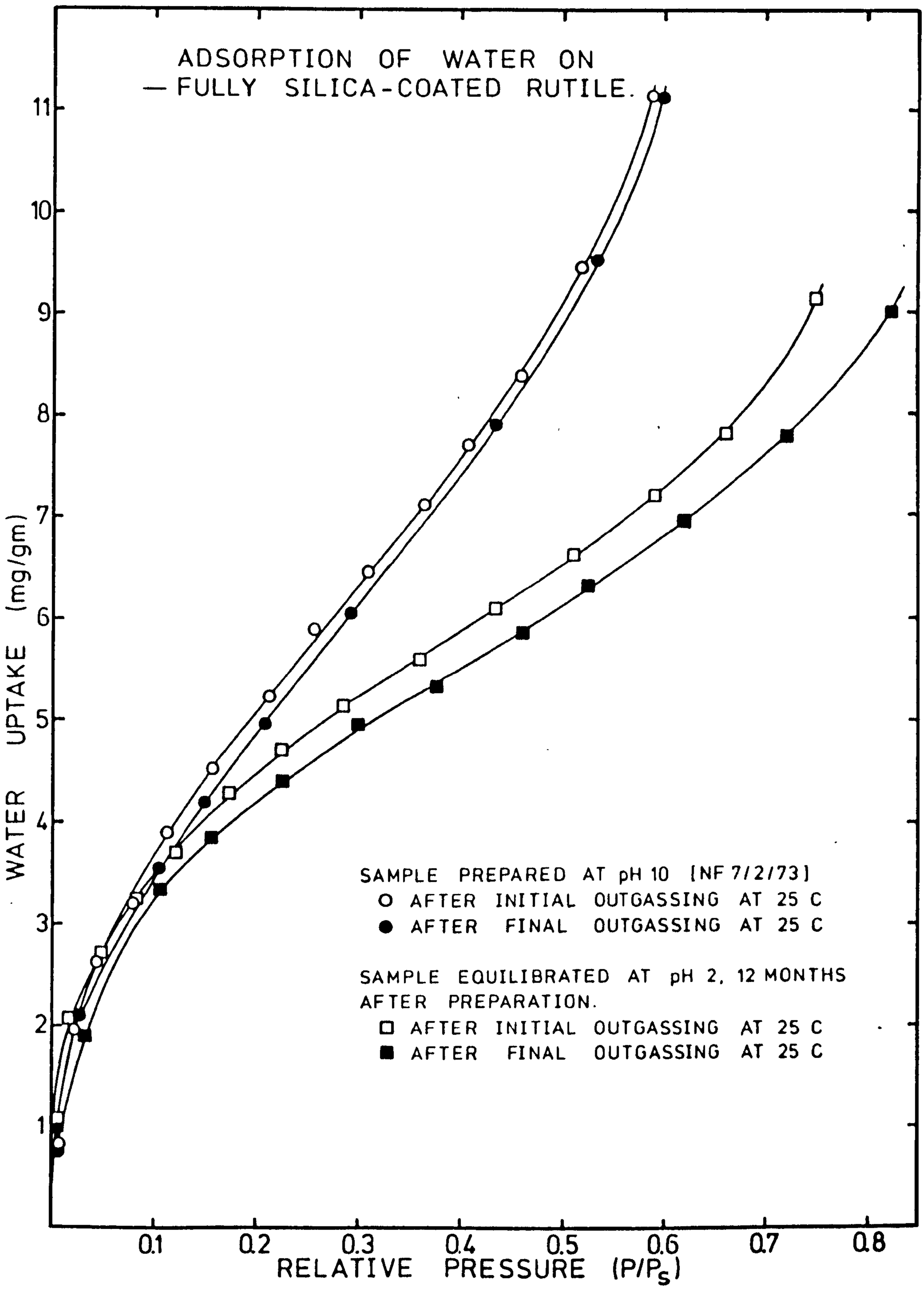

FIGURE 8-19

FRENKEL-HALSEY-HILL PLOTS

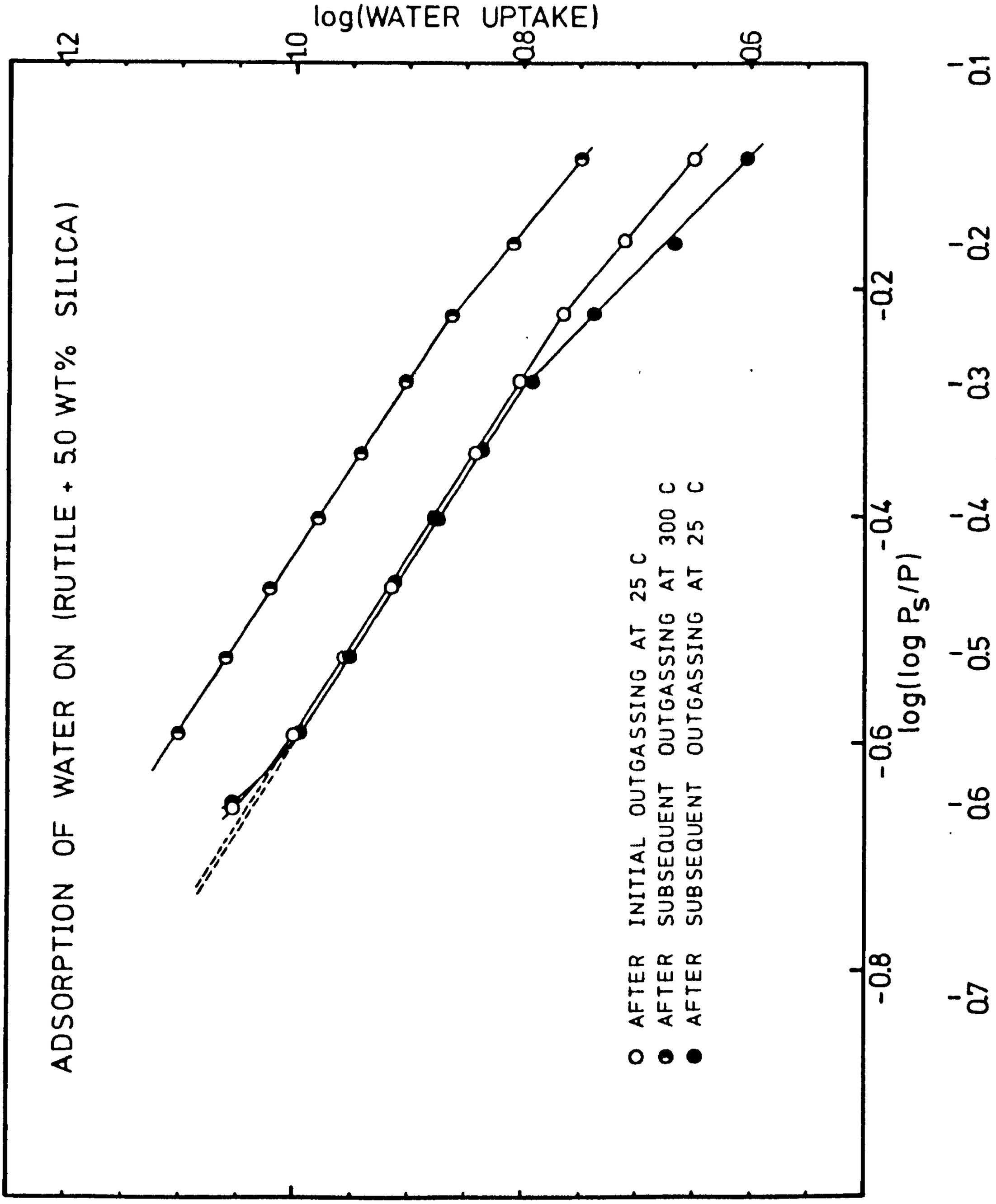

FIGURE 8-20

EFFECTS OF PRE-EQUILIBRATION pH

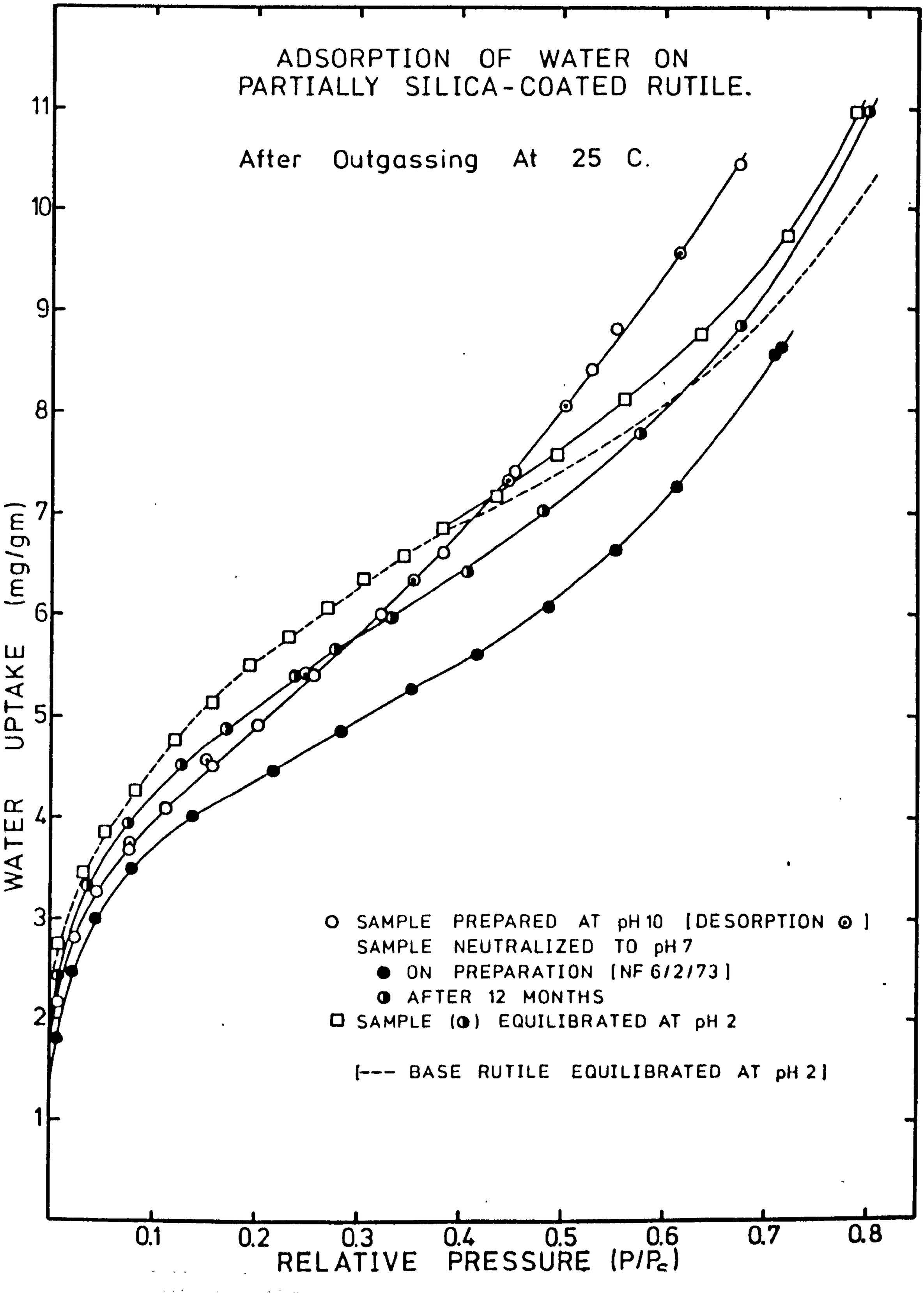

FIGURE 8-21

EFFECTS OF PRE-EQUILIBRATION pH

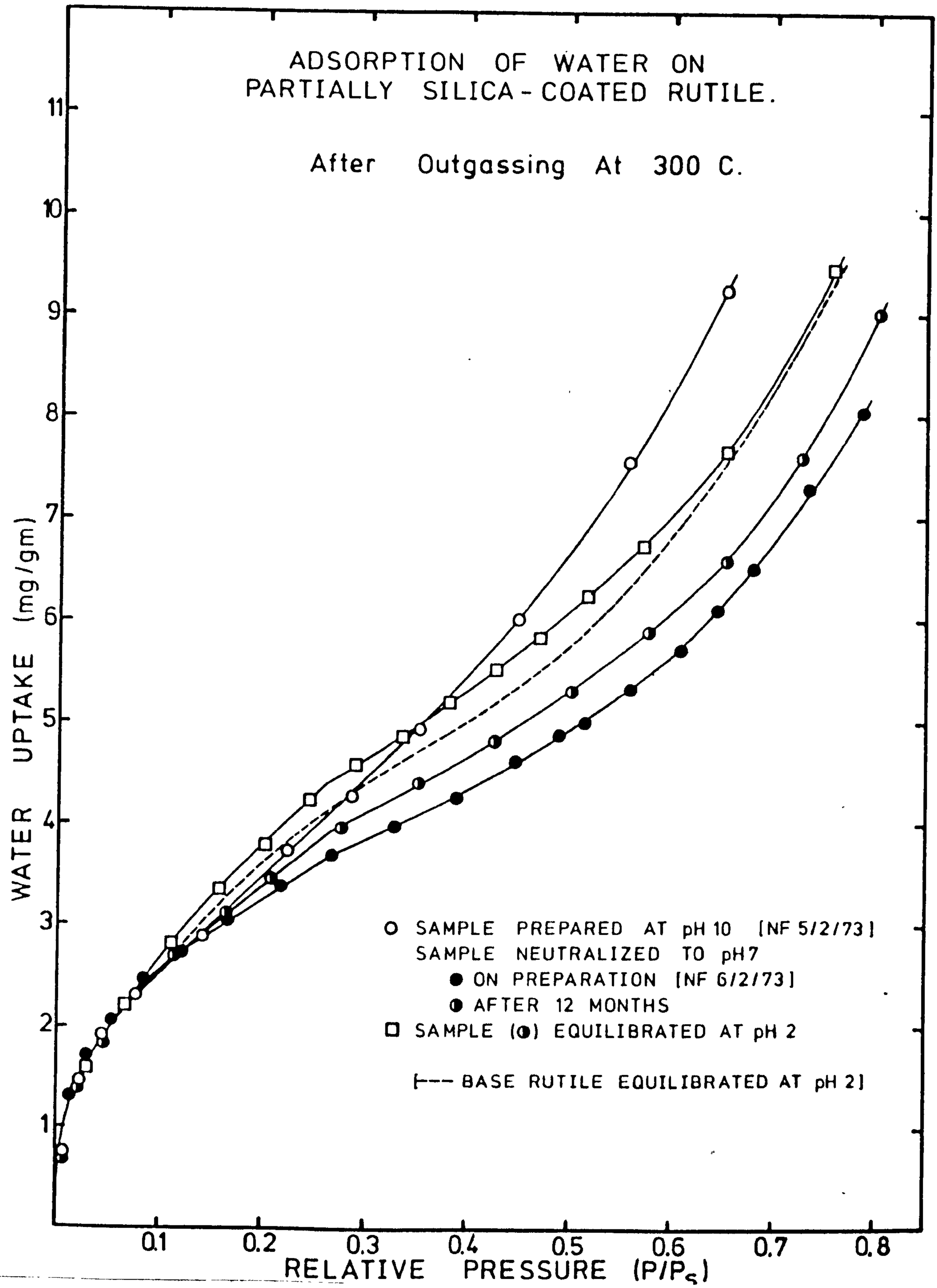

CHAPTER 9: GENERAL CONCLUSIONS

The aim of the present study was to investigate the deposition of amorphous silica from aqueous solution on to the surfaces of small rutile particles.

(A) The Nature of the Interacting Species: The coating preparation experiments (Chapter 5) and the electrokinetic studies (Chapter 6) indicate that uniform silica coatings are formed when adsorption of monomeric silica is followed by polymerization of silica at the solid/liquid interface. There is evidence that adsorbed monomer species anchor the polymeric silica to the titanium dioxide surface although the exact nature of the silica-titania bond is unknown. Electrokinetic studies (Chapter 6) and water sorption studies (Chapter 8-3) indicate that some silica deposited under alkaline conditions can be removed by equilibration at low pH (< 3). The results of the present study are consistent with the formation of $Ti-O-Si(OH)_3$ surface species due to adsorption from solution of monomeric silica. Such species were suggested by Parfitt et al[143] following the hydrolysis of surfaces formed by the gas phase reaction between rutile and $SiCl_4$.

(B) Coverage of the Titanium Dioxide Surface: Five levels of silica coating in the range 0.6 to 5.0 wt.% silica have been investigated.

All studies undertaken show the 0.6 wt.% silica sample to consist of partially-silica-covered rutile particles. This amount of silica corresponds to 0.33 nm^2 per SiO_2 unit on the base rutile used. Nitrogen and argon adsorption studies (Chapter 7) indicate that the high energy

components of bare rutile surfaces were masked by the addition of the 0.6 wt.% of silica. Studies of water sorption versus outgassing temperature (Chapter 8-1) show that ligand water molecules attached to Ti cations on bare rutile were not present on the 0.6 wt.% silica sample and that this sample exhibited multilayer water sorption characteristics similar to those of the uniformly silica-coated samples. The ageing studies (Chapter 8.3) indicate that removal of some silica from the 0.6 wt.% silica sample was sufficient to restore rutile-like behaviour for the adsorption of water vapour. The addition of 0.6 wt.% of silica to the base rutile had little effect on its isoelectric point - a parameter believed to depend essentially on the behaviour of surface hydroxyl groups. The differential energies of adsorption of nitrogen and argon (Chapter 7-3), and the water sorption data (Chapter 8), suggest that the 0.6 wt.% silica sample contains both Si-OH and Ti-OH surface groups.

If the model of Jones and Hockey[162] for the rutile surface is used, viz:

60% of the surface consists of the (110) plane with 5.1 Ti ions/nm^2

20% " " " " " " (100) " " 7.4 " " "

20% " " " " " " (101) " " 7.9 " " "

then it can readily be shown that a monolayer of $-O-Si(OH)_3$ species on the base rutile, formed by a 1 : 1 reaction with surface titanium ions, would require approximately 1.2 wt.% of silica (expressed as SiO_2). Indeed all the experimental techniques used indicate that the 1.4 wt.% silica sample prepared by the aqueous coating process consists of rutile particles completely covered by silica. The

electrokinetic experiments and the water sorption/ageing studies indicate that the silica coating in the 1.4 wt.% silica sample is sufficiently thin to allow its removal on equilibrating in acid solution.

The 2.6 and 5.0 wt.% silica samples have been shown to consist of base rutile particles covered by a multilayer of silica. The silica coatings can be seen to be approximately uniform under the electron microscope.

As far as electrokinetic behaviour and adsorption of nitrogen, argon and water vapour are concerned, the coatings control the physical and chemical characteristics of these latter two samples.

(C) Coating Structure: A systematic study of the texture of the silica coatings prepared has not been undertaken. Nevertheless some conclusions can be derived from the characterization studies performed, with the proviso that the effects on the coatings of drying and outgassing at room temperature are not known.

The majority of the characterization studies were performed on samples of silica-coated rutile neutralised to pH 7 on preparation. It was expected from literature data on the polymerization of silica in aqueous solution that such coatings would consist of fully internally condensed amorphous silica. These pH 7 coatings were shown in general to contain little internal volume accessible to water, nitrogen or argon. Electrokinetic studies were consistent with some internal hydroxyl groups being accessible to hydrogen and hydroxyl ions from aqueous solution.

The water sorption studies on silica-coated rutile samples pre-equilibrated at pH 10, 7 and 2 indicate that coating structure is drastically changed between pH 10 and 7. Polymerization at pH 10 produced silica coatings containing narrow channels accessible to water molecules, even in low silica content samples. As already stated neutralization to pH 7 removed accessible internal volume in coatings, but because samples were neutralized at pH 7 for varying short times, the degree of internal cross-linking achieved varied from sample to sample.

REFERENCES

1. Springborn, G.D., Chemische Industrie 12, (1971), 841.
2. Kampfer, W.A., Pigment Handbook, 1, (1973), 1.
3. Samsonov, G.V., The Oxide Handbook (I.F.I./Plenum 1973).
4. Murley, R.D., J. Oil Colour Chem. Assoc., 45(1), (1962), 16.
5. Cunningham, J. and Perry, A.L., J. phys. Chem., 78(9), (1974), 870.
6. Bickley, R.I. and Stone, F.S., J. Catalysis, 31(3), (1973), 389.
7. Bickley, R.I. and Stone, F.S., J. Catalysis, 31(3), (1973), 398.
8. Tanaka, K-I., J. phys. Chem., 78(5), (1974), 555.
9. Cunningham, J., Finn, E. and Perry, A.L., Chemica Scripta, 6(2), (1974), 87.
10. Cockayne, B. and Jones, D.W., (Ed) Modern Oxide Materials (Academic Press, 1972).
11. Iammartino, N.R., Chemical Engineering, 79(9), (1972), 34.
12. Hurlen, T., Acta chem. scand., 13, (1959), 365.
13. Cromer, D.T. and Herrington, K., J. Am. chem. Soc., 77, (1955), 4708.
14. Horn, M., Schwerdtfeger, C.F. and Meagher, E.P., Z. Kristallographie, 136(3/4), (1972), 18.
15. Abrahams, S.C. and Bernstein, J.L., J. chem. Phys., 55, (1971),3206.
16. Weiners, G., Chem. anlagen Verfahren, 12, (1971), 43.
17. Shaulov, Yu. Kh., Shtrambrand, Yu. M., Shinkarev, A.M., Andreeva, N.I. and Ryabenko, E.A., Russ. J. phys. Chem., 47(10), (1973), 1530.
18. Bobyrenko, Yu. Ya., Russ. J. phys. Chem., 47(3), (1973), 399.
19. Antipov, I.V., Lipkes, Ia. M., Grofman, L.M. and Suchko, T.P., Lakok. Mater. Ikh. Primen, 4, (1972), 9.

20. Weyl, W.A. and Forland, T., Ind. Engng. Chem., 42, (1950), 257.

21. Londergan, M.C. and Spengeman, W.F., J. Paint Technology, 42(543), (1970), 260.

22. Renz, C., Helv. chim. Acta, 4, (1921), 961.

23. Goodeve, C.F., Trans. Faraday Soc., 33, (1937), 340.

24. Jacobsen, A.E., Ind. Engng. Chem., 41, (1949), 523.

25. McTaggart, F.K. and Bear, J., J. appl. Chem., 5, (1955), 643.

26. Mazurkevich, Ya. S., Fedotova, I.M., Fitileva, V.V., Kozlova, T.V. and Smogorzhevskii, A.V., Lakok. Mater. Ikh. Primen, 3, (1968), 14.

27. Gerteis, R.L. and Elm, A.C., J. Paint Technology 43(555), (1971), 99.

28. Voelz, H.G. and Koempf, G., Farbe Lack, 78(11), (1972), 1037.

29. Ashmead, B.V., Bowrey, M., Burrill, P.M., Hendrick, T.C. and Owen, M.J., J. Oil Colour Chem. Assoc., 54, (1971), 403.

30. Dubois, J.C. and Gazard, M., French Patent 2,144,024.

31. Barksdale, J., Titanium (Ronald Press, N.Y., 1966).

32. Preuss, H.P., Pigments in Paint (Noyes Data Corp., N.J., 1974).

33. Rutter, E.G., Oil Colour Chem. Assoc. (Trans), 28(304), (1945), 187.

34. Tinsley, S.G. and Bowman, A., J. Oil Colour Chem. Assoc., 32(348), (1949), 233.

35. Campbell, J.G. and Hughes, W., J. Oil Colour Chem. Assoc., 39(435), (1956), 481.

36. Ermolaeva, T.A., Abramson, D.L., Anufrieva, N.S., Prytkova, G.A. and Potopova, M.P., Lakok. Mater. Ikh. Primen, 2, (1969), 17.

37. Siddle, G.R., Paint Technology, 35(12), (1971), 6.

38. Day, R.E., Progress in Organic Coatings, 2, (1973/4), 269.

39. Wilska, S., Farbe Lack, 71(1), (1965), 39.

40. Smith, H., Nature, 211(5046), (1966), 292.

41. Kaempf, G. and Voelz, H.G., Farbe Lack, 74(1), (1968), 37.

42. Barcucci, U. and Torlaschi, S., 9th F.A.T.I.P.E.C. Congress, Section 1, (1968), 73.

43. Herrington, K.D. and Lui, Y.K., J. Colloid Interface Sci., 34(3), (1970), 447.

44. Murray, J.W., Pigment Handbook, 3, (1973), 77.

45. Doorgest, T., J. Oil Colour Chem. Assoc., 50, (1967), 1079.

46. Urwin, D., J. Oil Colour Chem. Assoc., 52, (1969), 697.

47. Rechmann, H., Farbe Lack, 75(1), (1969), 51.

48. Zettlemoyer, A.C., Micale, F.J. and Scheidt, P., Chem. Phys. Appl. Surface Active Subst., Proceedings 4th Int. Congress 1964, 2, (1967), 181.

49. Wiseman, T.J., J. Oil Colour Chem. Assoc., 50(6), (1967), 545.

50. Parfitt,G.D. and Ramsbotham, J., J. Oil Colour Chem. Assoc., 54, (1971), 356.

51. Parfitt, G.D., J. Oil Colour Chem. Assoc., 54, (1971), 717.

52. Ermolaeva, T.A., Potopova, M.P. and Abramson, D.L., Lakok. Mater. Ikh. Primen, 5, (1972), 17.

53. Parfitt, G.D., Croatica Chemica Acta, 45, (1973), 189.

54. Zettlemoyer, A.C. and Chessick, J.J., Advances in Chemistry Series,43, (1964), 88.

55. Dawber, J.G., Guest, L.B. and Lambourne, R., Thermochimica Acta, 6, (1973), 411.

56. Steig, F., J. Paint Technology, 43, (1971), 36.

57. Sherwood, A.F. and Rybica, S., J. Oil Colour Chem. Assoc., 49, (1966), 648.

58. Urwin, D., Ph.D. Thesis, Brunel University, 1973.

59. Iler, R.K., U.S. Patent 2,885,366 (1959).

60. Iler, R.K., Surface and Colloid Science, 6, (1973), 1.

61. Tanabe, K., Ito, M. and Sata, M., J. chem. Soc. chem. Comms., (1973), 676.

62. Ito, M., Hattori, H. and Tanabe, K., J. Catalysis, 35(2), (1974), 225.

63. Hosaka, H., Kawashima, N. and Meguro, K., Bull. chem. Soc. Japan, 45(11), (1972), 3371.

64. Overbeek, J.Th.G., "Electrokinetic Phenomena" in Colloid Science 1,(1952),195, Ed. H.R. Kruyt (Elsevier Publ. Co.).

65. Lyklema, J., Croatica Chemica Acta, 43, (1971), 249.

66. Overbeek, J.Th.G., Reference 64, page 115.

67. Parsons, R., in "Modern Aspects of Electrochemistry" 1, (1954), 103, (Butterworths, Ed. J.O'M. Bockris and B.E. Conway).

68. Haydon, D.A., in "Recent Progress in Surface Science" 1, (1964), 94, (Academic Press, Ed. J.F. Danielli, K.G.A. Pankhurst and A.C. Riddiford).

69. Smith, A.L., in "Dispersion of Powders in Liquids" (1973), 86 (Applied Science Publishers Ltd., Ed. G.D. Parfitt).

70. von Helmholtz, H., Ann. Physik, 7, (1879), 337.

71. Perrin, J.J., J. chem. Phys., 2, (1904), 601.

72. Gouy, G., J. Physique [4], 9, (1910), 457.

73. Gouy, G., Compt. Rend., 149, (1910), 654.

74. Gouy, G., Ann. Physique [9], 7, (1917), 129.

75. Chapman, D.L., Phil. Mag. [6], 25, (1913), 475.

76. Grahame, D.C., Chemical Reviews, 41, (1947), 441.

77. Bérubé, Y.G. and de Bruyn, P.L., J. Colloid Interface Sci., 28, (1968), 92.

78. Bolt, G.H., J. Colloid Sci., 10, (1955), 206.

79. Levine, S. and Bell, G.M., Discuss. Faraday Soc., 42, (1966), 69.

80. Bell, G.M. and Levine, S., J. Colloid Interface Sci., 41(2), (1972), 275.

81. Hunter, R.J., J. Colloid Interface Sci., 22, (1966), 231.

82. Wiese, G.R., James, R.O. and Healy T.W., Discuss. Faraday Soc., 52, (1971), 302.

83. Fuerstenau, D.W. and Modi, H.J., J. electrochem. Soc., 106, (1959), 336.

84. Sonntag, H. and Strenge, K., Coagulation and Stability of Disperse Systems, (Halstead Press, 1969).

85. Sennett, P. and Olivier, J.P., Ind. Engng. Chem., 57(8), (1965), 33.

86. Grahame, D.C., J. chem. Phys., 18, (1950), 903.

87. Stern, O., Z. elektrochem., 30, (1924), 508.

88. Langmuir, I., J. Am. chem. Soc., 38, (1916), 2221; 39, (1917),1885; 40, (1918), 1361.

89. Verwey, E.J.W. and Overbeek, J.Th.G., Theory of the Stability of Lyophobic Colloids, 1948, (Elsevier Publ. Co.).

90. Gileadi, E. and Conway, B.E., in "Modern Aspects of Electrochemistry" 3, (1964), 347, (Butterworths, London).

91. Matijevic, E., Janauer, G.E. and Kerker, M., J. Colloid Sci., 19(4), (1964), 333.

92. Loeb, A.L., Overbeek, J.Th.G. and Wiersema, P.H., The Electrical Double Layer Around a Spherical Colloid Particle (1961), (M.I.T. Press, Cambridge).

93. James, R.O. and Healy, T.W., J. Colloid Interface Sci., 40, (1972), 53.

94. Grahame, D.C., J. electrochem. Soc., 98(9), (1951), 343.

95. Grahame, D.C. and Soderberg, B.A., J. chem. Phys., 22(3), (1954), 449.

96. Lyklema, J., Trans. Faraday Soc., 59, (1963), 418.

97. Devanthan, M.A.V., Trans. Faraday Soc., 50, (1954), 373.

98. Bockris, J.O'M., Devanthan, M.A.V. and Müller, K., Proc. R. Soc., A274, (1963), 55.

99. Anderson, T.N. and Bockris, J.O'M., Electrochim. Acta, 9, (1964), 347.

100. Levine, S., Mingins, J. and Bell, G.M., J. electroanal. Chem., 13, (1967), 280.

101. Levine, S., Bell, G.M. and Calvert, D., Canadian J. Chemistry, 40, (1962), 518.

102. Levine, S., Robinson, K. and Fawcett, W.K., J. electroanal. Chem., 54, (1974), 237.

103. Verwey, E.J.W. and Niessen, K.F., Phil. Mag., 28, (1939), 435.

104. Levine, P.L., Levine, S. and Smith, A.L., J. Colloid Interface Sci., 34(4), (1970), 549.

105. Grimley, T.B. and Mott, N.F., Discuss. Faraday Soc., 1, (1947), 3.

106. Grimley, T.B., Proc. R. Soc., 201, (1950), 40.

107. Honig, E.P., Trans. Faraday Soc., 65, (1969), 2248.

108. Honig, E.P. and Hengst, J.H.Th., J. Colloid Interface Sci., 31(4), (1969), 545.

109. Honig, E.P., Nature, 225, (1970), 537.

110. Ahmed, S.M. and Maksimov, D., J. Colloid Interface Sci., 29(1), (1969), 97.

111. Wright, H.J.L. and Hunter, R.J., Aust. J. Chem., 26, (1973), 1183.

112. Ball, B., J. Colloid Interface Sci., 30(3), (1969), 424.

113. Ahmed, S.M., Proc. 1972 Miami Symposium - Oxide/Electrolyte Interfaces,(1973), 1 (Ed. R.S. Alwitt).

114. Levine, S. and Smith, A.L., Discuss. Faraday Soc., 52, (1971), 290.

115. Wright, H.J.L. and Hunter, R.J., Aust. J. Chem., 26, (1973), 1191.

116. Yates, D.E., Levine, S. and Healy, T.W., J. chem. Soc.-Faraday Trans. I, 10, (1974), 1807.

117. Fuerstenau, D.W., Pure appl. Chem., 24, (1970), 135.

118. Hunter, R.J. and Wright, H.J.L., J. Colloid Interface Sci., 37(3), (1971), 564.

119. Lyklema, J., J. electroanal. Chem., 18, (1968), 341.

120. Abendroth, R.P., J. Colloid Interface Sci., 34, (1970), 591.

121. Bérubé, Y.G. and de Bruyn, P.L., J. Colloid Interface Sci., 27(2), (1968), 305.

122. Dröst-Hansen, W., Ind. Engng. Chem., 57(4), (1965), 18.

123. Griot, O., Trans. Faraday Soc., 62, (1966), 2904.

124. Van Lier, J.A., De Bruyn, P.L. and Overbeek, J.Th.G., J. phys. Chem., 64, (1960), 1675.

125. Watillon, A. and de Backer, R., J. electroanal. Chem., 25, (1970), 181.

126. Levine, S., Smith, A.L. and Brett, A.C., Chem; Phys. Chem. Anwendungstech. Grenzflaechenaktiven Stoffe, Ber. Int. Kongress (VI) 1972 , 2(2), (1973), 603.

127. Perram, J.W., Hunter, R.J. and Wright, H.J.L., Chem. Phys. Letters, 23(2), (1973), 265.

128. Perram, J.W., Hunter, R.J. and Wright, H.J.L., Aust. J. Chem., 27, (1974), 461.

129. Helmy, A.K., J. chem. Phys., 59(6), (1973), 3101.

130. Tadros, Th.F. and Lyklema, J., J. electroanal. Chem., 17, (1968), 267.

131. Ahmed, S.M., in "Oxides and Oxide Films", 1, (1972), (Marcel Dekker Inc. N.Y., Ed. J.W. Diggle).

132. Herczyńska, E. and Prószyńska, K., J. inorg. nucl. Chem., 26, (1964), 1429.

133. Atkinson, R.J., Posner, A.M. and Quirk, J.P., J. phys. Chem., 71(3), (1967), 550.

134. Ahmed, S.M., J. phys. Chem., 73, (1969), 3546.

135. Blok, L. and de Bruyn, P.L., J. Colloid Interface Sci., 32(3), (1970), 533.

136. Blok, L. and de Bruyn, P.L., J. Colloid Interface Sci., 32(3), (1970), 527.

137. Bowden, J.W., Bolland, M.D.A., Posner, A.M. and Quirk, J.P., Nature (Physical Science), 245, (1973), 81.

138. Herczyńska, E., J. inorg. nucl. Chem., 26, (1964), 2127.

139. Napper, D.H. and Hunter, R.J., "Surface Chemistry and Colloids" 7, (1972), 241, (Butterworths, Ed. M. Kerker).

140. Liberti, A., Chiantella, V. and Corifliano, F., J. inorg. nucl. Chem., 25, (1963), 415.

141. Latimer, W.L., "Oxidation Potentials", (Prentice-Hall Inc. 1952).

142. Garrels, R.M. and Christ, C.L., "Solutions, Minerals and Equilibria", (Harper and Row, 1965).

143. Parfitt, G.D., Ramsbotham, J. and Rochester, C.H., J. Colloid Interface Sci., 41(3), (1972), 437.

144. Fukuda, H. and Miura, M., J. Sci. Hiroshima Univ. Ser. A, 36(2), (1972), 77.

145. Purcell, G. and Sun, S.C., Soc. Mining Engineers A.I.M.E.(Trans) 226, (1963), 6.

146. Smith, G.W. and Salman, T., Canadian Metallurgical Quarterly 6(2), (1967), 167.

147. Parks, G.A., Advances in Chemistry Series, 67, (1967), 121.

148. Parks, G.A. and de Bruyn, P.L., J. phys. Chem., 66, (1962), 967.

149. Mackenzie, J.M.W., Minerals Sci. Engng., 3(3), (1971), 25.

150. Hunter, R.J., J. Colloid Interface Sci., 22, (1966), 231.

151. Lyklema, J. and Overbeek, J.Th.G., J. Colloid Sci., 16, (1961), 501.

152. Zettlemoyer, A.C., Micale, F.J. and Scheidt, P., Chemistry, Physics-Practical Application of Surface Active Substances. Proceedings of Fourth Int. Congress, 2, (1967), 181.

153. Schmets, J. and Pourbaix, M., C.I.T.C.E., 6th Conference 1954, 167.

154. Brown, J., Japp, W.J. and Ritchie, J., J. appl. Chem. (London), 9, (1959), 153.

155. I.U.P.A.C. Manual - Definitions, Terminology and Symbols in Colloid and Surface Chemistry - Part 1. (1972), (Butterworths, Ed. D.H. Everett).

156. Crowell, A.D., in "The Solid-Gas Interface", 1, (1967), 175. (E. Arnold Publ., Ed. E.A. Flood).

157. Steele, W.A., Advances in Colloid and Interface Science, 1, (1967), 3.

158. Barrer, R.M., J. Colloid Interface Sci., 21, (1966), 415.

159. Young, D.M. and Crowell, A.D., Physical Adsorption of Gases, (Butterworths, 1962), 53.

160. Gregg, S.J. and Sing, K.S.W., Adsorption, Surface Area and Porosity, (Academic Press, 1967).

161. Kiselev, A.V., Russ. J. phys. Chem., 41(10), (1967), 1339.

162. Jones, P. and Hockey, J.A., Trans. Faraday Soc., 67, (1971), 2679.

163. Munuera, G. and Stone, F.S., Discuss. Faraday Soc., 52, (1971), 205.

164. Peri, J.B., J. phys. Chem., 69, (1965), 220.

165. Anderson, P.J., Horlock, R.F. and Oliver, J.F., Trans. Faraday Soc., 61, (1965), 2754.

166. Carruthers, J.D., Payne, D.A., Sing, K.S.W. and Stryker, L.J., J. Colloid Interface Sci., 36(2), (1971), 205.

167. Everett, D.H. and Haynes, J.M., Specialist Periodical Report-Colloid Science, 1, (1973), 123, (The Chemical Society, London).

168. Kington, G.L. and McLeod, A.C., Trans Faraday Soc., 55, (1959), 1799.

169. Drain, L.E., Trans Faraday Soc., 49, (1953), 650.

170. Gregg, S.J., Surface Chemistry and Colloids - Physical Chemistry - Series 1., 7, (1972), 189, (Butterworths, Ed. A.D. Buckingham and M. Kerker).

171. Brunauer, S., Deming, L.S., Deming, W.T. and Teller, E., J. Am. chem. Soc., 62, (1940), 1723.

172. Flood, E.A., The Solid-Gas Interface Volumes 1 and 2, 1967, (E. Arnold Publishers).

173. Brunauer, S., The Adsorption of Gases and Vapours, 1944. (Oxford Uni. Press, London).

174. Dubinin, M.M., J. Colloid Interface Sci., 23, (1967), 487.

175. Marsh, H. and Rand, B., J. Colloid Interface Sci., 33, (1970), 101.

176. Everett, D.H., in "The Solid-Gas Interface", 2, (1967), 1055, (E. Arnold Publ., Ed. E.A. Flood).

177. Sing, K.S.W., Specialist Periodical Report, 1, (1973), 1, (The Chemical Society, London).

178. Schay, G., J. Colloid Interface Sci., 35(2), (1971), 254.

179. Drain, L.E., Science Progress 42, (1954), 608.

180. Pace, E.L., in "The Solid-Gas Interface", 1, (1967), 105, (E. Arnold Publ., Ed. E.A. Flood).

181. Hill, T.L., J. chem. Phys., 17(6), (1949), 520.

182. Everett, D.H., Trans. Faraday Soc., 46, (1950), 453.

183. Everett, D.H., Trans. Faraday Soc., 46, (1950), 942.

184. Everett, D.H., Trans. Faraday Soc., 46, (1950), 957.

185. Everett, D.H., Colloques Internationaux Du CNRS, No. 201 Thermochimie-1972, 45.

186. Denbigh, K., Principles of Chemical Equilibrium (Cambridge Uni. Press, 1964).

187. Sing, K.S.W., Colloques Internationaux Du CNRS, - No 201 Thermochimie-1972, 435.

188. Flood, E.A., in "The Solid-Gas Interface", 1, (1967), 11. (E. Arnold Publ., Ed. E.A. Flood).

189. Létoquart, C., Rouquerol, F. and Rouquerol, J., J. Chim. phys. 3, (1973), 559.

190. Brunauer, S., Emmett, P.H. and Teller, E., J. Am. chem. Soc., 60, (1938), 309.

191. Langmuir, I., J. Am. chem. Soc., 38, (1916), 2221.

192. Langmuir, I., J. Am. chem. Soc., 40, (1918), 1361.

193. Brunauer, S., Copeland, L.E. and Kantro, D.L., in "The Solid-Gas Interface", 1, (1967), 85, (E. Arnold Publ., Ed. E.A. Flood).

194. Ross, S., Proc. Int. Symp. Surface Area Determination, (1969), 143 and 205, (Butterworths, 1970, Ed. D.H. Everett and R.H. Ottewill).

195. Halsey, G.D., J. chem. Phys., 16, (1948), 931.

196. Barrer, R.M., Mackenzie, N. and McLeod, D., J. chem. Soc., (1952), 1736.

197. Singleton, J.H. and Halsey, G.D., Canadian J. Chemistry, 33, (1955), 184.

198. Yaryshev, G.M. and Sevtin, P.E., Russ. J. phys. Chem., 46(10), (1972), 1512 and 1514.

199. Morimoto, T. and Nagao, M., J. phys. Chem., 78(11), (1974), 1116.

200. Sing, K.S.W. and Madeley, J.D., J. appl. Chem., 3, (1953), 549.

201. Génot, B., J. Colloid Interface Sci., 50(3), (1975), 413.

202. Sing, K.S.W. and Madeley, J.D., J. appl. Chem., 12, (1962), 445.

203. Aristov, B.G. and Kiselev, A.V., Russ J. phys. Chem., 37, (1963), 1359.

204. McClellan, A.L. and Harnsberger, H.F., J. Colloid Interface Sci., 23, (1967), 577.

205. Mikhail, R.Sh. and Shebl, F.A., J. Colloid Interface Sci., 34, (1970), 65.

206. Hagymassy, J. and Brunauer, S., J. Colloid Interface Sci., 33, (1970), 317.

207. Halsey, G.D., Discuss. Faraday Soc., 8, (1950), 54.

208. Knowles, A.J. and Moffat, J.B., J. Colloid Interface Sci., 41(1), (1972), 116.

209. Litvan, G.G., J. phys. Chem., 76(18), (1972), 2584.

210. Carruthers, J.D., Payne, D.A., Sing, K.S.W. and Stryker, L.J., J. Colloid Interface Sci., 36(2), (1971), 205.

211. Jaycock, M.J. and Waldsax, J.C.R., J. chem. Soc. - Faraday Trans. I. 70(8), (1974), 1501.

212. Dawson, P.T., J. phys. Chem., 71, (1967), 838.

213. Zettlemoyer, A.C., Iyengar, R.D. and Scheidt, P., J. Colloid Interface Sci., 22, (1966), 172.

214. Day, R.E. and Parfitt, G.D., Trans. Faraday Soc., 63, (1967), 708.

215. Brunauer, S., Skalny, J. and Bodor, E.E., J. Colloid Interface Sci., 30(4), (1969), 546.

216. Hill, T.L., J. chem. Phys., 14(4), (1946), 263.

217. Kemball, C. and Schreiner, G.D.L., J. Am. chem. Soc., 72, (1950), 5605.

218. Day, R.E., Parfitt, G.D. and Peacock, J., J. Colloid Interface Sci., 46(1), (1974), 17.

219. Kington, G.L. and Aston, J.G., J. Am. chem. Soc., 73(5), (1951), 1929.

220. Drain, L.E. and Morrison, J.A., Trans. Faraday Soc., 48, (1952), 318.

221. Frenkel, J., Kinetic Theory of Liquids,(Clarendon Press, 1946).

222. Halsey, G.D., J. chem. Phys., 16(10), (1948), 931.

223. Hill, T.L., J. chem. Phys., 14(4), (1946), 263; 14(7), (1946), 441; 15(11), (1947), 767.

224. Champion, W.M. and Halsey, G.D., J. phys. Chem., 57, (1953), 646.

225. Halsey, G.D., J. Am. chem. Soc., 73, (1951), 2693.

226. Hill, T.L., J. chem. Phys., 17(6), (1949), 590.

227. Halsey, G.D., J. Am. chem. Soc., 74, (1952), 1082.

228. Pierce, C. and Ewing, B., J. Am. chem. Soc., 84, (1962), 4070.

229. Pierce, C., J. phys. Chem., 64, (1960), 1184.

230. Pierce, C., J. phys. Chem., 63, (1959), 1076.

231. Zettlemoyer, A.C., J. Colloid Interface Sci., 28(3/4), (1968), 343.

232. McCafferty, E. and Zettlemoyer, A.C., J. Colloid Interface Sci., 34(3), (1970), 452.

233. Jurinak, J.J., J. Colloid Sci., 19, (1964), 477.

234. Harkins, W.D. and Jura, G., J. Am. chem. Soc., 66, (1944), 1366.

235. House, W.A. and Jaycock, M.J., J. Colloid Interface Sci., 47(1), (1974), 50.

236. Rudzinski, W. and Jaroniec, M., Surface Science, 42, (1974), 552.

237. Dormant, L.M. and Adamson, A.W., J. Colloid Interface Sci., 38(2), (1972), 285.

238. Krauskopf, K.B., Geochim. cosmochim. Acta, 10, (1956), 1.

239. Stöber, W., Advances in Chemistry Series, 67, (1967), 161.

240. Jorgensen, S.S., Acta chem. scand., 22, (1968), 335.

241. Greenberg, S.A., J. phys. Chem., 61, (1957), 196.

242. Greenberg, S.A. and Price, E.W., J. phys. Chem., 61, (1957), 1539.

243. Alexander, G.B., Heston, W.M. and Iler, R.K., J. phys. Chem., 58, (1954), 453.

244. Iler, R.K., The Colloid Chemistry of Silica and Silicates, (Cornell University Press, 1955).

245. Shell, H.R., in Treatise on Analytical Chemistry Part II - Analytical Chemistry of the Elements, 2, (1962), 120, (Interscience Publ., Ed. I.M. Kolthoff and P.J. Elving).

246. Lewin, J.C., Geochim. cosmochim. Acta, 21, (1961), 182.

247. Johnston, J.H., Ind. Hyg. Occup. Med., 1, (1950), 323.

248. Prigogine, M. and Fripiat, J.J., Bull. Soc. Royal Sci. Liège, 43(7/10), (1974), 449.

249. Smith, F.G., Physical Geochemistry-Chapters 12 and 13, (Addison-Wesley Publ., 1963).

250. Iler, R.K., J. Colloid Interface Sci., 43(2), (1973), 399.

251. Brown, J., Jaap, W.J. and Ritchie, P.D., J. appl. Chem., 9, (1959), 153.

252. Alexander, G.B., J. phys. Chem., 61, (1957), 1563.

253. Elmer, T.H. and Nordberg, M.E., J. Am. chem. Soc., 41, (1958), 517.

254. Weldes, H.H. and Lange, K.R., Ind. Engng. Chem., 61(4), (1969), 29.

255. Lagerström, G., Acta chem. scand., 13, (1959), 722.

256. Freund, E., Bull. Soc. chim. Fr., (7/8), (1973), 2238.

257. Stöber, W., Kolloid Z., 147(3), (1956), 131.

258. Ingri, N., Acta chem. scand., 13, (1959), 758.

259. Dent Glasser, L.S. and Sharma, S.K., British Polymer J., 6(6),(1974),283.

260. Alexander, G.B., J. Am. chem. Soc., 75, (1953), 5655.

261. Kopejkin, V.A. and Mikhajlov, A.S., Dokl. Akad. Nauk. SSSR., Ser. Geokhimija, 191, (1970), 917.

262. Fortnum, D. and Edwards, J.O., J. inorg. nucl. Chem., 2, (1956), 264.

263. Earley, J.E., Fortnum, D., Wojcicki, A. and Edwards, J.O., J. Am. chem. Soc., 81, (1959), 1295.

264. Iler, R.K., J. phys. Chem., 57, (1953), 604.

265. Lentz, C.W., Inorganic Chemistry, 3(4), (1964), 574.

266. Aveston, J., J. chem. Soc., (1965), 4444.

267. Stumm, W., Hüper, H. and Champlin, R.L., Environmental Science and Technology, 1(3), (1967), 223.

268. Debye, P. and Nauman, R.V., J. Am. chem. Soc., 65, (1961), 5.

269. Greenberg, S.A., J. phys. Chem., 61, (1957), 960.

270. Scheel, L.D., Fleischer, E. and Klemperer, F.W., Ind. Hyg. Occup. Med., 8, (1953), 564.

271. Debye, P. and Nauman, R.V., J. Am. chem. Soc., 65, (1961), 10.

272. Brady, A.P., Brown, A.G. and Huff, H., J. Colloid Sci., 8, (1953), 252.

273. Bechtold, M.F., J. phys. Chem., 59, (1955), 532.

274. Heald, I.A., Coates, K.B. and Edwards, J.E., J. appl. Chem., 5, (1955), 425.

275. Greenberg, S.A. and Sinclair, D., J. phys. Chem., 59, (1955), 435.

276. Alexander, G.B., J. Am. chem. Soc., 76, (1954), 2094.

277. Dollimore, D. and Heal, G.R., J. appl. Chem., 12, (1962), 445.

278. Iler, R.K. and Pinkney, P.S., Ind. Engng. Chem., 39(II), (1947), 1379.

279. Depasse, J. and Watillon, A., J. Colloid Interface Sci., 33(3), (1970), 430.

280. Acker, E.G., J. Colloid Interface Sci., 32(1), (1970), 41.

281. Audsley, A. and Aveston, J., J. chem. Soc., (1962), 2320.

282. Bechtold, M.F., Vest, R.D. and Plambeck, L., J. Am. chem. Soc., 90(17), (1968), 4590.

283. Wieker, W. and Hoebbel, D., Z. anorg. allg. Chem., 336, (1969), 139.

284. Jones, A.M., Practical Physical Chemistry, (J. and A. Churchill Ltd.,1967).

285. Bennett, H., Trans. Br. Ceram. Soc., 61, (1962), 649.

286. Insley, M.J. and Parfitt, G.D., Trans. Faraday Soc., 64(7), (1968), 1945.

287. Bennett, H., Hawley, W.G. and Eardley, R.P., Trans. Br. Ceram. Soc., 57, (1958), 1.

288. Klug, H.P. and Alexander, L.E., X-Ray Diffraction Procedures for Polycrystalline And Amorphous Materials, (J. Wiley and Sons, 1954).

289. van Gils, G.E. and Kruyt, H.R., Kolloidbeihefte, 45, (1936), 60.

290. Skrivan, P., Heyl, V. and Riman, R., Colln. Czech. chem. Commun., 38, (1973), 2557.

291. Jackson, P. and Parfitt, G.D., Kolloid Z.u.Z. Polymère, 239(1), (1970), 611.

292. Fukuda, H. and Miura, M., J. Sci. Hiroshima Univ., Ser. A., 36(2), (1972), 74.

293. Riddick, T.M. and Ravina, L.A., Ind. Engng. Chem., 62(7), (1970), 70.

294. Wiersema, P.H., Loeb, A.L. and Overbeek, J.Th.G., J. Colloid Interface Sci., 22, (1966), 78.

295. Sengupta, M. and Biswas, D.N., J. Colloid Interface Sci., 29, (1969), 536.

296. Honig, E.P. and Hengst, J.H. Th., J. Colloid Interface Sci., 29, (1969), 510.

297. Day, R.E., Parfitt, G.D. and Peacock, J., Discuss. Faraday Soc., 52, (1972), 215.

298. Gregg, S.J., Nashed, S. and Malik, M.T., Powder Technology, 7, (1973), 15.

299. Baker, F.S., Ph.D. Thesis, Brunel University, 1974.

300. Cahn, L. and Schutz, H.R., Vacuum Microbalance Techniques, 3, (1962), 29.

301. Thomas, J.M. and Williams, B.R., Quarterly Reviews, (Chemical Society), 19, (1965), 231.

302. Poulis, J.A. and Thomas, J.M., J. Sci. Inst., 40, (1963), 95.

303. Sing, K.S.W. and Ramakrishna, V.R., Colloques Internationaux Du CNRS - No 201 - Thermochimie (1972), 433.

304. Morimoto, T., Nagao, M. and Tokuda, F., Bull. chem. Soc. Japan, 41, (1968), 1533.

305. Rouquerol, J., Private Communication.

306. Boehm, H.P. and Hermann, M., Z. anorg. allg. Chem., 352, (1967), 156.

307. Pope, M.I. and Sutton, D.I., Powder Technology, 10, (1974), 251.

308. Rimmer, D.L. and McIntosh, R., Canadian J. Chemistry, 52(22), (1974), 3699.

309. Chenion, J. and Lang, F.M., Bull. Soc. chim. Fr., 12(1), (1973), 3273.

310. Hagymassy, J., Brunauer, S. and Mikhail, R.Sh., J. Colloid Interface Sci., 29(3), (1969), 485.

311. Kantro, D.L., Brunauer, S. and Weise, C.H., Advances in Chemistry Series, 33, (1961), 199.

312. Ikeda, S., Kito, A., Imae, T. and Maeda, H., J. Colloid Interface Sci., 48(2), (1974), 256.

313. McBain, J.W. and Bakr, A.M., J. Am. chem. Soc., 48, (1926), 690.

314. Payne, D.A., Ph.D. Thesis, Brunel University, 1970.

315. Calvet, E. and Prat, H., Recent Progress in Microcalorimetry, (Pergamon Press), (1963), 25.

316. Rouquerol, J. and Boivinet, P., Differential Thermal Analysis 2, (1972), 23.

317. Melville, H. and Gowenlock, B.G., Experimental Methods in Gas Reactions, (Macmillan, 1964).

318. Chen, H.H., Aziz, R.A. and Lim, C.C., Canadian J. Physics, 49, (1971), 1569.

319. Rouquerol, J., Colloques Internationaux Du CNRS - No 201 - Thermochimie, (1972), 537.

320. Rouquerol, F., Partyka, S. and Rouquerol, J., Colloques Internationaux Du CNRS - No 201 - Thermochimie, (1972), 547.

321. Carman, C.P. and Raal, F.H., Proc. R. Soc., 209A, (1951), 59.

322. Wade, W.H., J. phys. Chem., 69, (1965), 322.

323. Tayyab, M., Ph.D. Thesis, Brunel University, 1970.

324. Kiselev, A.V., Structures and Properties of Porous Materials (1958), (Butterworths, Ed. D.H. Everett and F.S. Stone).

325. Smith, W.R. and Ford, D.G., J. phys. Chem., 69, (1965), 3587.

326. Rouquerol, J., J. Thermal Analysis, 2, (1970), 123.

327. Rouquerol, J. and Lafitte, M., Colloques Internationaux Du CNRS - No 201 - Thermochimie, (1972), 181.

328. Gardiner, R.G., Mansfield, W.W. and Willing, R.I., Aust. J. Chem., 24, (1971), 681.

329. Davies, K.N. and Holliday, A.K., Trans. Faraday Soc., 48, (1952), 1061.

330. Parks, G.A., Chem. Reviews, 65, (1965), 177.

331. Johansen, P.G. and Buchanan, A.S., Aust. J. Chem., 10, (1957), 398.

332. Morimoto, T. and Sakamoto, M., Bull. chem. Soc. Japan, 37, (1964), 719.

333. Parfitt, G.D., Progress in Surface and Membrane Science, (1975)-in Press.

334. Morimoto, T., Nagao, M. and Tokuda, F., J. phys. Chem., 73(1), (1969), 243.

335. Gonzalez, F. and Munuera, G., Revue De Chimie Minérale, 7, (1970), 1021.

336. Jones, P. and Hockey, J.A., Trans. Faraday Soc., 67, (1971), 2669.

337. Jackson, P. and Parfitt, G.D., Trans. Faraday Soc., 67, (1971), 2469.

338. Primet, M., Pichat, P. and Mathieu, M-V., J. phys. Chem., 75(9), (1971), 1216.

339. Chu, C.W., Phys. Rev. Ser. 3., B(1), (1970), 4700.

340. Guderjahn, C.A., Paynter, D.A., Berghausen, P.E. and Good, R.J., J. phys. Chem., 63, (1959), 2066.

341. Clark, W.C. and Broadhead, P., J. appl. Chem., 20, (1970), 354.

342. Allen, L.H. and Matijevic, E., J. Colloid Interface Sci., 31, (1969), 287.

343. Parfitt, G.D., Ramsbotham, J. and Rochester, C.H., J. chem. Soc. - Faraday Trans. I., (1972), 17.

344. Beckwith, R.S. and Reeve, R., Aust. J. soil Res., 1, (1963), 157.

345. Hingston, F.J. and Rapauch, M., Aust. J. soil Res., 5, (1967), 295.

346. Hingston, F.J., Posner, A.M. and Quirk, J.P., J. soil Sci., 23, (1972), 177.

347.(a) James, R.O. and Healy, T.W., J. Colloid Interface Sci., 40(1), (1972), 42.

(b) James, R.O. and Healy, T.W., J. Colloid Interface Sci., 40(1), (1972), 53.

(c) James, R.O. and Healy, T.W., J. Colloid Interface Sci., 40(1), (1972), 65.

348. Hall, E.S., Discuss. Faraday Soc., 42, (1966), 197.

349. Kononov, O.V., Barskii, L.A. and Ratmirova, L.P., Abstract in Russ. J. phys. Chem., 47(11), (1973), 1651.

350. Fuerstenau, M.C., Gutierrez, G. and Elgillani, D.A., Soc. Mining Engineers A.I.M.E. (Trans)., 241, (1968), 319.

351. Tanabe, K., Sumiyoshi, T., Shibata, K., Kiyoura, T. and Kitagawa, J., Bull. chem. Soc. Japan, 47(5), (1974), 1064.

352. Miura, M., Naono, H. and Iwaki, T., J. Sci. Hiroshima Uni., Ser. A-II, 30(1/2), (1966), 57.

353. Boehm, H.P., Angewandte Chemie, 5(6), (1966), 533.

354. Schindler, P.W. and Gamsjäger, H., Kolloid Z.u.Z. Polymère, 250, (1972), 759.

355. Shannon, R.D., J. appl. Physics, 35(11), (1964), 3414.

356. Bystrov,V.I., Avksent'ev, V.V. and Sokolov, V.A., Russ. J. phys. Chem., 10, (1973), 1441.

357. Wade, W.H. and Hackerman, N., J. phys. Chem., 65, (1961), 1681.

358. Ettre, L.S., Pigment Handbook, 3, (1973), 139.

359. Parfitt, G.D., Urwin, D. and Wiseman, T.J., J. Colloid Interface Sci., 36(2), (1971), 217.

360. de Boer, J.H., The Structure and Properties of Porous Materials, (Butterworths, 1958), 68.

361. Lippens, B.C., Linsen, B.G. and de Boer, J.H., J. Catalysis, 3, (1964), 32.

362. Bhambhani, M.R., Cutting, P.A., Sing, K.S.W. and Turk, D.H., J. Colloid Interface Sci., 38, (1972), 109.

363. Barrer, R.M. and McLeod, D.M., Trans. Faraday Soc., 50, (1954), 980.

364. Hollabaugh, C.M. and Chessick, J.J., J. phys. Chem., 65, (1961), 109.

365. Lewis, K.E. and Parfitt, G.D., Trans. Faraday Soc., 62, (1966), 204.

366. Yates, D.J.C., J. phys. Chem., 65, (1961), 746.

367. Iwaki, T., Komuro, M. and Miura, M., Bull. chem. Soc. Japan, 45, (1972), 2343.

368. Kiselev, A.V. and Uvarov, A.V., Surface Science, 6, (1967), 399.

369. Omiri, T., Imai, T., Nagao, M. and Morimoto, T., Bull. chem. Soc. Japan, 42, (1969), 2198.

370. Armistead, C.G., Tyler, A.J., Hambleton, F.H., Mitchell, S.A. and Hockey, J.A., J. phys. Chem., 73(11), (1969), 3947.

371. Fripiat, J.J. and Uytterhoeven, J., J. phys. Chem., 66, (1962), 800.

372. Kubelková, L. and Jiru, P., Colln. Czech. chem. Commun., 37(9), (1972), 2853.

373. Erkelens, J. and Linsen, B.G., J. Colloid Interface Sci., 29(3), (1969), 464.

374. Cornier, G., Baverez, M. and Bastick, J., Bull. Soc. chim. Fr., 7, (1968), 2707.

375. Kondo, S. and Muroya, M., Bull. chem. Soc. Japan, 43(8), (1970), 2657.

376. Klier, K., Shen, J.H. and Zettlemoyer, A.C., J. phys. Chem., 77(11), (1973), 1458.

377. Young, G.J., J. Colloid Sci., 13, (1958), 67.

378. Tyler, A.J., Taylor, J.A.G., Pethica, B.A. and Hockey, J.A., Trans. Faraday Soc., 67(2), (1971), 483.

379. Peri, J.B., J. phys. Chem., 70(9), (1966), 2937.

380. Bassett, D.R., Boucher, E.A. and Zettlemoyer, A.C., J. Colloid Interface Sci., 27(4), (1968), 649.

381. Kondo, S., Muroya, M. and Fuju, K., Bull. chem. Soc. Japan, 47(3), (1974), 553.

382. Koberstein, E. and Voll, M., Z. phys. Chem. Neue Folge, 71, (1970), 275.

383. Hockey, J.A. and Pethica, B.A., Trans. Faraday Soc., 57, (1961), 2247.

384. Bailey, A., Cadenhead, D.A., Davies, D.H., Everett, D.H. and Miles, A.J., Trans. Faraday Soc., 67, (1971), 231.

385. Clark-Monks, C. and Ellis, B., J. Colloid Interface Sci., 44(1), (1973),37.

386. Lange, K.R., J. Colloid Sci., 20, (1965), 231.

387. Huang, Yun-Yang , J. Catalysis, 25, (1972), 131.

388. Sing, K.S.W., Proc. Int. Symp. Surface Area Determination - Bristol 1969, 25 (Butterworths).

389. Drain, L.E. and Morrison, J.A., Trans. Faraday Soc., 48, (1952), 840.

390. Drain, L.E. and Morrison, J.A., Trans. Faraday Soc., 49, (1953), 654.

391. Harris, L.B., Surface Science, 13(2), (1969), 377.

392. Ross, S. and Olivier, J.P., On Physical Adsorption, (Interscience, 1964).

393. van Dongen, R.H., Surface Science, 39(2), (1973), 341.

394. Ottewill, R.H. and Tiffany, J.M., J. Oil Colour Chem. Ass., 50, (1967), 844.

395. Bosacek, V., Patzelova, V. and Tvaruzkova, Z., J. Catalysis, 36(3), (1975), 371.

396. Aristov, B.G. and Kiselev, A.V., Russ. J. phys. Chem., 38(8), (1964), 1077.

397. Whalen, J.W., J. phys. Chem., 71(6), (1967), 1557.

398. Gregg, S.J. and Nashed, S., Colloques Internationaux Du CNRS - No 201 - Thermochimie, (1972), 461.

399. Cancela, G.D., Rouquerol, F. and Rouquerol, J., J. Chim. phys., 67(3), (1970), 609.

400. Wittman, A., Osterreichische Chemiker Zeitung, 62(8), (1961), 245.